ISSN 1980-9743

Soils and Rocks

Soils and Rocks

An International Journal of Geotechnical and Geoenvironmental Engineering

Volume 36, N. 1
January-April 2013

Soils and Rocks Volume 36, N. 1 2013

SOILS and ROCKS

An International Journal of Geotechnical and Geoenvironmental Engineering

Editor André Pacheco de Assis - University of Brasilia, Brazil

Co-editor Manuel Matos Fernandes - University of Porto, Portugal

Soils and Rocks publishes papers in English in the broad fields of Geotechnical Engineering, Engineering Geology and Geo-environmental Engineering. The Journal is published in April, August and December. Subscription price is US$ 90.00 per year. The journal, with the name "Solos e Rochas", was first published in 1978 by the Graduate School of Engineering, Federal University of Rio de Janeiro (COPPE-UFRJ). In 1980 it became the official magazine of the Brazilian Association for Soil Mechanics and Geotechnical Engineering (ABMS), acquiring the national character that had been the intention of its founders. In 1986 it also became the official Journal of the Brazilian Association for Engineering Geology and the Environment (ABGE) and in 1999 became the Latin American Geotechnical Journal, following the support of Latin-American representatives gathered for the Pan-American Conference of Guadalajara (1996). In 2007 the journal acquired the status of an international journal under the name of Soils and Rocks, published by the Brazilian Association for Soil Mechanics and Geotechnical Engineering (ABMS), Brazilian Association for Engineering Geology and the Environment (ABGE) and Portuguese Geotechnical Society (SPG). In 2010, ABGE decided to publish its own journal and left the partnership.

Soils and Rocks

1978,	1 (1, 2)
1979,	1 (3), 2 (1,2)
1980-1983,	3-6 (1, 2, 3)
1984,	7 (single number)
1985-1987,	8-10 (1, 2, 3)
1988-1990,	11-13 (single number)
1991-1992,	14-15 (1, 2)
1993,	16 (1, 2, 3, 4)
1994-2010,	17-33 (1, 2, 3)
2011,	34 (1, 2, 3, 4)
2012,	35 (1, 2, 3)
2013,	**36 (1,**

ISSN 1980-9743 CDU 624.131.1

ISSN 1980-9743

SOILS and ROCKS

An International Journal of Geotechnical and Geoenvironmental Engineering

Publication of

ABMS - Brazilian Association for Soil Mechanics and Geotechnical Engineering

SPG - Portuguese Geotechnical Society

Volume 36, N. 1, January-April 2013

Table of Contents

ARTICLES

Trial Embankment on Gold Mine Tailings
J.A.R. Ortigao, P. Paiva, A. Fahel, A. Landi, R. Souto 3

Influence of Pile-Soil-Raft Parameters on the Behavior of Piled Raft and Conventional Piled Group Foundations
R.P. Cunha, M. Pando 21

Tailings Liquefaction Analysis Using Strength Ratios and SPT/CPT Results
W. Pirete, R.C. Gomes 37

A Method for Predicting Pile Bearing Capacity From Dynamic Penetration Tests
F. Schnaid, M.J. Langone 55

A Preliminary Assessment of the Distribution and Consequences of Natural and Some Anthropogenic Hazards in Brazil
L.V. Zuquette, O.J. Pejon, R.E. Lima, M. Dantas-Ferreira, V. Guimarães 67

Application of Risk Analysis Methods on Tailings Dams
T. Espósito, L.R. Palmier 97

Performance of In-Line Sediment Control Devices Under Field Conditions
C.P. Cavalhieri, S.J.A.M. Campos, A.L.C.F. Gallardo, O.Y. Bitar 119

TECHNICAL NOTE

Explicit Numerial Iterative Methods Applied to the Three-Parameter Infiltration Equation
A.L.B. Cavalcante, L.C.S.M. Ozelim, P.K. Swamee, P.N. Rathie 129

Articles

Soils and Rocks
v. 36, n. 1

Trial Embankment on Gold Mine Tailings

J.A.R. Ortigao, P. Paiva, A. Fahel, A. Landi, R. Souto

Abstract. This paper describes the behaviour of a 10 m high trial embankment built on silt gold mine tailings of Morro do Ouro Dam, Brazil. The dam is the country's largest tailings dam having 120 m in height and 4 km in length. This trial aimed at investigating tailings strength behaviour, which field experience has already indicated to be better than predicted by in situ and laboratory tests. The embankment foundation was instrumented with piezometers, settlement plates, profiler and inclinometers. Just after placing the first 2 m embankment layer, one observed water surges, interpreted as static liquefaction taking place at low stress level. Large porepressures and displacements were recorded during construction. The embankment height was taken to 10 m, much higher than predictions based on in situ and laboratory tests. The foundation strength was also analysed.

Keywords: tailings, trial embankment, liquefaction.

1. Introduction

How to obtain the shear strength of mine tailings for the design of a hundred metres high tailings dam?

Engineers at RPM Rio Paracatu Mining (now Kinross), Minas Gerais, Brazil, faced this challenge by means of a comprehensive approach employing in situ, laboratory testing and a full scale trial embankment, described in this paper.

This mine produces about 6 tonnes/year of gold and 17 to 22 Mtpa (million tonnes per annum) of tailings. A large expansion project took place between 2005 and 2008 to increase production to 30 Mtpa of tailings. Another tailings dam is currently under construction.

Mine tailings are disposed at the Morro do Ouro Dam, whose current dimensions are 120 m high and 4 km long, the country's largest tailings dam.

The dam project started some 30 years ago and the same Brazilian designers have been involved since the start and continue their work to date. This has been pointed out by the international design reviewer's board, as a safety measure in a long time project, as the project history is well known.

Dam safety is analysed every year by local and international consultants, with at least three hierarchy reviewers' levels above the designers. This has been very important for the successful history of this project, as all safety measures - including this trial embankment - deserve attention by the reviewers, designers and mine managers.

Morgenstern (2002) reviewed the dam design and site investigation results and recommended a low value in the order of 0.08 to 0.12 for the tailings undrained strength index (c_u/σ'_{vo}). This value is lower than the one given by undrained triaxial tests and piezocone analyses, which are in the order of 0.20 to 0.22.

Nevertheless, field experience from building dykes and access roads on the tailings demonstrated that failure is rare. Therefore, actual tailings shear strength looked well above what is predicted by in situ and laboratory tests.

One way to shed light on this dilemma was to build a trial embankment section on the tailings. This approach has been is use on soft clays in Brazil (Ortigao *et al.*, 1983; Ortigao, 1991) and overseas by many researchers (*e.g.*, Leroueil, *et al.*, 1985, 1990; Hunter & Fell, 2003). Nevertheless, there are only a few documented case histories of trial embankments tailings, apart from the Canadian liquefaction experiment programme CANLEX (Byrne *et al.*, 2000; Wride *et al.*, 2000).

Such a full-scale trial would lead to a better understanding of tailings behaviour and savings in further stages of the Morro do Ouro Dam.

This paper summarises tailings properties, describes the experiment, presents factual instrumentation data and stability analyses.

2. Trial Embankment Design

The trial embankment was located at the back of the tailings lake, far from the dam, and about 500 m from the tailings discharge point.

The test section dimensions (Figs. 2, and 3) were: 10 m in height with a front slope 1.5:1 and a gentle slope in the back. At this height, the foundation would have failed, according to predictions based on strength from laboratory and in situ tests. The top of the embankment was 30 m long, so that approximately plane strain conditions apply.

J.A.R.Ortigao, PhD, Terratek Ltd, Av Érico Veríssimo 901/302, 22621-180 Rio de Janeiro, RJ, Brazil. e-mail: ortigao@terratek.com.br.
P Paiva, Civil Engineer, Geo HydroTech Consultants Ltd, São Paulo, SP, Brazil, e-mail: ppaivafk@uol.com.br.
A Fahel, PhD, Samarco Mining, Formerly Geotechnical Consultant, Mariana, MG, Brazil. e-mail: andre.fahel@samarco.com
Antonio Landi, BSc, Mining Engineering, Kinross Mining, Belo Horizonte, MG, Brazil. e-mail: landi.borges@gmail.com.
Romulo Souto, Civil Engineer, Yamana Gold, formerly at Kinross RPM Mining, Jabobina, BA, Brazil. e-mail: romulo.souto@yamanagold.com.
Submitted on May 18, 2011; Final Acceptance on February 14, 2013; Discussion open until August 30, 2013.

Figure 1 - Morro do Ouro tailings dam.

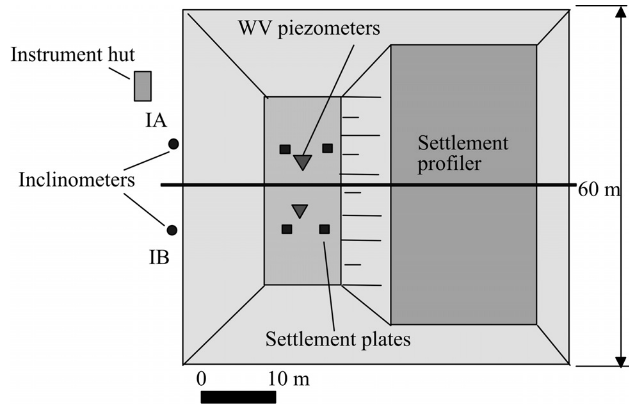

Figure 3 - Plan view, test embankment.

The foundation instrumentation included: electrical vibrating wire piezometers, settlement plates, a settlement profiler and inclinometers.

The loading rate was as fast as possible, to match the worst loading conditions and maximum porepressures build-up. The final height was reached in just seven days. Earthworks took place around the clock, 24 h a day.

Figures 4 to 6 show the embankment under construction and at the end of the project.

3. Tailings Properties

Previous studies and laboratory tests indicate that Mina do Ouro tailings is a soft dark grey silty material having 15% of clay size particles and about 60% silt.

Atterberg limits are: liquid limit LL is 28%, plasticity index PI = 4%, water content w = 50% and average unit weight γ = 17.4 kN/m^3.

3.1. Laboratory triaxial tests

Stress-strain-strength assessment was carried out through load controlled K_0-consolidated undrained triaxial compression tests (CK$_0$U-C tests) on reconstituted samples

Figure 4 - Embankment at 5 m height.

of varying densities. Only the loose state, corresponding to a dry unit weight of 8 kN/m^3, will be presented here.

Specimens were moist tamped in four soil layers in the triaxial mould until the desired density and void ratio was achieved. Saturation, then, took place by water seepage over 12 hours, followed by back-pressuring in small 25 kPa stages until reaching a minimum of porepressure parameter

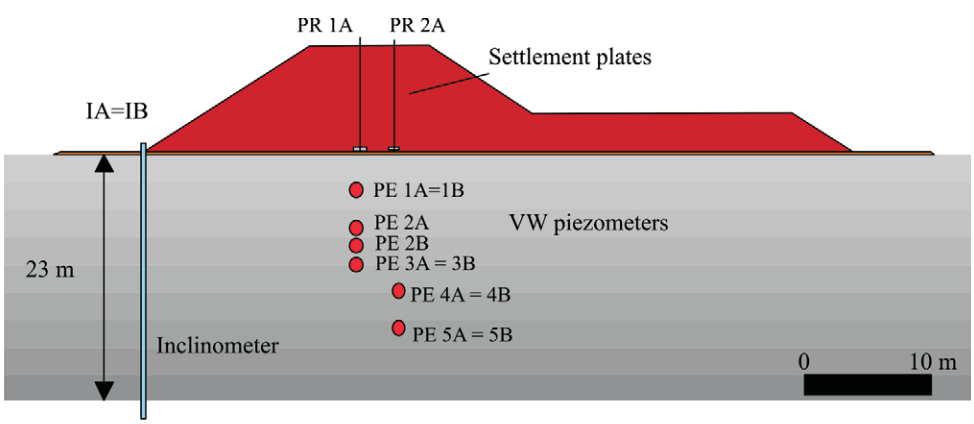

Figure 2 - Cross section of the test embankment.

Figure 5 - Access road.

Figure 6 - Finished embankment.

B of 0.97. Shear was then applied by a static loading frame by increasing deviator stress in controlled increments.

Figure 7 presents stress-strain and porepressure behaviour of loose specimens. The co-ordinates are $p' = (\sigma'_1 + \sigma'_2 + \sigma'_3)/3$, $q = \sigma_1 - \sigma_3$ and void ratio e. The confining stress levels varied from 25 to 200 kPa.

Figure 8 shows the p': q: e plot. The specimen under 200 kPa confining stress shows little deformation under 1% strain, followed by large deformation and porepressure rise tending to reach failure under constant stress.

The stress paths enable the definition of a CSL (critical state line), which present a friction angle of $\phi' = 32^{\circ}$.

The p': e plot yields the following approximate equation for the CSL: (p' in kPa).

$$e = 2.3 - 0.5 \log p'$$

All tests enable the definition of an intermediate line between the K_0 and the CSL, whose deformation magnitude and rate seem to increase by a large amount. This line has been named either instability or collapse line.

The loose specimens at lower confining stresses show a peak strength value followed by very high deformation, which leads to failure. This is typical of static liquefaction behaviour under low confining stress, which presents strong strain-softening under low confining stress that can be detected under strain-controlled tests (Yamamuro & Lade, 1997 and Yamamuro & Covert, 2001).

As confining stress increases, the strain softening tends to decrease and eventually the loose tailings show strain-hardening, as in the loose specimen tested at 200 kPa confining stress.

The undrained strength ratio at (c_u/σ'_{vc}) can be taken at the point where the stress path crossed the instability line, which leads to $c_u/\sigma'_{vc} = 0.2$.

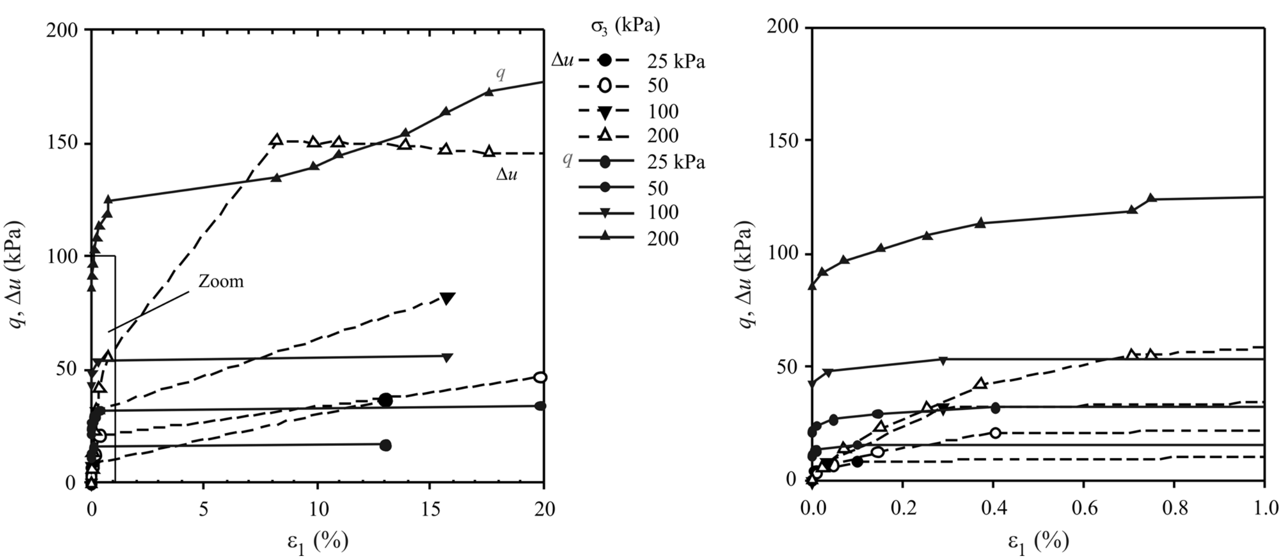

Figure 7 - Stress-strain and porepressure behaviour, loose specimens (left normal view, right zoomed view).

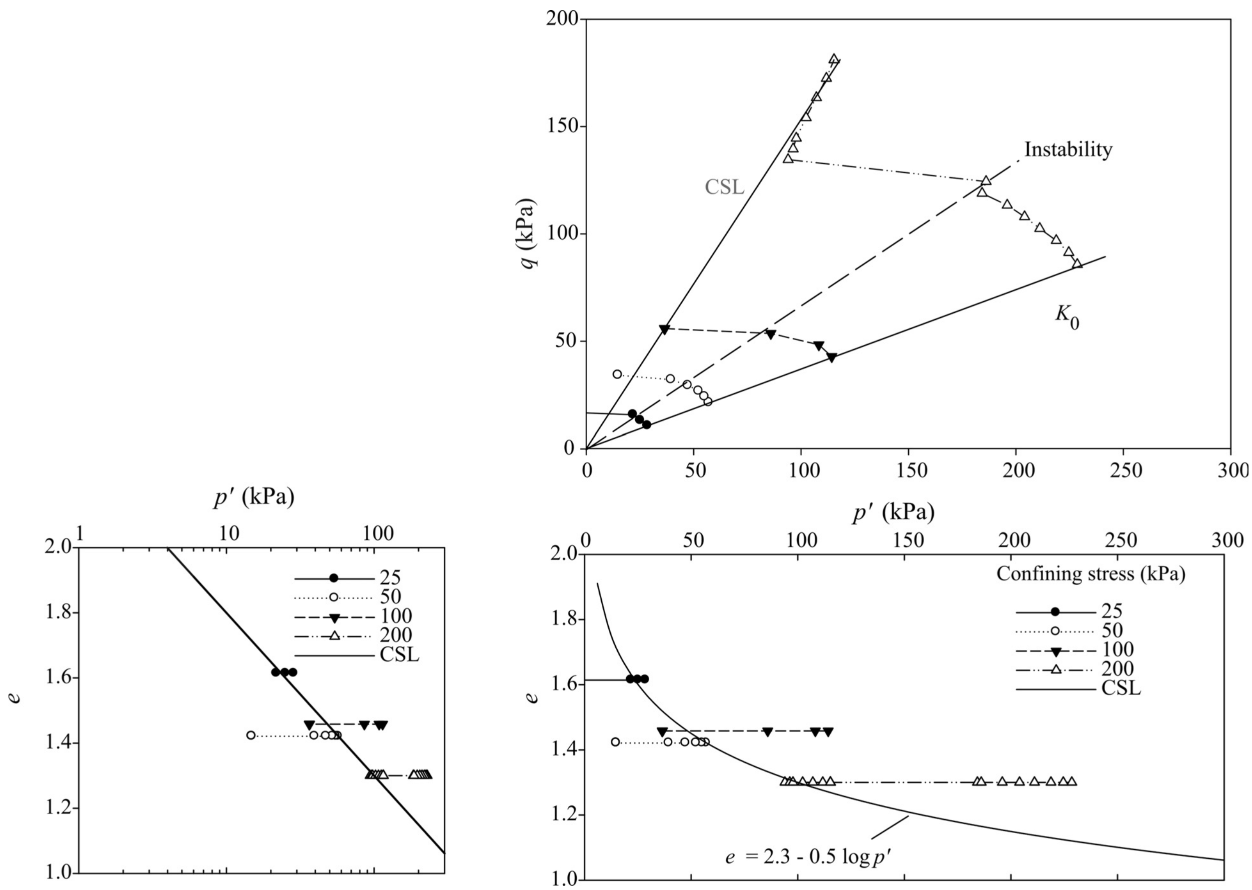

Figure 8 - Stress paths, loose specimens.

3.2. In situ tests

The tailings site investigation programme included some 15 seismic piezocone tests (CPTUS).

Figure 9 shows a typical result of a test carried out close to the trial embankment site. It presents plots of tip resistance q_t; friction ratio, R_f, porepressures u_2 and hydrostatic u_0, I_c, the Soil Behaviour Type or SBT index (Robertson, 2012). Figure 10 shows the normalised CPT parameters for the tip resistance, Q_{tn}, local friction, F, and porepressure B_q described elsewhere (*e.g.*, Robertson, 2012).

The tip resistance through the upper uncompacted embankment fill is greater than 1 MPa down to 12 m depth and then decreases in the tailings below. The friction ratio R_f lies in the range 2 to 4% in the fill and then increases in the tailings to values above 8%. This plot also shows a decrease in R_f below 27 m depth, which is an indication of increase in sand content.

The porepressure u_2 in nearly nil in the fill, but reaches high values in the tailings, well above u_0. The porepressure parameter B_q increases dramatically in the tailings just below the fill and reaches values of above 1. Porepressure dissipation rate in the tailings is so high that full dissipation is achieved during the short time spent at adding steel rods. This is the cause of the zig-zag in the u_2 plot of all boreholes.

Porepressure dissipation rates are very fast yielding a coefficient of consolidation from 3000 to 4000 m^2/ year, *i.e.*, about 800 times a typical soft sedimentary clay (taken as 5 m^2/year, *e.g.*, Ortigao, 1995). This raises the argument that a partial drained behaviour could be assumed for the tailings, especially if loading rate is slow.

Figure 11 shows q_t and shear wave velocity V_s profiles close to the dam crest closer to the trial embankment site. Lower q_t values at tests at the back of the pond, far away from the dam, is because they are closer to the tailings discharge point at the back of the tailings. The CPTUS closer to the dam has a 18m thick fill at the top. On the other hand, the one at the trial embankment site has just 5 m of fill. V_s values are in the range of 100 to 200 m/s in the tailings.

3.3. Flow liquefaction assessment from CPTU

This section looks at flow liquefaction using recent work by Robertson (2009, 2010), who updated a previous method (Robertson & Wride, 1998). Shuttle & Cunning (2007) discussed Robertson and Wride's method limitations. The work presented here is based on an updated version of the original Robertson and Wride's method (1998), details of which were given in Robertson (2008, 2010)

This updated method takes into account cyclic softening and evaluates post liquefaction undrained strength ratio based on case histories recorded by Olson & Stark (2002, 2003).

Robertson's (2010) method consists of obtaining the normalised CPT parameters for tip resistance (*Q*) and friction (*F*) and plotting the data as in the SBT chart as Fig. 12,

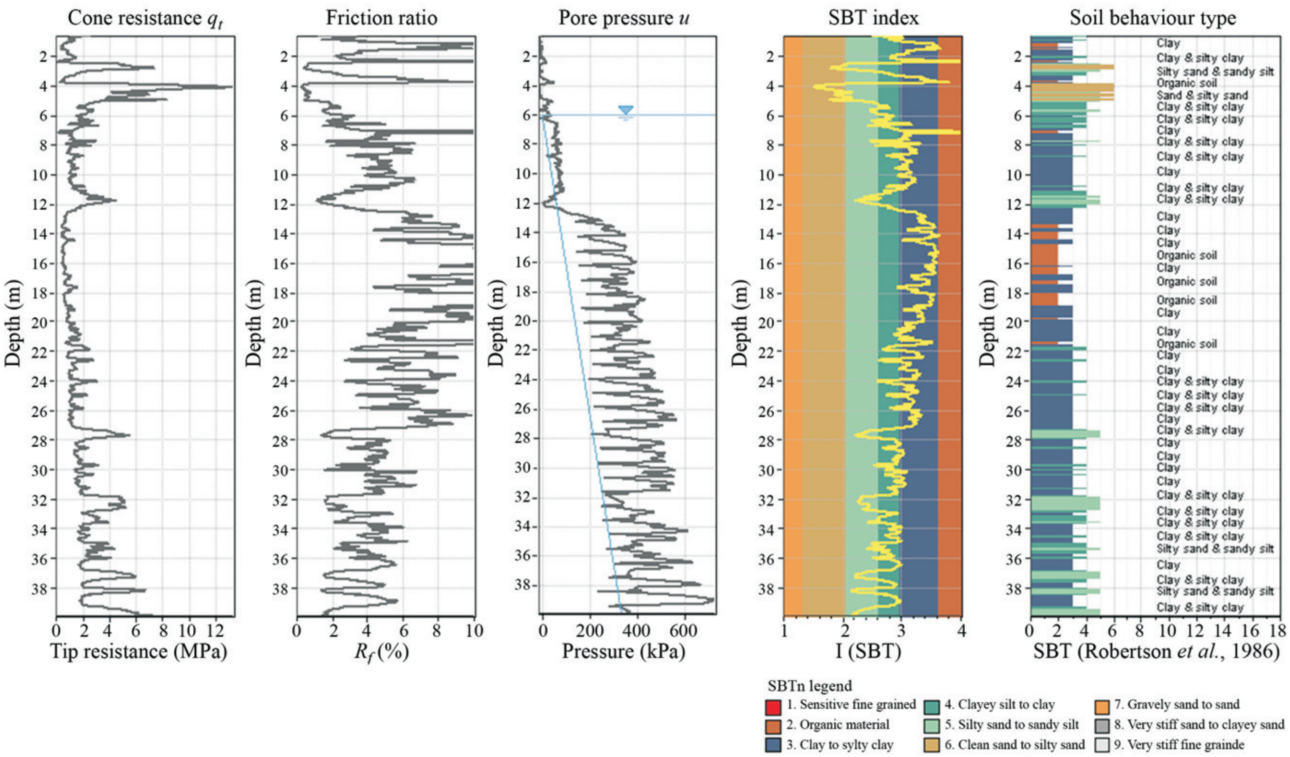

Figure 9 - Typical CPTU results.

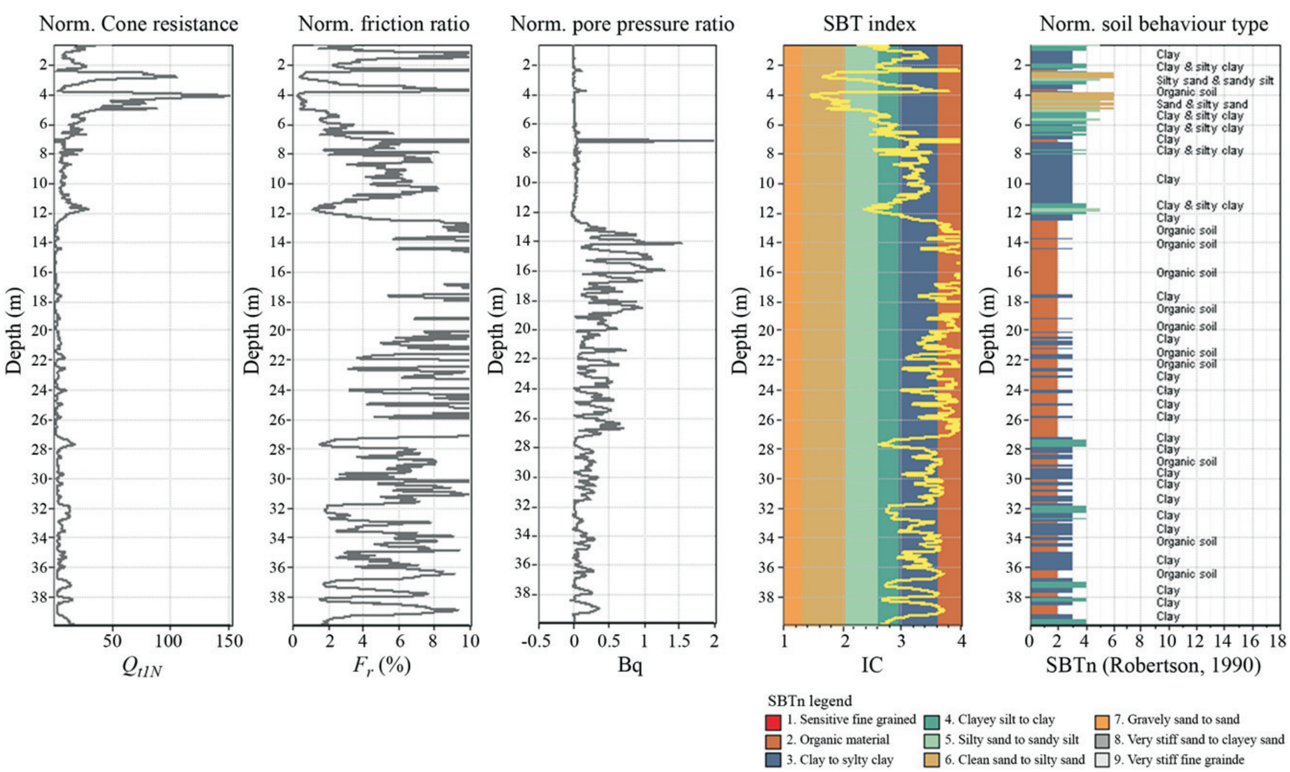

Figure 10 - CPTU normalised results.

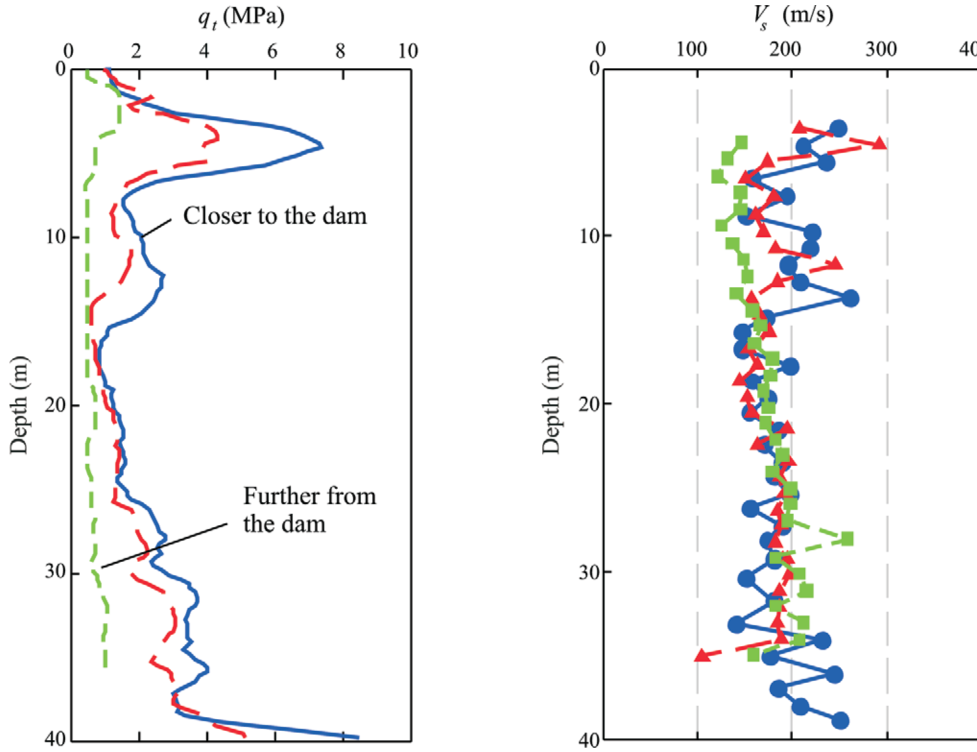

Figure 11 - CPTUS seismic results as a function of the distance from the dam crest.

as done for these CPTU data. Zones A_1 and A_2 are the zones where cyclic and flow liquefaction are possible.

The next step is to plot the data in Fig. 13, which shows (a) the tip resistance, (b) K_c, a correction factor which depends on the grain characteristics, (c) and Q_{tncs}, the normalised tip resistance equivalent to a clean sand value (Robertson & Wride, 1998). Q_{tncs} parameter values above 70 indicates contractive soils and correlates well with state parameter $\Psi > 0$ (Jefferies & Been, 2006). Figure 13 shows $Q_{tncs} > 70$ in the tailings, thus contractive behaviour takes place. On the right of Fig. 13 there is: (d) a plot of the pre and post liquefaction undrained ratio. The latter shows values as low as 0.1 in the tailings from 13 to 19 m depth.

3.4. Comparison between undrained strength predictions

This section compares undrained strength predictions from different methods, plotted in Figure 14, discussed as follows.

3.4.1. Olson and Stark's method

Figure 14 plots undrained strength ratio and values for pre and post liquefaction from CPTU correlation proposed by Olson & Stark (2002, 2003). It yields the ratio corresponding to pre (or triggering) and post liquefaction conditions, yielding the following parameters:

c_{uLiq}/σ'_{v0} = pre and post liquefaction undrained strength ratio to the effective overburden stress;

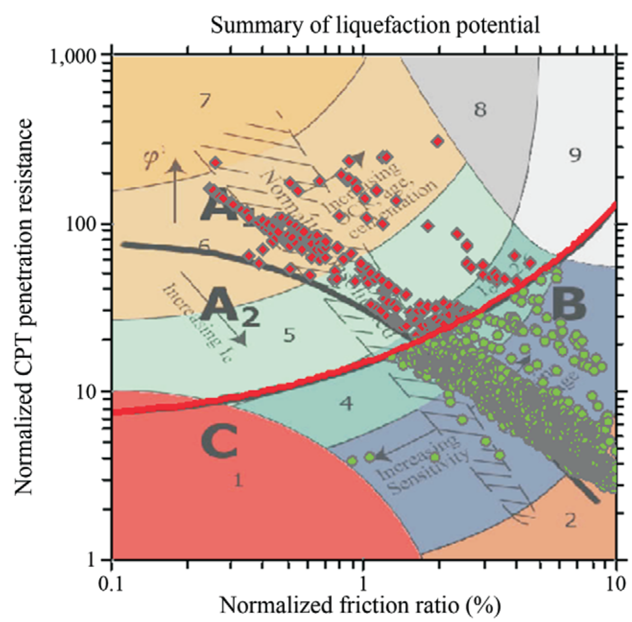

Zone A1: Cyclic liquefaction likely depending on size and duration of cyclic loading
Zone A2: Cyclic liquefaction and strength loss likely depending on loading and ground geometry
Zone B: Liquefaction and post-earthquake strength loss unlikely, check cyclic softening
Zone C: Cyclic liquefation and strength loss possible depending on soil plasticity, brittleness/sensitivity, strain to peak undrained strength and ground geometry

Figure 12 - CPT x SBT - Soil Behaviour Type chart for liquefaction.

c_{uLiq} = pre and post liquefaction undrained strength at the tailings (kPa).

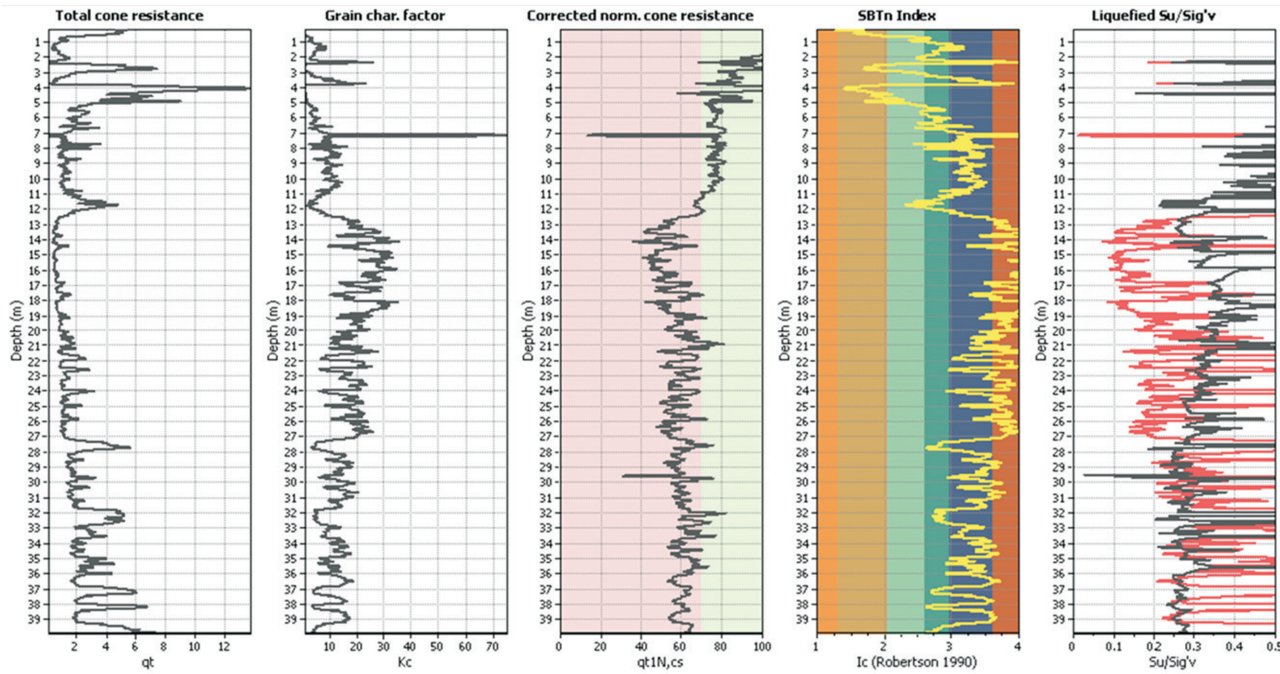

Figure 13 - Flow liquefaction assessment, according to Robertson (2008, 2010).

3.4.2. Jefferies and Been's CSSM

Jefferies & Been (2006) book summarises their work on the application of CSSM (critical state soil mechanics) to understanding the behaviour of tailings and loose sands. They provide a useful spreadsheet to analyse CPTU data and this yielded post liquefaction or residual undrained values (c_{ur}) also plotted in Fig. 14, which yields very low values.

3.4.3. N_{kt} approach

Figure 14 presents empirical values for the undrained strength based on N_{kt} and compares with strength obtained by means of the equation:

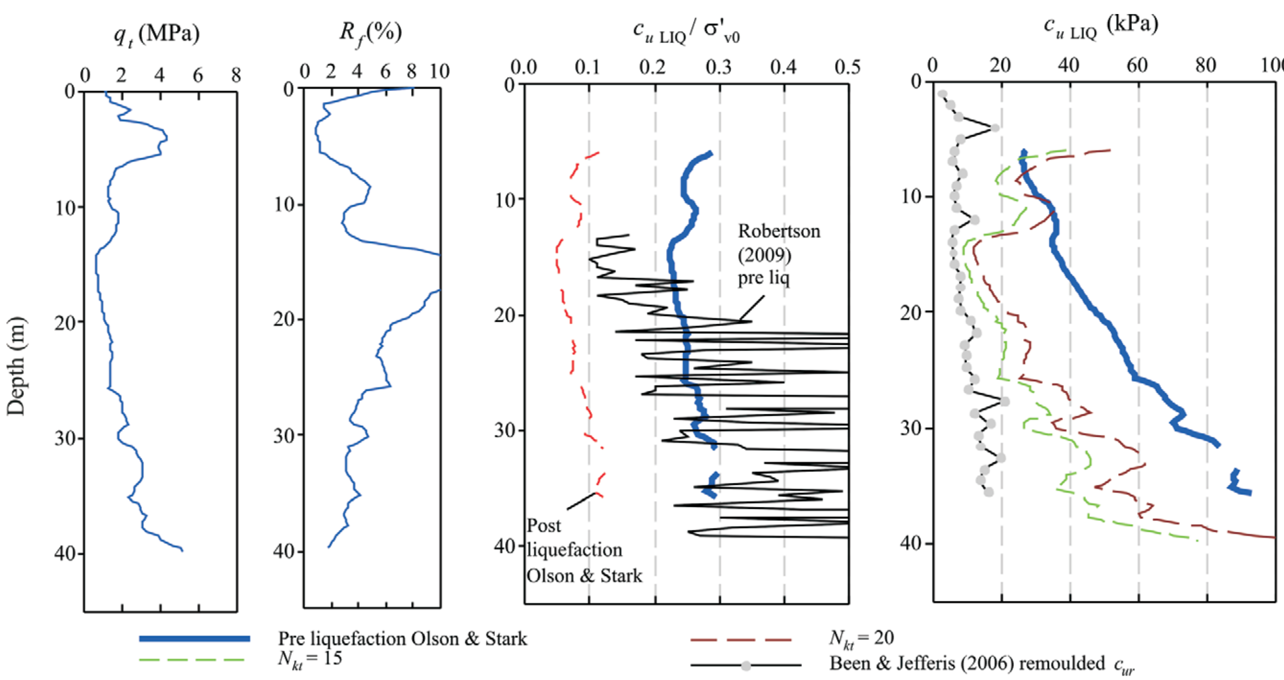

Figure 14 - Comparison between undrained strength predictions: Olson & Stark (2003), Jefferies & Been (2006), N_{kt} and Robertson (2010) methods.

$$c_u = \frac{q_t}{N_{kt}} \qquad (1)$$

where N_{kt} is an empirical coefficient. This work assumes N_{kt} equals to 15 and 20, which is the range for most clays.

As discussed previously in this paper the instability or collapse line yields the undrained strength (c_u/σ'_{vc}) ratio of 0.2, which is just in between Olson and Stark's results (Fig. 14).

4. Embankment Construction

The borrow material was a residual silt from a nearby area, ripped by dozers from the top soil to a depth of about 1.5 m. The embankment was about 100 m from the beach on the top of a minimum of 20 m thick tailings. An access road was built from the borrow pit to the embankment location.

A 400 g/m^2 non-woven geosynthetic was placed over the entire area (Fig. 15), followed by a 80-90 cm thick embankment layer. The geosynthetic aimed at improving and reducing thickness of the first layer, which was the minimum necessary to allow dozers and lorries to operate. However, this first layer led to high initial settlements on the soft tailings. Boreholes carried out through this first layer indicated that the total fill thickness was about 2 m, therefore, the initial settlement was about 1.1 to 1.2 m.

Light dozers, D4 type, spread the fill material. After this work platform was in place, construction stopped to allow instrumentation installation and initial or baseline readings. This phase took about one month.

4.1. Loading rate

Figure 16 presents the time-history of embankment loading. It was the fastest possible rate under given conditions of the embankment dimensions, distance to the borrow pit and earthwork equipment.

Earthworks took place around the clock, 24 h a day, with one hour breaks for changing shifts at 6:00 and 18:00 h. Other breaks occurred at 12:00 and 24:00 h for meals.

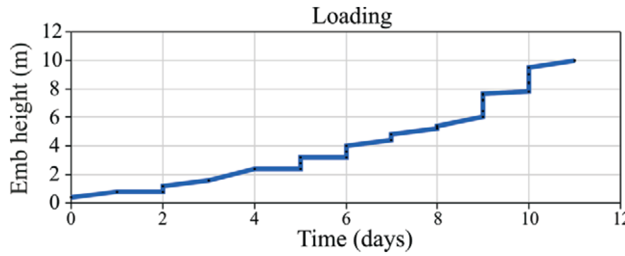

Figure 16 - Embankment loading rate.

The initial rising rate was slow, as the spreading area was too large, and it took two days to reach 2 m in height, and another two days to reach the level of the berm. From this point, the rise was fast, and the embankment reached 10 m height in only six days.

4.2. Liquefaction

Just after placing the first embankment layer, evidence of liquefaction took place. Figures 17 to 20 present photographic records of the events. Firstly, a small water spring or *sand boil* surged on the top of the embankment and continued until forming a "volcano" of tailings, about one metre in diameter. This phenomenon took place only under the first embankment layer.

Indeed, static liquefaction seems to have occurred under very low confining stress only. Laboratory evidence supports this conclusion, as loose specimens at low confining stress showed very large deformation after instability or collapse, with a considerable rise in porepressures.

4.3. Instrumentation

The instrumentation consisted of ten vibrating wire (VW) piezometers in the foundation, two inclinometer access tubes at the embankment toe, a hydraulic settlement profiler along the base of the main cross-section and four

Figure 15 - Placing the geosynthetic on the tailings.

Figure 17 - Sand boils on the top of the first layer.

Figure 18 - Sand boils on the top of the first embankment layer.

Figure 19 - Sand boils.

Figure 20 - Sand boils, zoomed view.

settlement plates. A benchmark was installed on firm ground close to the borrow pit area and an observation well close to the embankment.

The VW piezometers were installed in *H* size (100 mm diameter) boreholes into a one-metre high sand bulb and sealed with 0.5 m thick seal of bentonite balls followed by filling with bentonite mud to the top of the borehole.

Electrical cables were extended in shallow trenches to the instrument hut located in front of the embankment. A portable read-out unit read the piezometers both during installation and after construction. A data acquisition system installed in the instrument hut read piezometer data during construction at regular intervals of about half an hour.

Inclinometer access tubes 80 mm in diameter were installed in *P* size (150 mm) holes drilled a few metres into firm ground, beyond the tailings bottom-line. A bentonite-cement grout filled the annular space between tubes and borehole wall. They were surveyed with a digital inclinometer probe.

A 50 mm diameter access steel tube was placed in a shallow trench along the embankment cross section, and backfilled. This tube was surveyed regularly with a hydraulic settlement profiler which slides in the access tube, providing settlement readings at 5 m intervals. This unit consisted of an electrical VW low pressure transducer connected to a constant level water reservoir outside the embankment. The system enables atmospheric pressure and temperature corrections. The overall accuracy is about $\pm$ 5 mm.

Four settlement plates were installed. Their protruding rods spoil earthworks, however, they are very important for post-construction monitoring. They were surveyed with an engineer's level relatively to the benchmark.

The field crew took inclinometer and settlement profiler readings twice a day during changing shifts at 6:00 h and 18:00 h. Settlement plates were read once a day at noon. Piezometers were read nearly continuously.

The field crew carried out baseline readings, field calibration and redundant checking of all instruments before and after installation for over a fortnight before embankment construction started. Readings were also obtained by RPM crew with a second VW readout box and inclinometer probe. This ensured the high data quality needed for this experiment.

Settlement and porepressure readings continue for post-construction monitoring, although these data will be analysed in another paper.

4.4. Observations during construction

The first fill layer led to a settlement of about 1.1 to 1.2 m, which was not taken into account in the calculations.

The observation well indicated that the water table coincided with tailings surface. This instrument was located too close to the embankment toe, and showed porepressure rise during loading. This report assumed that the ground water remained unchanged through the experiment.

When the embankment reached 5 m in height, the tailings surface on the lakeside of the embankment showed signs of bulging. Inclinometers and piezometers also recorded jumps at the same time, and will be discussed later. This was, then, interpreted as a local failure at that stage.

At the end of loading, the embankment was thoroughly inspected and presented no visible signs of failure or cracking.

5. Instrumentation Results

5.1. Porepressures

Figures 21 to 28 summarise porepressure measurements in separate plots for vertical A and B, showing that porepressures built up considerably during loading.

Figures 21 and 22 present excess porepressures Δu *vs.* time and embankment height.

Figures 23 and 24 plot excess porepressures Δu during loading as a function of total vertical stress increment $\Delta\sigma_v$, which is the increase in overburden stress $\Delta\sigma_v = \gamma H$ due to the embankment loading. The rate of porepressure build-up is higher in the initial phase until the embankment reached 6 m in height, and then decreases slightly. This could be the influence of dissipation rate.

One can observe a sharp drop in porepressures when the embankment reached about 5 m in height, followed by a recovery with loading. This was accompanied by a jump in horizontal displacements measured by the inclinometers, which will be discussed later. Ortigao *et al.* (1983) observed a similar porepressure decrease during failure of a test embankment on soft clay. This can be explained by local yielding due to dilation taking place close to piezometer sensors.

The plots of Δu *vs.* $\Delta\sigma_v$ include a $\Delta u = \Delta\sigma_v$ line, which corresponds to fully undrained case of porepressure increase. Piezometers located close to the centre of the tailings layer show higher porepressures and they plot closer to this line, whereas those close to the top plot well below this line, due to porepressure dissipation.

Figures 25 and 26 present porepressure isochrones. Instruments in the centre of the tailings layer show larger porepressures than those close to the top. This is a typical phenomenon caused by faster dissipation closer to drainage boundaries.

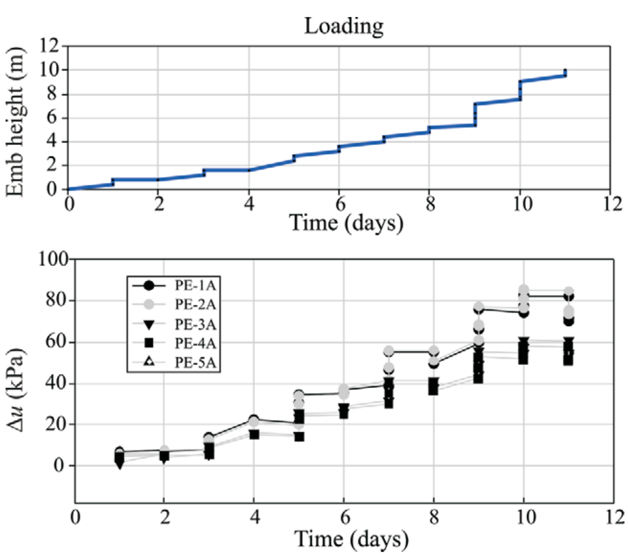

Figure 21 - Porepressures during loading, vertical A.

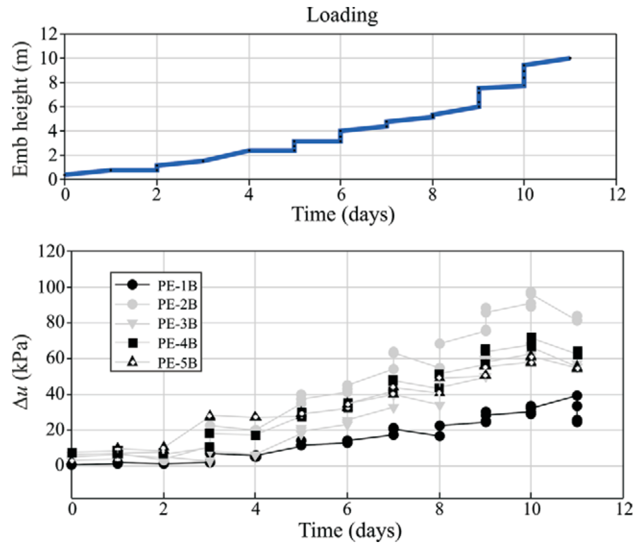

Figure 22 - Porepressures during loading, vertical B.

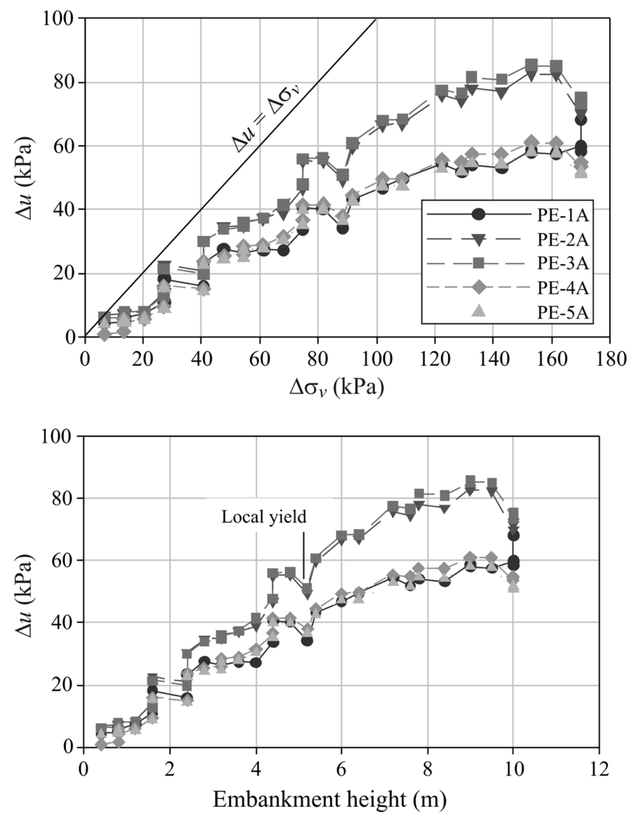

Figure 23 - Excess porepressures during loading, vertical A.

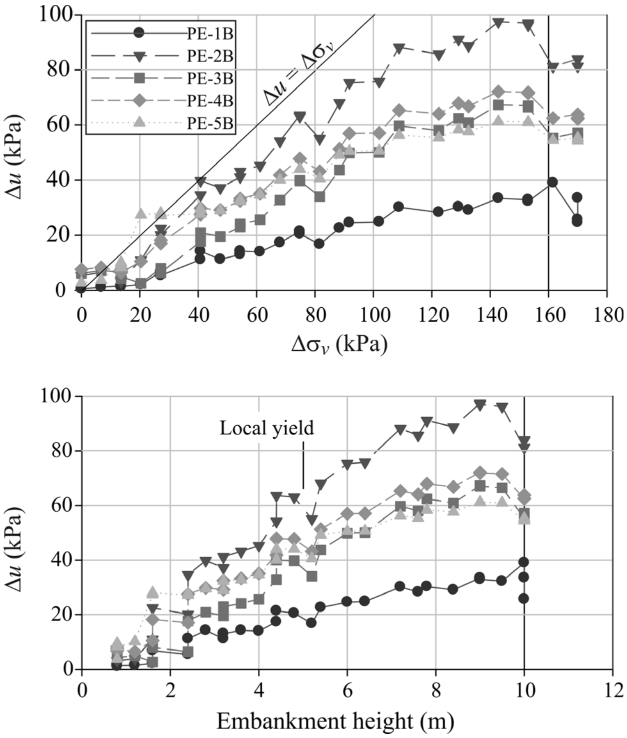

Figure 24 - Excess porepressures during loading, vertical B.

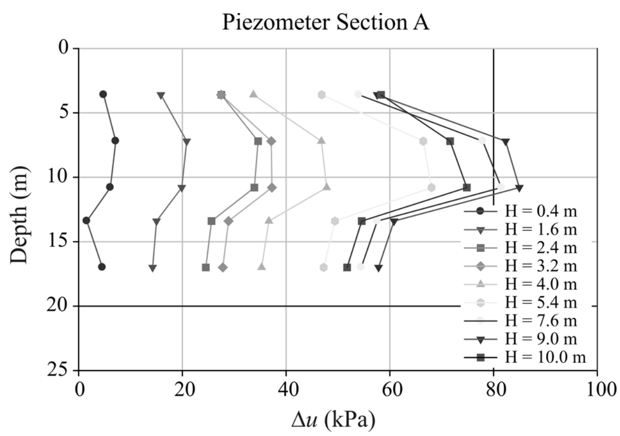

Figure 25 - Porepressure isochrones, vertical A.

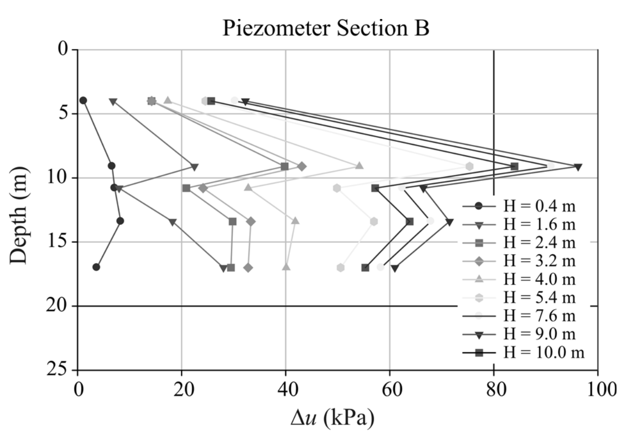

Figure 26 - Porepressure isochrones, vertical B.

Porepressure isochrones are re-plotted in Figs. 27 and 28, presenting normalised porepressure parameter $B = \Delta u/\Delta\sigma_v$ *vs.* normalised depth z/D, where D is the depth of the tailings. These plots demonstrate that the measured porepressures follow the typical behaviour observed in a number of cases of loading on soft clay, where partial dissi-

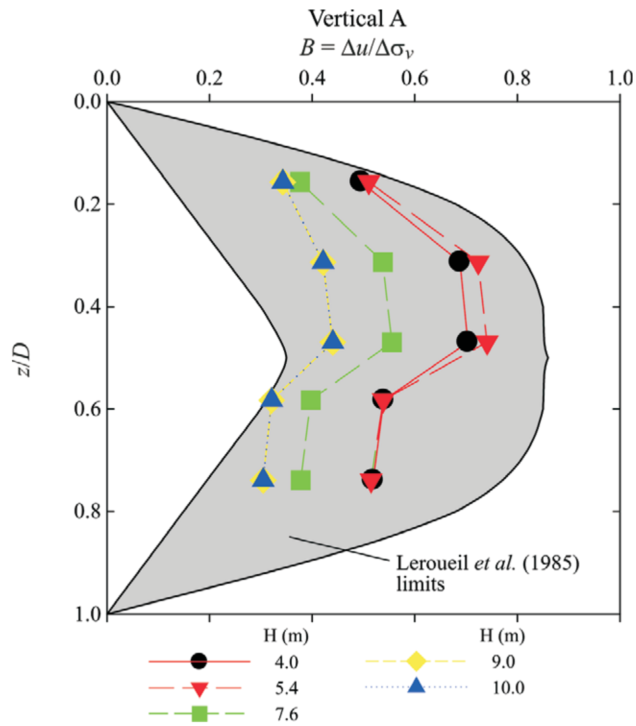

Figure 27 - Porepressure parameter B, vertical A.

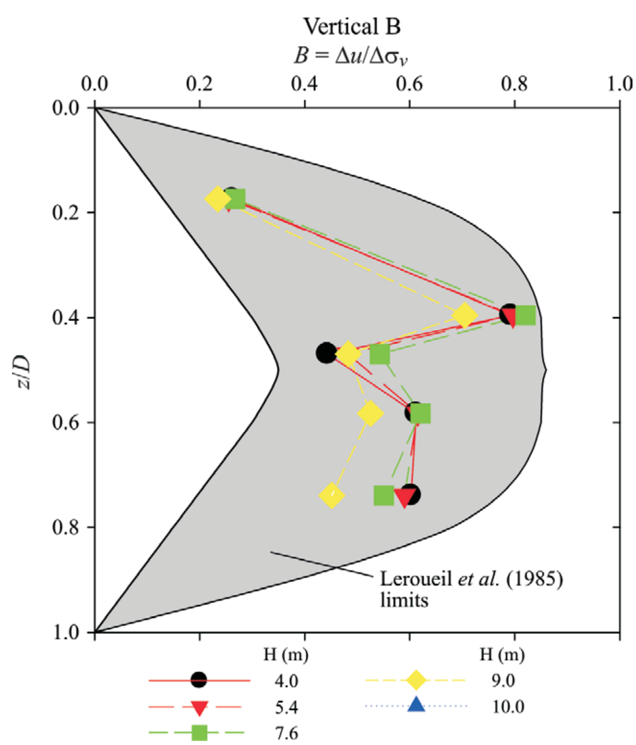

Figure 28 - Porepressure parameter B, vertical B.

pation takes place. Leroueil *et al.* (1985) observed this phenomenon in a number of cases in soft clays, when the clay is still at the overconsolidation stress range. Indeed, measurements at this test embankment fall within the limits proposed by these authors, also observed for other Brazilian soft clays (Ortigao *et al.*, 1983).

5.2. Porepressure dissipation after construction

Figure 29 presents porepressures *vs.* time for piezometers under vertical A, showing fast dissipation rates after construction, which took 10 days to achieve complete dissipation. This figure also plots results from a very simple one-dimensional Terzaghi dissipation model. The coefficient of consolidation was varied until an agreement was obtained, leading to the value of this coefficient in the vertical direction of $c_v = 4000 m^2/year$.

It is interesting to compare this value with the coefficient of consolidation in the horizontal direction (c_h) from many piezocone dissipation tests in the tailings. Figure 30 is a histogram of CPTU data and includes the back-figured value from the trial embankment dissipation. The results are in good agreement, showing that c_v and c_h values are very close for the tailings. This also shows that the piezocone dissipation radial model is a good approximation to the test, as well as, the simple vertical 1D consolidation model. Additionally, the tailings show homogeneous permeability behaviour.

5.3. Inclinometer measurements

Figures 31 to 35 present horizontal displacements measure with inclinometers at the toe. The plots in Figs. 31, 32 and 33 present calculated displacements and change of

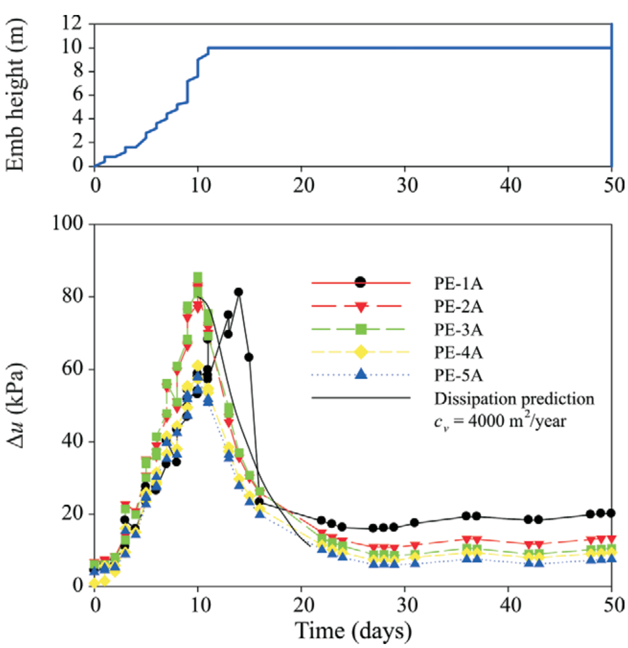

Figure 29 - Porepressure dissipation after construction, vertical A.

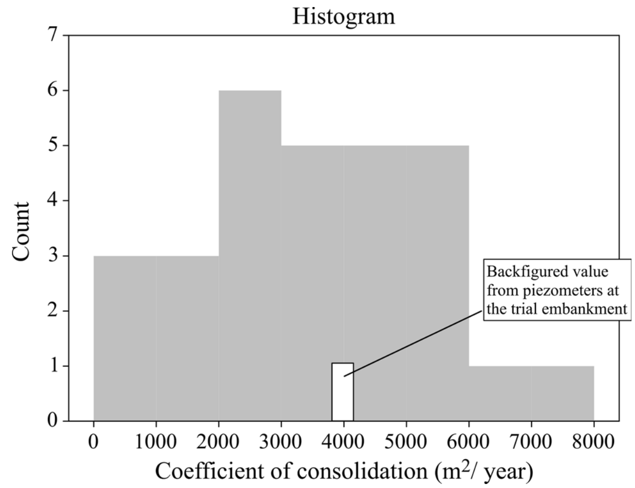

Figure 30 - Coefficient of consolidation from piezocone and piezometer dissipation.

readings with depth for various heights. Maximum horizontal displacements are about 150 mm and 110 mm at 7 m depth in inclinometer IA and IB, respectively.

When the embankment reached 5 m in height these plots show a sharp jump in the deformation, consistent with local yielding also detected at the piezometers.

The change of readings is proportional to soil distortion. The largest value possibly indicates the location of a slip surface and is related to shear strain of soil, as discussed by Ortigao *et al.* (1983b). The measurements show large distortions at 15 m depth, with consistent results in both tubes.

Measurements at the two access tubes show similar results on axis *A* (main axis, across the embankment), but quite different behaviour along the secondary axis *B*. Inclinometer IA presented negligible lateral displacements and the results are not included. On the other hand, considerable lateral spreading took place at inclinometer IB (Fig. 33). Maximum displacements were about 60 mm.

Figures 34 and 35 present horizontal displacements measured by the inclinometers and corresponding change of readings as a function of the embankment height.

The amount of angular deflection θ is obtained from the change in inclinometer readings (change), according to the following equation:

5.4. Settlements

Figure 36 presents recorded settlements *vs.* time and *vs.* embankment height. Figure 37 gives settlement results obtained by the settlement profiler. In both cases, the initial settlement caused by the working mat has not been included.

The maximum settlement at the end of construction was 800 mm in the settlement plates and about 700 mm in the settlement profiler. Certainly, the settlement plates give the correct result, while the profiler gives the shape. The reason is that, for very large settlements, corrections should

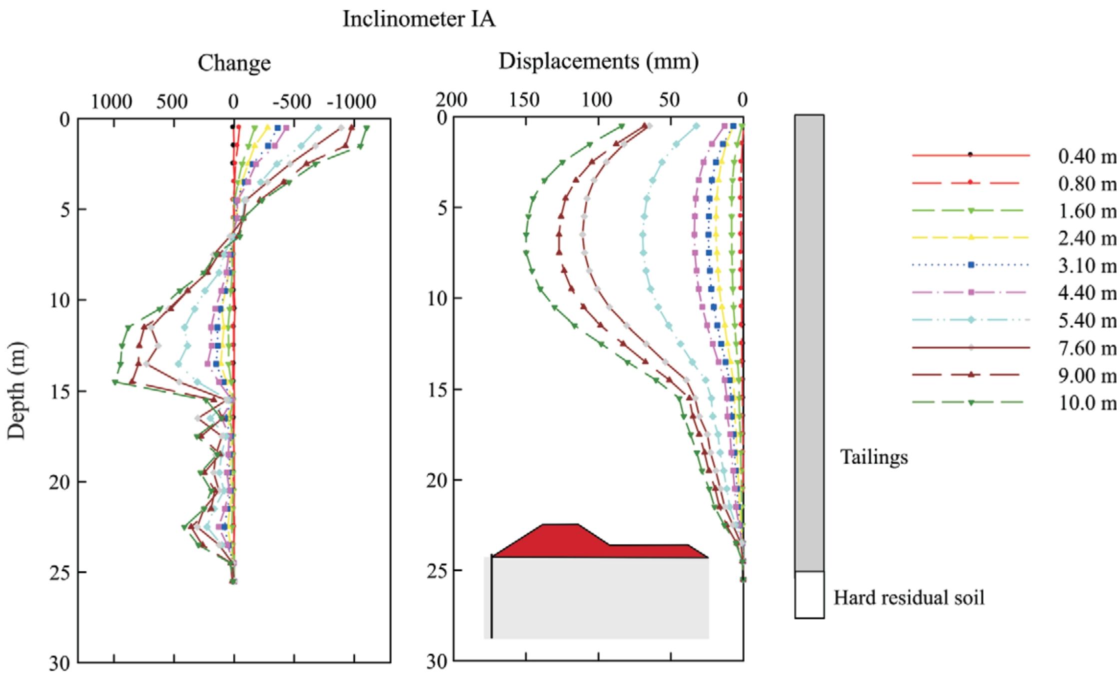

Figure 31 - Inclinometer IA results.

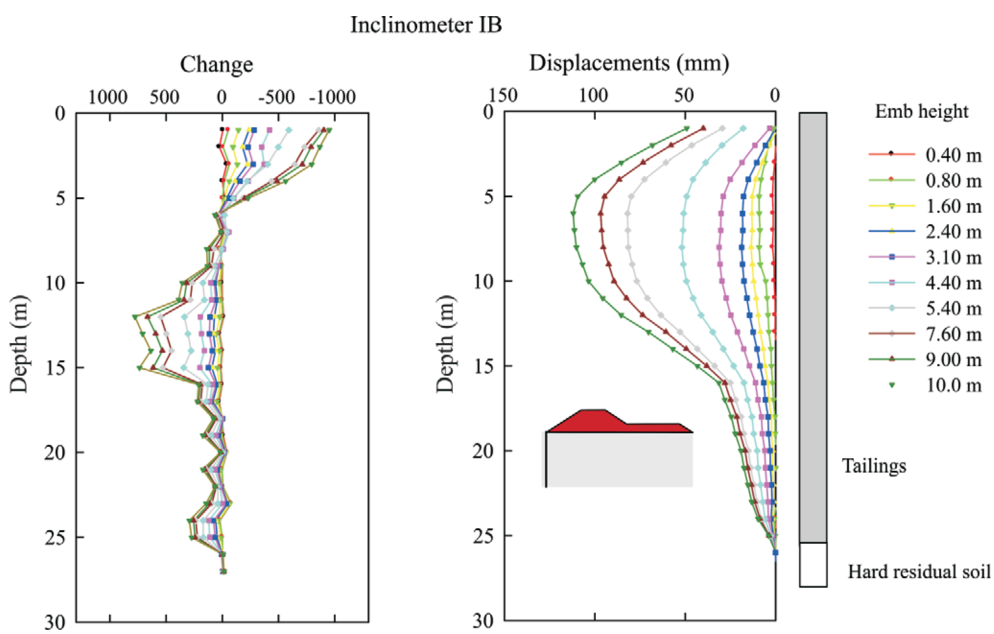

Figure 32 - Inclinometer IB results, main axis.

be made for the curvature of the profiler, as the access tube deforms.

5.5. Horizontal displacements *vs.* settlements

Figure 38 presents a plot of maximum settlements *vs.* maximum horizontal displacements measured at the same embankment height. On the same figure there are dashed lines proposed by Leroueil *et al.* (1985) for drained and undrained behaviour, based on similar measurements at several embankments on soft clay. The trial embankment data in Figure 38 plot close to the drained behaviour line.

5.6. Prediction of impending failure from instrumentation results

This embankment shows very clearly that inclinometer results are very sensitive to impending failure. Plots of incli-

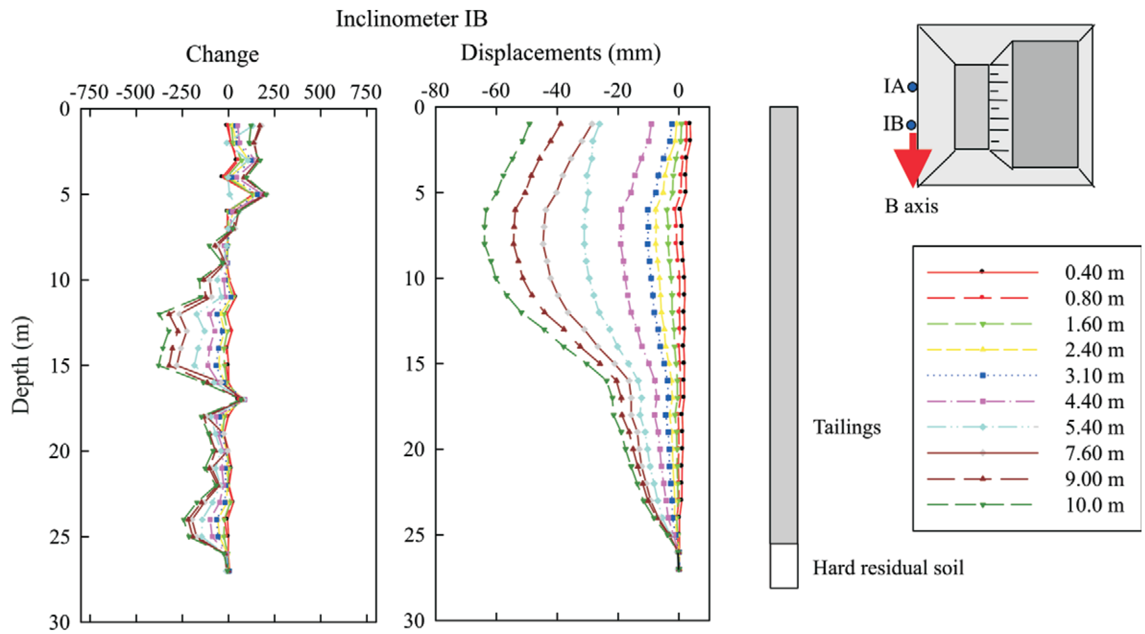

Figure 33 - Inclinometer IB results, lateral axis.

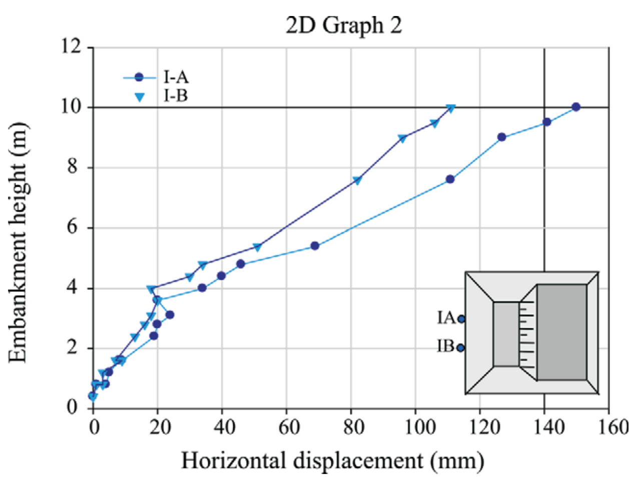

Figure 34 - Horizontal displacements *vs.* embankment height.

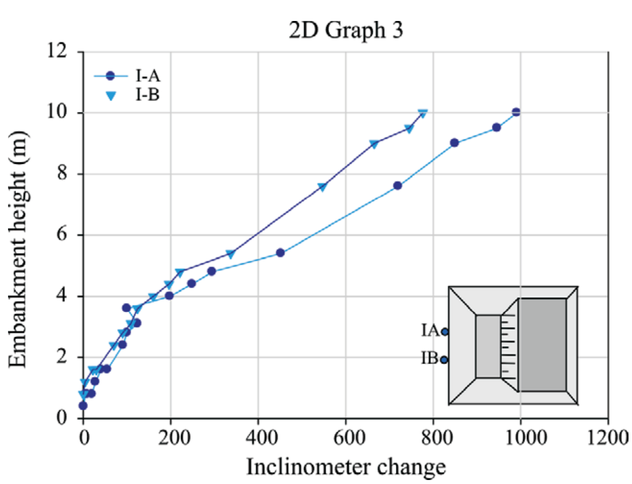

Figure 35 - Inclinometer change of readings *vs.* embankment height.

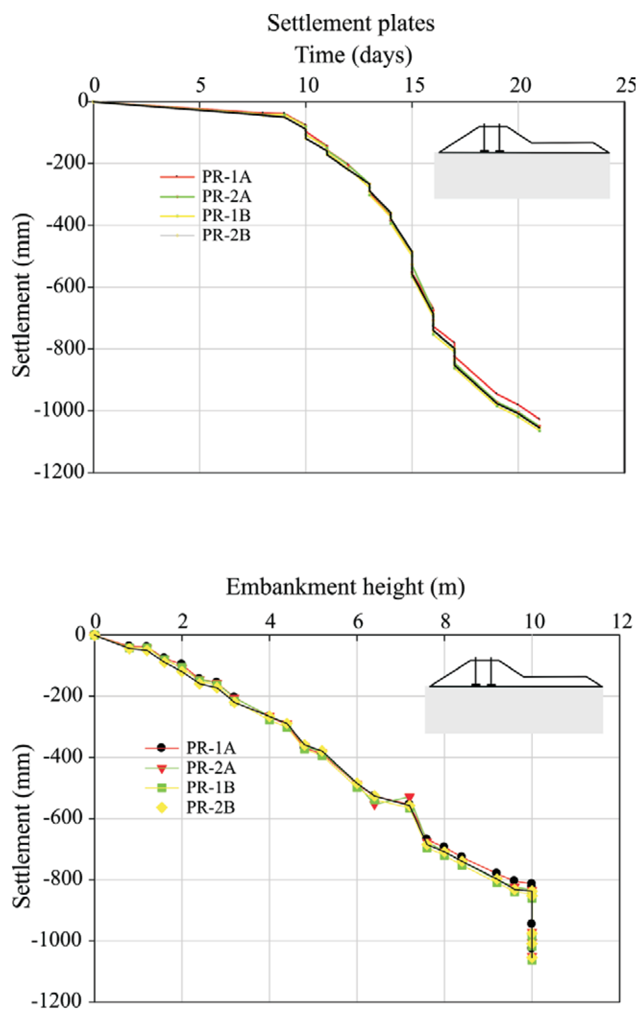

Figure 36 - Settlement plates results.

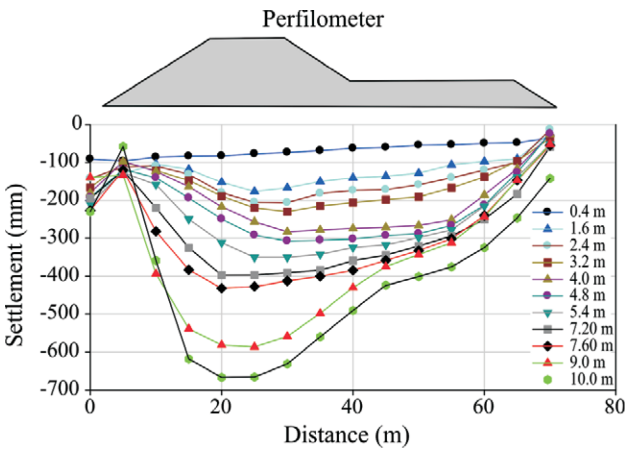

Figure 37 - Results from the settlement profiler.

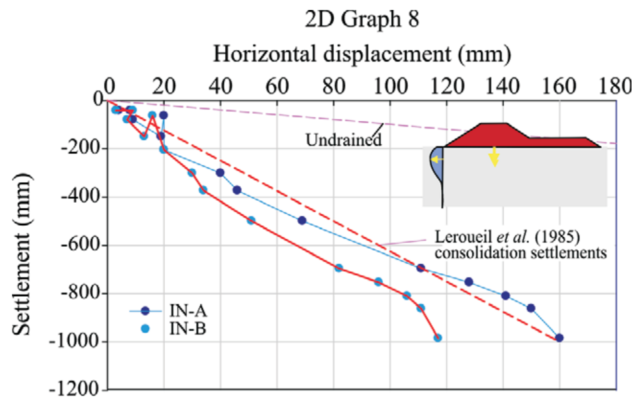

Figure 38 - Relationship of settlements and horizontal displacements.

nometer distortions are especially useful for this purpose, as discussed long ago by Ortigao *et al.* (1983a, 1983b). Jumps in readings indicate that failure is approaching.

In addition to inclinometers, the only useful instrument to indicate impending failure, is a piezometer, but never as clear as inclinometer data.

Hunter & Fell (2003) analysed 13 case histories of embankment of soft soils and suggested that the following observations can be a good indication of imminent failure of embankment foundations: (a) lateral displacement at the embankment toe; vertical deformation at or just beyond the toe; (c) inclinometer observations at the toe; (d) embankment cracking and (e) porepressure behaviour.

Past experience with a few embankments on soft clay in Brazil (Ortigao *et al.*, 1983a,1983b, Ortigao, 1991) has led the authors to rely mainly on inclinometer data followed by piezometers. Surface marks yield useless data for failure prediction in most cases.

6. Stability Analyses

Limit equilibrium stability analyses were carried out to evaluate the strength of the tailings at the end of construction with Bishop's simplified method and circular slip surfaces. The Slide 5 computer program was used. The embankment fill parameters were set as $\gamma = 17$ kN/m^3, $c = 0$ and $\phi = 30^o$.

6.1. TSA total stress analyses

The tailings parameters varied according to the analysis case. Firstly, total stress analyses (TSA) were carried out with undrained strength assumptions for the tailings. The tailings parameters were $\gamma = 17$ kN/m^3 and the undrained cohesion and friction were taken as $c_u = 0.1\ \sigma'_v$, $\phi_u = 0$, as suggested in Morgenstern (2002) report and used in stability analyses of the dam. This resulted in FS = 0.171 (Fig. 39), which is too low.

A search was then conducted to check which undrained strength value would yield a FS just above 1, for end of construction conditions. The ratio c_u/σ_v was increased until FS was just above one. Figure 40 presents the results which yielded $c_u/\sigma_v = 1.4$.

6.2. ESA effective stress analyses

The ESA consisted of a sensitivity analysis of FS as a function of the porepressure parameter *B*. The effective friction angle for the tailings was taken as $\phi' = 32°$. The ESA analyses were run varying *B*. Figure 41 presents the results which shows that FS = 1 for *B* in the order of 0.9. This value is higher than observed at the end of construction, which was in the order of 0.5 to 0.7, which, in turn, would yield a FS value of about 1.2 to 1.3.

7. Discussion

The outcome of stability analyses is that TSA was unable to predict the embankment behaviour. The reason is clear: drainage. Indeed, Fig. 29 shows that all excess porepressures dissipated within 10 days after the end-of-construction. Therefore, a considerable amount of drainage took place during construction, despite a placement rate, which was as fast as possible, but still not sufficient to impede drainage.

ESA with porepressure parameter *B* = 0.9 yields FS close to one. Therefore, assuming that at the end-of-construction FS might have been close to 1.2-1.3, based on actual porepressure measurements, it is concluded that ESA is the only possible way to analyse stability.

Conclusions

This field experiment has led to the following conclusions:

- The gold mine tailings behave like a loose silt material. Undrained triaxial tests on loose specimens show static liquefaction taking place under low confining stresses.
- Just after placing the first embankment layer, water and tailings surged through the fill. This phenomenon can be interpreted as static liquefaction taking place at low confining stress, as also observed in the triaxial tests.

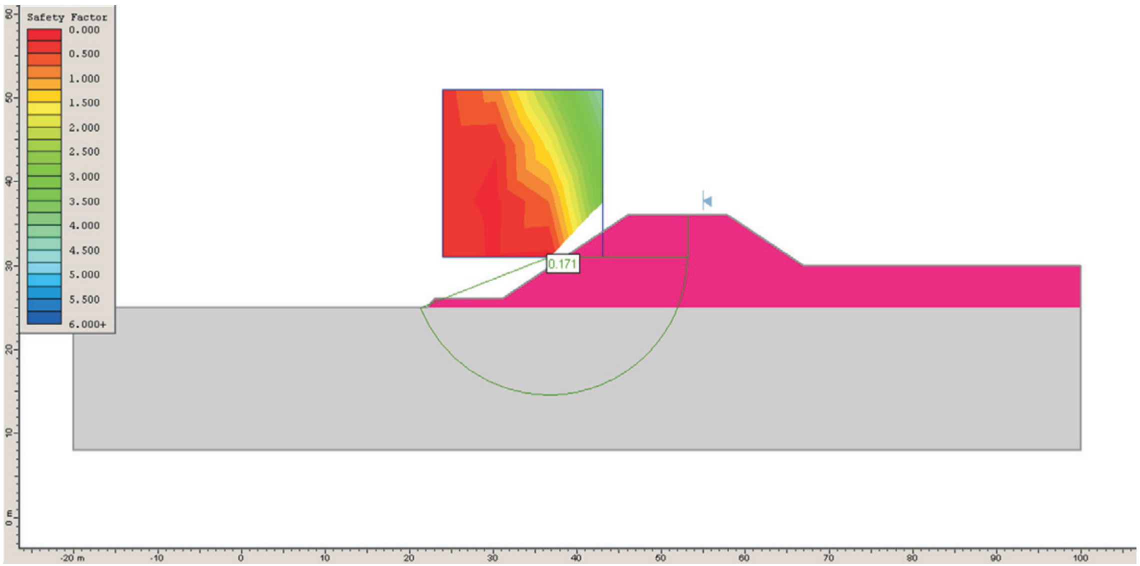

Figure 39 - TSA stability analyses with $c_u = 0.1\ \sigma'_v$ yielding FS = 0.171.

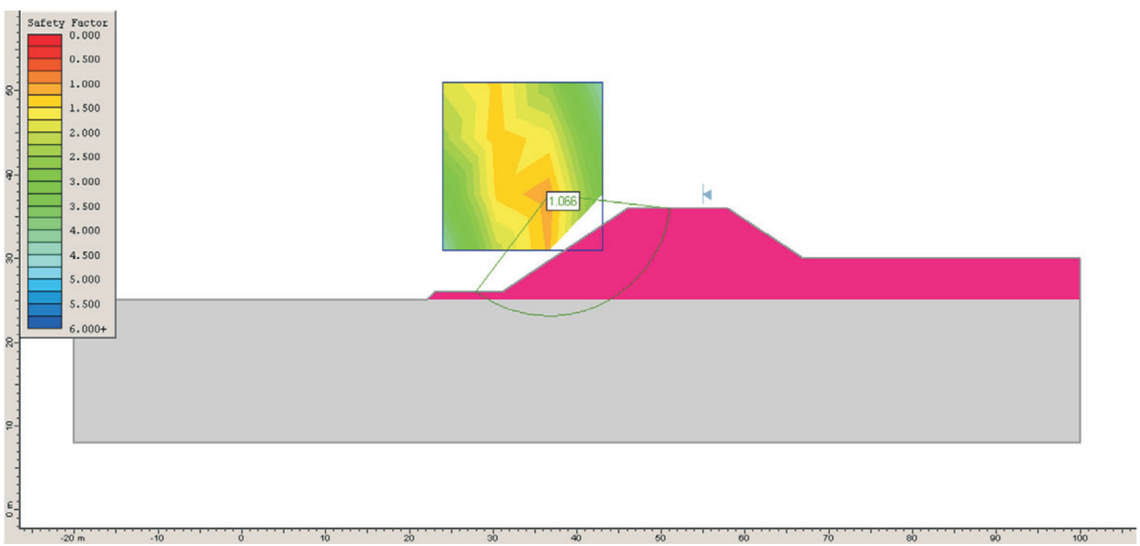

Figure 40 - TSA stability analyses with $c_u = \sigma'_v = 1.4$, yielding FS = 1.066.

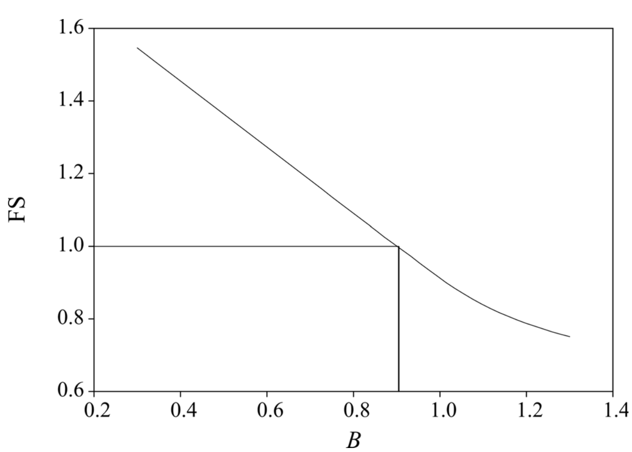

Figure 41 - ESA sensitivity analyses, FS *vs.* B.

- Local yielding and lateral bulging at the tailings took place when the embankment reached 5 m height. This was clearly observed at the inclinometer IB and affected measured porepressures in all piezometers, which showed a small, but sharp porepressure drop, followed by recovery.
- At the end of construction the embankment was stable without any visible cracks or large visible deformation;
- The performance of the instrumentation was very good, yielding a large amount of accurate and reliable data;
- The construction rate was fast enough to yield high porepressure built-up in the tailings, followed by fast dissipation rates after the end of construction;

- Porepressure dissipation analyses showed that the coefficient of consolidation agrees well with piezocone dissipation test results;
- Back-figured TSA analyses at the end of construction yielded a very high undrained strength ratio of about 1.4, much higher than any other method based on CPTU and laboratory values. None of the undrained strength methods were able to predict the embankment behaviour.
- Effective stability analyses with estimated porepressure parameter B values indicated that failure would take place with B close to 0.9. This is by far larger than measured values at the end of the construction, which, in turn, shows a FS value in the order of 1.2-1.3. Therefore, the authors conclude that effective stress analyses is the only way to analyse stability on these tailings.

Acknowledgments

The decision to carry out this experiment was supported by RPM mine geotechnical consultants: Mr S. Cale, Scott Wilson Mining Ltd, Mr D. Welch, Golder Associates and Mr B. Brown from Rio Tinto Mining. Dr S. Teixeira supervised the tests at the University of São Paulo, São Carlos Campus soils laboratory. Cimcop Contractors carried the earthworks. Mr John Ioannides from Geologismiki provided valuable software support. Dr M. Jefferies and Professor P.K. Robertson kindly reviewed the manuscript and gave many suggestions. To all the authors express our gratitude. RPM's permission to publish these results is kindly acknowledged.

References

Byrne P, Puebla H, Chan DH, Soroush A, Morgenstern NR, Cathro DC, Gu WG, Phillips R, Roberston PK, Homan BA, Wride C, Sego D, Plewes HD, List BR & Tan S (2000) CANLEX full-scale experiments and modelling. Canadian Geotechnical Journal, v. 37, p. 543-562.

Leroueil S, Magnan JP & Tavenas F (1985) Remblais sur argilles molles, LCPC Laboratoire Central des Ponts et Chaussées et Technique et Documentation Lavoisier, Paris, 342 pp.

Hunter G & Fell R (2003) Prediction of impending failure of embankments on soft ground. Canadian Geotechnical Journal, v. 40, p. 209-220.

Jefferies M & Been K (2006) Soil Liquefaction: A Critical State Approach. Taylor & Francis, 479 pp.

Morgenstern N (2002), Review and Sign-off Report, Mina do Ouro Dam. RPM Unpublished Report, 2002.

Olson, SM & Stark, TD (2002) Liquefied strength ratio from liquefaction flow failure case histories. Canadian Geotechnical Journal, v. 39, p. 629-647.

Olson SM & Stark TD (2003) Yield strength ratio and liquefaction analysis of slopes and embankments. ASCE Journal of Geotechnical and Geoenvironmental Engineering, ASCE, v. 129:8, p. 727-737.

Ortigao JAR (1995) Soil mechanics in the light of critical state theories. AA Balkema, Rotterdam, 299 pp.

Ortigao JAR, Werneck MLG & Lacerda WA (1983a) Embankment failure on Rio de Janeiro clay. ASCE Journal of Geotechnical Engineering, v. 109:11, p. 1460-1479.

Ortigao JAR, Lacerda WA & Werneck MLG (1983b) The behaviour of the instrumentation of an embankment on clay, Proc. Int. Symp. on Field Measurements in Geomechanics, Zürich, Balkema, v. 1, pp. 703-707.

Ortigao JAR (1991) Embankment failures on soft clay in Brazil. Geotechnical News, v. 9:4, p. 68-70.

Roberson PK & Wride CE (1998) Evaluating cyclic liquefaction potential using the cone penetration test. Canadian Geotechnical Journal, v. 35, p. 442-459.

Robertson PK (2008) Discussion on Shuttle and Cunning (2007) Liquefaction potential of silts from CPTU. Canadian Geotechnical Journal, v. 45, p. 140-141.

Robertson PK (2009) Discussion on Boulanger and Idriss "Evaluation of cyclic softening in silts and clays", ASCE Journal of Geotechnical Engineering and Geoenvironmental Engineering, v. 135:2, p. 306-307.

Robertson PK (2010) Evaluation of flow liquefaction and liquefied strength using the CPT, ASCE Journal of Geotechnical and Geoenvironmental Engineering, v. 136:6, p. 842-853.

Robertson PK (2012) Guide to cone penetration testing, Gregg Drilling, www.greggdrilling.com.

Shuttle DA & Cunning J (2007) Liquefaction potential of silts from CPTU. Canadian Geotechnical Journal, v. 44, p. 1-19.

Yamamuro JA & Covert KM (2001) Monotonic and cyclic liquefaction of very loose sands with high silt content. Journal of Geotechnical and Geoenvironmental Engineering, v. 127:4, p. 314-324.

Yamamuro JA & Lade PV (1997) Static liquefaction of very loose sands. Canadian Geotechnical Journal, v. 34, p. 905-917.

Wride (Fear) CE, Robertson PK, Biggar KW, Campanella RG, Hoffmann BA, Hugues JM O, Küpper A & Woeller DJ (2000) Interpretation of in situ test results from the CANLEX site. Canadian Geotechnical Journal, v. 37, p. 505-529.

Influence of Pile-Soil-Raft Parameters on the Behavior of Piled Raft and Conventional Piled Group Foundations

R.P. Cunha, M. Pando

Abstract. In the Central Area of Brazil, particularly in the city of Goiânia (and in limited cases of the Brazilian capital Brasília), it is becoming common to observe in few foundation projects the design of a single, thick and large raft, supported by several piles, particularly for the central highly loaded and slender part of very tall buildings. In fact, many of these piles are designed as "settlement reducer" ones, behaving as "floating piles" with distinct geometries or relative pile stiffness (pile-soil) ratios. They are defined with basis on some rationalized procedure adopted to minimize the differential and total settlements of the raft, also based on its relative raft stiffness (raft-soil) together with aforementioned aspects. In such conditions, the calculation is usually done using a capacity and settlement based design approach that is normal in the case of "piled raft" foundation systems. Therefore, this paper aims to investigate this particular topic, scrutinizing numerical results of piled raft cases (and its comparison with "conventional" pile groups) under both cases of horizontal and vertical load conditions. It focuses on the influence of some key parameters of piled raft systems (related to overall pile, soil and raft geometric & mechanical characteristics) on their hypothetical design behavior. It further explores the possible advantages of designing under the concept of piled rafts under few particular conditions, yielding generalized conclusions from a "practical" point of view for those interested in such design methodology.
Keywords: piled raft, deep foundation, numerical analysis, parametric assessment, relative stiffness, displacement.

1. Introduction

In the heavily centered loaded portion of tall buildings under construction in the Central Area of Brazil, it may be now common to find a foundation designed with basis on a single raft supported by piles. This foundation raft generally encompasses several columns of the central projection of the building, and is structurally calculated to withstand shear, moment and concentrated loads under a combined set of conditions ("dead", "live", wind and "occasional" loads at distinct directions) set by Brazilian specific norms.

It is calculated also in geotechnical terms to withstand the same combination of loads, under two basic general guidelines recently set out by the Brazilian ABNT (2010) foundation Standard. This same standard allows the foundation to be designed as a conventional or standard "group of piles", as commonly done (so far) in the majority of foundation projects where no superstructure load is supported by the soil underneath the raft, or by the raft itself. Nevertheless, this standard also recognizes and allows the foundation to be designed as "piled raft", in which the contact of the base of the raft with the superficial soil can be taken on consideration - as long as the *overall* safety factor does not drop below advocated values.

One should however realize that the term "piled raft", as originally presented by Ottaviani (1975), Hain & Lee (1978), Mandolini & Viggiani (1997) and Poulos (1998), to name few key publications, is expressed in the present paper with the same definition as previously put forward by Janda *et al.* (2009). That means, as a "foundation system in which both structural components (piles and top raft) interact with each other and with the surrounding soil to sustain vertical, horizontal or moment loads coming from supported superstructures".

It is emphasized that this is valid independently if the piles of such system are designed as "settlement reducers" (as initially advocated by some authors) or not. Actually, according to Mandolini (2003), "piled rafts" refer to foundations that can be designed in any manner (under "capacity and settlement based design", "capacity based design" or as "differential settlement based design") as long as there is load sharing between the elements. That means that the understanding of the entire foundation system requires knowledge not only about the single pile interaction with the soil environment, but also the mutual influence of individual piles within the group plus the raft and the soil (the "foundation-structure" general interaction allowed in current designs by the new ABNT (2010) standard).

The paper therefore explores a parametric analysis of a nine floating pile group under a combined (non simultaneous) set of vertical and horizontal distributed loading, in contact and without contact with an idealized superficial soil layer. The analyses are carried out under distinct overall conditions, to be described.

Renato P. Cunha, Ph.D., Associate Professor, Departamento de Engenharia Civil e Ambiental, Programa de Geotecnia, Universidade de Brasília, Brasília, DF, Brazil. e-mail: rpcunha@unb.br.
Miguel Pando, Ph.D., Associate Professor, Departamento de Engenharia Civil e Ambiental,Department of Civil and Environmental Engineering, University of North Carolina, Charlotte, USA. e-mail: mpando@uncc.edu.
Submitted on September 8, 2011; Final Acceptance on April 25, 2013; Discussion open until August 30, 2013.

That means, under particular conditions of vertical and horizontal loading, it seizes the influence of the Poisson's Coefficient, the slenderness ratio[1]1 of the piles, the relative pile-soil and raft-soil stifnesses, and the soil contact type, in relation to typical design variables as the normalized displacement, the load sharing between raft and piles, and the distribution among (and along) piles at different positions.

The paper re-evaluates and further extends the outcome from an already published data within a past M.Sc. Dissertation Thesis from the University of Brasília (Bezerra, 2003), taking on account (and summarizing) some of the recent developments put forward by other publications in this same line of knowledge, as those from Sales *et al.* (1999, 2005), Cunha & Sales (1998), Cunha *et al.* (2000a, b & c, 2001, 2002, 2004, 2006), Bezerra *et al.* (2005), Cunha & Zhang (2006), Janda *et al.* (2009) and Ayala (2013), among others.

For instance, Janda *et al.* (2009) demonstrated that it is possible, although not straight forward, to simulate and generalize some key aspects of the behavior of piled raft and conventional foundation systems founded in rather complex soils (in their case, the Brasília "porous" clay), solely on the basis of numerical analyses of "typical" systems. They proved that the feasibility of the analyses for a future "real" design could be reached by using readily available parameters from pile load tests or site and laboratory investigations, allied to a good dose of common sense.

Thus, the objectives of this paper are rather the same as those from aforementioned authors, *i.e.* guidelines for the geotechnical behavior and for the design approach of such systems will be cautiously envisaged with basis on generalizations of parametric studies that encompass analyses of typical foundation setups. The systems, relative to piled raft and conventional groups, will be simulated under distinct conditions of overall geometry and soil/structural pile-raft mechanical values.

2. Numerical Model and Software

This paper adopts a numerical program developed exclusively for groups of deep foundations and piled rafts under general loading, named APRAFR, which was developed in the doctoral thesis of Zhang (2000) at University of Sydney. This program extends the "finite layer" method to accommodate a simultaneous general loading on top of piled raft foundations, allowing the establishment of coupled relationships between displacements (in all three directions), rotations (in two directions), and external loads. The origin of this method, and the adopted software, are briefly explained next.

2.1. Historical developments

Hain & Lee (1978) developed a method which considered the interactions of the piles, raft and soil, but the rotations and horizontal movements of a pile head induced by a vertical load applied to an adjacent pile or the soil surface were ignored. Soon later, Small & Booker (1984, 1986) and Booker & Small (1988) developed the finite layer method to analyze the behavior of stratified media of horizontal layers of finite thickness, when submitted to vertical loading. Hence, Lee & Small (1991) applied this theoretical method to the simulation of axially loaded piles founded in isotropic or cross-anisotropic elastic medium, where the nodes of the piles (intersection between horizontal soil layers and pile vertical surfaces) were stressed by annular uniform loads.

Ta & Small (1996, 1997) extended aforementioned models to developed a new numerical tool for the analysis of piled rafts (with the raft on or off the ground) and, as for Hain and Lee's method, the solutions were only for vertical loads. This method used finite elements to model the raft and the finite layer to model the soil, taking on account heterogeneity problems and system interactions.

Zhang & Small (2000a), subsequently surpassed the limitations from previous methods and developed a new numerical approach for the analysis of piled raft foundations, now subjected to both vertical and horizontal loadings. In this method, the interactions between raft and piles, raft and soil, piles and piles, piles and soil, and soil and soil were fully considered. However, the method could only deal with piled foundations clear of the ground, *i.e.*, "conventional" pile groups.

2.2. Establishment of the software APRAF

Zhang (2000) in his doctoral Thesis, and Zhang & Small (2000b) have introduced an extension of the method presented by Zhang & Small (2000a), where the raft could be in contact with the ground surface. Similarly as before, this approach uses a combination of the finite layer method for modeling the soil and the finite element method for simulating the raft and piles. The piled raft foundation can be subjected to horizontal and vertical loads as well as moments, and the movements of the piled raft in three directions (x, y, z) and rotations in two directions (x, y) may be computed by a program named APRAFR (analysis of piled raft foundations). In this program the raft could have any structural flexibility, and the stratified soil could have variable modulus along depth. Nevertheless the analysis still continued to be a linear elastic one. However, these authors have successfully made comparisons of the new solutions with those of the finite element method, and the effects of

1 Although the Merriam Webster on line dictionary defines "slenderness ratio" as the ratio of the length of a structural member (as a column) to its least radius of gyration, this ratio was defined herein as the relation between pile's length to diameter (*L/D*). One shall also notice that according to the New Webster's Dictionary "slender" means a thin, narrow or "week" element – which do contrast with the definition of this paper. A higher slenderness ratio (increase in L for a constant adopted d) does not necessarily mean a weaker pile.

parameters (adopted for soil and raft) on the behavior of piled rafts have been examined.

As shown in Fig. 1, reproduced from Zhang & Small (2000b), the problem of the piled raft foundation can be solved by assuming that the forces between the piles and layered soil can be treated as a series of ring loads applied to `nodes' along the pile's shaft. These loads are both horizontal and vertical. The contact stresses that act between the raft and the soil can be considered to be made up of uniform rectangular blocks of pressure approximating to the actual stress distribution. These can be considered uniform vertical blocks of pressure or uniform horizontal shear stresses. The displacement of the layered soil can then be computed, as the solution for a layered soil subjected to ring loads at the layer interfaces is found from finite layer theory.

Firstly, the response of the piles and soil (with no raft) is computed by applying unit surface loads to the rectangular regions on the ground surface, or unit ring loads to the soil along the pile's shaft, or a unit uniform circular load at the base of the pile. The deflections so computed can be used to form the influence matrix for the soil. For the piles, a stiffness relationship may be written based on shaft loads and on applied load at the pile heads. Three noded linear bending elements are used to model the piles.

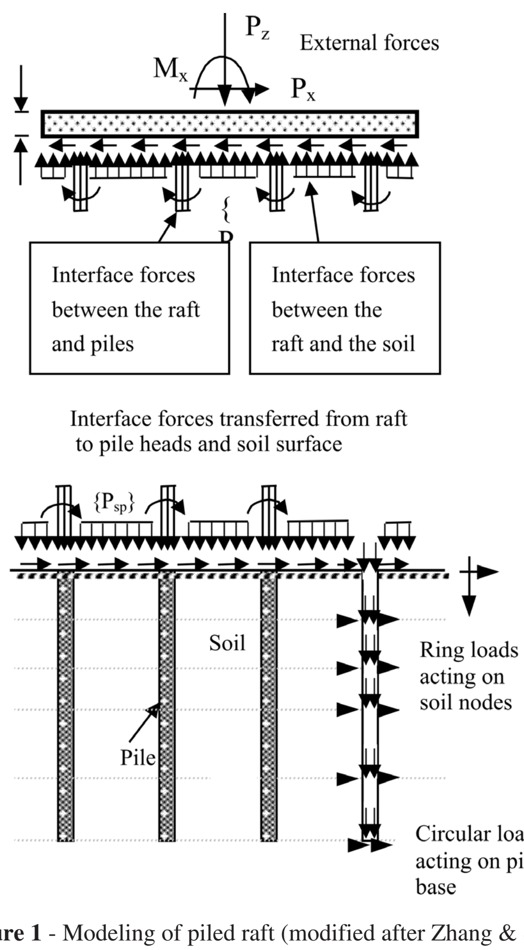

Figure 1 - Modeling of piled raft (modified after Zhang & Small (2000b).

Deflections of the soil or of the piles can be obtained for loads applied to the pile heads from the final stiffness relationship for the pile-soil continuum. This method is not as efficient computationally as computing the interaction between two piles only (*i.e.* by using the interaction factor method as advocated by Poulos, 1998 in his well known GARP software). However, it is much more accurate, especially for piles at close spacing because all the piles are considered at once.

Since the deflection of the piles can be computed when one is loaded at the head, or when the ground surface is loaded, this can be used to determine the behavior of the raft. Thus, by applying unit loads to the raft, its influence matrix may be obtained. By applying unit pressures to the ground, or unit pressures and moments to the pile heads, an influence matrix for the soil-piles may be obtained.

Finally, by considering equilibrium of applied forces and moments acting on the piles and raft, and compatibility of displacements of the soil and raft (and of displacement and rotation of the pile head and raft) enough equations may be assembled to obtain the solution under general loading. One should realize that there is full displacement compatibility between raft and soil, hence, no "soil-slip" at interface can be assumed.

3. Analyses and Results

The previously cited solutions were incorporated within the APRAFR software, used in this paper to perform a series of parametric analyses to be described and discussed now. Generalized conclusions, although limited somehow for the studied cases, are also provided.

3.1. Set up of the problem

The study of piled raft foundations involve a great range of interdependent variables that form a complex problem that, most of the time, is necessary to be solved with the adoption of some simplified hypotheses and/or configurations. A certain set of parameters is also needed to set up a model to study the system's behavior. So, using simple elements it is possible to depict in Fig. 2 the overall aspects of the systems which were simulated herein.

In this figure it is noticed the square layout of the raft and the position of the piles, in plan view, and a particular cross section in mid-position of the raft with the respective pile and soil profiles. A closer view of a small insert shows in detail the denomination used for distinct pile positions within the raft, from corner to center type locations.

The main difference in Fig. 2 from piled rafts and conventional group systems is the raft/soil contact, which is inexistent in the latter case and present (physically bonded via nodal points) in the former one.

Table 1 complements the information from aforementioned figure, stating the main physical parameters adopted in the analyses, and their ranges and magnitudes.

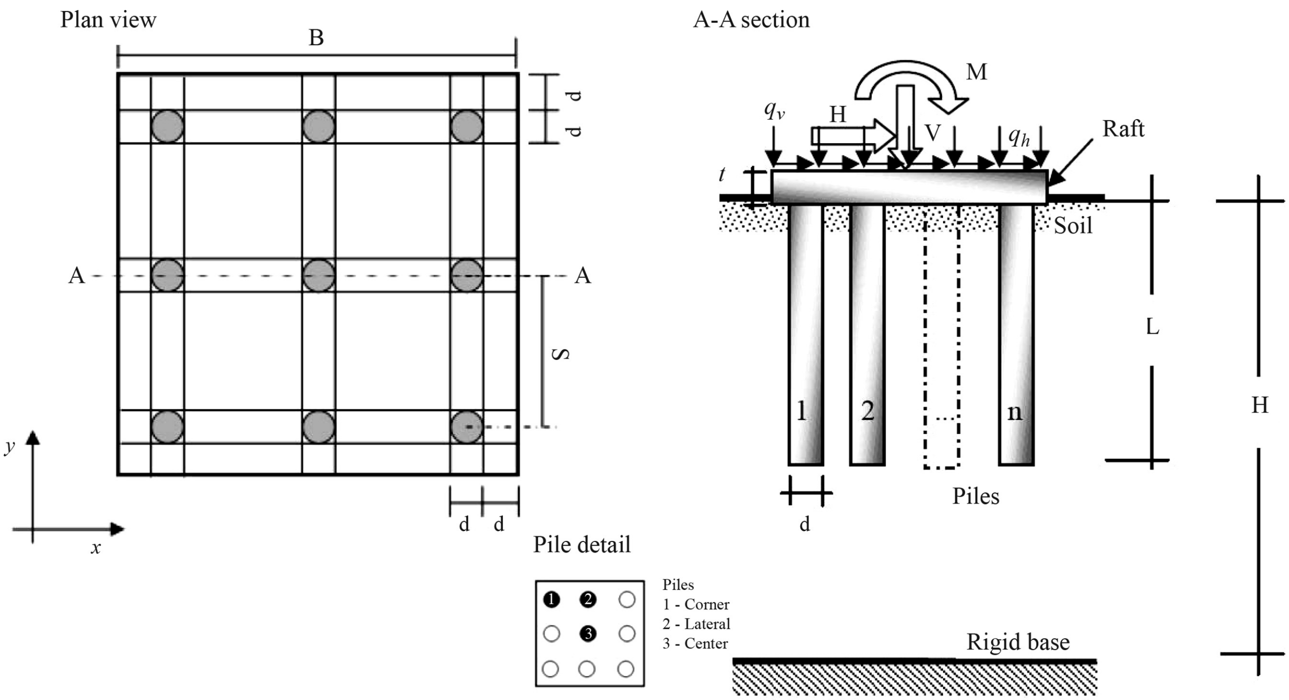

Figure 2 - Layout of the studied foundation system (modified from Bezerra, 2003).

They were originally established from standard geometric configurations and soil-raft values backanalyzed in Cunha & Sales (1998) field load tests at the Research Site from the University of Brasília, and later on from Sales (2000) and Cunha *et al.* (2004), as they may relate to standard values of interest to be regionally adopted for the design of such structures.

Besides, the range of variation for the parameters was selected to fit within magnitudes from a previous (and classical) similar exercise presented by Clancy & Randolph (1993), where squared piled rafts up to 36 piles were thoroughly simulated.

It shall be noted in Table 1 that the following equations do apply:

$$K_{RS} = \frac{4\, E_R\, t^3\, [1-\nu^2]}{3\pi\, E_S\, B^3\, [1-\nu_R^3]} \tag{1}$$

in accordance to Brown (1975) for square (B x B) rafts, where all the parameters are specified in this same table.

$$I_\alpha = \frac{E_S\, d u_\alpha}{q_\alpha\, B^2} \tag{2}$$

a non-dimensional variable, where α refers to vertical (v) or horizontal (h) directions. I_α is the normalized displacement, u_α is the displacement at the center of the raft, and q_α the distributed stress on the raft.

$$\Delta = \frac{u_{v-corner}}{u_{v-center}} \tag{3}$$

a non-dimensional differential settlement ratio based on vertical displacements in distinct pile positions, in accordance to the detail in Fig. 2. In other words, the higher is the value of Δ the more homogeneous or uniform are the settlements around the raft, and vice versa.

Therefore, for the appreciation of the key design aspects of the problem, as it was set up in this paper, the main (output) variables of interest, as settlement or shared load of the piles, were obtained and plotted. The results are presented and discussed along the next figures. Similarly as Fig. 2, all the subsequent ones have also been thoroughly modified after the original data published in Bezerra (2003).

3.2. Cases of load in the vertical direction

This item and respective sub items deal exclusively with comparisons between piled raft and standard group systems under vertical distributed load, for distinct values of the pile slenderness ratio (L/d). The influence of the key parameters L/d, ν, K_{RS}, K_{PS} and foundation system are evaluated and discussed.

3.2.1. Effect of L/D, ν and foundation type

The effect of some initial parameters of design respectively on the normalized central settlement and on the percentage of load absorbed by the pile group (the remainder goes to the raft alone), can be visualized through Figs. 3

Table 1 - Adopted parameters in analyses.

Parameter	Value
Soil Young Modulus E_S	6 MPa
Structural Young Modulus of Pile (E_P)	18000 Mpa and variable (600-6000000)*
Structural Young Modulus of Raft (E_R)	20000 MPa
Number of piles (n)	9
Soil Poisson's Coeff. (ν)	0.35 and variable (0.1-0.5)**
Structural Poisson's coeff. of Pile (ν_P) and Raft (ν_R)	0.2
Pile length (L)	Variable 12.5-50 m
Pile diameter (d)	0.5 m
Pile spacing (S)	2.5 m
Position of rigid base (H)	10 times L
Raft breadth or length (B)	6 m
Raft thickness (t)	0.5 m and variable (0.25-1.25)***
Pile spacing ratio (S/d)	5
Depth along pile's Shaft (z)	Variable 0 to L
Pile slenderness ratio (L/d)	Variable 25 to 100
Pile-soil stiffness ratio ($K_{PS} = E_P/E_S$)	Variable 100-1000000
Raft-soil stiffness ratio (K_{RS})	Variable 0.1-12
Distributed vertical stress on raft (q_v)	0.1 Mpa
Distributed horizontal stress on raft (q_h)	0.1 MPa
Normalized central settlement in vert. direction (I_v)	Result in accordance to Eq. 2
Normlzd. central displacement in horizontal direction (I_H)	Result in accordance to Eq. 2
Differential settlement ratio in vertical direction (Δ)	Result in accordance to Eq. 3

Observations:
(1) V Load = load in vertical direction;
(2) H Load = Load in horizontal direction;
*Variable in plots with the K_{PS} parameter;
**Variable in plots with the ν parameter;
***Variable in plots with the K_{RS} parameter and Eq. 1.

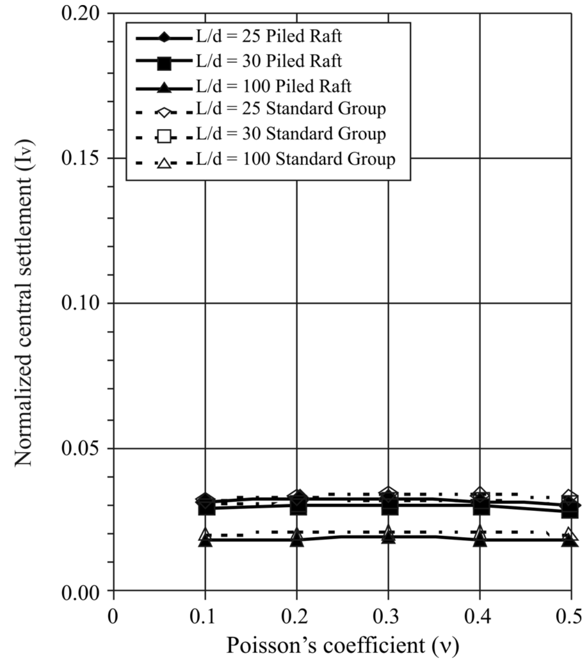

Figure 3 - Effect of the variation of some initial parameters on the settlement value.

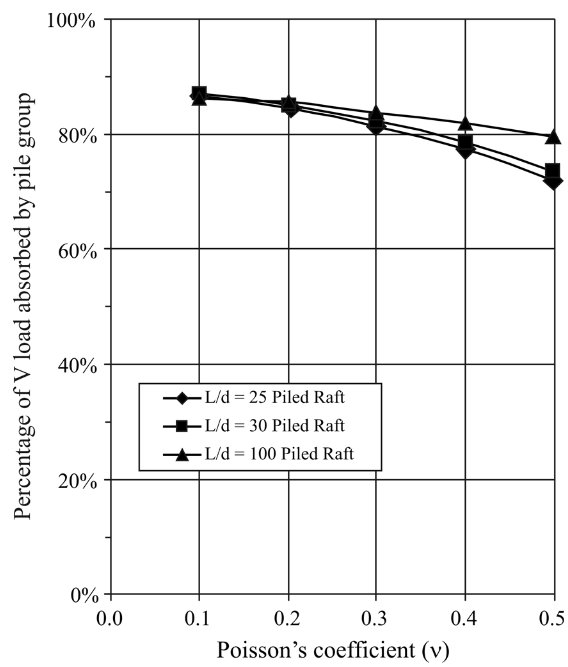

Figure 4 - Effect of the variation of some initial parameters on the load distribution.

and 4. It is noticed that such comparisons were carried out in terms of a constant E_P of 18000 MPa (K_{PS} = 3000) and raft thickness of 0.5 m, besides of distinct L/d, as previously mentioned, with a range from 25 to 100 that covers most practical cases. The Poisson's Coeff. varied from 0.1 to 0.5, and all other parameters are in accordance to Table 1.

From this set of figures, the following main observations can be drawn:

- The sensitivity of the vertical normalized central settlement to variations in ν is negligible for both cases of system;
- Piled raft systems do not appear to have a noticeable advantage in comparison to standard groups in terms of the reduction of the vertical total settlement of the raft;

- The pile slenderness ratio has more influence on the derived normalized settlement than the Poisson's Coeff., again for both cases. Also, the higher is *L/d* the lower will be the settlement;
- In the case of piled rafts only, the influence of the Poisson's Coeff. on the percentage of load absorbed by the piles is low. For practical (medium) values of ν, this influence tends to be rather small;
- However, differently as before, the higher is *L/d* the higher will be the load absorbed by the pile group within a piled raft system.

Given such observations, one can yield the following partial conclusions strictly valid to vertical loading:

- In design projects with either piled rafts or standard pile groups under vertical distributed load the estimation of the Poisson's Coefficient is not of concern, particularly when the interest is in the total central settlement of the system, or the load share within its elements;
- In order to decrease (to a low degree) the vertical settlement for both systems, the slenderness ratio of the pile shall be increased. This procedure will also lead, in piled raft systems, to a slight increase in the load absorbed by the piles, in detriment (*i.e.* with corresponding decrease) of the raft's load;
- If the major design interest is in the total vertical central settlement of the raft, there is no advantage in designing the foundation as a piled raft system.

3.2.2. Effect of the pile-soil stiffness ratio

The effect of the relative Pile-Soil stiffness ratio (K_{PS}), *i.e.* the relation between the Young modulus of the pile (E_P) and of the soil (E_S) was also evaluated in regard to the normalized central settlement and to the percentage of load absorbed by the pile group, among other variables. Similarly as before, this was carried out for both piled raft and standard group systems with. Such comparisons were carried out in terms of a constant ν of 0.35, raft thickness of 0.5 m, besides of distinct *L/d*, as previously commented. The E_P of the pile varied from 600 to 6000000 MPa in order to respectively yield K_{PS}'s from 100 to 1000000. All other parameters in accordance to Table 1.

Figures 5 and 6 show aforementioned results, again in terms of distinct slenderness ratios ranging from 25 to 100. From the analyses, it is possible to observe that:

- The sensitivity of the vertical normalized central settlement to variations in K_{PS} is more pronounced, in both systems, for relatively "deformable" or ordinary pile cases, *i.e.*, piles with relative stiffness ratios around and lower than 1000. In this regard, the higher is the compressibility of the pile (the lower is K_{PS}) the higher is the normalized vertical settlement. On the other hand, for less deformable or "incompressible" piles (very high K_{PS}), the influence of K_{PS} is negligible;
- The pile slenderness *L/d* ratio does not appear to have pronounced influence on the derived normalized settlement for more compressible piles (ratios ≤ 1000). For less compressible or incompressible piles, the influence of this ratio is of note, and similar for both systems, that means, the higher is *L/d* the lower will be the settlement;
- In the case of piled rafts only, the influence of K_{PS} on the percentage of load absorbed by the piles is low for in-

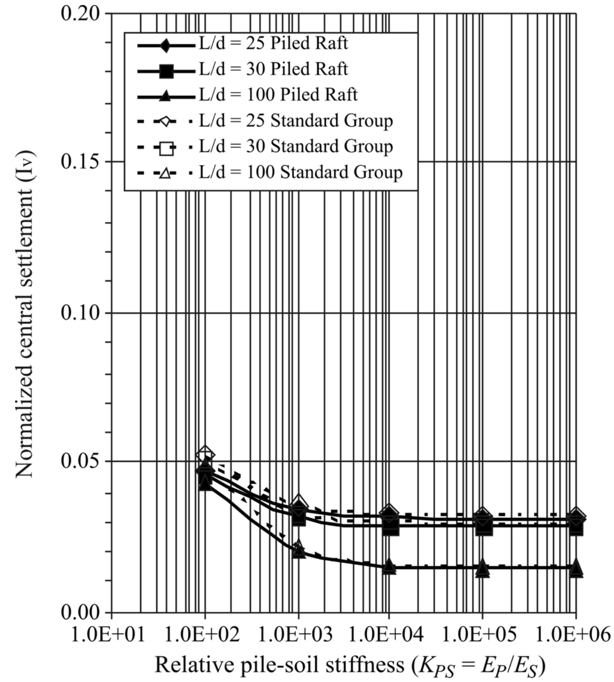

Figure 5 - Effect of the variation of the Relative Pile-Soil stiffness on the settlement value.

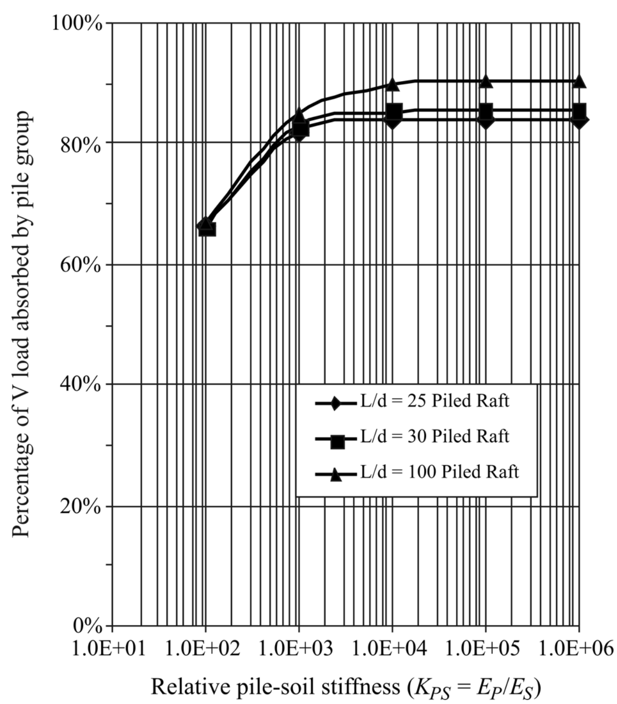

Figure 6 - Effect of the variation of the Relative Pile-Soil stiffness on the load distribution.

compressible piles. For more compressible ones, the higher is the compressibility of the pile (the lower is K_{PS}) the lower will be the load absorbed by the pile elements (more load to the raft). Besides, *L*/*d* slenderness ratio has only influence on incompressible piles, increasing their absorbed loads with the increase of *L*/*d*;

- It is finally noticeable the inverse correspondence of results from absorbed load and settlement in the range of incompressible piles, for piled raft systems.
- The effect of the relative Pile-Soil stiffness ratio (K_{PS}) concerning the differential settlement ratio (Δ) is presented in Fig. 7 for both systems. In this figure it is possible to notice that:
- Similarly as the vertical normalized total settlement, Δ is also very sensitive to variations in K_{PS}, in both systems, for relatively "deformable" pile cases. Again, the higher is the compressibility of the pile (lower is K_{PS}) the lower is the differential settlement ratio (less uniform settlements). For incompressible piles there is no influence of K_{PS}, *i.e.*, and the settlement of the raft becomes much more homogeneous (higher values of Δ);
- The pile slenderness *L*/*D* ratio does not appear to have a pronounced influence on Δ in all spectrum of K_{PS} variation, although some slight tendency of the decrease of Δ with the increase of *L*/*D* may be observed for piles that are more compressible;
- Both foundation systems have similar values of Δ varying with K_{PS}, although slight higher (Δ) numbers were obtained for the standard groups, *i.e.*, this latter system allowed slightly more uniform settlements along raft;

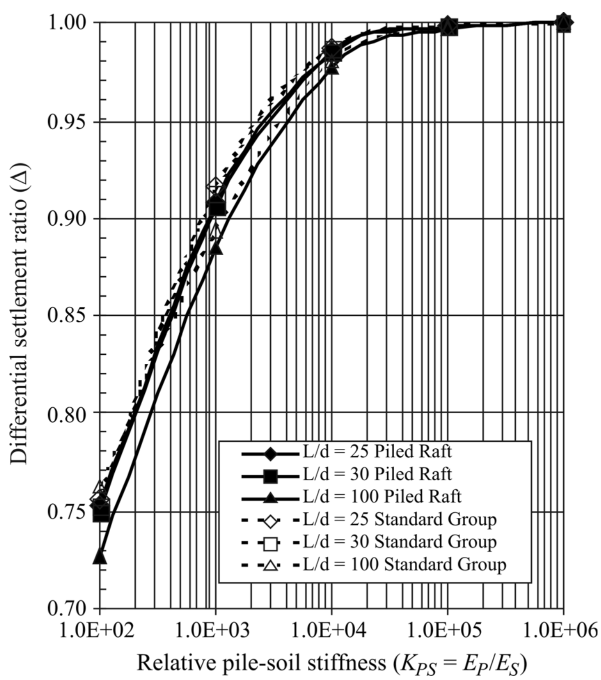

Figure 7 - Effect of the variation of the Relative Pile-Soil stiffness on differential settlement.

- All aforementioned aspects and trends have been similarly obtained by Zhang (2000), and by Clancy & Randolph (1993) (regarding normalized central settlement), in their numerical analyses.

Taking on account the detailed group configuration from the insert of Fig. 2, it is now possible to evaluate the load distribution within the piles of each system (in percentage to the total) in relation to variations on the relative Pile-Soil stiffness ratio. Figure 8 (a) and (b) respectively presents the results for a piled raft and a conventional group system, in regard to corner, center or laterally positioned piles.

From this one, it is noted the following points:

- The percentage of vertical load absorbed by the piles in each particular position is similar irrespective of the system. The piled raft, however, allows slightly less load to be transmitted to the piles, as part of the total applied load is absorbed by the raft;
- The load distribution concerning the pile's position is also a function of the relative Pile-Soil stiffness. For instance, for more compressible piles, where (as noticed before) total settlements are higher and differential ones more pronounced, the load at each position tends to be more uniform and similar. For less compressible, or incompressible piles, where differential settlements tends to be homogeneous along the raft, it is clear that center piles take lesser loads than lateral ones, and this one lesser loads than corner piles - the latter absorbing the highest load. Besides by decreasing the compressibility of the piles (hence increasing K_{PS}) the center piles will tend to slightly decrease their share of load in detriment to corner piles;
- In regard to the pile's slenderness ratio, it is also clear that, in the case of an incompressible pile, an increase of this ratio will tend to turn more "uniform" the loads within the pile elements (for both cases). That means, by increasing the pile's *L*/*D* center and lateral piles (those with lower loads) will tend to increase their share of load in detriment to corner piles (originally with higher loads), which on the other hand will tend to decrease their share of load.

Given such observations, one can yield the following partial conclusions, strictly valid for vertical loading:

- The adoption of a particular relative pile-soil stiffness ratio has the same effect for both piled raft and standard group systems when the main variable of interest is either the differential vertical settlement of the raft or the percentage of load absorbed by the piles. Although the piled raft system allows less load to be transmitted to the piles, as the raft shares part of the load, it does not seem to be so advantageous in design in comparison to standard groups, as both systems yielded similar values of normalized central and differential raft settlements;
- Nevertheless, if a piled raft is adopted one should try, whenever possible, to increase the relative stiffness of

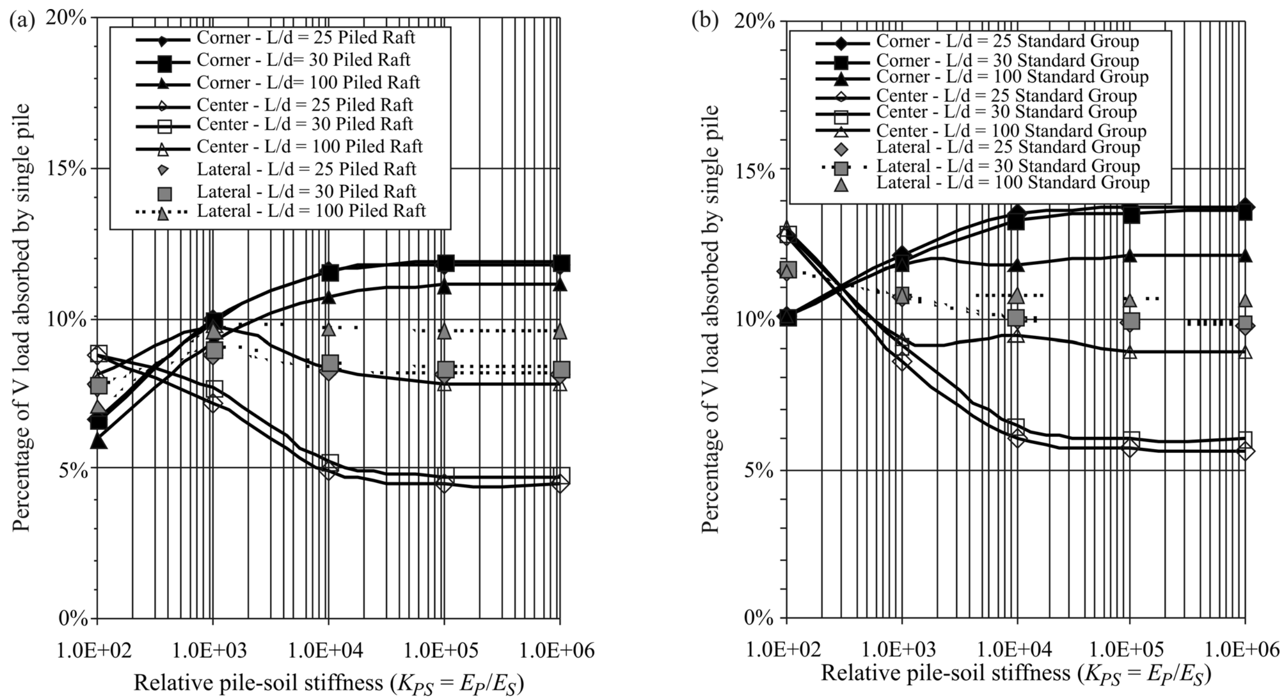

Figure 8 - Effect of the variation of the Relative Pile-Soil stiffness on the single pile's load for (a) piled raft and (b) conventional pile group.

the pile in regard to the surrounding soil (if possible with K_{PS} > 1000, *i.e.* turning the pile less deformable). As the results show, an increase of K_{PS} beyond a given value does not significantly influence both results of settlement and absorbed loads;

- By designing piled rafts with incompressible piles, one should also try to increase their slenderness ratios, since there will be a positive tendency of reduction of the total central settlement of the system with the increase of *L*/*D*, although the influence on the differential settlement will be negligible. Nevertheless, this will also lead to a corresponding increase of the absorbed load from the piles (with simultaneous decrease of raft's load);
- In terms of load share within the elements of the system, by adopting incompressible piles and by allowing them to have high slenderness ratios (if practical, much above 30), it is possible to obtain foundation systems with more uniform loads. Perhaps, by having center and lateral piles with higher *L*/*D* than corner piles, such effect could be maximized (although it was not tested herein). Anyway, this "rationalized" design concept (some define it as an "optimization") has already been advocated before by Cunha *et al.* (2001), Reul & Randolph (2004) or Bezerra *et al.* (2005) among others, and is the next step in designing piled rafts.

3.2.3. Effect of the Raft-Soil Stiffness ratio

The effect of the relative Raft-Soil stiffness ratio (K_{RS}) was also done with the same variables studied before. Such comparisons were carried out in terms of a constant ν of 0.35 and E_P of 18000MPa (K_{PS} = 3000), besides of distinct *L*/*D*, as previously commented. All other parameters in accordance to Table 1.

The value of K_{RS} for each situation was calculated via Eq. 1 with the same parameters of Table 1, and a variable raft thickness (t) which varied from 0.25 to 1.25m in order to respectively obtain a range of K_{RS} from 0.1 to 12. That means, from very flexible rafts (≤ 0.1) to rigid or "incompressible" ones (≥ 10).

Figures 9 to 11 respectively present the results in terms of the normalized central settlement, the percentage of vertical absorbed load by the group, and the differential settlement ratio.

From these figures, the following comments apply:

- The sensitivity of the vertical normalized central settlement to variations in K_{RS} is negligible throughout the spectrum of stiffness variation. However, it is affected in the same manner by the pile slenderness ratio *L*/*D* for both systems, that means, the higher is *L*/*D* the lower will be the settlement at any stiffness ratio. In fact, according to Zhang (2000) in analyses for standard group systems, "the E_R/E_S stiffness ratio has only a minor effect on the vertical deflection" and "increase in pile length will greatly reduce the vertical displacements". Curiously according to this author this stiffness ratio seems to be more influential in reducing horizontal deflections rather than vertical ones, nevertheless this topic will not be covered later herein;

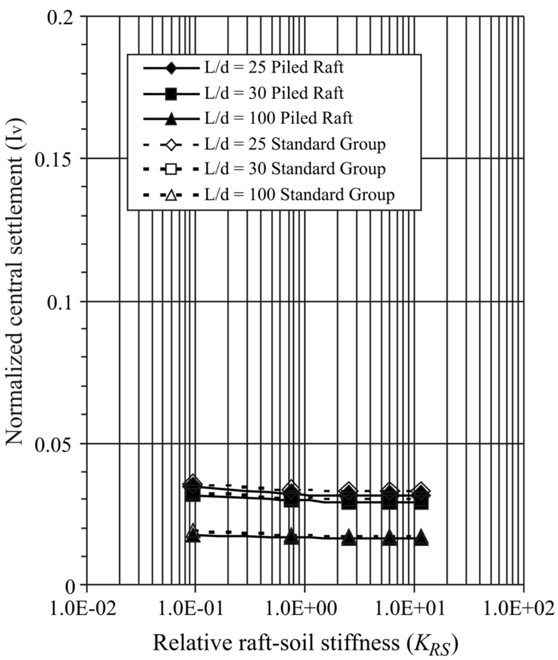

Figure 9 - Effect of the variation of the Relative Raft-Soil stiffness on the settlement value.

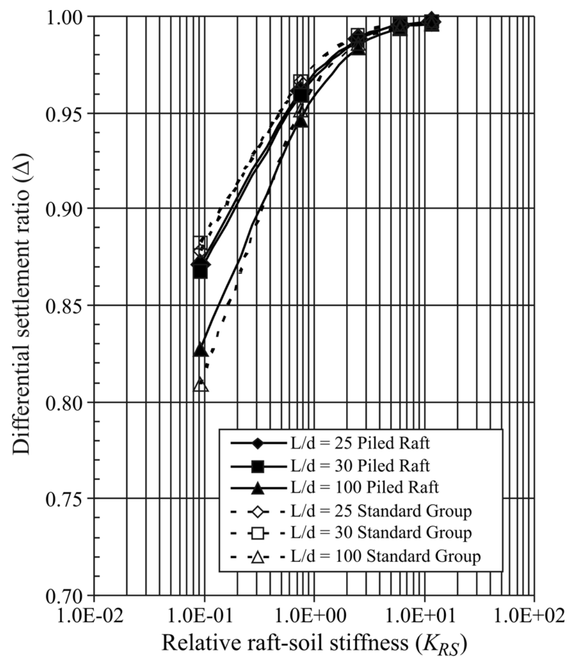

Figure 11 - Effect of the variation of the Relative Raft-Soil stiffness on differential settlement.

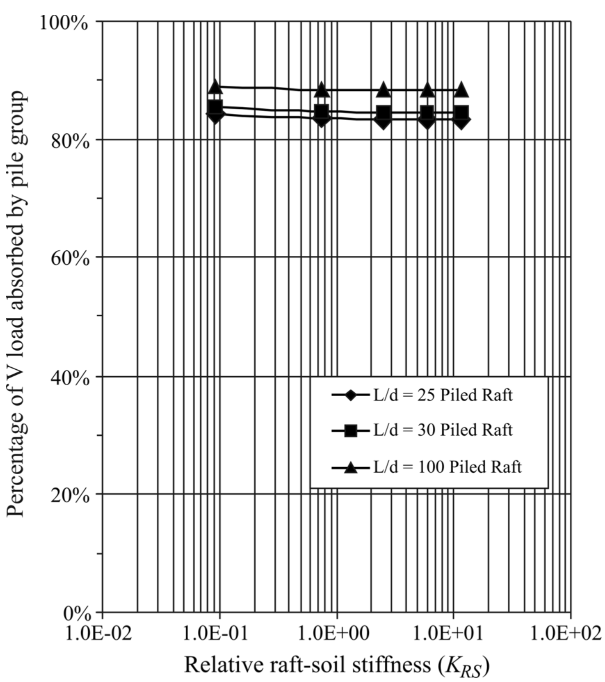

Figure 10 - Effect of the variation of the Relative Raft-Soil stiffness on the load distribution.

- On the other hand, the differential settlement ratio (Δ) is very sensitive to variations in K_{RS}, in both systems and for flexible rafts, *i.e.*, the higher is the flexibility (lower is the K_{RS}) the greater are the differences between the settlement at the corner and at the center of the raft (lower values of Δ), with the corner's settlement being always lower. For rigid rafts there is no influence of K_{RS} in both systems, *i.e.*, an increase of K_{RS} beyond a given value does not significantly influence the results;
- Differently to what has been noted in the case of the pile-soil stiffness, for K_{RS} it also seems that there is a more clear influence of the slenderness *L*/*D* ratio on Δ, for both system cases, when the raft is flexible. In this case, the higher is the pile slenderness ratio *L*/*D* the greater will be the differences between the settlement at the corner and at the center of the raft (*i.e.* the lower are the Δ values). For rigid rafts such effect is of negligible magnitude;
- In the case of piled rafts only, the influence of K_{RS} on the percentage of load absorbed by the piles is low or inexistent for any flexibility of the raft. Nevertheless, by increasing the *L*/*D* slenderness ratio there will be an increase of the absorbed load by the piles, with consequent fewer load being transferred to the raft.

Similarly as the previous sub item, the evaluation of the load distribution within the piles of each system is presented at this stage, now in relation to variations on the relative Raft-Soil stiffness ratio.

Hence, Fig. 12 (a) and (b) respectively show the results for a piled raft and a conventional group system, in regard to corner, center or laterally positioned piles.

From this figure some main observations can be given, as follows:

- Load distribution in regard to the position of the pile is influenced by the relative Raft-Soil stiffness. For instance, for flexible rafts, where differential settlements are more pronounced, the load at each position tends to

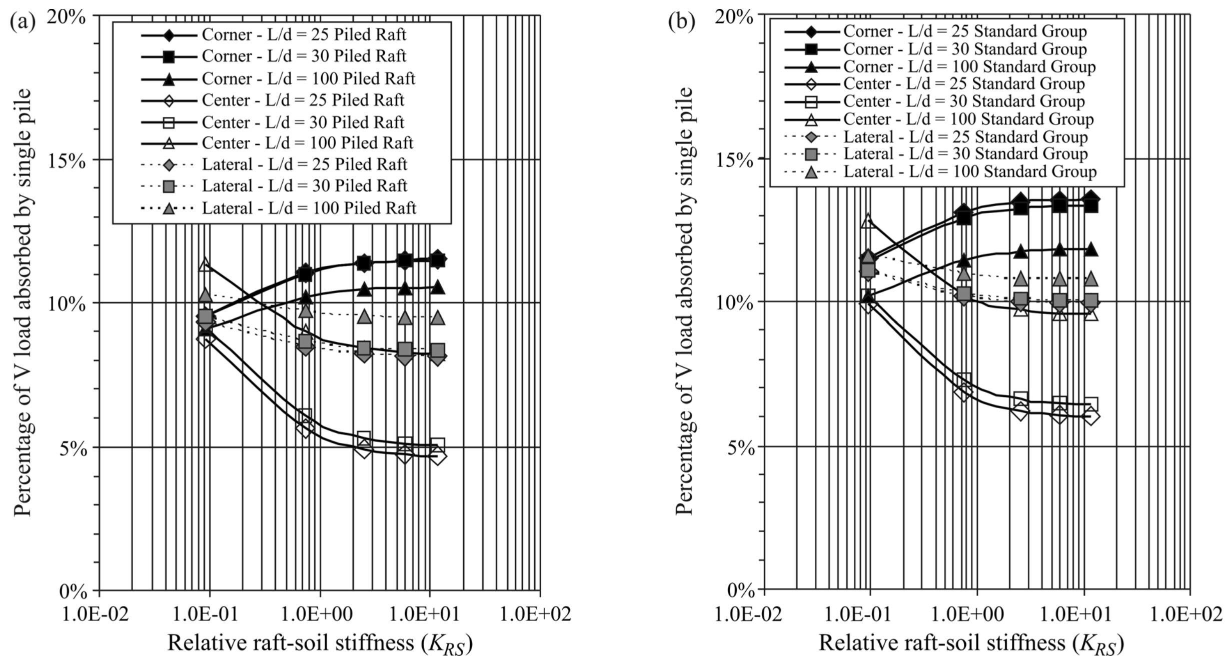

Figure 12 - Effect of the variation of the Relative Raft-Soil stiffness on the single pile's load for (a) piled raft and (b) conventional pile group.

be more uniform and similar (especially for K_{RS} = 0.1) than the equivalent one at respective positions in rigid rafts. For rigid rafts it is clear that center piles takes lesser loads than lateral ones, and this one lesser loads than corner piles - the latter absorbing the highest load (same observation as given for K_{PS});

- In relation to the pile's slenderness ratio, it is also clear that, in the case of a rigid raft (with more uniform settlements), an increase of this ratio will tend to homogenize the loads within the system elements (for both cases). In a similar way as depicted for K_{PS}, by increasing the pile's *L*/*D* ratio, center and lateral piles (with lower loads) will tend to increase their share of load in detriment to corner piles.

Partial conclusions can also be given with aforementioned observations, as it will be detailed next. Again, they are strictly valid for vertical loading:

- The adoption of a particular relative raft-soil stiffness ratio has the same effect for both piled raft and standard group systems when the main variable of interest is either the total or the differential vertical settlement of the raft;
- In any case one should always try, whenever possible, to increase the relative stiffness of the raft in regard to the supporting soil, turning the raft rigid. For engineering purposes, a value of K_{RS} equal or higher than 10 is enough to ensure practically uniform settlements within the raft;
- Nevertheless, by designing with flexible rafts one should be aware that by increasing the pile's slenderness ratio to values as high as 100 there will be a simultaneous decrease of the central settlement of the raft with a slight increase of its differential ratio (difference between corner and center displacements);
- In the case of rigid rafts it is advantageous to increase the pile's slenderness ratio, as it will decrease total settlements without collateral effects on the raft's differential values. In the case of piled rafts, this will also lead to a corresponding increase of the absorbed load from the piles (with simultaneous decrease of raft's load);
- In terms of the load share within the elements of the system, for both standard groups and piled rafts, it is possible to obtain a more uniform load distribution among the piles by allowing the raft to be rigid ($K_{RS} \geq 10$), and by designing with piles with high slenderness ratios. Such homogenization can also be achieved with very flexible rafts (at any pile's *L*/*D* ratio), but with the disadvantage of larger differential settlements within the raft.

3.3. Cases of load in the horizontal direction

This item is similar to the previous one, with the difference that it will now deal exclusively with load in the horizontal direction. The same magnitude of distributed stress (0.1 MPa) used in the (preceding) vertical cases was adopted here, as one notices in Table 1. However, in order to simplify the comparisons, and to cross compare the results to the vertical case, a unique slenderness ratio of 30 was adopted.

3.3.1. Effect of Poisson's coefficient

In a similar fashion as the previous data, the analyses carried out herein have also demonstrated that the influence of this parameter is negligible, and therefore can for all purposes be fixed in a foundation design. Similar results as those from former Figs. 3 and 4 have been obtained, and are not included in order to save paper's space.

3.3.2. Effect of the Pile-Soil Stiffness ratio

The effect of the relative Pile-Soil stiffness ratio K_{PS} was also evaluated concerning the horizontal load direction.

Their influence was assessed on the normalized central displacement (Eq. 2) and on the percentage of load absorbed by the pile group, as can be respectively visualized through Figs. 13 and 14.

From these figures one notices that:

- The sensitivity of the horizontal normalized central displacement to variations in K_{PS} is noticeable along all spectrum of relative pile stiffness, being more pronounced for standard pile groups than for piled rafts. Similarly as the vertical case, the higher is the compressibility of the pile (lower K_{PS}) the higher is the normalized horizontal displacement;
- On the other hand, in the horizontal direction piled raft systems do have a noticeable advantage in comparison to standard groups in terms of the reduction of the horizontal total displacement of the raft, as one observes in Fig. 13. This fact relates to the high percentage of load that is absorbed in the contact raft/soil, that, according to Fig. 14, ranges from around 80 to 35% (respectively from K_{PS} = 100 to 1000000). See for instance in Fig. 6 that in the vertical case the percentage of load absorbed by the raft was much lesser than in the horizontal one for all spectrum of K_{PS};

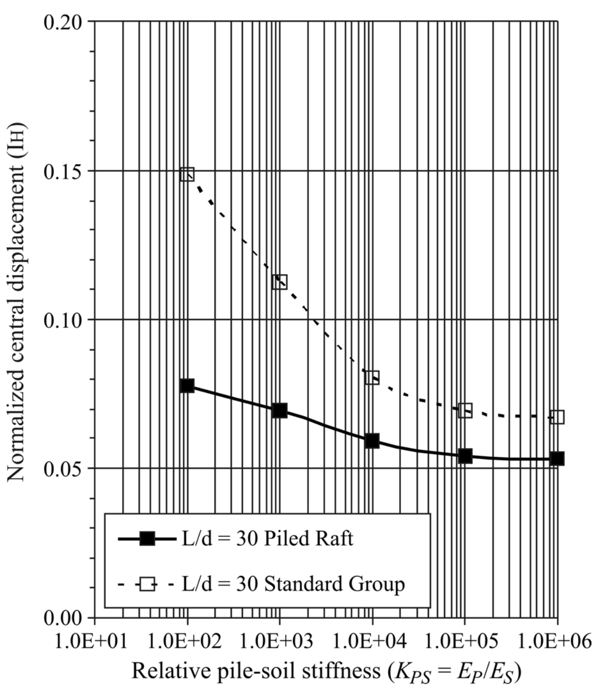

Figure 13 - Effect of the variation of the Relative Pile-Soil stiffness on the displacement value.

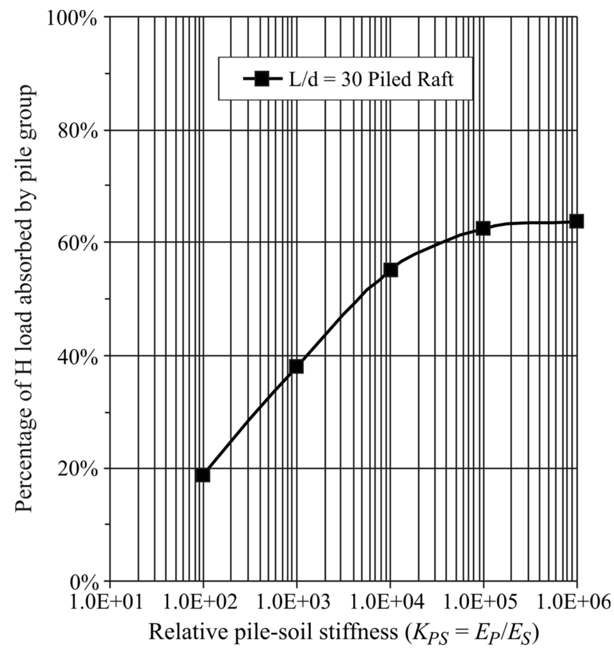

Figure 14 - Effect of the variation of the Relative Pile-Soil stiffness on the load distribution.

- It also seems in the case of piled rafts, comparing both situations of vertical and horizontal load at an equivalent K_{PS} (respectively at Figs. 5 and 13), that the lower is the load in the raft alone the lower will be the magnitude of displacement (in any direction);
- All aforementioned aspects and trends have been similarly obtained by Zhang (2000) in his analyses.

Taking on account the detailed group configuration from the insert of Fig. 2, it is also possible to evaluate the horizontal load distribution within the piles of each system (in percentage to the total) in relation to variations on the relative Pile-Soil stiffness ratio. Figure 15 (a) and (b) respectively presents the results for a piled raft and a conventional group system, in the same fashion as done for the vertical load.

From Fig. 15, one notices that:

- The trend of horizontal load distribution by the piles in each particular position is similar irrespective of the system. It is clear that center piles take lesser loads than lateral ones, and this one lesser loads than corner piles - the latter absorbing the highest load, in a similar fashion as observed for the vertical loading. Likewise, the piled raft allows slightly less load to be transmitted to the piles, as part of the total applied load is absorbed by the raft;
- The load distribution concerning the pile's position is a function of the relative Pile-Soil stiffness for both systems. For more compressible piles, where normalized horizontal displacements are higher, the load at each position tends to be more uniform and similar. For incompressible piles, the differences between the loads at each pile position are more pronounced and less uniform;

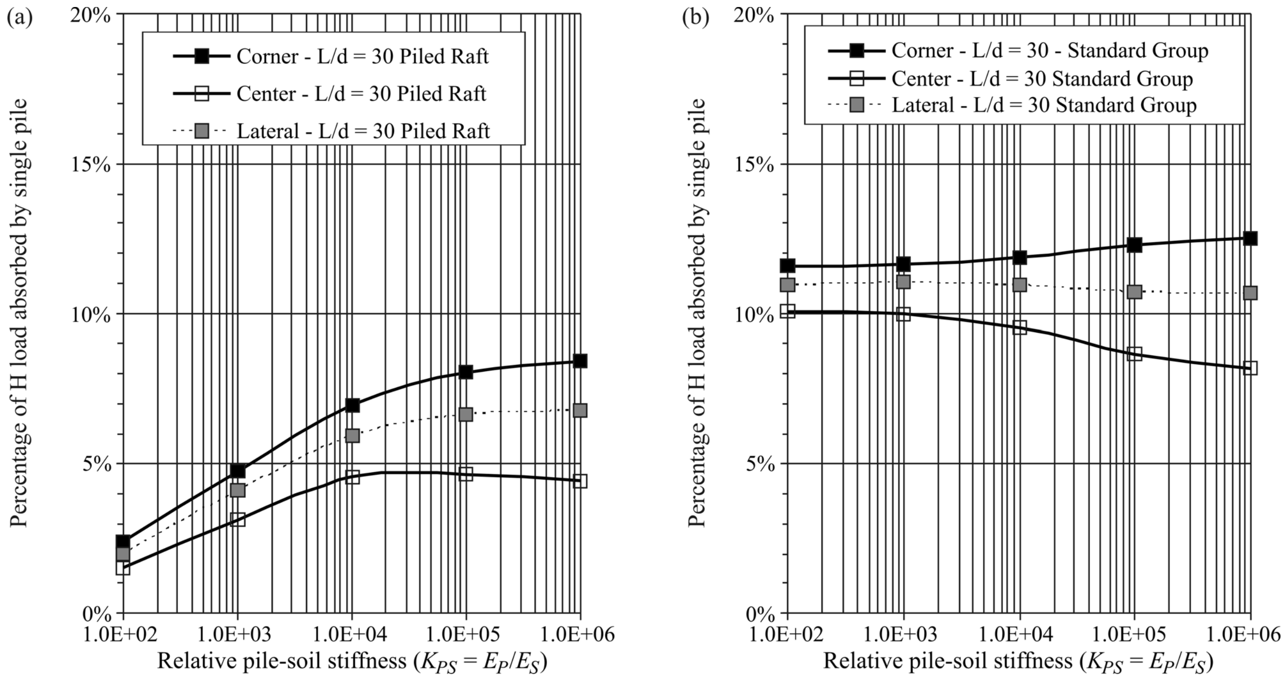

Figure 15 - Effect of the variation of the Relative Pile-Soil stiffness on the single pile's load for (a) piled raft and (b) conventional pile group.

- When comparing the situations of vertical and horizontal load shares at distinct pile positions with equivalent situations for both piled rafts and standard groups (respectively at Figs. 8 and 15), one notices that by decreasing the compressibility of the piles (hence increasing K_{PS}), center piles (those with lower loads) tend to decrease their share of load in detriment to corner piles (originally with higher loads). This will turn the load distribution more non-uniform within the system - as previously stated.

Given such observations, one can yield the following partial conclusions, strictly valid for horizontal loading:

- If the main variable of interest is the normalized central displacement of the raft it is of upmost importance to design the foundation as piled raft, with piles of high relative pile-soil stiffness K_{PS}, *i.e.* incompressible piles. This procedure will tend to decrease the horizontal displacements with a simultaneous decrease of the load being transferred to the raft. Nevertheless it will also induce a more non-uniform distribution of the (remaining) load within the piles of the system, with corner piles taking more load than center ones;
- On the other hand, if the system is designed as a standard pile group, it is also important to adopt incompressible piles in the project, besides of the aforementioned non uniformity of load distribution;
- In design projects with either piled rafts or standard pile groups under horizontal distributed load the estimation of the Poisson's Coefficient is not of concern.

3.4. Load distribution along pile

Figures 16 and 17 depict the load distribution along the shaft at distinct relative depths (z/L) for the (center) pile, with an L/D of 30 and at discrete values of K_{PS} for both foundation systems. They respectively relate to loading at vertical and horizontal directions.

The observed trend in aforementioned figures between the percentage of absorbed vertical and horizontal load at the top of the center pile, with K_{PS} variation (from 1000 to 10000), do agree with comments expressed on previous items respectively done for Figs. 8 and 15.

Nevertheless, one also notices from Figs. 16 and 17 that:

- For the horizontal direction, in any case, the distribution of load along the pile's length tends to be more "concentrated" (less homogeneous) on top positions of the shaft. This is especially noticeable for the top 50% of the pile (that means z/L up to around 0.5). Tension loads have also appeared on the remaining lower sections, denoting that a "neutral" point existed, where the top compressive loads turned into tension ones at the bottom;
- For the vertical direction, and also in any case, the distribution of the load is much more homogeneous along the depth;
- For the vertical direction, the magnitude of the load (in percentage to total) along the whole pile's length decreased with the increase of the pile-soil stiffness K_{PS}, whereas the opposite happens for the horizontal direction (in the aforementioned top region). In the latter case

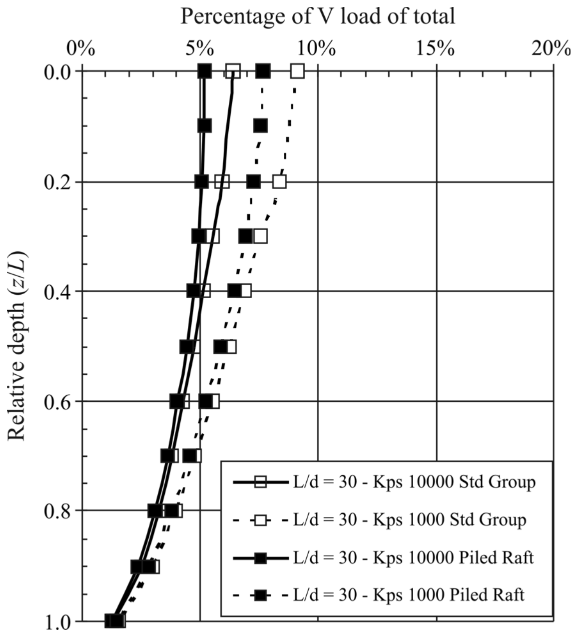

Figure 16 - Vertical load variation along (center) pile length at distinct conditions for both systems.

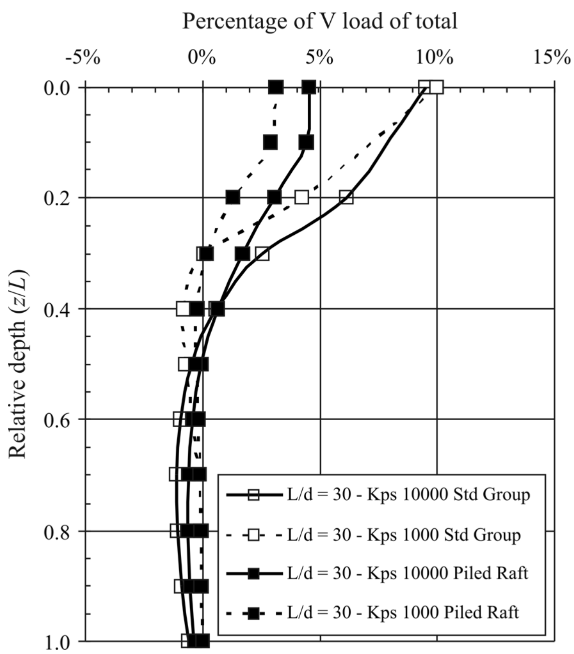

Figure 17 - Horizontal load variation along (center) pile length at distinct conditions for both systems.

the magnitude of the load along the pile's length increased with the increase of K_{PS}.

Such dissimilarities undoubtedly denote differences in the foundation behavior when loaded at distinct directions. Perhaps it could explain part of the differences observed on equivalent data when comparing it at each load direction. Nevertheless, more research is still needed to foster grounded conclusions in such behavioral aspect.

4. Conclusions

This paper investigated the individual behavior of piled rafts and standard pile groups with differing characteristics of relative stiffness (pile-soil, raft-soil), slenderness ratio (pile) and Poisson's Coeff. (soil), at both non simultaneous vertical and horizontal load conditions.

Although the range of the numerical parametric analyses was limited, generalized conclusions have been drawn. This knowledge can off course be referenced as an *initial* guideline in the design of similar foundation systems.

Therefore, based on aforementioned results and discussion, and bearing in mind the partial conclusions drawn in each sub item, it is possible to suggest that:

- Foundation systems can be designed (as usually done) as conventional groups if the main variable of interest is the vertical settlement (either total or differential). Nevertheless, the group should be preferably designed with a high slenderness ratio for the pile (longer piles as practically possible for a constant diameter), and high relative pile-soil (≥ 1000) and raft-soil (≥ 10) stiffnesses;
- Foundation systems must be designed (as it is not usual yet) as piled rafts if the main variable of interest is the horizontal displacement of the raft (total). It shall be preferably designed, again, with a high relative pile-soil (≥ 1000) and raft-soil (≥ 10) stiffness;
- If the system can not be designed as a piled raft, in the case of horizontal loading, it should at least have the same characteristics suggested at previous Item(1);
- Care should be taken in the structural reinforcement of the piles when adopting aforementioned suggestions, as by decreasing the pile compressibility there will be also a tendency of more non-uniform loads distributed within the system;
- In any case, the Poisson's Coefficient of the soil can be fixed without problems, as it seems to be not a parameter of strong influence on the final results;
- When designing the system as a piled raft, some sort of "rationalization" procedure, as advocated by some of the cited references of this paper, could be employed in order to enhance in design some of the (beneficial) features observed herein with the numerical analyses. Perhaps, for instance, by allowing center and lateral piles to have higher lengths than corner piles (although this possibility needs yet to be numerically better assessed). This feature is, nevertheless, already being implemented in the few piled raft projects of the city of Goiânia/Brazil (Sales 2013, personal communication).

Acknowledgments

This study was made possible through an existing joint technical co-operation research program from the Universities of Sydney in Australia and Brasília in Brazil, where students from both institutions were able to correspond and interact. In this regard, the authors are grateful to the kind support and comradeship provided by both (retired) Profs. H.G. Poulos and J.C. Small, and Dr. H. Zhang (SMEC Australia Pty Ltd.). The authors also thank the Brazilian sponsorship organizations CNPq and CAPES for all related support in this and in all other studies carried out by the GPFees Group, either in terms of personal research grants, or via sabbatical & student scholarships.

One of such scholarships allowed the MSc Student J.E. Bezerra to generate the raw data and illustrative plots used as basis of this paper. Although the paper considerably differs from the original knowledge generated by this particular Dissertation, as it expands and explores further its interpretation and conclusions, the authors are nevertheless indebted for the work done by Mr. Bezerra.

References

ABNT (2010) NBR6122. Projeto e Execução de Fundações. Brazilian Association of Technical Norms - ABNT, Rio de Janeiro, 91 pp.

Ayala, D.J.C. (2013) Uso da Técnica de Radier Estaqueado para Pequenos Edifícios Assentes sobre Solo Colapsível. M.Sc. Thesis, Dept. of Civil and Env. Enginnering, Univ. of Brasília, 147 pp.

Bezerra, J.E. (2003) Estudo do Comportamento de Fundações em Radier Estaqueado: Conceitos e Aplicações. M.Sc. Thesis, Dept. of Civil and Env. Enginnering, Univ. of Brasília, 193 pp.

Bezerra, J.E.; Cunha, R.P. & Sales, M.M. (2005) Optimization concepts for the design of piled raft foundation systems. Proc. 16th. Int. Conf. on Soil Mechanics and Geot. Engineering, Osaka, p. 1947-1950.

Booker, J.R. & Small, J.C. (1988) Finite layer analysis of layered pavements subjected to horizontal loading. Proc. 6th. Int. Conf. Num. Meth. Geomechanics, Insbruck, v. 3, p. 2109-2113.

Brown, P.T. (1975) Strip footing with concentrated loads on deep elastic goundations. Geotechnical Engineering, v. 6, p. 1-13.

Clancy, P. & Randolph, M.F. (1993) An approximate analysis procedure for piled raft foundations. Int. Journal Num. Anal. Methods in Geomechanics, v. 17, p. 849-869.

Clancy, P. & Randolpth, M.F. (1996) Simple design tools for piled raft foundation. Geotechnique, v. 46:2, p. 313-328.

Cunha, R.P. & Sales, M.M. (1998) Field load tests of piled footings founded on a tropical porous clay. Proc. of the 3rd Intern. Geotechnical Seminar on Deep Foundation on Bored and Auger Piles, Ghent, v. 1, p. 433-438.

Cunha, R.P.; Soares, J.M. & Mota, N.M.B. (2000a) Otimização de um projeto de fundações, através do uso de radier estaqueado. Simp. Int. Estrutura-Solo em Edifícios, São Carlos, CD ROM, 10 pp.

Cunha, R.P.; Small, J.C. & Poulos, H.G. (2000b) Class C analysis of a piled raft case history in Gothenburg, Sweden. Year 2000 Geotechnics - Geotechnical Engineering Conference, Bangkok, Asian Institute of Technology, v. 1, p. 271-280.

Cunha, R.P.; Small, J.C. & Poulos, H.G. (2000c) Parametric analysis of a piled raft case history in Uppsala, Sweden. IV Seminar of Special Foundations and Geotechnics, São Paulo, Brazilian Soil Mechanics Society, v. 2, p. 381-390.

Cunha, R.P.; Poulos, H.G. & Small, J.C. (2001) Investigation of design alternatives for a piled raft case history. ASCE Journal of Geotechnical and Geoenvironmental Engineering, v. 127:8, p. 635-641.

Cunha, R.P.; Bezerra, J.E.; Small, J.C. & Zhang, H.H. (2002) Parametric analysis of piled rafts founded on a tropical clay of Brazil. Proc. IX Int. Conf. of Piling and Deep Foundation, Nice, p. 249-256.

Cunha, R.P.; Bezerra, J.E.; Zhang, H.H. & Small, J.C. (2004) Back analyzed parameters from piled foundations founded on tropical porous clay. Int. Conf. on Cooperation and Innovation in the Geo-Industry. ASCE Geot. Special Pub. no. 124, p. 1003-1014.

Cunha, R.P.; Bezerra, J.E. & Zhang, H.H. (2006) Influência da rigidez relativa estaca/solo (Kps) em grupo de estacas convencionais e tipo "radier estaqueado" carregados vertical ou horizontalmente. Proc. XIII Braz. Cong. of Soil Mechanics and Geot. Engineering - Cobramseg, Curitiba, v. 2, p. 793-798.

Cunha, R.P. & Zhang, H.H. (2006) Behavior of piled raft foundation systems under a combined set of loadings. 10th. Int. Conf. on Piling and Deep Foundations - DFI_2006. Amsterdam, p. 242-251.

Hain, S.J. & Lee, I.K. (1978) The analysis of flexible raft-pile systems. Géotechnique, v. 28:1, p. 65-83.

Janda, T.; Cunha, R.P.; Kuklík, P. & Anjos, G.M. (2009) Three dimensional finite element analysis and back-analysis of CFA standard pile groups and piled rafts founded on tropical soil. Soil and Rocks, v. 32:1, p. 3-18.

Lee, C.Y. & Small, J.C. (1991) Finite layer analysis of axially loaded piles. Journal Geot. Eng. Div., ASCE, v. 117:11, p. 1706-1722.

Mandolini, A. (2003) Design of piled raft foundations: practice and development. Conference on Bored and Auger Piles, BAP III, Ghent, p. 59-80.

Mandolini, A. & Viggiani, C. (1997) Settlement of piled foundations. Géotechnique, v. 47:4, p. 791-816.

Ottaviani, M. (1975) Three-dimensional finite element analysis of vertically loaded pile groups. Géotechnique, v. 25, p. 159-174.

Poulos, H.G. (1998) The pile-enhanced raft - an economical foundation system. Keynote Lecture, Proc. XI Brazilian Congress on Soil Mechanics and Geotechnical Engineering, Brasilia, v.4, p. 27-43.

Reul, O. & Randolph, M.F. (2004) Design strategies for piled rafts subjected to nonuniform vertical loading. ASCE Journal of Geot. and Geoenv. Eng., v.130:1, p. 1-13

Sales, M.M. (2000) Análise do Comportamento de Sapatas Estaqueadas. Ph.D. Thesis, University of Brasília, Department of Civil and Environmental Engineering, Publication G.TD - 002A/00, 229 pp.

Sales, M.M.; Cunha, R.P. & Jardim, N.A. (1999) Analysis of piled footing tests on a tropical porous clay. Proceedings of the XI Panamerican Conference on Soil Mechanics and Geotechnical Engineering, Foz do Iguaçu, v. 3, p. 1395-1402.

Sales, M.M.; Cunha, R.P.; Poulos, H.G. & Small, J.C. (2005) Simplified approach for load-settlement curve estimation of piled rafts. Solos e Rochas, v. 28:1, p. 73-83.

Small, J.C. & Booker, J.R. (1984) Finite layer analysis of layered elastic materials using a flexibility approach. Part 1 - Strip loadings. Int. Journal Num. Meth. in Engineering, v. 20, p. 1025-1037.

Small, J.C. & Booker, J.R. (1986) Finite layer analysis of layered elastic materials using a flexibility approach. Part 2 - Circular and rectangular loadings. Int. Journal Num. Meth. in Engineering, v. 23, p. 959-978.

Ta, L.D. & Small, J.C. (1996) Analysis of piled raft systems in layered soils. Int. Journal for Num. & Anal. Meth. in Geomechanics, v. 20, p. 57-72.

Ta, L.D. & Small, J.C. (1997) An approximation for analysis of raft and piled raft foundations. Computers and Geotechnics, v. 20:2, p. 105-123.

Zhang, H.H. (2000) Finite Layer Method for Analysis of Piled Raft Foundations, PhD Thesis, University of Sydney. 362pp.

Zhang, H.H. & Small, J.C. (2000a) Analysis of capped pile groups subjected to horizontal and vertical loads. Computers and Geotechnics, v. 26:1, p.1-21.

Zhang, H.H. & Small, J.C. (2000b) Piled Raft Foundations Subjected to General Loadings. John Booker Memorial Symposium, A.A.Balkema, p. 431-444.

Tailings Liquefaction Analysis Using Strength Ratios and SPT/CPT Results

W. Pirete, R.C. Gomes

Abstract. Tailings dams constructed using the upstream method generally have relatively low- density materials with a high degree of saturation. Such conditions can generate the phenomena of liquefaction, which is potentially critical in slurry tailings disposal systems. Slope stability analyses involving liquefied soil require that the shear resistance of the softened soil be estimated and then, a good practical alternative is back-analyzed with field case studies involving slope failures, using commonly SPT and CPT results. The Olson (2001) and Olson & Stark (2003b) liquefaction analysis methodology based on strength ratios, included in this approach, is comprised of three stages: (i) liquefaction susceptibility analysis; (ii) triggering analysis; and (iii) post-triggering - flow failure stability analysis. In this paper, this approach was applied for stability assessments to verify liquefaction potential in an upstream tailings dam built by the hydraulic fill technique and located in the *Quadrilátero Ferrífero* (Iron Quadrangle) region, southeastern of Brazil. The results ratified the safety condition of the impoundment although they have demonstrated that the tailings tend to exhibit contractile behavior during shear, indicating liquefaction susceptibility.
Keywords: tailings, liquefaction, strength ratio, SPT tests, CPT tests.

1. Introduction

In general, liquefaction can be understood as the phenomenon of the strain-softening of contractive, saturated and cohesionless soils during undrained shear and can be triggered by static or seismic undrained loading or undrained deformation under constant load. This behavior results in a liquefaction flow failure in the field if the static shear stress is greater than the liquefied (or steady state) shear strength. The liquefied shear strength is defined as the shear strength mobilized by large deformation after liquefaction is triggered in saturated, contractive and cohesionless soils. In addition, this condition has also been referred to as undrained residual shear strength (Seed, 1987), undrained steady state shear strength (Poulos *et al.*, 1985), and undrained critical shear strength (Stark & Mesri, 1992).

Although ‘liquefaction’ is commonly used to describe all failure mechanisms resulting from the build-up of pore pressures during the undrained cyclic shear of saturated cohesionless soils, some ground failures attributed to ‘soil liquefaction’ are more correctly ascribed to ‘cyclic mobility’, since it results in limited soil deformations (Gomes, 2010). Liquefaction can occur even in unsaturated soils, with a sufficient saturation degree to induce contraction associated to water dissipation instead of air (Yoshimi *et al.*, 1989; Aubertin *et al.*, 2003). Laboratory tests have confirmed the possibility of liquefaction even in materials with a saturation degree of 80% (Martin, 1999).

Except for the fine fraction of ore bodies with substantial mineral clay content, tailings are usually cohesionless materials, conventionally deposited in the form of slurry by hydraulic fill techniques in raised embankments. Raised embankments can be constructed using upstream, downstream, or centerline methods (Vick, 1990). Each one of the structures is constructed in stages, with constructing material and fill capacity increasing incrementally with each successive raising.

Upstream construction, the most economical method, begins with a starter dam constructed at the downstream toe. The tailings are discharged peripherally from the crest of the starter dam using spigots or cyclones. This deposition develops a dike and wide beach area composed of coarse material that becomes the foundation of the next dike. These dikes can be built with borrow fill, or tailings can be excavated from the beach and placed by dragline or bulldozer. The single most important criteria for the application of the upstream construction method is that the tailings beach must form a competent foundation for the support of the next dike.

The phreatic surface exerts a large degree of control over the stability of the structure, under both static and seismic loading conditions. The primary method of maintaining a low phreatic surface near the embankment face is to guarantee an elevated hydraulic conductivity of the deposit in the direction of flow. There are four factors influencing the phreatic surface location: the permeability of the foundation relative to the tailings; the degree of grain-size segregation; the lateral permeability variation within the deposit; and the location of the reservoir relative to the embankment crest. Only the reservoir limit can be controlled through operational practices, by maintaining a large tail-

Romero César Gomes, Associate Professor, Universidade Federal de Ouro Preto, Ouro Preto, MG, Brazil. e-mail: romero@em.ufop.br.
Washington Pirete, Geotechnical Engineer, Vale S.A., Southern Ferrous System, Belo Horizonte, Brazil. e-mail: washington.pirete@vale.com.br.
Submitted on November 1, 2011; Final Acceptance on March 10, 2013; Discussion open until August 30, 2013.

ings beach extension. Water control and management are the most critical elements of tailings dam design and operation.

Tailings dams constructed using the upstream method generally have relatively low- density materials with a high degree of saturation. On the other hand, the wide ranges in the initial void ratio, together with the structure of tailings deposits, imply that predictions of the in situ undrained strength for these materials are highly uncertain. Such conditions generate the phenomena of liquefaction, which is potentially critical in these slurry tailings disposal systems (Troncoso & Verdugo, 1985; Vick, 1990; ICOLD & UNEP, 2001; Bray *et al.*, 2004).

Although such systems are very susceptible to liquefaction mechanisms under dynamic loading (Kramer, 1996; Seid-Karbasi & Byrne, 2004), mine tailings impoundments have demonstrated that more static liquefaction events than seismic induced events occur in function of the loading rates (Ishihara *et al.*, 1990; Davies *et al.*, 2002; Olson, 2006; Byrne, 2008). In fact, if the loading rate is quick enough or if the tailings present sufficiently low relative hydraulic conductivity, shear-induced pore pressures are generated and, as a result, effective stresses are reduced and both stiffness and shear strength degrade. In tailings impoundments, particularly upstream tailings dams, potential static liquefaction triggers include (Davies *et al.*, 2002):

- Increased pore pressures induced by an increase in the piezometric surface, and/or change of pore pressure conditions from below hydrostatic to hydrostatic, or to higher than hydrostatic.
- Excessive rate of loading due to the rapid rise of the impoundment;
- Removal of toe support from an overtopping event;
- Foundation movements, rapid enough to generate undrained loading in tailings susceptible to spontaneous collapse.

Several procedures have been proposed for estimating the liquefaction potential or susceptibility of soils or tailings. These techniques include commonly experimental procedures based on lab tests results (Poulos *et al.*, 1985; Sladen *et al.*, 1985; Ishihara, 1993; Yamamuro & Lade, 1997, Gomes *et al.*, 2002; Olson & Stark, 2003a; Pereira, 2005).

To determine liquefied shear strength, methodologies based on laboratory tests require high-quality samples and the adoption of correction factors to compensate for potential volume variations that occur during sampling and testing (Poulos *et al.*, 1985; Ishihara, 1993; Idriss and Boulanger, 2007). This is due to the fact that any errors in determining the levels of voids in situ may result in large differences in the results, since the position of the steady state line is influenced by the sample preparation technique, by the shear mode and by the effective confining stresses.

Thus, greater emphasis has been given to empirical methods that correlate corrected values of resistance from SPT and CPT tests with liquefaction failure results from case histories that were back-analyzed (Seed *et al.*, 1985; Stark and Mesri, 1992; Ishihara, 1993; Olson 2001, Olson and Stark, 2003b; Idriss and Boulanger, 2007a). These studies are based on classical concepts of soil mechanics, such as critical void ratio, steady state line, peak strength and liquefied shear strength (Casagrande, 1975; Castro, 1975; Poulos *et al.*, 1985; Kramer, 1996; Olson, 2001).

In this context, the estimated values of shear strength in these analyses constitute parameters that are more representative than those obtained in laboratory testing, because they embody the complex reality of actual deposits, the physical interaction of different materials and even the failure kinetics processes. However, there remain some uncertainties that affect the estimated values of resistance, mainly due to difficulties in establishing the rigid boundaries of the liquefaction zone, the location of the sliding surfaces and the drainage and pore pressures conditions mobilized during the flow.

The liquefaction methodology proposed by Olson (2001) consists of a triggering analysis based on field tests and does not require a suite of laboratory tests or correction procedures. The author collected thirty-three case histories of liquefaction flow failures that were back-analyzed to evaluate the yield and liquefied shear strength. Relationships between yield strength ratio and corrected SPT and CPT resistance were developed for use in liquefaction triggering analyses and also, those between liquefied strength ratio and corrected SPT and CPT resistance were developed for use in post-triggering stability analyses.

The general principles and technical basis of this methodology are set out below, covering three primary analyses: (i) liquefaction susceptibility analysis; (ii) triggering analysis; and (iii) post-triggering - flow failure stability analysis (Olson, 2001; Olson & Stark, 2003b).

2. Liquefaction Resistance Based on SPT and CPT Tests

2.1. Liquefaction susceptibility

The first step of a tailings liquefaction analysis is to determine whether a tailings deposit is in a contractive state, *i.e.*, susceptible to undrained strain-softening behavior and flow failure. These states are established based on correlations between overburden-stress normalized penetration resistance (either CPT tip resistance or SPT blow count - a measure of soil density) and vertical effective stress (pre-failure condition). The corrected blowcount, $(N_1)_{60}$, is defined as the SPT blowcount at a vertical effective stress of 100 kPa and an energy level equal to 60% of the theoretical free-fall hammer energy. The correct cone tip resistance, q_{c1}, is expressed as $q_{c1} = q_c \cdot C_q$, where C_q is the CPT based overburden correction factor.

Figures 1 and 2 respectively present SPT and CPT values based on flow failure susceptibility relationships

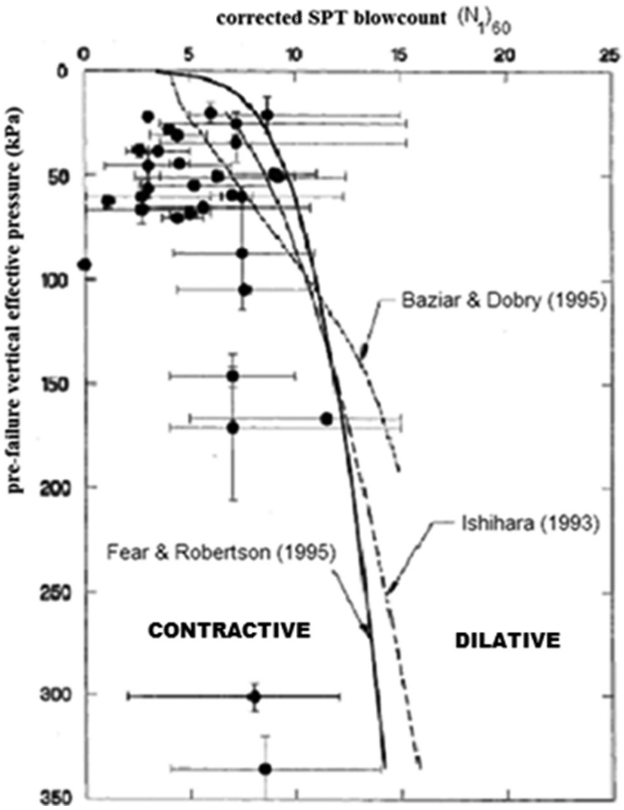

Figure 1 - Relationships separating contractive from dilative conditions using flow failure case histories and corrected SPT blowcount values (Olson, 2001).

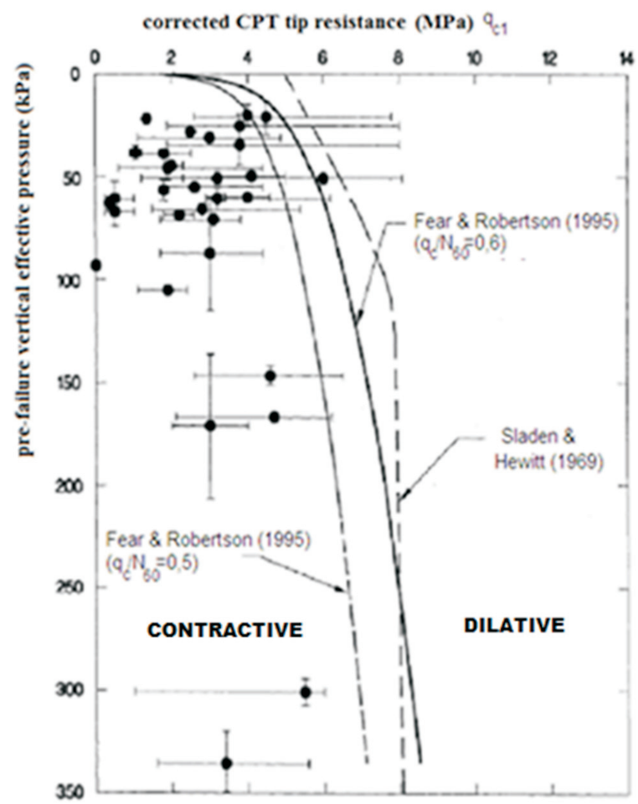

Figure 2 - Relationships separating contractive from dilative conditions using flow failure case histories and corrected CPT tip resistance values (Olson, 2001).

from literature with case history data. Based on the agreement with theory, laboratory results, and field case histories, the Fear & Robertson (1995) boundary was recommended by the author (Olson, 2001) to delineate field conditions susceptible and not to flow failure in both cases.

In a specific design, records of q_{c1} and/or $(N_1)_{60}$ should be plotted against vertical effective stress, including the recommended relationship.The liquefaction susceptibility analysis involves two hypotheses:

- Tailings exhibit dilative behavior: tailings liquefaction susceptibility is unlikely and the analysis is completed;
- Tailings exhibit contractive behavior: tailings liquefaction susceptibility is likely and this analysis should be complemented by the triggering analysis and post-triggering - flow failure stability analysis.

2.2. Triggering analysis

For tailings that show to be contractive under shear from the previous analysis, a liquefaction triggering analysis is performed to determine whether the imposed loading conditions (in these analyses, static loading) are sufficient to cause the soil to exceed its yield strength ratio and trigger liquefaction. This additional analysis is an extension of a traditional slope stability analysis typically performed with commercial software, and can be readily facilitated with the use of a spreadsheet and data obtained from the slope stability software.

The liquefaction triggering analysis is based on a limit equilibrium stability back-analysis (considering non-circular and circular surfaces), from the pre-failure geometry of the slope to estimate the average static shear stress (τ_d) in soils susceptible to liquefaction. A single value of shear strength is assumed, then, for soils susceptible to liquefaction and this resistance is continually changed to obtain FS = 1.0 and the corresponding critical surface rupture.

The critical failure surface is subdivided into a number of segments (10 to 15 segments are recommended) and is determined the weighted effective vertical stress, σ'_{v0} (average value) along the critical failure surface (within the zone of soil susceptible to liquefaction), and calculate the average static shear stress ratio τ_d/σ'_{v0}. If applicable, average seismic shear stresses (and other shear stresses applied to each segment of the yield failure surface) are evaluated using complementary analyses (Olson & Stark, 2003b).

In addition, yield strength ratios ($s_{u(yield)}/\sigma'_{v0}$), appropriate for each slice of the critical failure surface, are estimated based on corrected SPT and/or CPT penetration resistance values. In this analysis step, a desired level of conservatism can be incorporated by using a penetration resistance smaller than the mean value, or by selecting a yield strength ratio higher or lower than the mean value. In this manner, it is possible determine the liquefaction potential in each segment using a safety factor against liquefaction triggering that comprise two hypotheses:

- Segments with $(FS)_{triggering} > 1.0$ are unlikely to liquefy (post-triggering stability analysis is unnecessary if all segments have $(FS)_{triggering} > 1.0$);
- Segments with $(FS)_{triggering} \leq 1.0$ are likely to liquefy and these segments should be assigned the liquefied shear strength for a post-triggering stability analysis (segments with $(FS)_{triggering} > 1.0$ should be assigned their yield shear strength for a post-triggering stability analysis).

The authors recommend that both the critical circular and noncircular failure surfaces be analyzed, varying in depth and location within the zones of contractive tailings. If the circular and noncircular failure surfaces cross the zones of contractive soil at about the same location and depth, it is recommended that one or two additional potential failure surfaces that cross these zones at different locations be analyzed.

2.3. Post-triggering - Flow failure stability analysis

After the characterization phase of the liquefaction triggering, a post-triggering stability analysis of the structure, using the pre-failure geometry, must be conducted to determine whether the static shear forces are greater than the available shear resistance, including the liquefied shear strength. In this case, the liquefied shear strength ratio ($s_{u(liq)}/\sigma'_{v0}$), appropriate for each slice of the critical failure surface, is determined based on corrected SPT and/or CPT penetration resistance values. Appropriate values of liquefied shear strength are estimated (using the value of σ'_{v0} for the segment) and assigned to the segments of the critical failure surface predicted to liquefy from the triggering analysis. Fully mobilized drained or undrained shear strengths are assigned to the non liquefied soils.

This analysis should be conducted for all of the potential failure surfaces that were examined in the triggering analysis. Another level of conservatism can be incorporated by using a penetration resistance smaller than the mean value, or by selecting a yield strength ratio higher or lower than the mean value. The post-triggering analysis results comprise two hypotheses:

- Safety factor against flow failure $(FS)_{flow} \leq 1.0$: flow failure is predicted to occur; control procedures should be adopted to increase impoundment safety;
- Safety factor against flow failure $(FS)_{flow}$ such that $1.0 < (FS)_{flow} \leq 1.1$: flow failure has little possibility to occur, but some deformation is likely (the segments of the failure surface with $1.0 < (FS)_{flow} \leq 1.1$ should be reassigned their liquefied shear strength).

The post-triggering stability analysis should be repeated with the new segment shear strengths to determine a new $(FS)_{flow}$. This accounts for the potential for deformation-induced liquefaction and progressive failure of the structure. The minimum $(FS)_{flow}$ will be determined when liquefaction is triggered in all zones of contractive soil and assigned their liquefied shear strengths for the flow failure stability analysis.

Post-liquefaction behavior is characterized by a very complex process involving dissipation of excess pore water pressure, sedimentation, solidification and re-consolidation of the liquefied tailings resulting in large settlements of the deposit. If the results of the post-triggering stability analysis indicate $(FS)_{flow}$ below unity, then mitigation strategies are required. In tailings dams constructed using the upstream method, this approach consists basically in the maintenance of a large tailings beach extension, with adoption of rigid operational procedures of water control. For segments with $(FS)_{triggering} > 1.0$, the post-triggering analysis can be conducted in a similar way using yield shear strength.

Nevertheless, the reliability of any liquefaction evaluation depends directly on the quality of the site characterization, including mainly the quality of the in situ and/or laboratory test data.

Furthermore, it is often the synthesis of findings from several different procedures that provides the most insight and confidence in making final decisions. For this reason, the practice of using different testing methodologies constitutes the best approach for liquefaction analyses in tailings impoundments, so that semi-empirical methodologies based on back-analysis of field case studies involving slope failures are strongly recommended.

3. Case History: Córrego do Feijão Mine - Dam I

The liquefaction analysis methodology using the strength ratio approach proposed by Olson (2001) and Olson & Stark (2003b) was applied to a tailings impoundment located in the so-called *Quadrilátero Ferrífero* (Iron Quadrangle) region, located in the State of *Minas Gerais*, southeastern Brazil, corresponding to an area of about 7,000 km^2. This region is known worldwide for its immense deposits of iron ore, gold, manganese, and several other valuable minerals, which are mined by several industries, from large conglomerates up to countless small-to-medium-sized mining companies.

Dam I constitutes the tailings disposal system from the ore concentration plant of 'Córrego do Feijão', currently owned by Vale S.A. The dam was built using the upstream construction method with a starter dam comprised of fine ore and laterite. The impoundment has been in operation since 1976. Dam I had a maximum height of 81 m with nine raising dykes, built using tailings or compacted soil as construction materials (Fig. 3).

A large-scale investigation was conducted along the main cross-section of the dam (so-called 'reference section'- RS) involving conventional field testing (exploratory borings with standard penetration tests - SPT and cone pen-

Figure 3 - General view of Dam I - 'Córrego do Feijão' Mine.

etration tests - CPT). A total of 12 in situ tests were performed, with four couple SPT - CPT tests in adjacent points, and three SPT tests and one CPT test distributed in different points along the downstream slope of the dam (Fig. 4). In each of them, tailings samples were collected for laboratory tests.

In addition, an extensive laboratory test campaign was also developed in order to complete geotechnical characterization of the tailings, foundation materials and tailings impoundment, that are described and presented elsewhere (Pirete, 2010). The ore tailings from 'Córrego de Feijão' mine (CF tailings) generally consist of uniform fine silty sand (Fig. 5) containing about of 4% clay, 28% of silt,

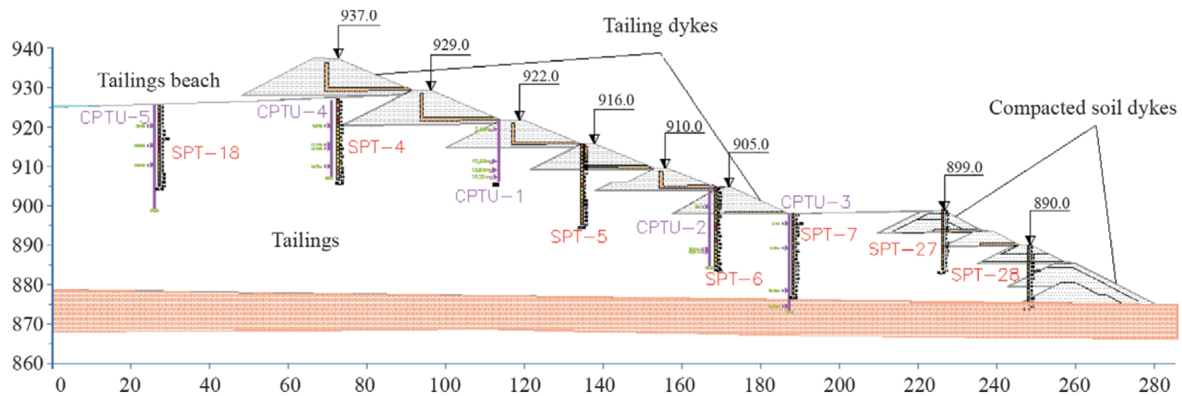

Figure 4 - Typical cross-section of the dam (RS section) and SPT and CPT locations.

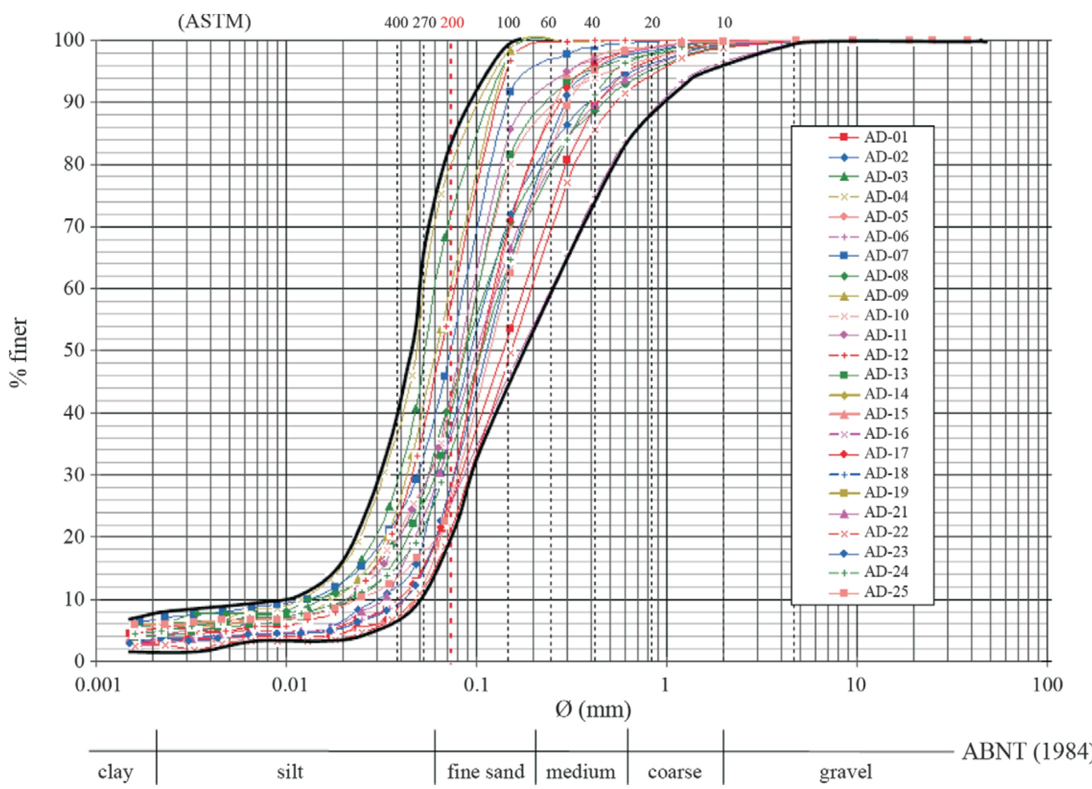

Figure 5 - Particle size distribution curves of CF tailings (ABNT, 1984).

56% of fine sand, 8% of medium sand, 3% of coarse sand and also 1% of gravel (ABNT, 1984). On the other hand, some strata tend to exhibit low plasticity ($w_L \leq 35\%$) with potential susceptibility to liquefaction mechanisms. The measured maximum void ratio was 1.47 and the minimum void ratio was 0.74. In tailings deposit, values of relative density index varied between 49% and 72%.

4. Liquefaction Analysis of CF Tailings Using Strength Ratios

4.1. CF tailings liquefaction susceptibility

As exposed previously, the first step in evaluating the potential for CF tailings liquefaction is to verify whether these residues are susceptible to undrained strain-softening behavior and flow failure (contractive or dilative behavior) by means of a susceptibility analysis using corrected SPT blowcount values or corrected CPT resistance tip values.

The measured SPT blowcount (N) is normalized for an energy level equal to 60% of the theoretical free-fall hammer energy applied to the drill system ($N_{60,}$ where ER is a called 'energy ratio') and for the overburden stress at the depth of the test (multiplying N_{60} by the overburden correction factor $C_N \leq 2.0$). The measured SPT blowcount is then corrected to a standardized value of $(N_1)_{60}$ as (Olson, 2001):

$$(N_1)_{60} = N\left(\frac{ER}{60}\right)\left(\frac{p_a}{\sigma'_{v0}}\right)^n = N\left(\frac{70}{60}\right)C_N \qquad (1)$$

where σ'_{v0} is the vertical effective stress at the depth of N and p_a is one atmosphere of pressure (approximately 100 kPa) in the same units as σ'_{v0}. The maximum value of 2.0 limits C_N at depths typically less than 1.5 m. The energy ratio ER should be measured for the particular SPT equipment used (70% in this study). Table 1 presents the corrected values for $(N_1)_{60}$ along the reference section of Dam I (CF - RS) for SPT-18, SPT-04, SPT-05, SPT-06 tests. Table 2 presents these factors for SPT-07, SPT-27 e SPT-28 tests.

The pairs of values $(N_1)_{60}$ and σ'_{v0}, calculated in Tables 3 and 4, were then correlated with the results of back-analysis of historical cases and with the Fear & Robertson (1995) boundary (Fig. 6), delineating field conditions susceptible and not susceptible to flow failure.

In the present analysis, CPT test results are also available, a fact that allows the review of susceptibility to liquefaction of CF - RS tailings based on corrected values of tip resistances, reevaluating the previous approach. However, unlike SPT tests, CPT tests include continuous records of the tailings deposit profile and then tip resistances values (q_c) only need to be corrected for vertical effective stress (q_{c1}).

The measured CPT tip resistance is then corrected to a standardized value of (q_{c1}) and is obtained as follows:

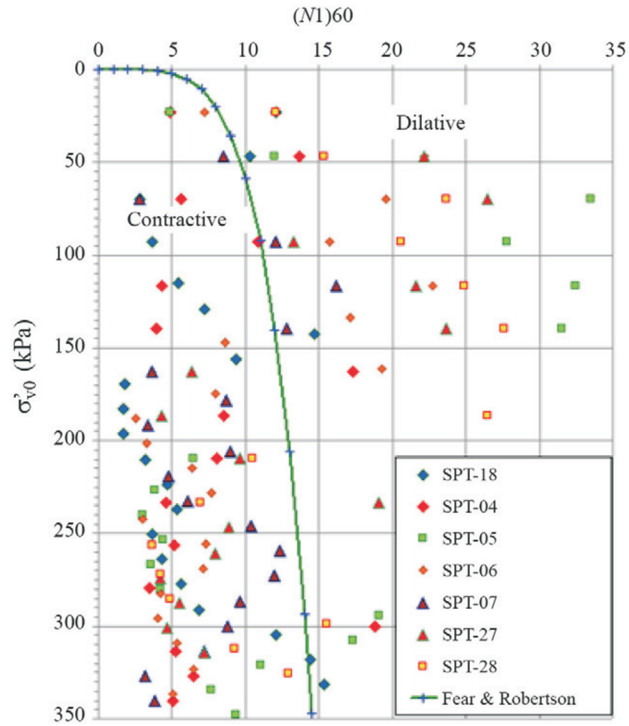

Figure 6 - Relationship $(N_1)_{60}$ *versus* σ'_{v0} for CF-RS tailings.

$$q_{c1} = C_q \cdot q_c = \frac{1.8}{0.8 + \left(\sigma'_{v0}/p_a\right)} \cdot q_c \qquad (2)$$

where σ'_{v0} is the vertical effective stress at the depth of (q_c) and p_a is one atmosphere of pressure (approximately 100 kPa) in the same units as σ'_{v0}. The factor C_q should be less or equal to 2.0 (Olson, 2001).

Table 3 presents the corrected values for (q_{c1}) along the reference section of Dam I from 'Córrego do Feijão' mine (CF - RS) for CPT-05, CPT-04 and CPT-01 tests and Table 4 presents these factors for CPT-027 and CPT-03 tests.

Similarly, the pairs of values (q_{c1}) and σ'_{v0}, calculated in Tables 3 and 4, were correlated with the results of back-analysis of historical cases and with the Fear - Robertson (1995) boundary (Fig. 7), delineating tailings susceptible and not susceptible to flow failure.

The results, in both the analysis of SPT and CPT analyses, demonstrate that the most points scored is located to the left of the Fear & Robertson boundary, corresponding to materials that tend to exhibit contractile behavior during shear, i.e., CF tailings liquefaction susceptibility is likely and this analysis should be complemented by the triggering analysis and post-triggering - flow failure stability analysis. For a better characterization of the tailings sub-layers susceptible to liquefaction, based on the SPT and CPT profiles, the authors of this paper developed a technique for further

Table 1 - Standardized values of $(N_1)_{60}$ for SPT-18, SPT-04, SPT-05, SPT-06 tests.

Depth. (m)	SPT - 18					SPT - 04					SPT - 05					SPT - 06				
	N	N_{60}	σ'_{vo} (kPa)	WT CN	4.90m $(N_1)_{60}$	N	N_{60}	σ'_{vo} (kPa)	WT CN	12.72m $(N_1)_{60}$	N	N_{60}	σ'_{vo} (kPa)	WT CN	9.33m $(N_1)_{60}$	N	N_{60}	σ'_{vo} (kPa)	WT CN	5.40m $(N_1)_{60}$
1	5	5.83	23.30	2.07	12.1	2	2.33	23.30	2.07	4.8	2	2.33	23.30	2.07	4.83	3	3.50	23.30	2.07	7.25
2	6	7.00	46.60	1.46	10.3	8	9.33	46.60	1.46	13.7	7	8.17	46.60	1.46	11.96	13	15.17	46.60	1.46	22.22
3	2	2.33	69.90	1.20	2.8	4	4.67	69.90	1.20	5.6	24	28.00	69.90	1.20	33.49	14	16.33	69.90	1.20	19.54
4	3	3.50	93.20	1.04	3.6	9	10.50	93.20	1.04	10.9	23	26.83	93.20	1.04	27.79	13	15.17	93.20	1.04	15.71
5	5	5.83	115.52	0.93	5.4	4	4.67	116.50	0.93	4.3	30	35.00	116.50	0.93	32.43	21	24.50	116.50	0.93	22.70
6	7	8.17	129.02	0.88	7.2	4	4.67	139.80	0.85	3.9	32	37.33	139.80	0.85	31.57	17	19.83	133.92	0.86	17.14
7	15	17.50	142.52	0.84	14.7	19	22.17	163.10	0.78	17.4	39	45.50	163.10	0.78	35.63	9	10.50	147.42	0.82	8.65
8	10	11.67	156.02	0.80	9.3	10	11.67	186.40	0.73	8.5	44	51.33	186.40	0.73	37.60	21	24.50	160.92	0.79	19.31
9	2	2.33	169.52	0.77	1.8	10	11.67	209.70	0.69	8.1	8	9.33	209.70	0.69	6.45	9	10.50	174.42	0.76	7.95
10	2	2.33	183.02	0.74	1.7	6	7.00	233.00	0.66	4.6	5	5.83	226.43	0.66	3.88	3	3.50	187.92	0.73	2.55
11	2	2.33	196.52	0.71	1.7	7	8.17	256.30	0.62	5.1	4	4.67	239.93	0.65	3.01	4	4.67	201.42	0.70	3.29
12	4	4.67	210.02	0.69	3.2	5	5.83	279.60	0.60	3.5	6	7.00	253.43	0.63	4.40	8	9.33	214.92	0.68	6.37
13	6	7.00	223.52	0.67	4.7	28	32.67	300.16	0.58	18.9	5	5.83	266.93	0.61	3.57	10	11.67	228.42	0.66	7.72
14	7	8.17	237.02	0.65	5.3	8	9.33	313.66	0.56	5.3	6	7.00	280.43	0.60	4.18	4	4.67	241.92	0.64	3.00
15	5	5.83	250.52	0.63	3.7	10	11.67	327.16	0.55	6.5	28	32.67	293.93	0.58	19.1	10	11.67	255.42	0.63	7.30
16	6	7.00	264.02	0.62	4.3	8	9.33	340.66	0.54	5.1	26	30.33	307.43	0.57	17.3	10	11.67	268.92	0.61	7.11
17	8	9.33	277.52	0.60	5.6	7	8.17	354.16	0.53	4.3	17	19.83	320.93	0.56	11.07	6	7.00	282.42	0.60	4.17
18	10	11.67	291.02	0.59	6.8	13	15.17	367.66	0.52	7.9	12	14.00	334.43	0.55	7.66	6	7.00	295.92	0.58	4.07
19	18	21.00	304.52	0.57	12.0	15	17.50	381.16	0.51	9.0	15	17.50	347.93	0.54	9.38	8	9.33	309.42	0.57	5.31
20	22	25.67	318.02	0.56	14.4	34	39.67	394.66	0.50	20.0	16	18.67	361.43	0.53	9.82	10	11.67	322.92	0.56	6.49
21	24	28.00	331.52	0.55	15.4	21	24.50	408.16	0.49	12.1	13	15.17	374.93	0.52	7.83	8	9.33	336.42	0.55	5.09

Table 2 - Standardized values of $(N_1)_{60}$ for SPT-07, SPT-27 e SPT-28 tests.

depth. (m)	SPT - 07					SPT - 27					SPT - 28			
	N	N_{60}	σ'_{vo} (KPa)	WT CN	7.20m $(N_1)_{60}$	N	N_{60}	σ'_{vo} (KPa)	WT CN	10.05m $(N_1)_{60}$	N	N_{60}	σ'_{vo} (KPa)	WT CN
1	17	19.83	23.30	2.07	41.09	21	24.50	23.30	2.07	50.76	5	5.83	23.30	2.07
2	5	5.83	46.60	1.46	8.55	13	15.17	46.60	1.46	22.22	9	10.50	46.60	1.46
3	2	2.33	69.90	1.20	2.79	19	22.17	69.90	1.20	26.51	17	19.83	69.90	1.20
4	10	11.67	93.20	1.04	12.08	11	12.83	93.20	1.04	13.29	17	19.83	93.20	1.04
5	15	17.50	116.50	0.93	16.21	20	23.33	116.50	0.93	21.62	23	26.83	116.50	0.93
6	13	15.17	139.80	0.85	12.8	24	28.00	139.80	0.85	23.68	28	32.67	139.80	0.85
7	4	4.67	163.10	0.78	3.65	7	8.17	163.10	0.78	6.39	45	52.50	163.10	0.78
8	10	11.67	178.56	0.75	8.73	5	5.83	186.40	0.73	4.27	31	36.17	186.40	0.73
9	4	4.67	192.06	0.72	3.37	12	14.00	209.70	0.69	9.67	13	15.17	209.70	0.69
10	11	12.83	205.56	0.70	8.95	25	29.17	233.00	0.66	19.1	9	10.50	233.00	0.66
11	6	7.00	219.06	0.68	4.73	12	14.00	246.99	0.64	8.91	5	5.83	256.30	0.62
12	8	9.33	232.56	0.66	6.12	11	12.83	260.49	0.62	7.95	6	7.00	271.76	0.61
13	14	16.33	246.06	0.64	10.4	6	7.00	273.99	0.60	4.23	7	8.17	285.26	0.59
14	17	19.83	259.56	0.62	12.3	8	9.33	287.49	0.59	5.50	23	26.83	298.76	0.58
15	17	19.83	273.06	0.61	12.00	7	8.17	300.99	0.58	4.71	14	16.33	312.26	0.57
16	14	16.33	286.56	0.59	9.65	11	12.83	314.49	0.56	7.24	20	23.33	325.76	0.55
17	13	15.17	300.06	0.58	8.76			327.99					339.26	
18	11	12.83	313.56	0.56	7.25			341.49					352.76	
19	5	5.83	327.06	0.55	3.23			354.99					366.26	
20	6	7.00	340.56	0.54	3.79			368.49					379.76	
21	4	4.67	354.06	0.53	2.48			381.99					393.26	

refinement of the data, according to the procedures described below.

4.2. CF-SR profile divided in tailings sub-layers susceptible to liquefaction

Initially, the values of the parameters $(N_1)_{60}$ were correlated with their respective elevations, in order to characterize the critical zones of potential liquefaction-induced flow along the tailings deposit, considering the domain limited by values of $(N_1)_{60} \leq 12$ (Eq. 5). The regions with average values of $(N_1)_{60} \leq 6$ were classified as zones of low resistance whereas the regions with average values of $6 < (N_1)_{60} \leq 12$ were classified as zones of medium resistance (Fig. 8).

This subdivision was extrapolated then for the CF - RS profile of the downstream slope of Dam I, resulting in nine layers susceptible to liquefaction (Fig. 9), with resistances given by the mean values obtained from the correspondent SPT profile zones.

Additionally, the values of the respective parameters (q_{c1}) were correlated with their elevations, in order to characterize the critical zones of potential liquefaction-induced flow along the tailings deposit, considering the domain limited by values of $(q_{c1}) \leq 6.5$ MPa (Eq. 6). The regions with average values of $(N_1)_{60} \leq 3.25$ MPa were classified as zones of low resistance whereas the regions with average values of 3.25 MPa $< (N_1)_{60} \leq 6.5$ MPa were classified as zones of medium resistance (Fig. 10).

This subdivision was extrapolated similarly to the CF - RS profile of the downstream slope of Dam I, resulting also in nine layers susceptible to liquefaction (Fig. 11), including SPT - 05 results for better characterization, with resistances given by the mean values obtained from the correspondent CPT profile zones.

The comparison between Figs. 9 and 11 indicates a good correlation of both geometries of the tailings deposit, with the characterization of nine layers that have a greater potential or susceptibility to liquefaction. The largest differences occurred for layers located near the edge of the intermediate dykes (layers 06, 07 and 08), both in terms of thickness and mean values of resistance. Based on this refined set of layers to the CF - RS profile of the downstream slope, the triggering analysis was then applied to the ore tailings deposited in Dam I from 'Córrego do Feijão' mine.

Table 3 - Standardized values of (q_{c1}) for CPT-05, CPT-04 and CPT-01 tests.

depth. (m)	CPT - 05					CPT - 04					CPT - 01				
	q_c (MPa)	σ'_{vo} (MPa)	σ'_{vo} (KPa)	WT Cq	4.90m q_{c1} (MPa)	q_c (MPa)	σ'_{vo} (MPa)	σ'_{vo} (KPa)	WT Cq	12.72m q_{c1} (MPa)	q_c (MPa)	σ'_{vo} (MPa)	σ'_{vo} (KPa)	WT Cq	13.20m q_{c1} (MPa)
1	1.903	0.02	23.30	1.74	3.32	3.48	0.023	23.30	1.74	6.1					
2	1.289	0.05	46.60	1.42	1.83	3.726	0.047	46.60	1.42	5.3	31.099	0.047	46.60	1.42	44.2
3	0.965	0.07	69.90	1.20	1.16	2.736	0.070	69.90	1.20	3.3	38.779	0.070	69.90	1.20	46.6
4	1.735	0.09	93.20	1.04	1.80	3.44	0.093	93.20	1.04	3.6	28.29	0.093	93.20	1.04	29.4
5	1.003	0.12	115.52	0.92	0.92	2.521	0.117	116.50	0.92	2.3	24.152	0.117	116.50	0.92	22.1
6	0.264	0.13	129.02	0.86	0.23	2.776	0.140	139.80	0.82	2.3	48.328	0.140	139.80	0.82	39.6
7	7.734	0.14	142.52	0.81	6.26	21.171	0.163	163.10	0.74	15.7	52.6	0.163	163.10	0.74	38.9
8	3.739	0.16	156.02	0.76	2.85	8.916	0.186	186.40	0.68	6.0	15.6	0.186	186.40	0.68	10.5
9	3.379	0.17	169.52	0.72	2.44	7.389	0.210	209.70	0.62	4.6	9.6	0.210	209.70	0.62	6.00
10	0.819	0.18	183.02	0.68	0.56	3.61	0.233	233.00	0.58	2.1	5.325	0.233	233.00	0.58	3.10
11	0.508	0.20	196.52	0.65	0.33	5.127	0.256	256.30	0.54	2.74	9.663	0.256	256.30	0.54	5.17
12	0.574	0.21	210.02	0.62	0.36	1.001	0.280	279.60	0.50	0.50	8.178	0.280	279.60	0.50	4.09
13	3.926	0.22	223.52	0.59	2.33	8.508	0.300	300.16	0.47	4.03	2.757	0.303	302.90	0.47	1.30
14	8.01	0.24	237.02	0.57	4.55	10.016	0.314	313.66	0.46	4.58	1.733	0.318	318.36	0.45	0.78
15	0.857	0.25	250.52	0.54	0.47	7.009	0.327	327.16	0.44	3.10	19.098	0.332	331.86	0.44	8.35
16	0.984	0.26	264.02	0.52	0.51	7.059	0.341	340.66	0.43	3.02	23.652	0.345	345.36	0.42	10.01
17	7.301	0.28	277.52	0.50	3.68	1.277	0.354	354.16	0.41	0.53					
18	16.419	0.29	291.02	0.49	7.97	4.455	0.368	367.66	0.40	1.79					
19	14.846	0.30	304.52	0.47	6.95	8.562	0.381	381.16	0.39	3.34					
20	14.997	0.32	318.02	0.45	6.78	26.112	0.395	394.66	0.38	9.90					
21	10.706	0.33	331.52	0.44	4.68										

Table 4 - Standardized values of (q_{c1}) for CPT-027 and CPT-03 tests.

depth. (m)	CPT - 02					CPT - 03				
	q_c (MPa)	σ'_{vo} (MPa)	σ'_{vo} (kPa)	WT Cq	5.40m q_{c1} (MPa)	q_c (MPa)	σ'_{vo} (MPa)	σ'_{vo} (kPa)	WT Cq	7.20m q_{c1} (MPa)
1	21.039	0.023	23.30	1.74	36.66	12.533	0.023	23.30	1.74	21.84
2	16.475	0.047	46.60	1.42	23.42	4.598	0.047	46.60	1.42	6.54
3	24.461	0.070	69.90	1.20	29.37	1.003	0.070	69.90	1.20	1.20
4	35.824	0.093	93.20	1.04	37.23	5.757	0.093	93.20	1.04	5.98
5	31.5	0.117	116.50	0.92	28.85	11.15	0.117	116.50	0.92	10.21
6	6.178	0.134	133.92	0.84	5.20	6.364	0.140	139.80	0.82	5.21
7	3.414	0.147	147.42	0.79	2.70	4.842	0.163	163.10	0.74	3.59
8	31.26	0.161	160.92	0.75	23.36	6.292	0.179	178.56	0.70	4.38
9	9.606	0.174	174.42	0.71	6.80	1.883	0.192	192.06	0.66	1.25
10	7.252	0.188	187.92	0.67	4.87	13.189	0.206	205.56	0.63	8.31
11	7.4	0.201	201.42	0.64	4.73	8.51	0.219	219.06	0.60	5.12
12	8.177	0.215	214.92	0.61	4.99	4.365	0.233	232.56	0.58	2.51
13	6.8	0.228	228.42	0.58	3.97	11.379	0.246	246.06	0.55	6.28
14	3.9	0.242	241.92	0.56	2.18	15.821	0.260	259.56	0.53	8.39
15	4.6	0.255	255.42	0.54	2.47	4.513	0.273	273.06	0.51	2.30
16	2.832	0.269	268.92	0.52	1.46	16.437	0.287	286.56	0.49	8.07
17	9.733	0.282	282.42	0.50	4.83	10.536	0.300	300.06	0.47	4.99
18	11.627	0.296	295.92	0.48	5.57	7.759	0.314	313.56	0.46	3.55
19	11.56	0.309	309.42	0.46	5.34	5.411	0.327	327.06	0.44	2.39
20	8.869	0.323	322.92	0.45	3.96	1.648	0.341	340.56	0.43	0.71
21						1.204	0.354	354.06	0.41	0.50

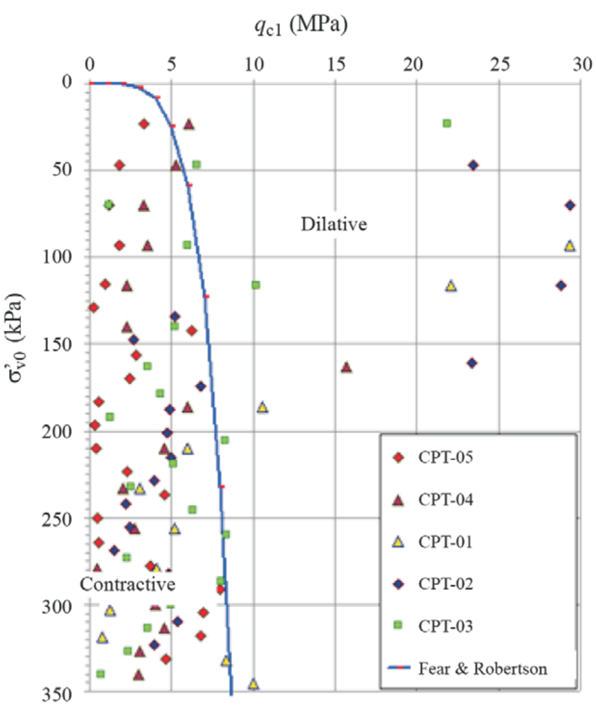

Figure 7 - Relationship (q_{c1}) *versus* σ'_{v0} for CF-RS tailings.

4.3. CF Tailings liquefaction triggering analysis

The methodology adopted for the triggering analysis included the following procedures (Olson and Stark, 2003b):

i From the liquefaction geometry of the reference section of the dam obtained from SPT test results (Fig. 9), limit equilibrium stability analyses were implemented using the method of Spencer (1967) and considering non-circular and circular surfaces (software Slide 5.043 from Rocscience International). Different values of shear strength were assumed for the soil layers susceptible to liquefaction, varying this resistance continually until obtaining FS = 1.0 and the corresponding critical surface rupture, defined for a critical value τ_d = 45 kPa (indicated in Fig. 9). The critical failure surface obtained in the analysis tends to extend from the seventh rising to the horizontal platform located between the third and fourth dykes (a 60 m displacement of the fourth dyke axle towards upstream was performed to improve general stability of the dam), crossing the layers 5 and 6 of the tailings sus-

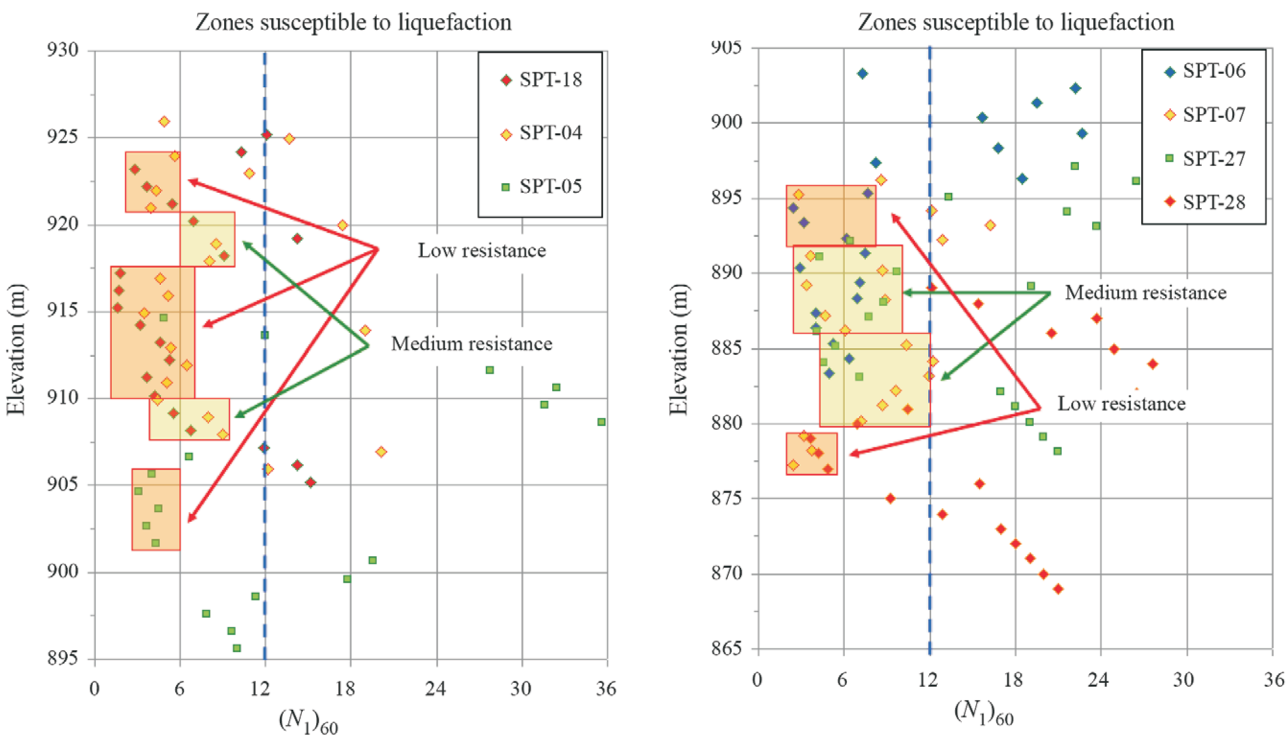

Figure 8 - RS - SPT profile divided in layers susceptible to liquefaction for $(N_1)_{60} \leq 12$.

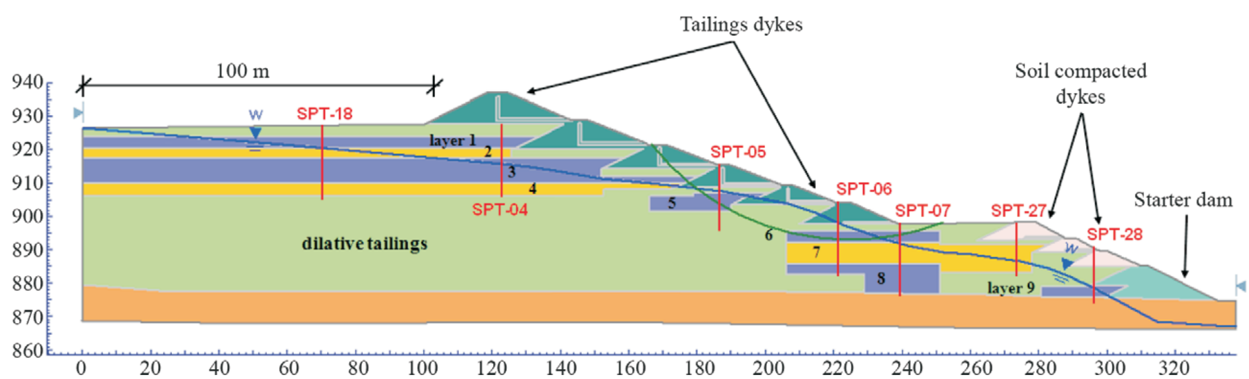

Figure 9 - CF - RS subdivided in nine layers susceptible to liquefaction (SPT analysis).

ceptible to liquefaction and that should therefore be subject to corresponding triggering analysis.

ii Division of the yield failure surface into 16 segments (Fig. 12)

iii From the determination of the weighted effective vertical stress, σ'_{v0} (Eq. 3), along the critical failure surface (within the domain of tailings susceptible to liquefaction), the average static shear stress ratio τ_d / σ'_{v0} (average value) was equal to 45 kPa / 217 kPa → 0.207.

iv Average seismic shear stress is not applicable in this case and then $(\tau_{sism})_{avg} = 0$.

v Table 5 presents the yield strength ratio values ($s_{u(yield)}/\sigma'_{v0}$) for layers 5 and 6 based on corrected SPT results.

The ratio values were used to obtain $S_{u(yield)}$ and τ_d for each segment based on respective σ'_{v0} values. For static loadings (Eq. 7), in this critical zone, the $(FS)_{triggering}$ is generally greater than 1.1 (typically varying between 1.14 and 1.21 as indicated in Table 6), indicating that CF - SR tailings are unlikely to liquefy.

Adopting the same methodology for the CPT results, the location of the critical surface rupture (for τ_d = 45 kPa)

Table 5 - Yield strength ratio values ($s_{u(yield)}/\sigma'_{v0}$) for layers 5 and 6 (SPT analysis).

Layers	$(N_1)_{60}$	$s_{u(yield)}/\sigma'_{v0}$
05	4.5	0.239
06	6.0	0.250

Table 6 - Liquefaction triggering results for CF - RS tailings (SPT analysis).

Segment N°	Liquefiable?	σ'_{vo} (kPa)	$(\tau_d)/\sigma'_{vo\ (average)}$	$s_u(yield)/\sigma'_{vo}$	s_u (yield)	$\tau_{driving}$ (τ_d)	$FS_{Triggering}$	Liquefaction triggered?
1	No	-	-	-	-	-	-	-
2	No	-	-	-	-	-	-	-
3	Yes	140.48	0.21	0.241	33.86	29.50	1.15	No
4	No	-	-	-	-	-		-
5	No	-	-	-	-	-		-
6	Yes	187.38	0.21	0.239	44.78	39.35	1.14	No
7	No	-	-	-	-	-	-	-
8	No	-	-	-	-	-	-	-
9	No	-	-	-	-	-	-	-
10	Yes	232.12	0.21	0.250	58.03	48.75	1.19	No
11	Yes	232.03	0.21	0.250	58.01	48.73	1.19	No
12	Yes	235.92	0.21	0.250	58.98	49.54	1.19	No
13	Yes	218.95	0.21	0.250	54.74	45.98	1.19	No
14	Yes	155.14	0.21	0.250	38.79	32.58	1.19	No
15	Yes	80.71	0.21	0.250	20.18	16.95	1.19	No
16	No	-	-	-	-	-	-	-

along the downstream slope of the tailings dam is indicated in Fig. 11 (crossing the layers 5 and 6 of the tailings susceptible to liquefaction), essentially similar to the previous critical surface (based on SPT results).

Considering its division into 16 segments and applying the steps (iii), (iv) and (v) from the methodology, were obtained the yield strength ratio values ($s_{u(yield)}/\sigma'_{v0}$) for layers 5 and 6 indicated in Table 7.

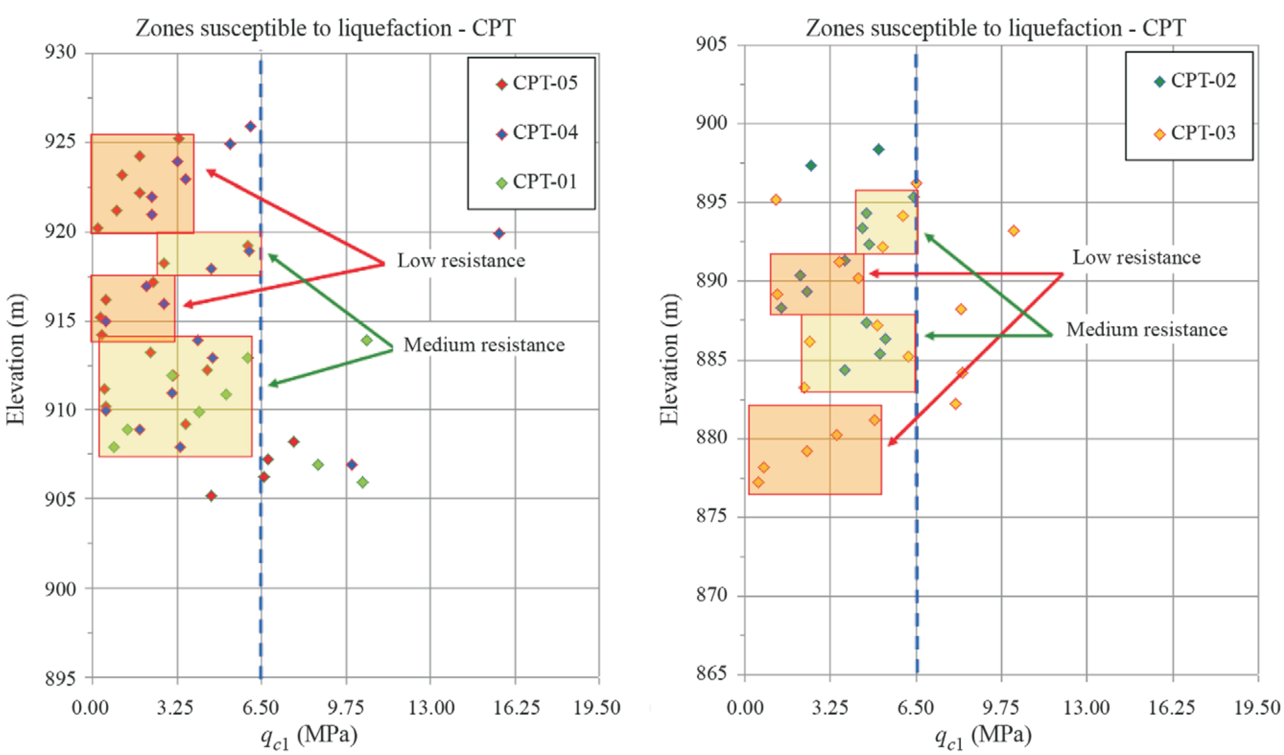

Figure 10 - RS - CPT profile divided in layers susceptible to liquefaction for $(q_{c1}) \leq 6.5$ Mpa.

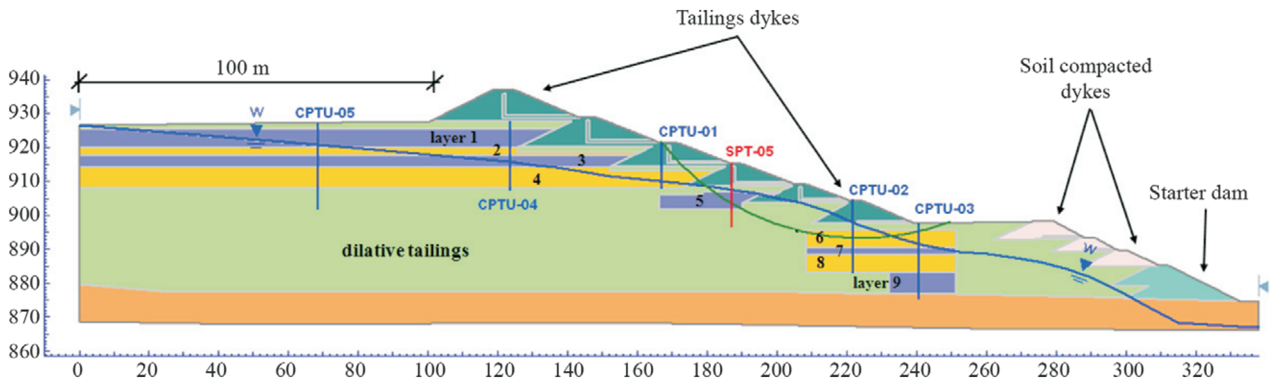

Figure 11 - CF - RS subdivided in nine layers susceptible to liquefaction (CPT analysis).

Table 7 - Yield strength ratio values ($s_{u(yield)}/\sigma'_{v0}$) for layers 5 and 6 (CPT analysis).

Layers	(q_{c1})	$s_{u(yield)}/\sigma'_{v0}$
05	4 5*	0.239
06	5.4 MPa	0.282

* $(N_1)_{60}$ parameter.

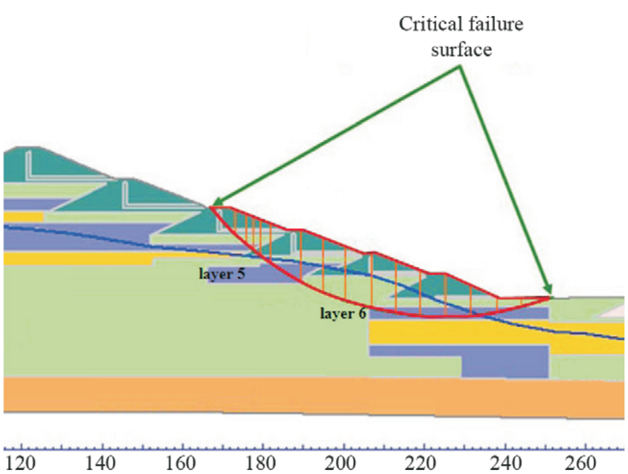

Figure 12 - Yield failure surface divided into 16 segments.

Once more, in the hypothesis of only static loading, the $(FS)_{triggering}$ is generally greater than 1.1 (typically varying between 1.15 and 1.36 as indicated in Table 8), indicating that CF - SR tailings are unlikely to liquefy.

4.4. CF Tailings liquefaction post-triggering analysis

In both triggering liquefaction analyses, using the results of SPT and CPT tests performed in the reference section of the Dam I, all segments from tailings critical zones have $(FS)_{triggering} > 1.0$ and then post-triggering stability analysis is unnecessary to verify whether the static shear forces exceed the available shear resistance (including liquefied shear strength). Nevertheless, a post-triggering slope stability analysis was appropriate since it was conducted using appropriate yield shear strength values instead of liquefied shear strength values.

Table 9 presents the geotechnical parameters used in stability analyses of the downstream slope. These parameters were obtained from a series of undrained triaxial compression tests performed under monotonic loading conditions on reconstituted samples of the tailings. All the specimens were isotropically consolidated at a mean effective pressure of 100 kPa, 200 kPa, 300 kPa and 400 kPa and then, subjected to undrained monotonic loading at a constant strain rate of 0.09 mm per minute, which was slow enough to allow the pore pressure change to equalize throughout the sample with pore pres-sure measured at the base of sample. All tests were con-tinued up to a 20% axial strain. The yield strength ratio values were taken from SPT results.

Phreatic surface location is one of the most important factors to influence tailings dam safety, under both static and seismic loading conditions (Vick, 1990). The major design premise is that the phreatic surface should not emerge from the embankment and should be as low as possible near the embankment face. Thus, any factors that might affect the phreatic surface affect directly the dam stability and can be caused by any changes in environmental or operating conditions (heavy rainfall, blockage of seepage outlets, rise in water levels of the pond, etc.)

For the post-triggering analysis, a rapid rise of the phreatic line was admitted through the tailings deposit emerging from the embankment and reaching the toes of the intermediate rising dykes, with complete saturation of tailings layers susceptible to liquefaction. The initial position of the phreatic line was given from readings given by dam piezometers and by a 100 m extension of the tailings beach. Figures 13 and 14 present the results of the stability analyses for a strong rise of the phreatic line in Dam I based on SPT and CPT configurations, respectively.

The results are closely similar in terms of the critical failure surface location and of the safety factor values against flow failure $(FS)_{flow}$ for SPT and CPT configurations (1.28 and 1.32, respectively). These values imply that the flow failure susceptibility of Dam I is low even under such

Table 8 - Liquefaction triggering results for CF - RS tailings (CPT analysis).

Segment N°	Liquefiable?	σ'_{vo} (kPa)	$(\tau_d)/\sigma'_{vo\ (average)}$	$s_u(yield)/\sigma'_{vo}$	s_u (yield)	$\tau_{driving}$ (τ_d)	$FS_{Triggering}$	Liquefaction triggered?
1	No	-	-	-	-	-	-	-
2	No	-	-	-	-	-	-	-
3	Yes	135 46	0 21	0 259	35 08	28 45	1 23	No
4	No	-	-	-	-	-	-	-
5	No	-	-	-	-	-	-	-
6	Yes	187 09	0 21	0 239	44 71	39 29	1 14	No
7	No	-	-	-	-	-	-	-
8	No	-	-	-	-	-	-	-
9	No	-	-	-	-	-	-	-
10	Yes	233 96	0 21	0 282	65 98	49 13	1 34	No
11	Yes	230 39	0 21	0 282	64 97	48 38	1 34	No
12	Yes	236 07	0 21	0 282	66 57	49 57	1 34	No
13	Yes	216 30	0 21	0 282	61 00	45 42	1 34	No
14	Yes	160 22	0 21	0 282	45 18	33 65	1 34	No
15	Yes	79 24	0 21	0 282	22 35	16 64	1 34	No
16	No	-	-	-	-	-	-	-

Table 9 - Geotechnical parameters for the post-triggering downstream slope stability analyses.

Material	y (kN/m^3)	C (kPa)	ø (°)	s_u (yield)/σ'_{vo}
Residual soil (foundation)	20	20	30	-
Starter dam (compacted soil)	20	5	36	-
Compacted soil	20	10	30	-
Compacted tailings	25	5	40	-
Dilative tailings	22	20	38	-
Layer 1	22	-	-	0.238
Layer 2	22	-	-	0.267
Layer 3 and 5	22	-	-	0.239
Layer 4	22	-	-	0.255
Layer 6 8 and 9	22	-	-	0.250
Layer 7	22	-	-	0.260

a critical loading event, based on the following proposed range to evaluate flow failure potential in these analyses:

- $(FS)_{flow}$ 3 1.5: → Unlike;
- $1.3 \leq (FS)_{flow} < 1.5$: → Low;
- $1.1 \leq (FS)_{flow} < 1.3$: → Moderate;
- $(FS)_{flow} < 1.1$: → High.

An extensive laboratory experimental program has been performed, including strain-controlled, undrained-triaxial tests to measure: (i) the peak undrained strength, (ii) the shear strain to peak undrained strength, and (iii) the drop-off in shearing resistance with continued strain after peak. Test specimens were con-solidated isotropically and anisotropically to stresses aiming to model in situ conditions. Based on these laboratory parameters, new stability analyses were performed and showed in good agreement with the results from the strength ratio analyses presented in this paper.

In addition, the management of the Dam I from 'Córrego do Feijão' has included a rigid water level control using both proper decanting and spigotting procedures to maintain a 100 m minimum distance between the pond's edge and the embankment crest, beyond a continuous program of inspection and maintenance of tailings deposition

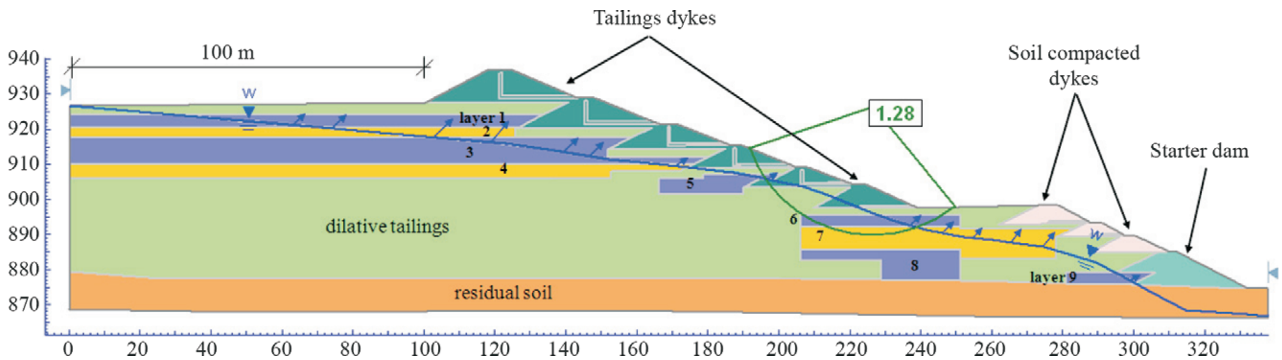

Figure 13 - CF - RS downstream slope: post-triggering stability (SPT analysis).

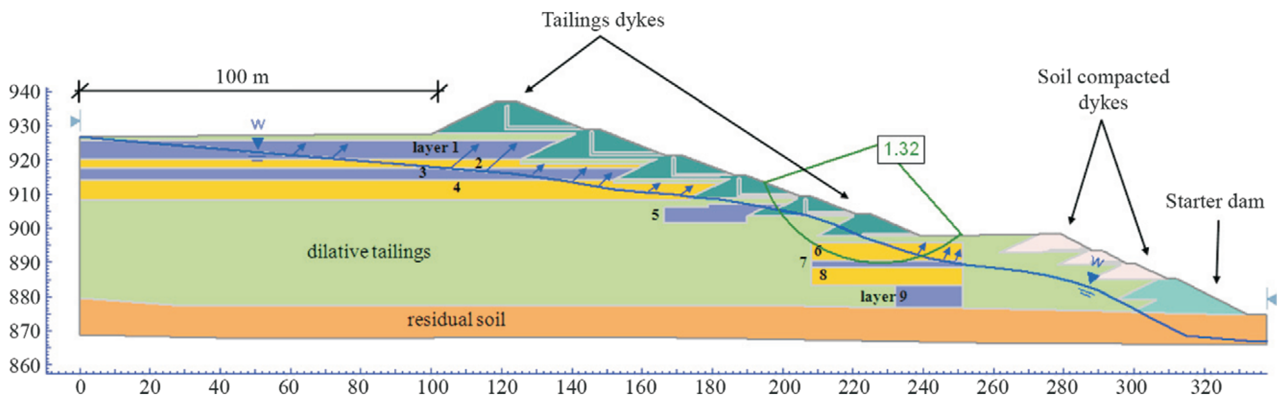

Figure 14 - CF - RS downstream slope: post-triggering stability (CPT analysis).

throughout the life of the dam by means of a very expert field technical crew.

5. Conclusions

Slope stability analyses involving liquefied soil require that the shear resistance of the softened soil be estimated. In light of the complex nature of excess pore pressure generation, large-strain development, and post-liquefaction strength gain accompanying drainage and large strain, most methods used in practice for estimating the residual strength of liquefied soil rely on back-analysis of field case studies involving slope failures. The most widely used methods based on SPT and CPT results. CPT's tests have the advantage that they are faster to perform and provide a con-tinuous, more reliable profile of penetration resistance.

In this context, Olson (2001) and Olson & Stark (2003b) liquefaction analysis, based on strength ratios approach, is too general, comprising three different approaches: (i) liquefaction susceptibility analysis; (ii) triggering analysis; and (iii) post-triggering - flow failure stability analysis. The method can be used to evaluate whether a specific loading (static or seismic) will produce shear stresses in a zone of a soil that is high enough to cause strength loss in that zone. The basic concept of the method is that strength loss will be triggered by a specific loading event if the sum of the static (gravity) shear stresses along a potential failure surface plus the eventual seismic (or other stresses) shear stresses exceed the yield (peak) undrained strength S_u (yield).

This liquefaction analysis procedure was applied to a Dam I from "Córrego do Feijão" mine, an 81 m high ore tailings disposal system (CF tailings), located in the *Quadrilátero Ferrífero* (Iron Quadrangle) region / Brazil, resulting in the following conclusions:

- CF tailings tend to exhibit contractile behavior during shear and then these materials are susceptible to liquefaction;
- The referenced subdivided section of the downstream slope of Dam I resulted in nine layers being susceptible to liquefaction with resistances given by the mean values obtained from both SPT or CPT profile zones;
- From the specific critical failure surfaces along the downstream slope of Dam I (obtained from SPT or CPT corrected values and subdivided into 16 segments), was obtained an average static shear stress ratio value (τ_d/σ'_{v0}) equal to 0,207 through the critical domain of tailings susceptible to liquefaction;
- In the hypothesis of only static loading, the $(FS)_{triggering}$ values varied between 1.14 and 1.36, indicating that CF - SR tailings are unlikely to liquefy;

- Considering a rapid rise of the phreatic line through the tailings deposit reaching the toes of the intermediate rising dykes, with complete saturation of tailings layers susceptible to liquefied, a post-triggering analysis indicated that the flow failure susceptibility of the Dam I is low even under a such critical loading event;
- The conclusions of these analyses, in addition to laboratory testing program results and based on rigid management procedures adopted in field, demonstrate that Dam I constitutes a safety structure against mechanisms from liquefaction-induced failures;
- Although the Olson (2001) and Olson & Stark (2003b) liquefaction analysis has been proposed mainly for cohesionless soils, the methodology is consistent and suitable for preliminary analyses of liquefaction potential in tailings deposits (generally relatively low- density materials with a high degree of saturation), particularly upstream tailings dams.

References

ABNT - NBR 7181 (1984) Solo - Análise Granulométrica (Grain Size Distribution). Brazilian Association of Technical Standards, Rio de Janeiro.

Aubertin, M.; Mbonimpa, M.; Bussiere, B. & Chapuis, R.P. (2003) A model to predict the water retention curve from basic geotechnical properties. Canadian Geotechnical Journal, v. 40:6, p. 1104-1102.

Bray, J.D.; Sancio, R.B.; Riemer, M. & Durgunoglu, H.T. (2004) Liquefaction susceptibility of fine-grained soils. Proc. 11th ICSD and 3th ICEGE, UC Berkeley, January 2004, pp. 7-9.

Byrne, P.M. (2008) Parecer Técnico (Technical Report), Mina do Cauê, Alteamento do Cordão Nova Vista, Complexo Minerador de Itabira. VALE, Itabira, Minas Gerais, 10 pp.

Casagrande, A. (1975) Liquefaction and cyclic deformation of sands - A critical review. Proc. 5th Pan-American Conference, Argentina, pp. 81-133.

Castro, G. (1975) Liquefaction and cyclic mobility of saturated sands. Journal of the Geotechnical Engineering Division, ASCE, v. 101:GT6, p. 551-569.

Davies, M.P.; McRoberts, E.C. & Martin, T.E. (2002) Static liquefaction of tailings - Fundamentals and case histories. Proc. Tailings Dams 2002. ASDSO/USCOLD, Las Vegas.

Fear, C.E. & Robertson, P.K. (1995) Estimating the undrained strength of sand: A theoretical framework. Canadian Geotechnical Journal, v. 32:4, p. 859-870.

Gomes, R.C. (2010) Mecânica da Liquefação dos Solos (Mechanics of Soil Liquefaction). NUGEO, Federal University of Ouro Preto, 112 pp.

Gomes, R.C.; Pereira, E.L.; Ribeiro, L.F.M. & Silva, J.T.G. (2002) Evaluation of liquefaction potential of fine grained tailings. Proc. International Congress on Environmental Geotechnics, ICEG, Rio de Janeiro. Swets and Zeitlinger, Netherlands, v. 1, p. 329-333.

ICOLD & UNEP (2001) Bulletin 121: Tailings Dams - Risk of Dangerous Occurrences. Lessons Learnt From Practical Experiences. Paris, ICOLD, 144 pp.

Idriss, I.M. & Boulanger, R.W. (2007) SPT- and CPT-based relationships for the residual shear strength of liquefied soils. Proc. Earthquake Geotechnical Engineering, 4th International Conference on Earthquake Geotechnical Engineering - Invited Lectures. K.D. Pitilakis, ed., Springer, The Netherlands, pp. 1-22.

Ishihara, K. (1993) Liquefaction and flow failure during earthquakes. Geotechnique, v. 43:3, p. 351-415.

Ishihara, K.; Yasuda, S. & Yoshida, Y. (1990) Liquefaction-induced flow failure of embankments and residual strength of silty sands. Soils and Foundations, v. 30:3, p. 69-80.

Kramer, S.L. (1996) Geotechnical Earthquake Engineering. Prentice Hall, Upper Saddle River, 653 pp.

Martin, T.E. (1999) Characterization of pore pressure conditions in upstream tailings dams. Proc. Tailings and Mine Waste '99, Fort Collins, Colorado, pp. 303-313.

Olson, S.M. & Mattson, B.B. (2008) Mode of shear effects on yield and liquefied strength ratios. Canadian Geotechnical Journal, p. 574-587.

Olson, S.M. (2001) Liquefaction Analysis of Level and Sloping Ground Using Field Case Histories and Penetration Resistance. Ph.D. Thesis, University of Illinois at Urbana-Champaign, Urbana III, 549 pp.

Olson, S.M. (2006) Liquefaction analysis of Duncan Dam using strength ratios. Canadian Geotechnical Journal, v. 43:5, p. 484-499.

Olson, S.M. & Stark, T.D. (2002) Liquefied strength ratio from liquefaction case histories. Canadian Geotechnical Journal, p. 629-647.

Olson, S.M. & Stark, T.D. (2003a) Use of laboratory data to confirm yield and liquefied strength ratio concepts. Canadian Geotechnical Journal, v. 40:6, p. 1164-1184.

Olson, S.M. and Stark, T.D. (2003b) Yield strength ratio and liquefaction analysis of slopes and embankments. ASCE Journal of Geotechnical and Geoenvironmental Engineering, v. 129:8, p. 727-737.

Pereira, E.L. (2005) Estudo do Potencial de Liquefação de Rejeitos de Minério de Ferro sob Carregamento Estático (Liquefaction Analysis of Iron Tailings Under Static Loading). Master Dissertation, Universidade Federal de Ouro Preto, Ouro Preto.

Pirete, W. (2010) Avaliação do Potencial de Liquefação Estática em Barragem de Rejeitos de Minério de Ferro com Base na Metodologia de Olson (Liquefaction Analysis of Iron Tailings Dams Using Olson Methodology). Master Dissertation, Universidade Federal de Ouro Preto, Ouro Preto.

Poulos, S.J.; Castro, G. & France, J.W. (1985) Liquefaction evaluation procedure. Journal of Geotechnical Engineering Division, ASCE, v. 111:6, p. 772-792.

Seed, H.B.; Tokimatsu, K.; Harder, L.F. & Chung, R. (1985) Influence of SPT procedures in soil liquefaction resistance evaluations. Journal of Geotechnical Engineering Division, ASCE, v. 111:12, p. 861-878.

Seid-Karbasi, M. & Byrne, P.M. (2004) Liquefaction, lateral spreading and flow slides. Proc. 57th Canadian Geotechnical Conf., Session 2c, pp. 23-30.

Sladen, J.A.; D'hollander, R.D. & Krahn, J. (1985) The liquefaction of sands, a collapse surface approach. Canadian Geotechnical Journal, p. 564-578.

Spencer, E. (1967) A method of analysis of the stability of embankments assuming parallel inter slice forces. Geotechnique, v. 17:1, p. 11-26.

Stark, T.D. & Mesri, G. (1992) Undrained shear strength of liquefied sands for stability analysis. Journal of Geotechnical Engineering, ASCE, v. 118:11, p. 1727-1747.

Troncoso, J.H. & Verdugo (1985) Silt content and dynamic behavior of tailings sands. Proc 11th ICSMFE, San Francisco, v. 3, pp. 131-1314

Vick, S.G. (1990) Planning, Design, and Analysis of Tailings Dams. 2nd edition. BiTech., Vancouver, 369 pp.

Yamamuro, J.A. & Lade, P.V. (1997) Effects of nonplastic fines on static liquefaction of sands. Canadian Geotechnical Journal, p. 918-928.

Yoshimi, Y.; Yanaka, K. & Tokimatsu, K. (1989) Liquefaction resistance of partially saturated sand. Journal of Soils and Foundations, v. 29:2, p. 157-162.

A Method for Predicting Pile Bearing Capacity From Dynamic Penetration Tests

F. Schnaid, M.J. Langone

Abstract. This paper presents a new method for predicting the axial capacity of piles from dynamic penetration tests which is based on the concepts of soil dynamics and principles of energy conservation. The energy delivered to the hammer-rod-sampler system and transferred to the soil is computed from the numbers of blow counts N_{spt} and is analytically converted in a penetration dynamic force. The dynamic force allows the unit resistance mobilized in the SPT sampler (model) to be determined, which is then used to predict the unit resistance mobilized in a prototype pile. The strong direct relationship between the ultimate resistance of driven steel piles and the SPT dynamic force, without any bias of soil type, validates the method. Extension of the method to other pile types requires empirical parameters to account for installation effects. Predictions of 89 instrumented static pile load test database demonstrate that the proposed methodology can be efficiently used in the assessment of axial pile capacity, providing a practical way of increasing reliability in pile design by accounting for effects controlling dynamic penetration.

Keywords: pile analysis, bearing capacity, penetration tests, energy conservation.

1. Introduction

The prediction of pile bearing capacity can be achieved using different methods of analysis such as interpretation of data from full-scale pile load tests, dynamic analysis and testing based on wave equations, static analysis based on soil properties and static analysis using the results of in situ tests. Given to the fact that penetration tests are used worldwide as the primary index test for site characterization, traditional methods of pile analysis and design often rely on empirical approaches based on SPT and CPT data (*e.g.* Bustamante & Giasenelli, 1982; Ruiter & Beringen, 1979; Aoki Velloso, 1975). These methods may produce inaccurate responses and unreliable predictions, because pile design depends on soil stratigraphy, pile characteristics, driving and installation methods, drainage and loading conditions. Applicability is therefore restricted to the database upon which the method has been developed and tested, and local experience and engineering judgment still plays an important role in pile analysis and design.

Among existing approaches, those established on the bases of SPT results receive severe criticism for their empirical nature, simplified assumptions, scattered predictions and discrepancies between predicted and measured loads. Although considerable literature is available on this matter, there is no single method of pile design based on dynamic penetration that has some theoretical background other than statistical.

Previous efforts have been made to estimate an average static resistance mobilized during sampler penetration (Schmertmann; 1979; Aoki *et al.*, 2004). An alternative method for the interpretation of dynamic penetration tests was proposed by Odebrecht *et al.* (2005) and Schnaid *et al.* (2008) from which the energy delivered to the rod string is used to calculate a dynamic force that represents the soil reaction to the penetration of the SPT sampler (F_d). Lobo (2007) used this dynamic force to develop an approach for predicting the axial bearing capacity of piles and Lobo *et al.* (2009) demonstrated the applicability of the approach by comparing measured and predicted ultimate loads from a database of 272 full scale load tests. Langone (2012) presented an independent assessment based on the interpretation of results from fully instrumented pile load tests. These results are presented in this paper and are used to validate a method for estimating the axial capacity of vertically loaded isolated piles.

2. Theoretical Developments

The proposed approach is based on the concepts of soil dynamics and principles of energy conservation. By computing the total energy delivered to the soil, Odebrecht *et al.* (2005) demonstrated that the potential energy (PE_{h+r}) has to be expressed as a function of the nominal potential energy (E^*), permanent sampler penetration ($\Delta\rho$) and weight of both hammer and rods, as well as three efficiency coefficients designed to account for energy losses during the energy transference process:

$$PE_{h+r} = \eta_3 \left[\eta_1 (0.75 + \Delta\rho) M_h g + \eta_2 \Delta\rho M_r g \right] \qquad (1)$$

where M_h is the hammer weight; M_r the rod weight; g the gravity acceleration; and η_1, η_2 and η_3 the efficiency coefficients. The nominal potential energy E^* represents a part of

Fernando Schnaid, PhD, Associate Professor, Departamento de Engenharia Civil, Universidade Federal do Rio Grande do Sul, Porto Alegre, RS, Brazil. e-mail: fernando@ufrgs.br.
Marcelo Júlio Langone, MSc, Civil Engineering, Petrobras Transporte S.A., Rio de Janeiro, RJ, Brazil. e-mail: marcelolangone@hotmail.com.
Submitted on April 9, 2012; Final Acceptance on March 1, 2013; Discussion open until August 30, 2013.

the hammer potential energy to be transmitted to the soil. An additional hammer potential energy is given by $M_h\, g\, \Delta\rho$ and the other part is transmitted by the rod potential energy $M_r\, g\, \Delta\rho$ which cannot be disregarded for tests carried out at great depths in soft soils, *i.e.* conditions in which $\Delta\rho$ and M_r are significant. Equation 1 requires a previous calibration of efficiency coefficients, which as a preliminary estimate for Brazilian SPT configurations can be assumed as $\eta_1 = 0.76$; $\eta_2 = 1$ e $\eta_3 = (1\text{-}0.0042l)$, where l is the total rod length, (Odebrecht *et al.*, 2005). Note that η_3 is adimensional, so the number before l has a m^{-1} dimension.

Since Eq. 1 gives the energy effectively delivered to the soil, with all losses accounted for by means of the efficiency coefficients, it is in principle possible to use this potential energy to calculate the mean dynamic reaction force (F_d) applied to the soil during sampler penetration (Schnaid *et al.*, 2007; Schnaid *et al.*, 2004; Schnaid, 2005):

$$F_d = \frac{\eta_3\eta_1(0.75M_h g) + \eta_3\eta_1(\Delta\rho M_h g) + \eta_3\eta_2(\Delta\rho M_r g)}{\Delta\rho} \qquad (2)$$

The sampler-soil interaction model is therefore represented by a dynamic mean reaction force that is calculated from the work produced by the non-conservative forces derived from the potential energy produced by the hammer-rod-sampler system.

The dynamic force F_d can now be used as an input value to compute the pile axial load by combining bearing capacity theory to the principles of cavity expansion. The ultimate axial load capacity of the pile (Qu) is the sum of two components: the end-bearing capacity (Q_p) and the shaft friction capacity (Q_L), which can be expressed as:

$$Q_u = Q_P + Q_L = A_p q_p + U\int_0^L f_l\, dL = A_p q_P + U\sum f_{l,i}\Delta L \qquad (3)$$

where q_p is the unit end bearing resistance, f_l local shaft friction, U the perimeter of the pile, A_p the area of the pile base and ΔL a pile length segment. Unlikely the cone, where the tip resistance q_c shows strong correlation with q_p and f_l, the dynamic force F_d has to be interpreted in order to estimate these two variables. Interpretation does not include specific considerations regarding the drainage paths around the penetrating sampler.

2.1. End-bearing

Estimating end bearing requires specific considerations regarding the mode of penetration of the sampler. Ideally a simple inspection of the soil plug inside the sampler is sufficient to identify whereas plugged or unplugged penetration has taken place at the depth of the pile tip. However this is not done in current investigation practice and, for the sake of simplicity, the proposed method was developed for piles embedded in stiff soils where sampler penetration is generally plugged (implying that floating piles would require different treatment). Plugged penetration is an assumption of the proposed methodology; other assumptions can be made within the same framework of energy propagation and energy conservation principles leading to slightly different results.

In a plugged penetration mode, the dynamic force is the sum of two terms: shaft friction and end-bearing resistance. By combing bearing capacity to cavity expansion (Vésic, 1972) it is possible to calculate the relative contribution of these two terms for a set of typical parameters. Use of Vésic's formulation follows recommendations from Eurocode 7 (1997) and API RP2A (2000). A parametric analysis demonstrates that end-bearing corresponds to 60% to 80% of the measured penetration force (Lobo *et al.*, 2009) which justifies considering the SPT bearing resistance $q_{p,spt}$ as 70% of the total measured penetration force:

$$q_{p,spt} = \frac{F_{d,p}}{a_p} = \frac{0.7\,F_d}{a_p} \qquad (4)$$

being a_p the area of the sampler base ($\pi 5.1^2/4 = 20.4\ cm^2$).

Extrapolating measurements from penetration tests to real scale pile load test data is therefore a direct process that is not biased by soil conditions, pile length (L), pile diameter (D) and pile aspect ratio (L/D). In doing so, a recommendation is made to calculated F_d from the average N value taken in the zone of 2.0 pile diameters (D) above and below the pile tip, which is consistent to previously reported studies in both SPT and CPT interpretation data (*e.g.* Bazaraa & Kurkur, 1986; Briaud & Tucker, 1988; Xu & Lehane, 2005).

2.2. Shaft friction

The shaft friction calculated by the SPT ($f_{l,spt}$) is simply the dynamic force divided by the inner and outer areas of the sampler, expressed as:

$$f_{l,spt} = \frac{F_d}{a_l} \qquad (5)$$

being a_l the area of the sampler shaft. In this case, friction components mobilized inside and outside the sampler are considered to be the same. This assumption has been numerically evaluated by Lobo (2010) and it is believed to reproduce the basic mechanism that takes place during penetration in soft and loose materials.

The measured values of $f_{l,spt}$ can then be integrated along depth to estimate the actual pile shaft, and by doing so a number of simplified considerations are necessary:

i the sampler shaft friction has been shown to be much greater than the actual pile shaft friction due to what has been generally recognized as scale effects. These effects need to be considered when extrapolating measurements from penetration tests to real scale pile load test data, as already established by previous interpretation methods using SPT and CPT results (*e.g.* De

Ruiter & Beringem, 1979; Bustamante & Gianeselli, 1982). Lobo *et al.* (2009) proposed reducing $f_{l,spt}$ by a factor of 0.2 based on a comprehensive analysis comprising 271 real scale pile load tests. Della Rosa (2009) observed scale effects of the same other of magnitude when performing tests using SPT with diameters ranging from 3.6 to 7.2 cm. Langone (2012) confirmed these observations when interpreting instrumented pile load tests;

ii the shaft friction developed on a pile in tension is smaller than that mobilized by a pile loaded in compression (*e.g.* Lehane *et al.*,1993; de Nicola & Randolph (1993); Jardine *et al.*, 2005; Lehane *et al.*, 2007). This effect is not considered in the current analysis which implies that the predicted friction resistance corresponds to a pile loaded in compressions and should be reduced for a pile under tension;

iii in driven piles, the shaft capacity is known to habitually increase with time (*e.g.* Axelsson, 1998; Jardine *et al.*, 2005a; Lehane *et al.*, 2005a. Data considered in the present analysis generally represents long term conditions where installation effects have been partially settled;

iv strains in the pile that have been mobilized before the start of the test due to residual load must be considered, and in cases where these values are reported the residual loads were adjusted before establishing the true load distribution (*i.e.* the true load is, mainly, the sum of the installation load distribution - locked in stresses - with the load measured during the load test);

The reasoning for these simplifying assumptions is to keep the method simple and straightforward for application in design, but it does not restrain future modifications within the same framework (that could be easily implemented).

In summary, the contributions of both end-bearing and shaft friction can be computed directly from the penetration force and the general formula for calculating the ultimate axial load capacity of the pile (Eq. 3) becomes:

$$Q_U = Q_L + Q_P = \frac{0.2U}{a_l} \sum F_d \Delta L + 0.7 F_d \frac{A_p}{a_p} \qquad (6)$$

The 0.2 value in Eq. 6 accounts for scale effects. In this general formula, a dynamic force is used to compute the static long term capacity of a pile which implies on disregarding visco-effects and pore-water pressures generated during the dynamic penetration of the sampler. As in all SPT-based methods ignoring these effects may induce errors in low permeable soils such as clays and silts. Since design procedures mainly involve considering the long term pile capacity, SPT data can be generally applied to sands, non-cohesive granular soils and most residual soil formations.

3. Database

An extensive search in the literature was conducted by Langone (2012) to identify instrumented pile load test publications with SPT penetration soundings adjacent to tested piles. A database of 89 instrumented incremental static load tests in different soil formations has been carefully reviewed in order to evaluate their suitability for the current research, considering availability of proper documentation on the pile data (installation and testing), subsurface exploration and general geotechnical laboratory and *in situ* testing data. Although all piles were subjected to static load tests, the loading procedure changed considerably reflecting local practice and standards, introducing errors and uncertainties to the overall analysis.

The ultimate axial load capacity for each pile was determined using the criterion recommended by the Brazilian Standard NBR 6122:2010, as illustrated in Fig. 1. Tests were chosen for their high degree of mobilization of pile capacity and the availability of reliable load-settlement relationships. However in several cases the *Vander der Veen* method (1953) had to be used to extrapolate the measured load-settlement curve of pile load tests that have not reached the required displacement of D/30 plus the elastic deformation of the pile.

Besides the proposed method, other semi-empirical and theoretical methodologies were employed for comparison purposes. The semi-empirical methods reflect the Brazilian engineering practice of foundation design: Aoki & Velloso (1975) and Décourt & Quaresma (1978). Since these methods were developed in Brazil, the energy efficiency is assumed to be of the order of 75%.

The theoretical approach uses bearing capacity theory associated with cavity expansion (Vésic, 1972). Vesic's approach to cavity expansion applied to cohesive-friction soils introduces some minor errors to the analysis because it does not consider the effect of cohesion in inhibiting dilation, as demonstrated by Mantaras & Schnaid (2002) and Schnaid & Mantaras (2003).

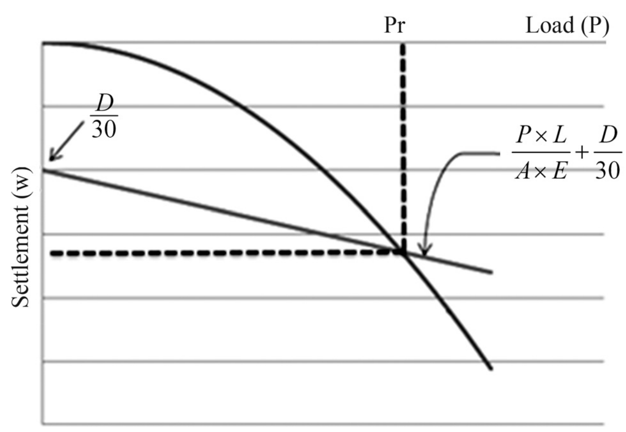

Figure 1 - Ultimate load based on the Brazilian Standard NBR 6122:2010.

When laboratory tests or soil parameters were not reported, SPT correlations were employed to estimate the friction angle (ϕ) and the Clam-Clay model ($S_u = 0.25\ \sigma'_v$) used to estimate the undrained shear strength.

4. Prediction and Performance

The ultimate axial load capacity of the pile predicted by dynamic penetration methods (Q_U) is compared to the measured pile capacity as obtained from the instrumented pile load tests using the Brazilian NBR 6122 failure criterion. By doing so, the predictive performance is presented and discussed. A summary of essential information related to the pile tests is shown in Table 1, including the pile size, type, length, location of the load test, the measured and predicted ultimate axial load capacity.

Initially the analysis concentrates on driven piles. End-bearing capacity (Q_P) and shaft friction capacity (Q_L) are computed from the measured data, as illustrated in Fig. 2 for a load test carried out in Brazil and reported by Falconi & Perez, (2008). This figure presents the load-settlement curve measured at the pile head and the actual load distribution along the pile at the final loading stage, as well as the SPT profile representative of ground conditions. The subsoil consists of a superficial 10 m thick fine silty sand layer, medium to dense, overlain a thick soft to very soft marine silty clay. Residual soil is encountered below 51 m depth. The tested H-pile was instrumented by strain gages placed at selected levels to determine the load distribution for each load applied to the pile head. Comparisons of measured and predicted loads cover the 4 methods used as reference in the present study. In this particular case, the the proposed method and the theoretical approach slightly underestimate the skin friction distribution whereas the semi- empirical methods overestimate the measured data.

Once the interpretation of each load test was completed, the measured and predicted values of Q_P, Q_L and Q_U were directly compared, as shown in Figs. 3, 4 and 5, respectively. In steel driven pile predictions, a limiting value of $N_{60} \leq 100$ was arbitrarily adopted.

Important observations derived from analysis can be summarized as follows:

- The proposed method predicts measured capacity values that are in general agreement with Brazilian practice;
- As previously stated, the method relies entirely on wave propagation and energy conservation, requiring a single empirical factor to account for scale effects;
- The arithmetic average and standard deviation of *measured* Q_m and *predicted* Q_P, Q_L and Q_U are indicators of the accuracy and precision of the prediction method. The proposed approach with average (QL/Qm) = 0.64 and deviation = 0.30 shows conservative estimated skin friction values with the lowest deviation when compared to other methods. Although Q_P is highly scattered, with average (QP/Qm) = 1.85 and deviation = 1.52, ultimate loads with average (QU/Qm) = 0.96 and deviation = 0.47 gives the best estimates. More importantly, in the proposed approach scatter could be reduced in the future by calibrating the SPT to derive local η efficiency factors (since average values have been used in the present analysis);

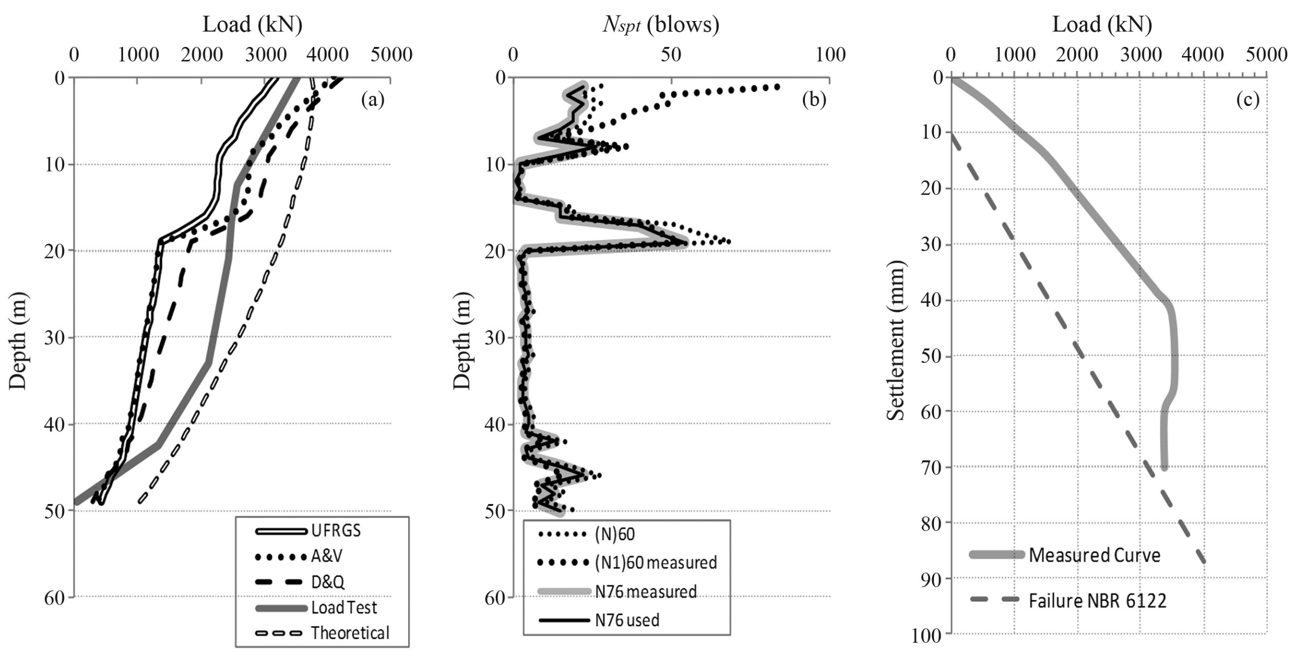

Figure 2 - Instrumented pile load test (a) predicted and measured load distribution (b) SPT profiles (c) load-settlement curve (adapted from Falconi & Perez, 2008).

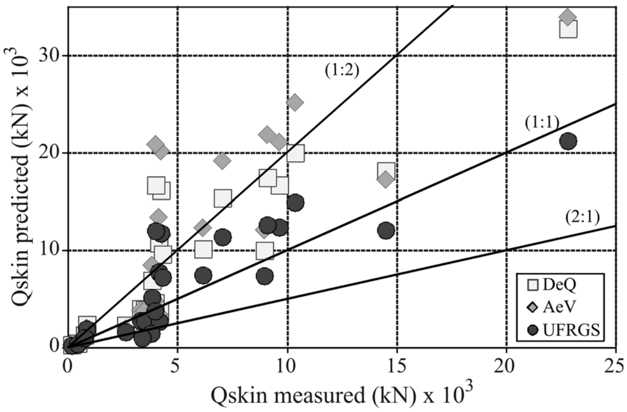

Figure 3 - Comparison of measured and predicted skin friction for steel piles.

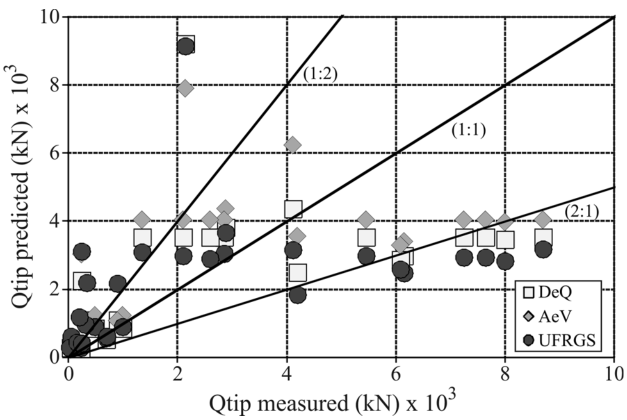

Figure 4 - Comparison of measured and predicted tip resistance for steel piles.

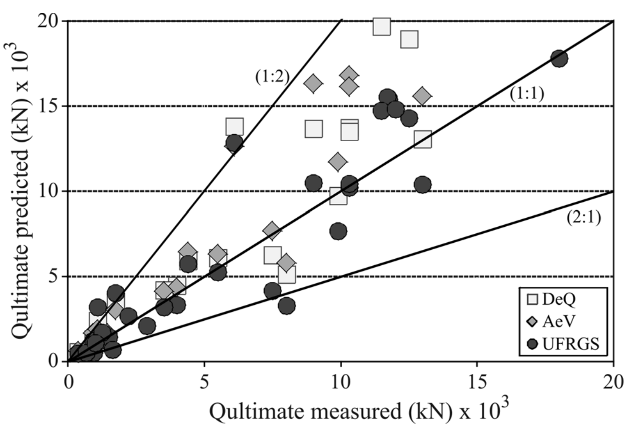

Figure 5 - Comparison of measured and predicted ultimate load for steel piles.

- The predictions of shaft resistance are much less scattered than predictions of end-bearing resistance. Errors in interpreting the measured values of end-bearing may be attributed to misleading evaluation of closed and open-ended piles, as well as the insufficient displacements at the pile tip during load tests to mobilize full end-bearing resistance;
- The proposed method shows no apparent bias of measured and predicted data with pile length (L), pile diameter (D), pile aspect ratio (L/D) and (more importantly) soil type. The principle of energy conservation combined to wave propagation analysis captures the influence of soil type.

5. Other Pile Types

The shaft friction and end-bearing resistance that can be developed on a pile are essentially related to the method of installation that dictates the magnitude of soil displacements and mobilized effective radial stresses. Embed on predicting the response of driven steel piles there is the assumption that q_p and f_l strongly correlates with F_d (or N_{spt}) since the mechanism of penetration, the large mobilized displacements imparted during installation and the interface friction angle shown some degree of similarity. Therefore variations in pile capacity developed by concrete driven piles, bored piles and continuous flight auger piles cannot be assessed from the same penetration measurement (being a SPT, LPT or CPT).

Extension of the approach to pile types other than driven steel piles requires two empirical factors, one for a proper evaluation of mobilized shaft friction and another for mobilized end bearing resistance:

$$Q_U = \alpha Q_L + \beta Q_P = \alpha \frac{0.2U}{a_l} \sum F_d \Delta L + 0.7 \beta F_d \frac{A_p}{a_p} \qquad (7)$$

where α and β are the pile type coefficients listed in Table 2 established from linear regression analysis (Lobo, 2005; Langone, 2012). Driven steel piles adopted as reference due to their similarity to SPT sampler penetration are represented by unitary values of α and β. Considering penetration restrain in hard layers and SPT reliability in case of discrete anomalies (localized high penetration values), the N_{spt} was arbitrarily limited according to values listed in Table 3.

Measured and predicted Q_P, Q_L and Q_U values are compared in Figs. 6 to 14 for precast concrete driven piles, bored piles and continuous flight auger piles. The following general conclusions can be drawn:

- *Precast concrete driven piles* have higher α coefficient than steel piles, reflecting the different nature of pile-soil friction interface. On average, predicted values of skin friction are of the same order of magnitude of measured loads, but slightly on the conservative side, *i.e.* predicted loads fall below the 1:1 best fit line for the predicted/measured pile capacities;
- Pedicted values of tip resistance show considerable scatter and a tendency to overestimate the measured resistance. Although this comparison may induce β values slightly lower than 1.1, the proposed value is justified by

Table 1 - Summary of instrumented steel pile test data.

Ref. / Fig.	Pile		Measured			UFRGS method						W_{lt}/W_{ult}	Observations	Similarity	Reference	Average N_{60} (Shaft)	Average N_{60} (point)	Shaft material	Tip material
						Predicted			Predicted/Measured										
	L	Φ	Qskin	Qtip	Qult	Qskin	Qtip	Qult	Qskin	Qtip	Qult								
1	48	0.30	3299	701	4000	2785	568.3	3354	0.8	0.8	0.8	0.6	H, variable section, SML, BRA		Gerdau, not published	11	18	MULT	silty sand
2	7	0.36	435	495	930	333.4	904.3	1238	0.8	1.8	1.3	2.4	OP, SML, residual loads considered, EUA	A	Paik *et al.*, 2003	14	22	gravelly sand	gravelly sand
3	49	0.31	3490	40	3530	2758	431.6	3190	0.8	10.8	0.9	1.6	H, variable section, QML, BRA		Falconi & Perez, 2008	10	12	MULT	RS sandy silt
4	9	0.27	154,9	225,2	380	195.8	285.1	480.9	1.3	1.3	1.3	1.5	CP, η_1 = 40%, EUA		Briaud & Tucker, 1989	8	10	sand	sand
5	7	0.36	455	995	1450	333.4	904.3	1238	0.7	0.9	0.9	2.5	CP, SML, residual loads considered, EUA	A	Paik *et al.*, 2003	13	22	gravelly sand	gravelly sand
6	17	0.35	845	905	1750	1870	2177	4047	2.2	2.4	2.3	2.3	H, SML, residual load considered, EUA		Seo *et al.*, 2009	20	69	MULT	silty clay
7	55	0.43	4148	6152	10300	7720	2486	10206	1.9	0.4	1.0	0.8	H, SPT extrap., CHN	B	Yu, 2008	37	145	RS silty sand	RS silty sand
8	40	0.45	3813	6088	9900	5097	2580	7677	1.3	0.4	0.8	1.3	H, SPT extrap., CHN	B	Yu, 2008	27	94	RS silty sand	RS silty sand
9	80	1.50	22800	16200	39000	21230	35657	56887	0.9	2.2	1.5	1.0	OP, QML, SPT extrap, JPN	C	Kikuchi, *et al.*, 2007	23	68	clay + sand	sand
10	66	1.50	14500	16000	30500	12041	38445	50486	0.8	2.4	1.7	1.3	OP, QML, SPT extrap, JPN	C	Kikuchi, *et al.*, 2007	15	68	clay	sand
11	36	0.61	4160	240	4400	2640	3117	5757	0.6	13.0	1.3	1.1	conical toe, TWN, QML, residual loads considered		Yen, 1989	13	30	sand+clay	sand
12	33	0.61	2620	2880	5500	1577	3666	5243	0.6	1.3	1.0	0.1	CP, SINGAPORE		Moh, 1994	8	43	sand	silty sand
13	15	0.70	3961	2139	6100	3717	9127	12844	0.9	4.3	2.1	0.5	OP, BRA		Lopes, 1986	34	71	MULT	silty sand
14	41	0.60	3800	4200	8000	1428	1842	3270	0.4	0.4	0.4	0.4	OP, bitumen 26.0 m, JPN	D	Gyoten *et al.*, 1982	7	20	sand+clay	MUL
15	38	0.60	3380	4120	7500	1016	3155	4171	0.3	0.8	0.6	0.4	OP, bitumen 26.0 m, JPN	D	Gyoten *et al.*, 1982	16	42	sand+clay	MUL
16	17	0.36	755	345	1100	1008	2183	3191	1.3	6.3	2.9	2.8	CP, EUA		Kim *et al.*, 2009	20	87	MULT	silty clay
17	52	0.37	9655	2100	11755	12389	2985	15374	1.3	1.4	1.3	1.0	H, SPT extrap., residual loads considered, HKG	E	Zhang & Wang, 2007	61	118	MULT sand	RS silty sand
18	45	0.37	8950	1350	10300	7345	3084	10429	0.8	2.3	1.0	1.0	H, SPT extrap., residual loads considered, HKG	E	Zhang & Wang, 2007	36	118	MULT sand	RS silty sand
19	48	0.37	6150	2850	9000	7451	3042	10493	1.2	1.1	1.2	1.2	H, SPT extrap., residual loads considered, HKG	E	Zhang & Wang, 2007	35	118	MULT sand	RS silty sand
20	59	0.37	9100	2600	11700	12606	2885	15491	1.4	1.1	1.3	1.0	H, SPT extrap., residual loads considered, HKG	E	Zhang & Wang, 2007	53	118	MULT sand	RS silty sand
21	39	0.37	4300	8700	13000	7232	3169	10400	1.7	0.4	0.8	1.0	H, SPT extrap., residual loads considered, HKG	E	Zhang & Wang, 2007	41	118	MULT sand	RS silty sand
22	56	0.37	4250	7250	11500	11775	2928	14703	2.8	0.4	1.3	0.7	H, SPT extrap., residual loads considered, HKG	E	Zhang & Wang, 2007	48	118	MULT sand	RS silty sand
23	53	0.37	7050	5450	12500	11324	2971	14295	1.6	0.5	1.1	0.8	H, SPT extrap., residual loads considered, HKG	E	Zhang & Wang, 2007	55	118	MULT sand	RS silty sand
24	60	0.37	4000	8000	12000	11977	2831	14808	3.0	0.4	1.2	0.7	H, SPT extrap., residual loads considered, HKG	E	Zhang & Wang, 2007	39	79	MULT sand	RS silty sand
25	56	0.37	10350	7650	18000	14861	2928	17789	1.4	0.4	1.0	0.4	H, SPT extrap., residual loads considered, HKG	E	Zhang & Wang, 2007	69	118	MULT sand	RS silty sand

W_{ult} = settlement at ultimate load (mm). SML = slow maintain load. CP = closed pipe pile. Loads in kN.
W_{lt} = load test maximum settlement (mm). QML = quick maintain load. OP = opened pipe pile. Dimensions in meters.
H = "H" section pile. SPT extrap. = extrapolated SPT. MULT = multilayered soil. RS = residual soil.

back-analysis of non-instrumented load tests (Lobo, 2007) and by the fact that the measured value may not truly represent the ultimate resistance given the large displacements required for full mobilization;

- *Bored piles* mobilize the lowest α and β coefficients when compared to other pile types, due to stress relieving

Table 2 - Coefficients α and β for pile bearing capacity analysis.

Pile type	α	β
Precast concrete driven pile	1.5	1.1
Steel driven pile	1.0	1.0
Continuous flight auger pile	1.0	0.6
Bored pile	0.7	0.5

Table 3 - N_{spt} limits.

Pile type	N_{60} limits	
	Shaft region	Tip region
Precast concrete driven pile	30	50
Steel driven pile	100	100
Continuous flight auger pile	50	50
Bored pile	50	50

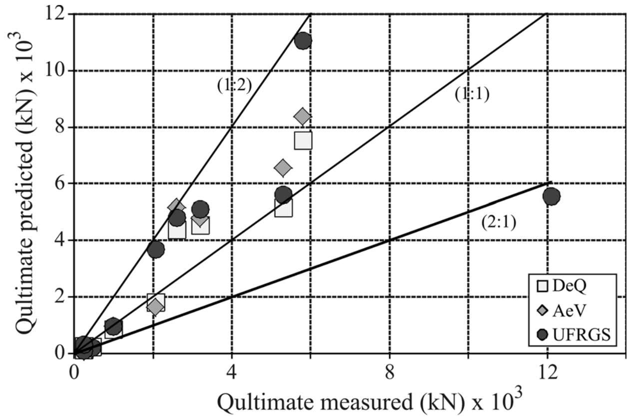

Figure 8 - Comparison of measured and predicted ultimate load for precast concrete piles.

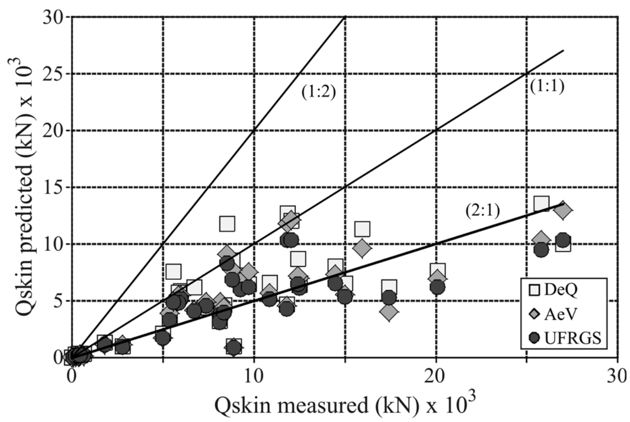

Figure 9 - Comparison of measured and predicted skin friction for bored piles.

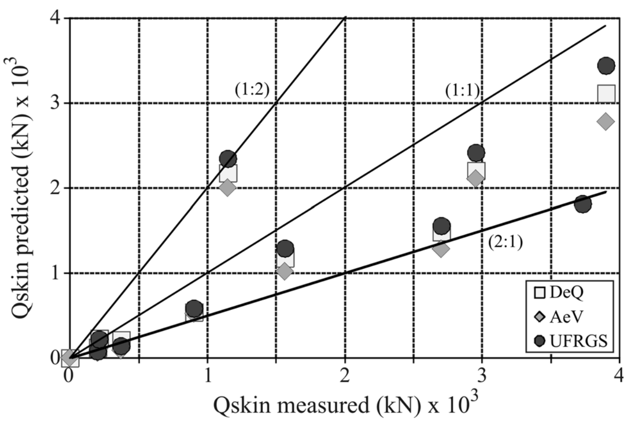

Figure 6 - Comparison of measured and predicted skin friction for precast concrete piles.

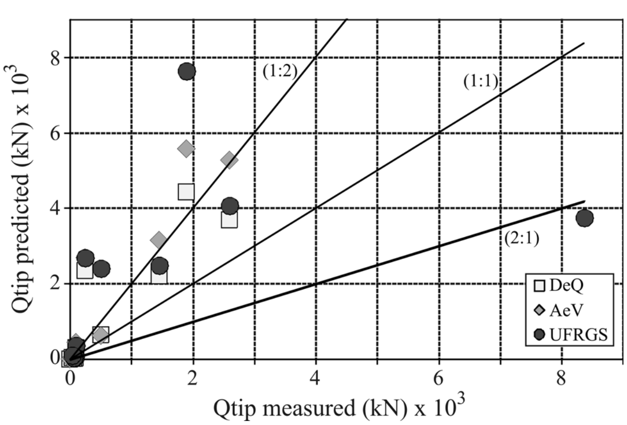

Figure 7 - Comparison of measured and predicted tip resistance for precast concrete piles.

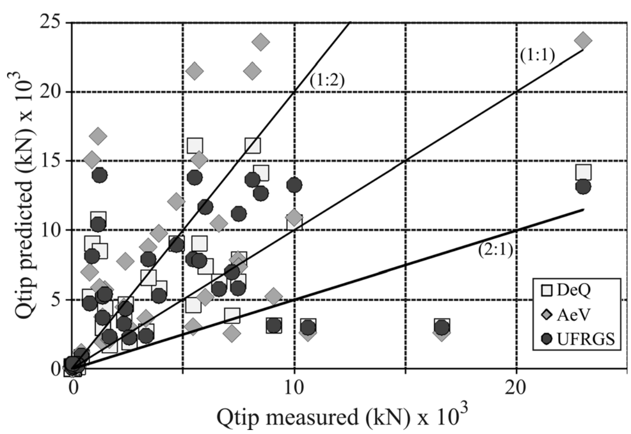

Figure 10 - Comparison of measured and predicted tip resistance for bored piles.

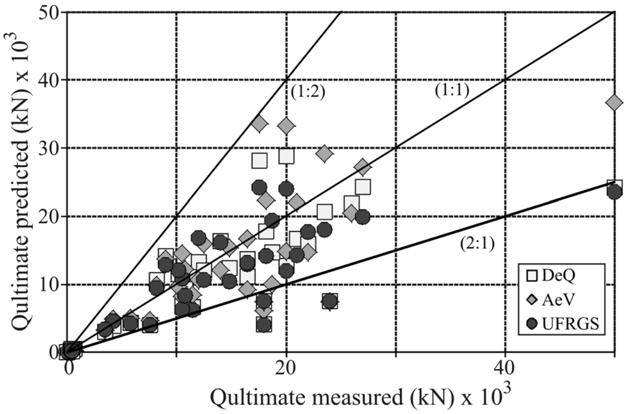

Figure 11 - Comparison of measured and predicted ultimate load for bored piles.

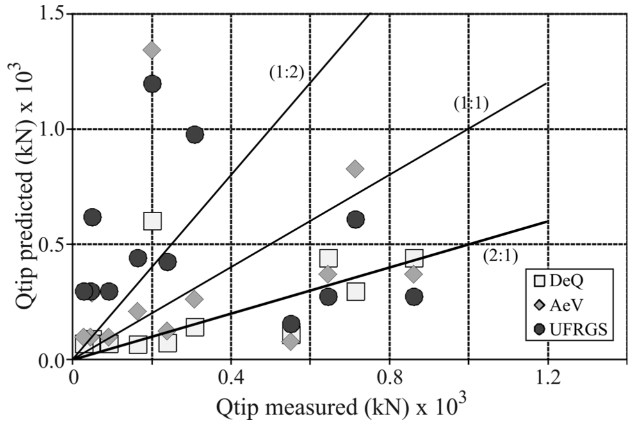

Figure 13 - Comparison of measured and predicted tip resistance for CFA piles.

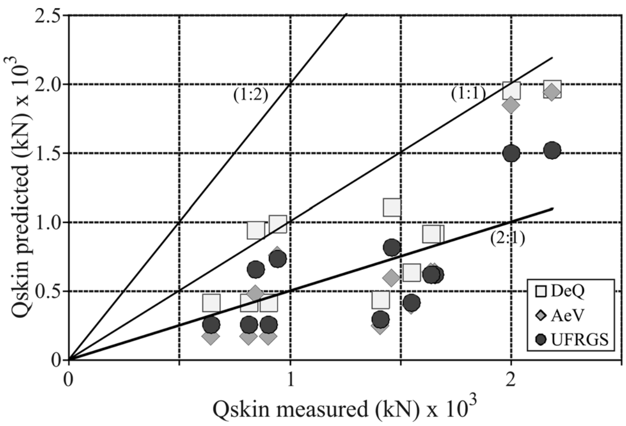

Figure 12 - Comparison of measured and predicted skin friction for CFA piles.

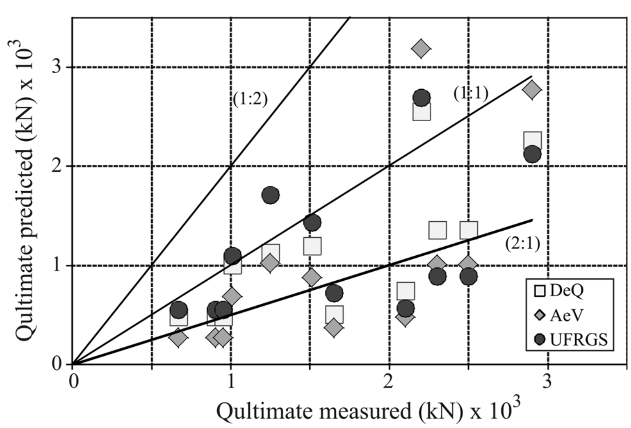

Figure 14 - Comparison of measured and predicted ultimate load for CFA piles.

induced by the excavation process. In average predicted skin friction underestimates measured values and tip resistance is scattered. Measured and predicted ultimate loads show good agreement;

- *Continuous flight auger piles*, *CFAP*, produce an intermediate condition between driven and bored piles. Although the α value of steel and CFA piles is the same, it does not necessarily represent similar pile-soil friction, because the oversupply of concrete or grout, and the consequent increase in diameter of CFAP, is disregarded in the analysis. In general predicted skin friction underestimates measured values and tip resistance is scattered. The proposed method is slightly conservative yielding predicted ultimate loads lower than measured.

In all predictions, the proposed method yields skin and tip resistance values within the range predicted by empirical methods classically adopted in Brazilian engineering practice. Predicted values generally lay around the best fit line for the predicted/measured pile capacities but, more importantly, for the database of instrumented load tests the method show the highest statistical probability of predicting values within 0.5*Qult* to 2*Qult* range. In addition, it is stressed that there is room for reducing scatter of predicted axial bearing capacity in a rational approach by calibrating energy efficiency coefficients to local SPT configurations.

6. Conclusions

This paper describes a new method developed for predicting the axial bearing capacity of individual piles, showing the strong relationship between the applied energy to SPT penetration test, its dynamic force and the ultimate resistance of steel driven piles. The method relies on energy conservation principles, wave propagation analysis and a number of hypotheses regarding the penetration mechanism. The main conclusions that can be drawn from the current analysis are:

- The method provides a valuable means of estimating the response of driven steel piles without having to rely on empirical statistical type of analysis;
- The proposed method can be extended to precast concrete driven piles, bored piles and continuous flight au-

ger piles, but empirical coefficients are necessary to account for the method of installation;

- Tthere appears to be room for reducing scatter of predicted axial bearing capacity by a proper calibration of energy efficiency coefficients representing the different configurations used in dynamic penetration tests;
- The proposed method shows no apparent bias of measured and predicted data with soil type, pile length (L), pile diameter (D), pile aspect ratio (L/D). Clearly the principle of energy conservation combined to wave propagation analysis captures the influence of soil type on the predicted values of axial bearing capacity;

These evidences and recommendations are supported by a final, overall picture given in Figs. 15 to 17, in which predicted/measured Q_P, Q_L and Q_U pile capacity values for driven, bored and continuous flight auger piles are simultaneously compared. The comparison to other established methods demonstrate the capability of the proposed SPT method in predicting the bearing capacity of piles: the method has been fully tested and is ready to be used in daily foundation design.

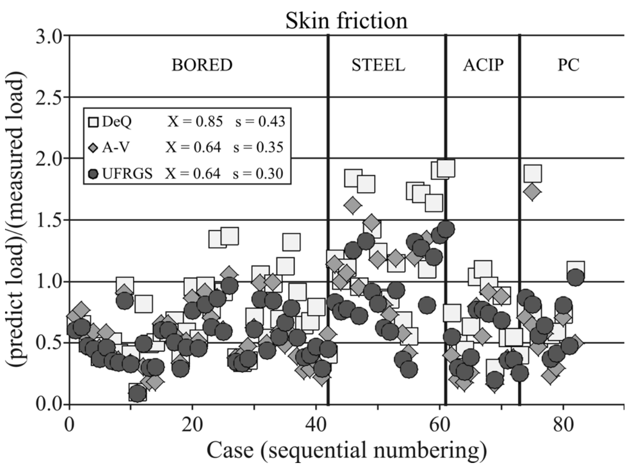

Figure 15 - Predictions of skin friction (after statistical cuts).

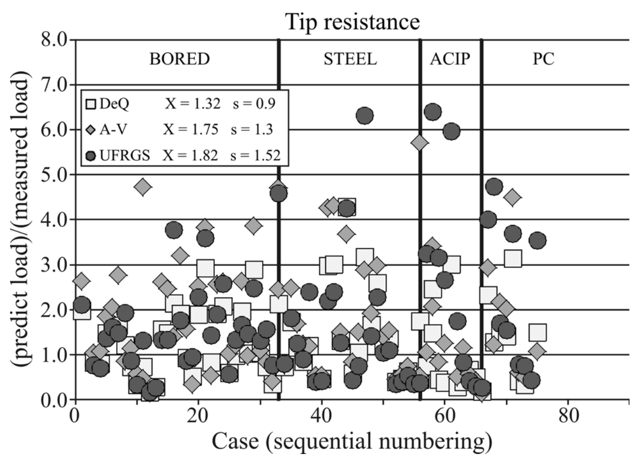

Figure 16 - Predictions of end bearing capacity (after statistical cuts).

Table 4 - Average and standard deviation of predictions (no statistical cuts).

		Predicted/measured							
		Proposed method		Aoki-Velloso		Décourt-Quaresma		Theoretical approach	
Pile type	Analysed aone	Average	SD	Average	SD	Average	SD	Average	SD
Steel	Skin friction	0.5	0.2	0.6	0.2	0.7	0.3	0.8	0.5
	Toe resistance	2.7	3.1	2.5	3.4	2.2	2.4	9.0	10.4
	Failure	0.8	0.3	0.8	0.4	0.8	0.3	2.0	1.0
Bored	Skin friction	1.2	0.7	1.9	1.2	1.7	0.9	0.7	0.4
	Toe resistance	2.3	3.2	2.4	2.8	2.0	2.2	3.2	5.8
	Failure	1.2	0.5	1.7	0.5	1.5	0.5	1.0	0.5
ACIP	Skin friction	0.5	0.2	0.5	0.3	0.7	0.3	0.5	0.1
	Toe resistance	4.0	4.1	2.0	2.2	1.0	0.9	10.4	10.6
	Failure	0.7	0.4	0.6	0.4	0.7	0.3	1.2	0.5
PC	Skin friction	0.8	0.5	0.7	0.4	0.8	0.4	0.6	0.4
	Toe resistance	3.2	3.1	2.9	3.3	2.4	2.8	4.5	3.5
	Failure	1.2	0.6	1.0	0.6	1.0	0.4	1.3	0.5

SD: Standard deviation.

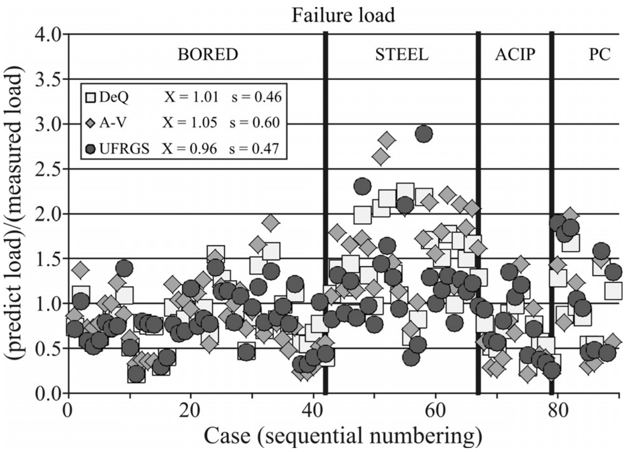

Figure 17 - Predictions of ultimate axial load capacity (after statistical cuts).

Acknowledgments

The writers wish to express their gratitude to the Federal University of Rio Grande do Sul, as well as to the Brazilian Research Council for the financial support to the research project and to the research group.

References

Aoki, N. & Velloso, D.A (1975) An approximate method to estimate the bearing capacity of piles. Proc. Panamerican Conference on Soil Mechanics and Foundation Engineering, Buenos Aires ISSMGE, pp. 116-127.

Axelsson, G. (1998) Long-term increase in shaft capacity of non-cohesive soils. M.Sc. Thesis, Royal Institute of Technology, Division of Soil and Rock Mechanics, Stockholm, 122 p.

Bazaraa, A.R. & Kurkur, M.M. (1986) N-values used to predict settlements of piles in Egypt. In: Use of In Situ Tests in Geotechnical Engineering. ASCE Geotechnical Special Publication n. 6, p. 462-47.

Briaud, J.L. & Tucker, L.M. (1988) Measured and predicted axial response of 98 Piles, Journal of Geotechnical Engineering, ASCE, v.114:9, p. 984-1001.

Briaud, J.L.; Tucker, L.M. & Ng, E. (1989) Axially loaded 5 pile group and single pile in sand. Proc. 12th International Conference of Soil Mechanics and Foundation Engineering, Rio de Janeiro, pp. 1121-1124.

Bustamante, M. & Gianeselli, L. (1982) Pile bearing capacity predictions by means of static penetrometer CPT. Proc. The Second European Symposium on Penetration Testing. 24-27 May, Balkema, Amsterdam, v. 2, p. 493-500.

Dalla Rosa, S. (2008) Study of Scale Effects in Dynamic Penetrarion Tests. M.Sc. Thesis, Programa de Pós-Graduação em Engenharia Civil, Universidade Federal do Rio Grande do Sul, 173 p. (in Portuguese).

Décourt, L. & Quaresma, R.A. (1978) Capacidade de carga de estacas a partir de valores de SPT. Anais do Congresso Brasileiro de Mecânica dos Solos e Engenharia de Fundações, Rio de Janeiro, ABMS, Rio de Janeiro, pp. 45-53.

De Mello, V.F.B. (1971) The standart penetration test state-of-the-art report. Proc. 4th Panamerican Conference on Soil Mechanics and Foundation Engineering, San Juan, pp. 1-86.

De Nicola, A. & Randolph, M.F. (1993) Tensile and compression shaft capacity of piles in sand. Journal of Geotechnical Engineering, ASCE, v. 119:12, p. 1952-1973.

De Ruiter, J. & Berigem, F.L. (1979) Pile foundation for large north sea structures. Marine Geotechnology, v.3:3, p. 276-314.

Falconi, F.F. & Perez Júnior, W. (2008) Estacas metálicas profundas de seção decrescente na Baixada Santista - Complemento aos estudos anteriores com base em novas provas de carga. Proc. Congresso Brasileiro de Mecânica dos Solos e Engenharia de Fundações, Búzios, ABMS/ABEF, São Paulo, CD -Rom.

Gyoten, Y.; Mizuhata, K. & Fukusumi, T. (1982) Tests on full-sized piles driven in reclaimed land. Soils and Foundations, Tokyo, v. 22:4, p. 81-95.

Jardine, R.; Chow, F., Overy, R. & Standing, J. (2005) ICP Design Methods for Driven Piles in Sands and Clays. Thomas Telford, London.

Jardine, R.J.; Standing, J.R. & Chow, F.C. (2005a) Field research into the effects of time on the shaft capacity of piles driven in sand. Proc. International Symposium on Frontiers in Offshore Geotechnics, Perth, Taylor & Francis.

Kikuchi, Y.; Mizutani, M. & Yamashita H. (2007) Vertical bearing capacity of large diameter steel pipe piles. Proc. Advances in Deep Foundations. International Workshop on Recent Advances of Deep Foundations, Yokosuka, Japan. Taylor & Francis, London, pp. 177-182.

Kim, D.; Bica, A.V.D.; Salgado, R. & Prezzi, M. (2009) Loading testing of a closed-ended pipe pile driven in multilayered soil. Journal of Geotechnical and Geoenvironmental Engineering, ASCE, v. 135:4, p. 463-473.

Langone, M.J. (2012) Método UFRGS de Previsão de Capacidade de Carga em Estacas: Análise de Provas de Carga Estáticas Instrumentadas. M.Sc. Thesis in Engineering, Programa de Pós-Graduação em Engenharia Civil, Universidade Federal do Rio Grande do Sul, 152 p.

Lehane, B.M.; Jardine, R.J.; Bond, A.J. & Frank, R. (1993) Mechanisms of shaft friction in sand from instrumented pile tests. Journal of Geotechnical Engineering, ASCE, v. 119:1, p. 19-35.

Lehane, B.M.; Schneider, J.A. & Xu, X. (2005) The UWA-05 method for prediction of axial capacity of driven piles in sand.Proc. International Symposium on Frontiers in Offshore Geotechnics. Perth, A.A. Balkema, pp. 683-689.

Lehane, B.M.; Schneider, J.A. & Xu, X. (2007) Development of the UWA-05 design method for open and closed ended driven piles in siliceous sand. Proc. Geo-Denver, New Peaks in Geotechnics, pp. 157-174.

Lobo, B.O. (2005) Método de Previsão de Capacidade de Carga de Estacas: Aplicação dos Conceitos de Energia do Ensaio SPT. M.Sc. Thesis in Engineering, Programa de Pós-Graduação em Engenharia Civil, Universidade Federal do Rio Grande do Sul, 121 p.

Lobo, B.O. (2009) Dynamics Penetration Mechanics in Cohesionless Soils. PhD Dissertation in Engineering, Programa de Pós-Graduação em Engenharia Civil, Universidade Federal do Rio Grande do Sul, 225 p.

Lobo, B.O.; Schnaid, F.; Odebrecht, E. & Rocha, M.M. (2009) Previsão de capacidade de carga de estacas através dos conceitos de energia do Ensaio SPT, Geotecnia, v. 115, p. 5-20.

Lopes, F.R. (1986) Medições de transferência de carga em estacas. Proc. Congresso Brasileiro de Mecânica dos Solos e Engenharia de Fundações, ABMS/ABEF, Porto Alegre, v. 8. p. 25-42.

Mantaras, F.M. & Schnaid, F. (2002) Cylindrical cavity expansion in dilatant cohesive-frictional materials. Geotechnique, v. 52:5, p. 337-348.

Moh, Z.C. (1994) Current deep foundation practice in Taiwan and Southeast Asia. Proc. International Conference on Design and Construction of Deep Foundations, FHWA, Orlando, p. 1137-1161.

Odebrecht, E.; Schnaid, F.; Rocha, M.M. & Bernardes, G.P. (2005) Energy efficiency for standard penetration tests. Journal of Geotechnical and Geoenvironmental Engineering, ASCE, v. 131:10, p. 1252-1263.

Paik, K.; Salgado, R.; Lee, J. & Kim, B. (2003) Behavior of open and closed ended piles driven into sands. Journal of Geotechnical and Geoenvironmental Engineering, ASCE, v. 129:4, p. 296-306.

Schnaid, F. (2000) Ensaios de Campo e suas Aplicações na Engenharia de Fundações. São Paulo, Oficina de Textos, p. 189.

Schnaid, F. (2005) Geocharacterisation and properties of natural soil by in situ tests. Proc. The 16th International Conference on Soil Mechanics and Geotechnical engineering, v. 1, p. 3-46.

Schnaid, F. & Mantaras, F.M. (2003) Cavity expansion in cemented materials: Structure degradation effects. Geotechnique, v. 53:9, p. 797-807.

Schnaid, F.; Odebrecht, E. & Rocha, M.M. (2007) On the mechanics of dynamic penetration test. Geomechanics and Geoengineering: An International Journal, v. 2:2 p. 137-146.

Schnaid, F. & Yu, H.S. (2007) Theoretical interpretation of the seismic cone test in granular soils. Geotechnique, v. 57:3, p. 265-272.

Schnaid, F. & Odebrecht, E.; Rocha, M.M. & Bernardes, G.P. (2009) Prediction of soil properties from the concepts of energy transfer in dynamic penetration tests. Journal of Geotechnical and Geoenvironmental Engineering, ASCE, v. 135:8.

Seo, H.; Yildirim, I.Z. & Prezzi, M. (2009) Assessment of the axial load response of an h pile driven in multilayered soil. Journal of Geotechnical and Geoenvironmental Engineering, ASCE, v. 135:12, p. 1789-1804.

Skempton, A.W. (1986) Standard penetration test procedures and the effects in sands of overburden pressure, relative density, particle size, ageing and overconsolidatin. Géotechnique, v. 36:3, p. 425-447.

Vesiæ A.S. (1972) Expansion of cavities in infinite soil mass. Journal of the Soil Mechanics and Foundations Division: Proc. The American Society of Civil Engineers, ASCE, v. 98, n. SM3.

Xu, X. & Lehane, B.M. (2005) Evaluation of end-bearing capacity of closed-ended pile in sand from cone penetration data. In: International Symposium on Fronties in Offshore Geotechnics, Perth, Taylor & Francis p. 19-21.

Yen, T.L.; Lin, H.; Chin, C.T. & Wang, R.F. (1989) Interpretation of instrumented driven steel pipe piles. Proc. Foundation Engineering: Current Principles and Practices. Evanston, ASCE, New York, v. 2, pp. 375-392.

Yu, F. (2011) Field tests on instrumented h-piles driven into dense sandy deposits. Electronic Journal of Geotechnical Engineering, EJGE, v. 14, 2008. Available in , accessed in Sep. 4, 2011.

Zhang, L.M. & Wang, H. (2007) Development of residual forces in long driven piles in weathered soils. Journal of Geotechnical and Geoenvironmental Engineering, ASCE, v. 133:10, p. 1216-1228.

A Preliminary Assessment of the Distribution and Consequences of Natural and Some Anthropogenic Hazards in Brazil

L.V. Zuquette, O.J. Pejon, R.E. Lima, M. Dantas-Ferreira, V. Guimarães

Abstract. This paper presents the results from a preliminary inventory of natural and man-made hazards and/or disasters in Brazil. The data were collected from previous studies, aerial photographs, satellite images and field studies. The data were obtained to evaluate the spatial distribution of natural and man-made hazards and disasters in different cities and states and to delimit the areas that have been the most affected during the last 50 years. A total of 28 different types of hazards/disasters were identified in Brazil; flooding, gravitational mass movements, continental and coastal erosion, silting and sinkholes are the more frequent, expensive, socially devastating and fatal types of hazards/disasters. Santa Catarina, São Paulo, Rio de Janeiro, Paraná, Pernambuco, Minas Gerais, Bahia, Rio Grande do Sul and Espirito Santo are the states most often affected by these hazards and disasters and thus experience the largest economic and social costs and the most casualties. Eight zones in which natural and anthropogenic hazards and associated disasters have occurred most frequently are described in this study. Among these, the coastal zone (zone 2) and mountainous regions in Eastern Brazil (zone 8) were found to have been intensely affected by hazards/disasters, with frequencies ranging from annual (*e.g.*, flooding) to once every five years (*e.g.*, high-magnitude gravitational mass movements). The greatest economic and social losses and the highest reported fatalities in Brazil have occurred in these two zones.

Keywords: natural and anthropogenic hazards, disasters, economic losses, Brazil.

1. Introduction

In recent decades, studies have focused on assessing natural and anthropogenic (*e.g.*, technologic, social, cultural and land use related) hazards and/or disasters and other types of environmental problems throughout the world to better understand the mechanism, predisposition and triggering factors to prevent social and economic losses (Zaruba & Mencl, 1969; Varnes, 1984; White & Haas, 1975; Bolt *et al.*, 1975; OAS, 1990; Alexander, 1993; Guzzetti, Cardinali & Reichenbach, 1994; Guzzetti, Stark & Salvati, 2005; Kovach, 1995; Brabb & Harrod, 1989; Alcántara-Ayala, 2002; Alcántara-Ayala, 2004; Korup, 2005; Guzzetti, Salvati & Stark, 2005; Dilley *et al.*, 2005; Yang *et al.*, 2005; Remondo *et al.*, 2005; Claessens *et al.*, 2007; Zhou, Wang, Wan & Jia, 2010; Balteanu *et al.*, 2010; Kirschbaum, 2010; Novelo-Casanova & Suárez, 2010; CNR/IRPI, 2010; Bonachea *et al.*, 2010; Van Den Eeckhaut & Hervás, 2011). In general, hazards are a consequence of natural processes (*e.g.*, geological, climatological and hydrological processes) and the interactions between land use and the environment (anthropogenic hazards). Damaging events that are related to hazards that generate human, social, environmental and economic losses are described as disasters (UNDRO 1984, 1991; Varnes, 1984). Glade & Crozier (2005) presented an interesting study that reports inventories of features of gravitational mass movements that occurred in several countries in Europe, Asia, South America, the South Pacific, North America and Africa. The Organization of American States (OAS, 1990) and the United Nations (UN) created organizations to advise countries on the problems resulting from hazardous events and to encourage the development of methodologies to forecast and mitigate these disasters.

Brazil does not experience volcanic events or high-magnitude earthquakes (> 7 on a Modified Mercalli Intensity scale), but other types of hazards and disasters have resulted in significant casualties and costly damages. In the last 50 years, several regions of Brazil have experienced natural processes, such as floods, gravitational mass movements, erosion, soil and water contamination and waste

L.V. Zuquette, PhD, Full Professor, Departamento de Geotecnia, Escola de Engenharia de São Carlos, Universidade de São Carlos, Avenida Trabalhador São Carlense 400, 13566-590 São Carlos, SP, Brazil. e-mail: email: lazarus1@sc.usp.br.
O.J. Pejon, PhD, Full Professor, Departamento de Geotecnia, Escola de Engenharia de São Carlos, Universidade de São Carlos, Avenida Trabalhador São Carlense 400, 13566-590 São Carlos, SP, Brazil. e-mail: email: pejon@sc.usp.br.
R.E. Lima, MSc, Associate Professor, Departamento de Geologia, Universidade Federal do Paraná, Centro Politécnico, Caixa Postal 19001, 81531-990 Curitiba, PR, Brazil. e-mail: renatolima@ufpr.br.
M. Dantas-Ferreira, PhD, Associate Professor, Departamento de Engenharia Civil, Universidade Federal de São Carlos, Rod. Washington Luis km 235, 13565-905 São Carlos, SP, Brazil. e-mail: marcilene.dantas@gmail.com.
V. Guimarães, PhD, Professor, Departamento de Geotecnia, Escola de Engenharia de São Carlos, Universidade de São Carlos, Avenida Trabalhador São Carlense 400, 13566-590 São Carlos, SP, Brazil. email: valguima@sc.usp.br.
Submitted on May 4, 2011; Final Acceptance on November 3, 2012; Discussion open until August 30, 2013.

spillage due to the ruptures of tailing dams, sanitary landfills and pipelines. However, the general population of Brazil has no clear understanding of the nature of these hazards and their direct and indirect economic consequences. In addition, hazardous events are often not distinguished from common events in the technical and scientific literature. Furthermore, no technical guidelines have been developed to forecast and respond to the different hazards and to avoid and mitigate disasters that are very common in Brazil.

Since the 1990s, studies have been conducted in Brazil by universities and independent research institutes (for example, Zuquette *et al.*, 1992; Gramani, 2001; IPT, 1995; CPRM, 2010; Cruz, 1974; Zuquette *et al.*, 1994a,c; IPT, 1995; Carvalho, 1996; Amaral & Palmeiro, 1997; Dorsi *et al.*, 1997; Bonuccelli, 1999; Herrmann, 2001; Bacellar, Lacerda & Coelho Neto, 2004; Herrmann *et al.*, 2004; CPRM, 2006), but public institutions have paid little attention to these hazards because in Brazil, there are no governmental centers to forecast these events. Most efforts of the governmental centers are concentrated on responding to the problems that follow the disasters.

Often, such governmental efforts are focused on the control of social problems rather than on the importance of forecasting and preventing the hazards (for example, Carvalho & Galvão, 2006; CENACID, 2010; DRM-RJ, 2011; GEORIO, 2011; BRASIL, 2011). These works have been developed based on predominantly in social and economical aspects of the affected places on the other side the geological and geotechnical data are secondarily considered. However, damages that occur as a consequence of natural and anthropogenic hazards can result in social losses, deaths and long-term economic losses. The effective management of these hazards requires a significant investment in rehabilitation, hazard control and problem-solving methods.

According to the data that have been collected by governmental institutions since 2007, approximately 800 disasters were recorded in several different regions (CENACID, 2010; CPRM 2010; Brazil, 2011; Brazil, 2012). The damages from these disasters ranged from 5,000 USD to more than 1,000,000 USD. Since 2008, several different types of natural disasters have occurred repeatedly in Brazil. These disasters have strongly affected the states in the southern and southeastern regions of the country. EM-DAT (2012) considered Brazil to be one of the most affected countries. Recently, Brazil was named by the UNITED NATIONS (2012) as the 3rd most affected country in terms of natural hazards and/or disasters in the world.

According to the data from the UN/ISRD (2010), the frequency of natural disasters has been steadily increasing in the world as well as in Brazil. The number of major recorded occurrences in the world has ranged from 70 to more than 400 annually between 1975 and 2010 (Fig. 1). The data allow us to distinguish five distinct periods directly associated with the growth and concentration of the population worldwide and in Brazil. Following this trend since 1965, Brazil has experienced a continuously increasing number of recorded disasters, which has coincided with the growth and concentration of the population in urban areas. According to the International Red Cross, Brazil is the country that is most affected by disasters related to natural hazards in the Americas. Between 1994 and 2011, there were more than 10,000 deaths, but according to governmental information, in 2010 alone, approximately 8 million people were affected, and 1,500 died, mainly because of gravitational mass movements, floods, droughts and other smaller disasters. This increase in damages is due to both an increase in the number of hazards and the fact that a greater proportion of hazards have affected a significant number of people (more than 20,000,000), mainly because disasters have occurred in the most populated regions. Since 2007, more than 300 significant disasters (each characterized by economic and social costs greater than 500,000 USD and casualties) have occurred in Brazil. In the last five years, more than 5 billion USD have been spent to aid areas affected by disasters that had resulted from natural processes and/or environmental problems. However, a limited amount of money has been invested in the forecasting of such events, and in some cases, a portion of this small amount of money is lost in the public system.

Given the large numbers of hazards and disasters resulting from natural processes and human activities, we developed a basic inventory of hazards and disasters for

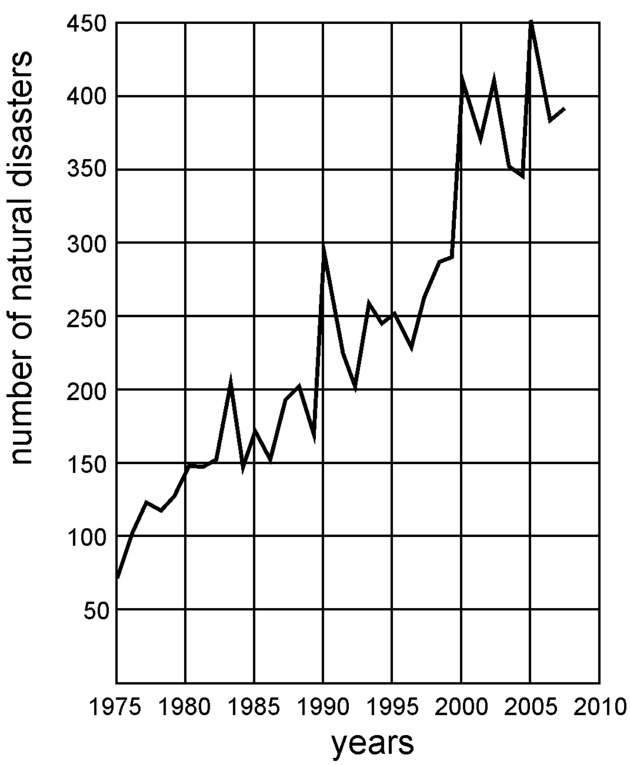

Figure 1 - The number of natural disasters worldwide between 1975 and 2010. From UN/ISRD (2010).

Brazil. The goal was to assess the distribution of hazards and disasters in each state and in the cities with the largest populations, which could be the most affected by such disasters. The records obtained would allow us to specify and define the most affected areas in Brazil and elaborate on the specific hazards and/or disasters threatening each state.

2. Challenges to Developing an Inventory of Natural and Man-Made Hazards and Disasters in Brazil

Studies of natural and man-made hazards are generally conducted after these hazards have led to consequent disasters. However, few studies aim to forecast the hazards and their associated risks. In general, the relevant studies can be classified into three groups. The first group includes studies that consider specific events; the goals of these studies are primarily related to the geological, geomorphologic and geotechnical characterization, design and installation of structural measures to prevent the problem from recurring in the future (for example, Pichler, 1957; Barata, 1969; Jones, 1973; Ploey & Cruz, 1979; Wolle, 1988; Elbachá, 1992; Cerri, 1993; Lacerda, 1997; Guimarães *et al.*, 2003; D'Orsi, Feijó & Paes, 2004, Déstro *et al.*, 2009). Approximately 75% of the studies conducted in Brazil are of this type. The second group is related to the discontinuous inventory of natural events. These studies emphasize susceptibility zoning, which uses engineering geological mapping at scales of less than 1:25,000. These maps are mainly based on qualitative data, but some studies have used quantitative geomorphological and rock substrate data and heuristic methods involving overlapping maps, with or without weighting (for example, Zuquette *et al.*, 1991; Zuquette *et al.*, 1994b; Augusto Filho, 1994; Amaral, 1996; Hach-Hach, 1998; Alheiros, 1998; Macedo, Costa & Salles, 1999; Herrmann, 2001; MINEROPAR, 2005; Amaral Junior, 2007; Dantas-Ferreira, 2008; Lollo, 2008). The third group is composed of hazard and risk mapping developed predominantly by universities at scales of less than 1:25,000 (rarely larger) and based primarily on semi-quantitative data (for example, Wolle & Carvalho, 1989; Ahrendt & Zuquette, 2003; Dias & Zuquette, 2004; Augusto Filho, 2004; Nunes Bandeira & Coutinho, 2008; Silva & Zuquette, 2010).

Several factors influence hazard studies in Brazil, such as the following:

- The large territorial extent of Brazil.
- The absence of governmental programs to develop continuous inventories. There are some data banks in various stages of development in the CPRM and in other organizations at the state level (for example, the MINEROPAR in Parana and the DRM in Rio de Janeiro), but these data banks exhibit serious problems involving data sources and registering predominantly landslides. A large part of the data contained in the different databases is the same as those obtained from surveys after the disasters.
- The lack of topographic maps at adequate scales for different parts of Brazil; the scales are generally less than 1:50,000, with a curve equidistance of greater than 20 m. In some regions, there are orthophotos at different scales and for different periods, but these photos are not linked to adequate topographic maps, which provide the fundamental basis for putting together information about natural and anthropogenic events.
- The lack of regular studies by governmental centers to map environmental factors at adequate scales (unconsolidated materials maps, rock substrate maps, drainage maps and continuous inventory maps, among others).
- The lack of regular surveys to obtain aerial photographs. High-resolution satellite images are expensive and have only been obtained for some specific areas where the economic losses were very high. Lower-resolution satellite images exist, but they are not fine enough to record the events. Brazil urgently needs a program to obtain continuous, high-resolution satellite images over extensive areas to create continuous inventories.
- Because of the climate in Brazil, most of the damaged and affected sites are quickly modified. Thus, identifying the affected areas becomes very difficult or even impossible.
- Most of the hazards are not reported. Only large disasters are registered.
- Records can sometimes be difficult to obtain because people are not accustomed to reporting small losses (less than 5,000 USD). However, in some regions, these losses are very common, especially when the events do not occur very rapidly, as they do with soil collapse and subsidence.

3. Materials and Methods

A central database of the natural and anthropogenic hazards and disasters does not exist in Brazil. Between 2007 and 2012, there was a large effort to compile the existing scattered information held by various organizations into a single database. The data search was conducted according to the following steps:

i The selection and preparation of basic data on the geology, relief and climatic conditions of Brazil to define and delimit the zones most affected by hazards and/or disasters. The geological data were collected based on the previous maps developed by CPRM (1971, 1983) and DNPM (1984) at scales of less than 1:1,000,000 and other maps that were produced for the states at scales between 1:500,000 and 1:1,000,000 (DAEE/UNESP, 1984; MINEROPAR, 2005; UNB, 2008; CPRM, 2007; IBGE, 2007). The relief data were collected from (Ab'Saber, 1964), FIBGE (1990), (Miranda & Coutinho, 2004), CPRM (2007) and IBGE (2007). The climatic map was prepared considering the annual variation in rainfall and temperature and the length of the dry season in different parts of Brazil obtained from (Nimer, 1989), INPE/CPTEC (2007) and IBGE (2007).

ii Data on the hazards and the associated economic losses were obtained from technical reports, theses (master's and doctorate) from the database of the most important universities of Brazil, magazines, state newspapers and other publications. These additional publications included the annals and proceedings of the national congresses and symposia supported by the Associação Brasileira de Geologia de Engenharia e Ambiental - Brazilian Association of Environmental and Engineering Geology (ABGE, 2007), the Associação Brasileira de Mecânica dos Solos (ABMS) - Brazilian Association of Soil Mechanics and proceedings of the international congresses of the International Association of Engineering Geology and Environment (IAEGE) and the International Society of Soil Mechanics and the Geotechnical Engineering (ISSMGE), as well as the proceedings from the International Congresses of Landslides. Most of these sources provided very localized and specific data. Natural and man-made hazards and disasters were assessed using a group of similar concepts of hazards, disasters, vulnerability and consequences proposed by (Varnes, 1984), UNDRO (1984), Crozier & Glade (2004), ISSMGE (2004) and (Fell *et al.*, 2008).

iii The geographical location of the recorded hazards and disasters. The geographical locations of the recorded hazards and disasters were only loosely provided, and the geographical coordinates were rarely given. To evaluate the distribution of the natural and man-made processes in Brazil, each data point needed to be placed on a map with all of the acquired information. Because of the vast extent of Brazil, the geographical position of each record was approximated based on an urban area or district, a natural slope, a valley of a natural drainage channel, or an escarpment.

iv Post-event aerial photographs and satellite images of the areas affected by hazards and disasters were analyzed to delimit the affected area and damage. However, these materials are scarce, and post-event analysis was only possible for a few areas.

v Fieldwork was conducted to assess great part of the areas that were greatly affected by hazards and disasters, to evaluate the reliability of the information in situ and to obtain new data on the events, such as the type, magnitude and size.

vi Using GIS and manual works, the spatial assessment of the data from the inventory was performed considering one or more of the following: the distribution of hazards and disasters in urban, forested and rural areas, the economic, social, environmental and humanitarian losses related to the disasters, the magnitudes and intensities of the natural events and the density and frequency of the natural and man-made events. For many of the recorded events, we could collect only one or two of these data.

vii The evaluation of the density (low - < $1/km^2$, moderate - 1 to $3/km^2$ and high - > $3/km^2$) and frequency (*e.g.*, monthly, annually or once every 5 years) of the natural and man-made hazards and disasters in the main urban areas was performed for the main urban areas in each state of Brazil.

viii An assessment of each state was conducted that considered the density and distribution of the various types of hazards and disasters. The magnitude of the economic, social, human and environmental losses was used to classify each state in terms of hazard/disaster into one of six levels (1 is the lowest and 6 is the highest) related to the attributes described above. These levels are described as follows: Level 1 - low-density (< $1/km^2$), small affected areas (< 10 km^2) associated with minor economic losses (< 100,000 USD); Level 2 - low to moderate-density, small affected areas associated with moderate economic losses (100,000 to 500,000 USD); Level 3 - low to moderate-density, medium-sized affected areas (10 to 100 km^2) associated with moderate economic and social losses; Level 4 - moderate-density (1 to $3/km^2$), medium-sized to large affected areas associated with moderate economic, social and environmental losses; Level 5 - moderate and high-density, large affected areas (> 100 km^2) associated with moderate economic, social, human and environmental losses; and Level 6 - high-density (> $3/km^2$), large affected areas associated with high economic, social, human and environmental losses (> 500,000 USD).

ix The most severely affected zones were defined based on the type of hazard and density of disasters considering the frequency and intensity associated with the human, economic and social losses, which were related to the geological, geomorphological and climatic aspects. The zones were displayed on a map of Brazil along with the main drainage channels to facilitate the delimitation of the zonal boundaries. After delimitation of the zones, a description of the relief, geology, and climatic conditions associated with the economic, social, environmental and human losses were formulated. The steps developed to delimit the zones were as follows: the evaluation of the density distribution of the hazards and disasters in the states, the analysis of the density distribution within the geological units based on the lithology, the identification of the most affected areas based on the geological units experiencing a high density of events, for the zones mentioned above, consideration of the characteristic altitude and relief, mainly using the hydrographic map (DNPM, 1984; IBGE, 2007), which permitted the fine-tuning the zonal boundaries, accounting for the climatic conditions that were considered to produce extreme rainfall events and the greatest hazards and disasters for each zone and the selection of typical examples of hazards and disasters associated with the economic, social, human and environmental losses.

x Considering the hazard and disaster zoning, population density and infrastructure, we developed an assessment of the degree of vulnerability for each of the more affected zones. The assessment considered 3 levels (low, moderate and high degree of vulnerability) based on the following 2 aspects: first, the hazard types and their intensity/magnitude and frequency (Low degree - hazards with low frequency and intensity/magnitude; Moderate degree - hazards with moderate frequency and intensity/magnitude; High degree - hazards with high frequency and intensity/magnitude) and second, the population density, affected environmental elements and urban and/or regional infrastructure (Low degree - low population density, small affected areas (less than 5 ha) and low density of infrastructure; Moderate degree - medium population density, medium-sized affected areas (6 to 50 ha) and low density of infrastructure but of great social and economic importance; High degree - high population density, large affected areas (> 50 ha) and medium to high density of infrastructure).

4. The General Environmental Characteristics of Brazil

Brazil is located between the latitudes of 34º South and 5º North and is approximately 4,300 km in the longest north-south direction and 4,150 km in the longest east-west direction, covering 8.5 million km^2 in the Northern and Southern Hemispheres. Climatically, the country includes seven major zones (Fig. 2), varying from wet tropical to sub-humid mesothermic; the main characteristics of the regions are listed in Table 1.

The relief of Brazil includes altitudes varying from 0 to 3,000 m. Approximately 99% of the country is from 0 to 1,200 m (0 to 200 m - 41%; 200 to 500 m - 37%; 500 to 800 m - 15%; 800 to 1,200 m - 6%); 0.5% from 1,200 to 1,800 m; and 0.5% higher than 1,800 m. The population density (Fig. 3) is divided into three categories: less than 10 inhabitants per km^2 (predominantly the northern and western portions), between 10 and 50 inhabitants per km^2 and greater than 50 inhabitants per km^2 (mainly in the south-eastern and southern regions). The population data were obtained from IBGE (2010).

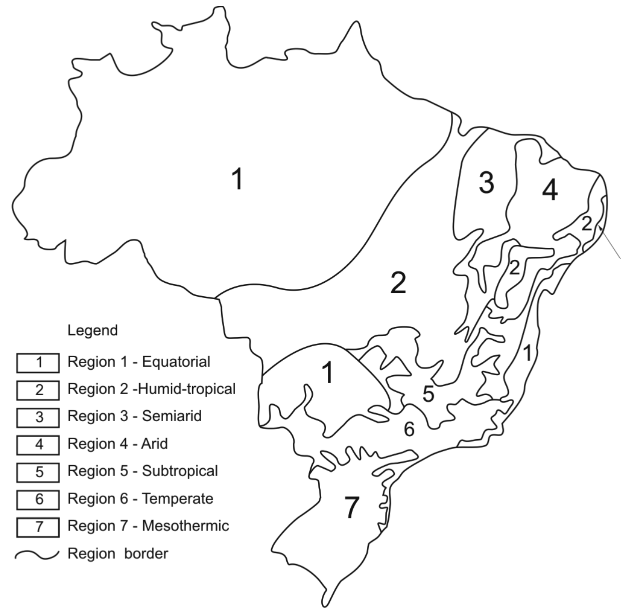

Figure 2 - The main climatic regions of Brazil.

5. Hazard Sources on Brazil

Generally, a hazard is characterized as an event that has a probability of occurrence associated with a specific area and whose intensity is greater than a predetermined limit (a safety threshold) that makes it different from a common event. However, when an event exceeds the safety threshold, it is classified as a hazard with different probabilities and intensities. Some of these hazards result in disasters, producing heavy economic, social and environmental losses or even killing hundreds of people.

The main observed natural and anthropogenic hazard sources that occur in Brazil are generally of a climatologi-

Table 1 - The basic characteristics of the main climatic regions of Brazil.

Main climatic region	Wetness	Average Temperature (°C)	Dry season (months)	Variation of rainfall (mm)
1	Humid	Tropical - > 18	< 3	1, 750 to 3,300
2	Humid	Tropical - > 18	4 to 5	1,000 to 2,250
3	Semiarid	Tropical - > 18	6	750 to 1,500
4	Arid	Hot - > 18	7 to 11	300 to 1,000
5	SubHumid	Subtropical - 15 to 18 at least 1 month	4 to 6	700 to 1,750
6	Humid	Temperate - 15 to 18 at least 1 month	< 3	1,200 to 4,500
7	SubHumid	Mesothermic - 10 to 15	< 5	1,250 to 2,300

Figure 3 - The population density in Brazil.

cal or geological-geotechnical nature, including seismic events, wind, tides, dry season, air pollution, salinization/saline soils, flooding, continental and coastal erosion, silting/sedimentation, subsidence (karst and underground excavation), gravitational mass movements, expansive soil and rock, groundwater pollution, compressible and collapsible soils, pipeline and dam ruptures, spontaneous combustion of turf materials, desertification, surface water pollution, soil pollution, dangerous components in the soil and water, frost, soil liquefaction, dune movements, radioactive spills, natural radiation, wastes and earth fill on the slopes, surface water flow and sanitary landfills. The main triggers of the natural and many anthropogenic hazards in Brazil are rainfall (time and intensity greatly impact its effects) and land use, both of which have an adverse effect on other environmental factors. However, the occurrence of geological, geotechnical and some anthropogenic hazards is directly influenced by the intrinsic properties and variability of the geological materials (unconsolidated materials, rock substrate and the depth of the saturated zone) and their spatial distributions.

6. The Distribution of Hazard Sources

The distribution of hazards and disasters in Brazil was determined based on data collected from the different types of records and considering hazards of all magnitudes and intensities.

According to the data, 28 different types of geological, geotechnical, hydrological, climatological and man-made hazard sources were observed. The distribution of the main hazard sources for each state in Brazil is shown in Fig. 4. The economic, environmental, human and social losses in Brazil have increased significantly over the last 50 years due to disasters resulting from such natural and man-made hazards. Even low-magnitude seismic activity has produced economic losses.

In 2010, Brazil had 5,561 municipalities, and approximately 1,200 have been heavily affected by some hazard over the previous 10 years. Because of the lack of adequate engineering geological mapping, hazard maps or risk charts, territorial planning in the country is not adequate. This lack of planning associated with the lack of adequate laws and sub-optimal land use practices, have led to the increased number of disasters that have resulted in economic losses on the order of billions of USD per year.

As of January 2012, more than 500 municipalities have been affected by hazards that caused disasters (drought, landslides, flooding) in Brazil (300 of them are in the most populous regions), with economic losses greater than 7 billion USD, and a total of 5 million people have been seriously affected, distributed in two groups of states: (i) the states of Minas Gerais, Rio de Janeiro and Espirito Santo, where the economic losses were greater than 5 billion USD; and (ii) the states of Rio Grande do Sul, Santa Catarina, Paraná, Bahia and São Paulo, where the economic losses due to drought were greater than 2.5 billion USD.

Table 2 shows the number of municipalities per state and the main large cities, predominantly state capitals (locations shown in Fig. 5), that were affected by natural and man-made hazards and/or disasters, which might result in social, economic and environmental losses. These municipalities and cities require the adoption of structural measures for prevention and control, and they also require the development of new disaster mitigation policies. The level of knowledge of the environmental components of the ground, especially the geological aspects, is below the level necessary for technical analysis. The areas where prevention and control measures have begun represent a very

Figure 4 - The distribution of the recorded geological, geotechnical, hydrological, climatological and some anthropogenic hazard sources and/or disasters in Brazil. Legend: 1-Seismic activity, 2-Wind, 3-High tides, 4-Drought, 5-Air pollution, 6-Saline soils/salinization, 7-Flooding (natural and human-induced), 8-Continental and coastal erosion, 9-River, lake and reservoir sedimentation, 10-Subsidence (karst and underground excavation), 11- Gravitational mass movements, 12-Expansive soils and rocks, 13-Groundwater pollution, 14-Settlement and collapsible soils, 15-Pipeline and dam (tailing and power) ruptures, 16-Spontaneous fire in peat bogs, 17-Desertification, 18-Surface water pollution, 19-Soil pollution, 20-Dangerous components in soil and water, 21-Hoarfrost condition, 22-Soil liquefaction, 23-Dune movements, 24-Radioactive spill, 25-Natural radioactivity, 26-Uncontrolled earth fill and waste disposal on slopes, 27-Concentrated surface water flow, 28-Pollutant sources.

small percentage of the total area of Brazil. These cities urgently need geological and geotechnical studies to produce engineering geological and hazard maps for the development of risk charts.

7. Hazard and Disaster Zoning

After the inventory was developed, it was analysed, and the collected data permitted the delimitation of the

Table 2 - The number of municipalities and major cities affected and registered as hazard and disaster sources in Brazil.

State	Number of municipalities affected	Most populous city affected by the disasters		Hazard sources
			Population (10^6 inhabitants)	
São Paulo	173	Metropolitan Region of São Paulo	20	Flooding, gravitational mass movements, silting, subsidence, erosion, groundwater pollution
Rio de Janeiro	52	Metropolitan Region of Rio de Janeiro	10	Flooding, gravitational mass movements, silting, subsidence, erosion, settlement
Minas Gerais	335	Metropolitan Region of Belo Horizonte	5	Flooding, gravitational mass movements, silting, subsidence, erosion
Rio Grande do Sul	320	Metropolitan Region of Porto Alegre	5	Flooding, gravitational mass movements, silting, subsidence, erosion
Paraná	180	Curitiba	4	Flooding, gravitational mass movements, silting, subsidence, erosion, expansive materials
Pernambuco	38	Recife	3	Flooding, gravitational mass movements, silting, subsidence, erosion, groundwater pollution
Bahia	48	Salvador	4	Flooding, gravitational mass movements, expansive materials
Ceara	31	Fortaleza	3	Flooding, gravitational mass movements, silting, subsidence, erosion, groundwater pollution, dune movements
DF		Brasília	3	Erosion, collapsible soils
Amazonas	15	Manaus	1	Flooding, erosion, gravitational mass movements
Mato Grosso	51	Cuiabá	1.5	Flooding, erosion, silting
Rio Grande do Norte	23	Natal	1	Dune movements, coastal erosion
Santa Catarina	293	Florianópolis	0.5	Flooding, gravitational mass movements, streambank erosion, erosion
Mato Grosso do Sul	78	Campo Grande	1	Erosion, collapsible soils
Para	35	Belém	1	Flooding ,coastal erosion
Espírito Santo	26	Vitória	1	Flooding ,gravitational mass movements
Goiás	50	Goiânia	2	Erosion
Rondônia	7	Porto Velho	0.5	Flooding, streambank erosion
Alagoas	15	Maceió	0.5	Flooding, landslides, erosion
Acre	10	Rio Branco	0.3	Flooding, erosion, collapsible soil
Tocantins	16	Palmas	0.2	Flooding, gravitational mass movements
Sergipe	8	Aracaju	0.6	Flooding, gravitational mass movements
Amapá	3	Macapá	0.4	Flooding, streambank erosion
Roraima	3	Boa Vista	0.45	Flooding, erosion, wet areas
Paraíba	10	João Pessoa	0.7	Flooding, erosion
Piauí	20	Teresina	0.8	Flooding, erosion, silting
Maranhão	15	São Luis	1	Flooding, erosion

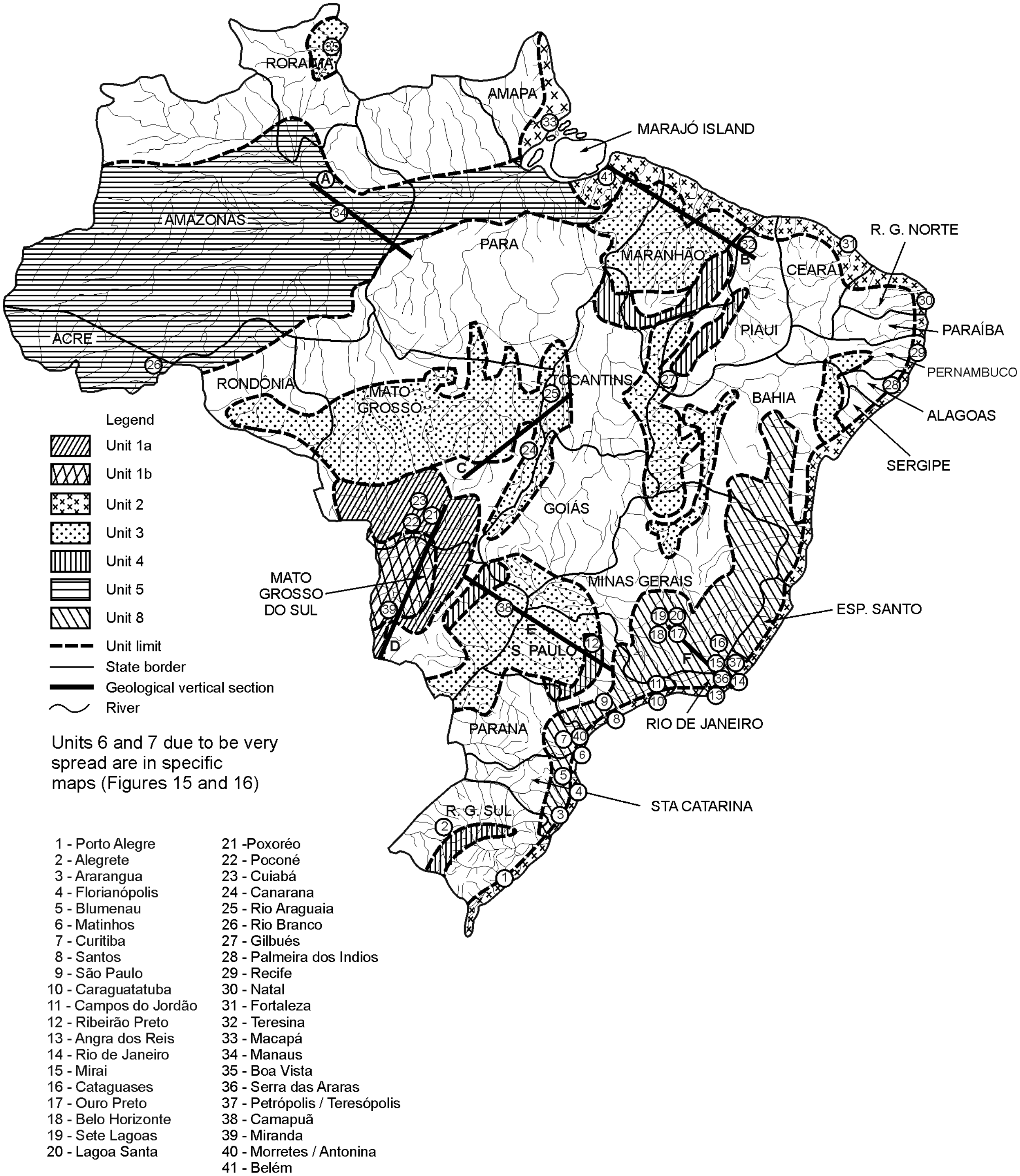

Figure 5 - The distribution of the terrain zones most affected by hazards and/or disasters in Brazil.

eight most affected zones considering the types and intensities of natural and man-made hazards and disasters. For different zones, selected examples that are representative of the hazards and disasters common in the zone are presented. These examples were selected to show the primary mechanisms, magnitudes, affected areas and intensities. Specific locations of all of the cities, sites and examples considered in each zone are shown in the maps. The geological vertical sections were based on geological maps from CPRM (1971), DNPM (1984), CPRM (1983), DAEE/UNESP (1984), MINEROPAR (2005), UNB (2008), CPRM (2007) and IBGE (2007). Figure 5 shows six zones: Zone 1 - Pantanal Basin (flooding, silting and erosion hazards), Zone 2 - Coastal zone and continental strip, Zone 3 - Composed of sandstones and sandy unconsolidated materials, Zone 4 - Aeolian sandstones, Zone 5 - The Amazon region and Zone 8 - Areas affected by natural disasters. The others two zones (Zone 6 - Areas affected by seismic activity and Zone 7 - Areas composed of carbonate rocks) are represented in specific maps.

7.1. Zone 1 - Pantanal Basin (flooding, silting and erosion hazards)

With regard to altitude and geological material, the basin can be divided into two parts (Fig. 6). Zone 1.a is a marshland of Tertiary and Quaternary sediments with an average altitude of approximately 100 m (flooded portion). This zone is composed of an extremely vulnerable and unique landscape (Ab'Sáber, 1988). During the rainy season, this area receives water from the higher portions of the basin (Zone 1.b) via several large rivers that drain large areas. The waters transport a major sediment load derived from the erosion of sandy geological materials (rock and unconsolidated materials). This scenario causes intense silting, the creation of sand bars and marginal erosion. The southern portion of Zone 1.a, near the cities of Miranda and Aquidauana (Mato Grosso do Sul State) (site 39 - Fig. 5), suffered intense flooding in March of 2011, and the water reached 15 m above the normal level of the rivers (see the great extent of the affected areas in Fig. 5) and covered more than 10,000 km^2. The second portion (Zone 1.b) ranges in altitude from 100 to 900 m and is used extensively for agriculture and as a pasture. In this area, diffuse, gully and marginal erosional processes are intense. This area is also characterized by the silting of rivers and dam reservoirs as a result of erosion and collapsing soils. Sandy geological materials and intense rains are responsible for the intense erosive processes and the dangers associated with collapsible soils. The city of Cuiabá in Mato Grosso (Site 23 - Fig. 5) is frequently affected by intense flooding. The largest recorded flood occurred in 1974, when the water reached 11 m above the normal level. This flood affected thousands of people and resulted in losses of 1 billion USD.

In this region, there are intense erosional processes (thousands of erosion features) and earth flows, which generate a large amount of sediments. Consequently, the sediment load transported to Zone 1.a has increased significantly, resulting in the silting of the rivers and lakes (Fig. 7).

7.2. Zone 2 - Coastal zone and continental strip

This zone can presents as wide as 100 km (*e.g.*, in the states of Maranhão, Pará and Piauí), encompassing portions of 18 states (Fig. 5). The width depends on the changes in the landscape from the wave break line. Two large areas can be distinguished within Zone 2. The first area is composed of a range of Quaternary and Tertiary sediments. This area is heavily affected by flooding, intense coastal erosion, dune movement, settlement, high tides, expansive materials and man-made hazards. A number of areas within the zone are prone to silting. The second part is made up of igneous and metamorphic rocks overlain by

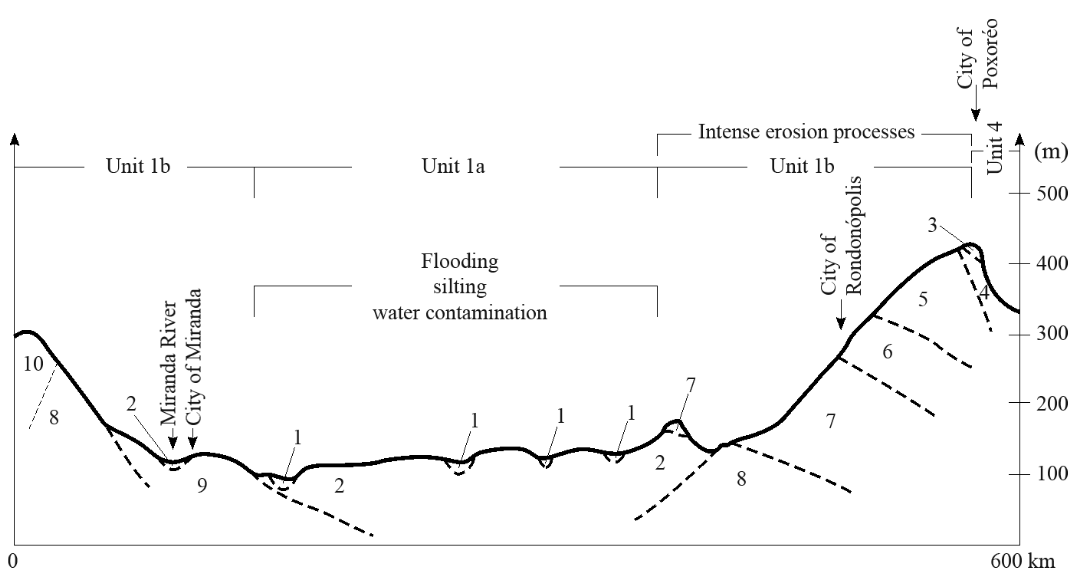

Figure 6 - A schematic geological vertical section of Zone 1 (section D - Fig. 5). Legend: 1 - Alluvial sediments (Quaternary); 2 - Alluvial sediments with gravel layers (Quaternary); 3 - Sandstones, minor siltstones, claystones and conglomerates (Cretaceous); 4 - Aeolian sandstones (Cretaceous); 5 - Sandstones, siltstones, arkoses, shales, rhythmites and diamictites (Carbo-Permian); 6 - Siltstones, shales and sandstones (Devonian); 7 - Sandstones, conglomerates and siltstones (Silurian-Devonian); 8 - Limestones, marls, dolomites, and shales (late Proterozoic); 9 - Phyllites, graphites and hematite phyllites, meta-arkoses, meta-sedimentary rocks and meta-volcanics (middle Proterozoic); and 10 - Schists, quartzites, migmatites and gneisses (undifferentiated Precambrian).

transported and residual unconsolidated materials with different thicknesses, significant relief amplitudes and slopes ranging from moderate to steep. Erosion and gravitational mass movements occur predominantly in this part. Among the cities cited in Table 2, fifteen are located in this zone; all have been heavily affected by disasters with significant economic losses during the last 30 years. In this zone, rainfall can reach as much as 500 mm per month; however, the most frequent monthly high is approximately 300 mm. There is intense coastal erosion in portions of the states of Rio Grande do Sul, Santa Catarina, Paraná (Matinhos region), Rio de Janeiro, São Paulo, Bahia, Pernambuco (Porto de Galinhas region), Rio Grande do Norte and Ceará (city of Fortaleza). Figure 8 shows sites in the cities of Fortaleza and Matinhos that are heavily affected by coastal erosion. More than 100 locations have been affected along the Brazilian coast, resulting in high economic losses due to the disruption of and damage to facilities. Dune movements have been promoted the silting of rivers and affect homes in the urban part of the city of Natal (in the state of Rio Grande do Norte). Major disasters occurred in the city of Salvador (Site 27 - Fig. 5) in 1989 and 1995 due to landslides, where more than 150 people were killed, and dozens of houses and buildings were damaged. The city of Recife (Site 24 - Fig. 5) suffered landslides in 1996, when more than 50 peo-

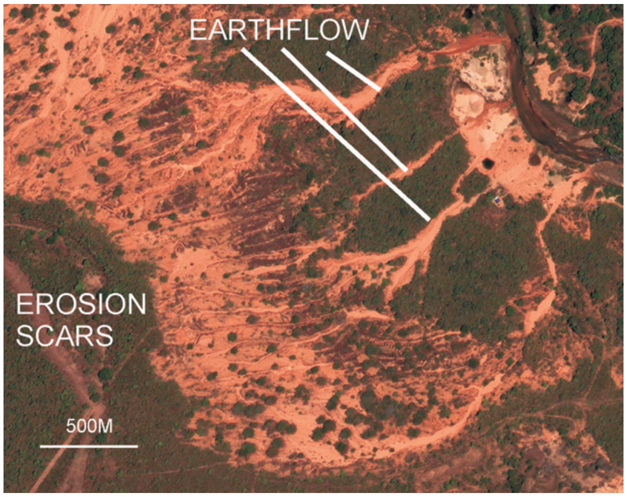

Figure 7 - A general view of an area showing the erosion features associated with earth flows (Site 21 - Fig. 5) in the northern portion of the Pantanal Basin (Poxoréo region - Mato Grosso State).

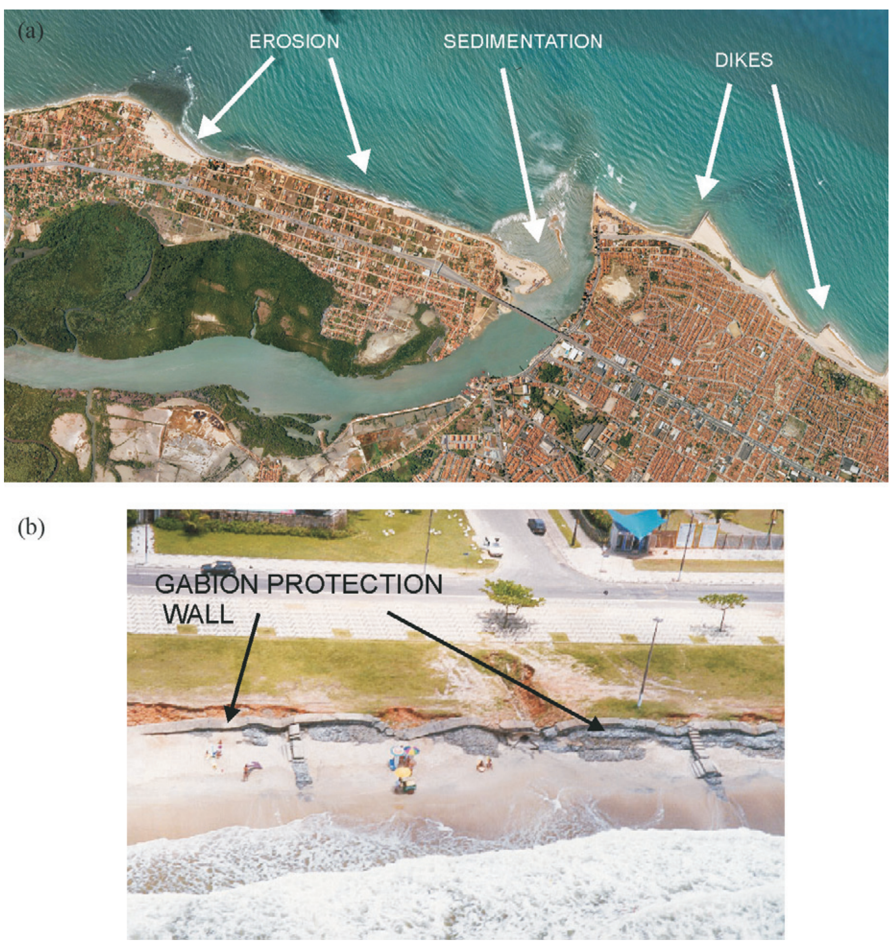

Figure 8 - Examples of sites affected by coastal erosion: a - the city of Fortaleza (Ceará State) with erosion and some dikes to control the sediment flow (Site 31 - Fig. 5); and b - the city of Matinhos (Paraná State) with facilities destroyed (Site 6 - Fig. 5).

ple were killed and hundreds of buildings were damaged. In June 2010, approximately 500 mm of rain fell in the states of Alagoas and Pernambuco, and approximately 40 cities were affected by flooding, erosion and other types of hazards; some cities were more than 80% destroyed. These cities are located in the coastal zone and in areas at higher altitudes. The economic and social damage caused by these disasters required more than $1.5 billion USD to cover direct damage and reconstruction.

7.3. Zone 3 - Composed of sandstones and sandy unconsolidated materials

This zone is composed of areas with sandy sediment, sandstones with different degrees of cementing and sandy transported and residual unconsolidated materials (Fig. 5). The rocky materials are normally covered by up to 100 m of sandy, unconsolidated materials with high porosity, low mechanical resistance, high erodibility index values and a high rate of potential infiltration. Erosive processes; soil collapse; and the desertification and silting of rivers, dams and lakes predominantly occur in these areas. Zone 3 is distributed across different parts of Brazil (Fig. 5), and, as examples, we present two geological vertical sections representative of areas in Figs. 9 and 10 (for one region in the northern part and another in the western part). Intense erosion and silting problems are very common in these areas. In all regions classified as Zone 3, there was estimated to be more than 100,000 erosion features classified as gullies. These intense erosional processes result from intense uses for agriculture and pasture in combination with sandy geological materials and high rainfall intensities and durations. Fig. 11 shows sand deposition (sand bars) in the Parnaíba River (Site 32 - Fig. 5, Piauí State) and erosion features in the Camapuã region (Site 38 - Fig. 5, northeastern part of Mato Grosso do Sul State).

7.4. Zone 4 - Aeolian sandstones

This zone includes areas made up of Triassic sandstones with different degrees of cementing. These sandstones are spread over more than 1 million km^2, but much of that area is covered by other geological materials, as can be seen in the vertical geological section shown in Fig. 12. These geological materials are the most important aquifer in Brazil. Environmental problems, such as sub-superficial water pollution, erosion, silting, desertification and collapsible soils, exist in this area. These sandstones are generally considered to contain good groundwater reservoirs, but the recharge of these reservoirs is directly affected by the use and management of the soil. Another problem is the intense erosive processes associated with the sandy residual unconsolidated material from the sandstones of the lower layers. The southwestern portion of the state of Rio Grande do Sul has been suffering greatly (during the period from November 2011 to March 2012) from intense drought. The economic losses caused by this phenomenon and its associated agricultural damage are on the order of 3 billion USD.

7.5. Zone 5 - The Amazon region

This zone is composed mainly of unconsolidated materials (sediments of Quaternary and Tertiary ages) and weakly cemented sedimentary rocks (Fig. 13). The natural process most common in this region is flooding, but it does not heavily affect the population in small cities because the population density is generally small near the rivers, with the exception of some large cities such as Manaus, Belém, Santarém and Parintins. There are fewer than 10 large cities in the region. Small urban areas near the rivers are prepared

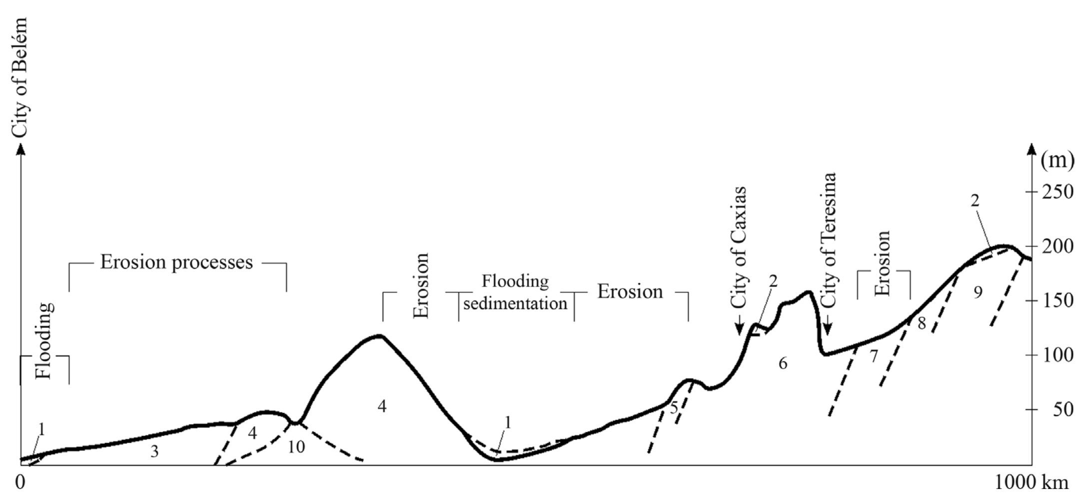

Figure 9 - A schematic vertical geological section of Zone 3 - northern portions (section B - Fig. 5). Legend: 1 - Alluvial sediments (Quaternary); 2 - Clastic sediments and laterites (Tertiary); 3 - Sandstones, siltstones and conglomerates (Tertiary); 4 - Sandstones, limestones, marls and shales (Cretaceous); 5 - Sandstones, shales and limestones (Cretaceous); 6 - Sandstones, siltstones, shales and limestones (Permian); 7 - Sandstones (Carbo-Permian); 8 - Sandstones, siltstones, shales and coal layers (Carbo-Permian); 9 - Sandstones, siltstones and shales (Devonian); and 10 - Phyllites, quartzites and metasedimentary rocks (late Proterozoic).

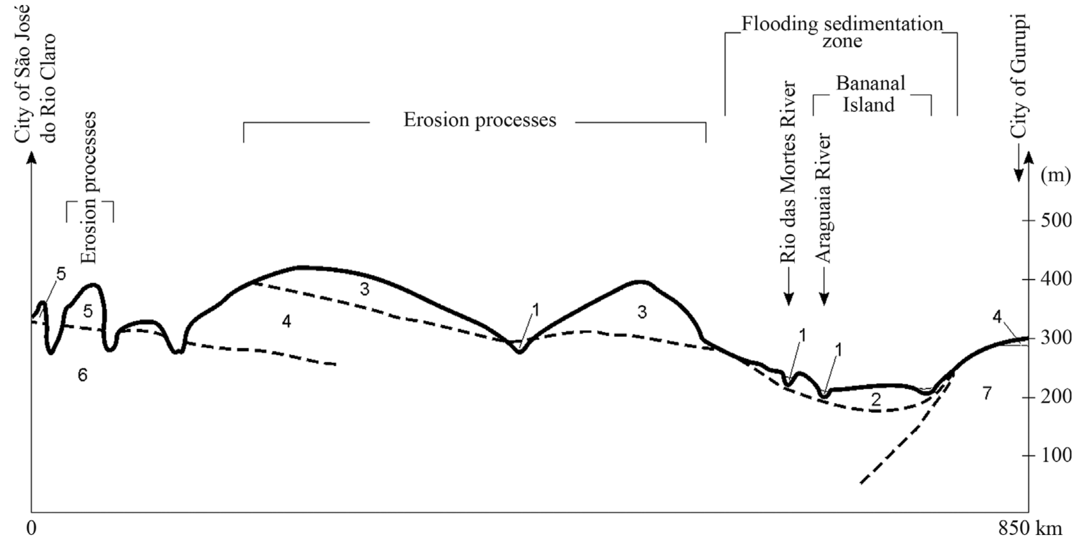

Figure 10 - A schematic vertical geological section of Zone 3 - western portion (section C - Fig. 5). Legend: 1 - Alluvial sediments (Quaternary); 2 - Sandy sediments with gravel layers (Quaternary); 3 - Sandy-silty sediments and laterites (Tertiary-Quaternary); 4 - Clastic sediments and laterites (Tertiary); 5 - Sandstones (Cretaceous); 6 - Sandstones, conglomerates, siltstones and claystones (Palaeozoic-Mesozoic); and 7 - Quartzites, schists, marbles and other metamorphic rocks (middle Proterozoic).

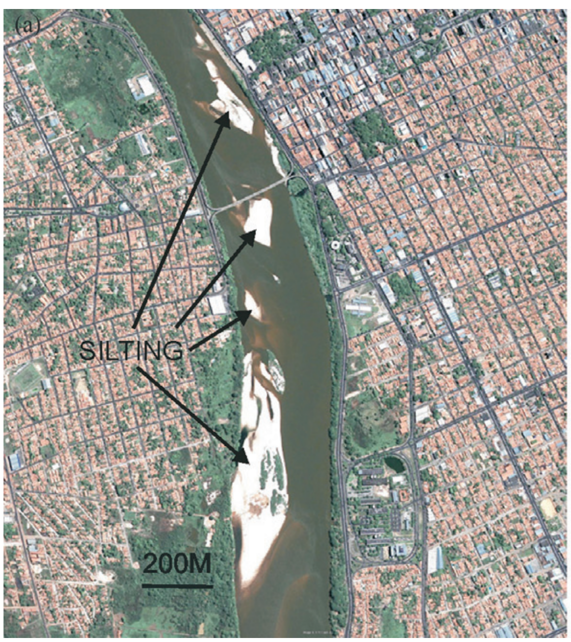

Figure 11 - Areas strongly affected by erosional processes and silting: a) sediment deposits (Site 32 - Fig. 5) in the Parnaiba River (city of Teresina - Piauí State) and b) gullies in the Camapuã region (northeast portion of Mato Grosso do Sul State, Site 38 - Fig. 5).

for and accustomed to this natural process. The floods are intense because the rivers drain very large areas, and the rainfall is controlled by the climatological conditions of the Northern and Southern Hemispheres. However, this region suffers heavily from dry periods when the river water levels decrease so that it is impossible to navigate small boats, which are the main form of transportation and are also used for tourism and fishing, which are very important economic activities.

Urbanisation has affected the equilibrium of the geological materials, generating gravitational mass movements, erosion and other natural processes in the main urban areas such as Manaus, Belem and Macapá (Fig. 14). The metropolitan regions of Belém, Para State, (Site 41 - Fig. 5), and Manaus, Amazonas State, (Site 34 - Fig. 5) have been affected by flooding of up to 15 m (in April 2012). Due to the very flat topography (with an average relief amplitude of less than 5 m) the flooding covers large ar-

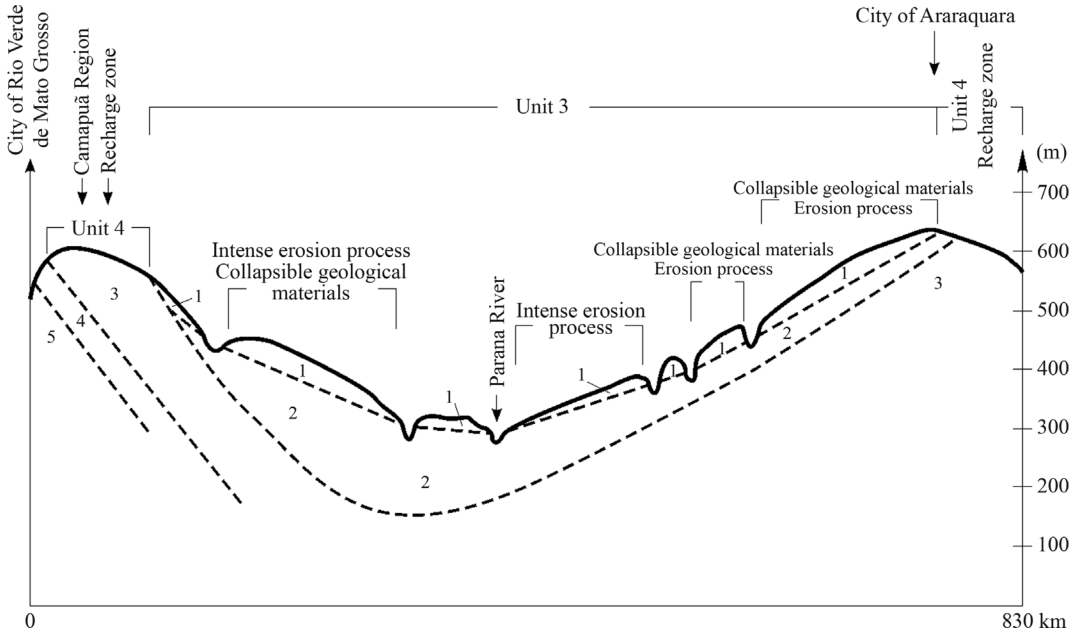

Figure 12 - A schematic vertical geological section of Zones 3 and 4 (section E - Fig. 5). Legend: 1 - Sandstones, siltstones and minor claystones (Cretaceous); 2 - Basalts (Juro-Cretaceous); 3 - Aeolian sandstones (Jurassic); 4 - Sandstones and siltstones (Carboniferous-Permian); and 5 - Siltstones and shales (Devonian).

eas. The Acre and Roraima states were affected by flooding in the January, February and March of 2013.

7.6. Zone 6 - Areas affected by seismic activity

This zone includes areas where the frequency of seismic activity is higher than average for Brazil (Fig. 15). These areas are associated with specific geographic positions that are associated with geological structures. Some of these areas have not suffered economic losses because they have not been affected by high-magnitude seismic activity. However, this area is experiencing increased development, and the seismic aspects have been considered as dynamic parameters in these projects. The majority of earthquakes recorded in Brazil since the 1800s have had Modified Mercalli Intensity lower than 4, with a small percentage (5%) ranging from 6 to 7. The highest recorded intensity according to the Modified Mercalli Intensity scale is 6. Approximately 80% of earthquakes recorded in Brazil between 1800 and the present occurred in the areas noted in Fig. 15.

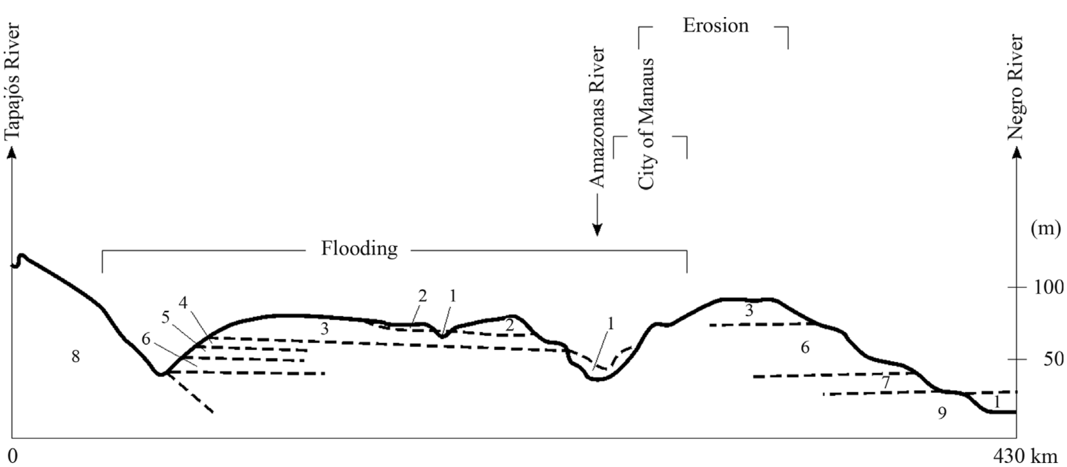

Figure 13 - A schematic vertical geological section of Zone 5 (section A - Fig. 5). Legend: 1 - Alluvial sediments (Quaternary, Tertiary); 2 - Weakly cemented sandstones (Quaternary, Tertiary); 3 - Sandstones, siltstones and shales (Cretaceous); 4 - Sandstones, siltstones, shales and limestones (Carbo-Permian); 5 - Sandstones, siltstones and shales (Devonian); 6 - Sandstones, siltstones and shales (Ordo-Silurian); 7 - Arkoses, conglomerates and sandstones late Proterozoic); 8 - Acid and intermediate volcanics (middle Proterozoic); 9 - Hornblende-gneisses, schists, amphibolites and diorite (Archean).

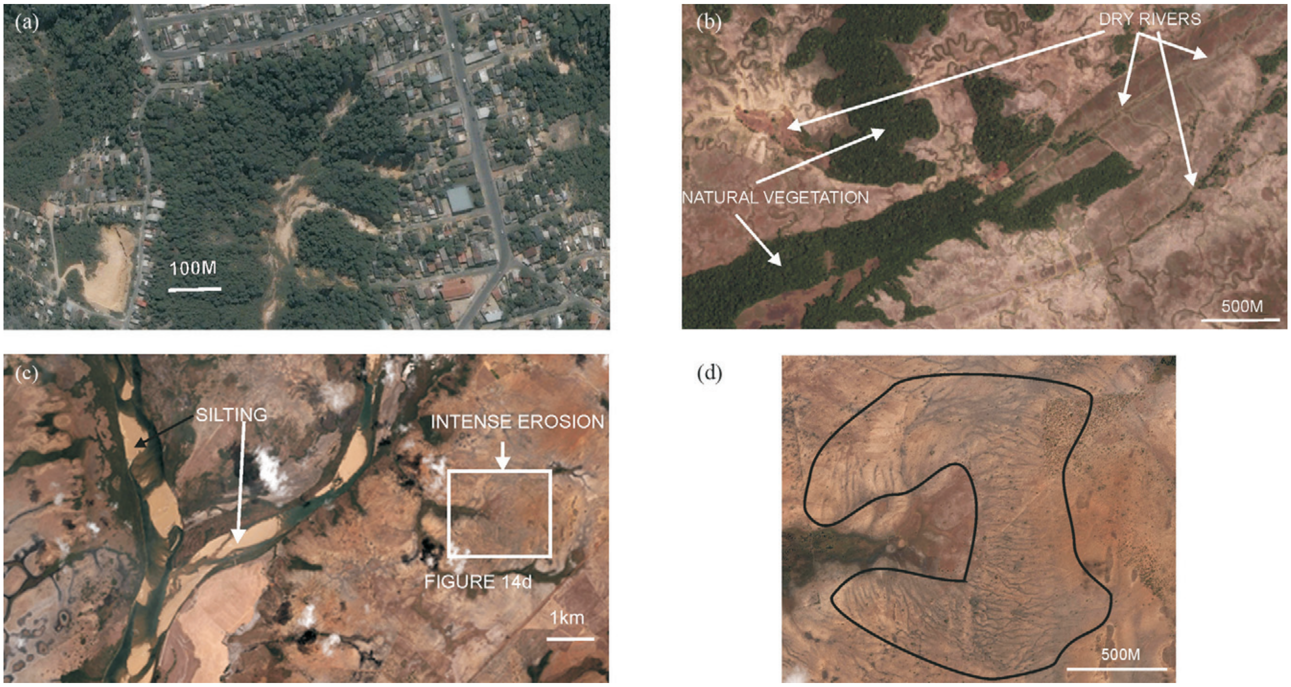

Figure 14 - Degraded areas due to deforestation, overcultivation and overgrazing: (a) Erosion and gravitational mass movement in the city of Manaus, Amazonas State (Site 34 - Fig. 5); (b) Degraded land in the Macapá region, Amapá State (Site 33 - Fig. 5); (c) A river highly affected by silting due to erosional processes in the Boa Vista region, Roraima State; and (d) Detail of intense erosional processes

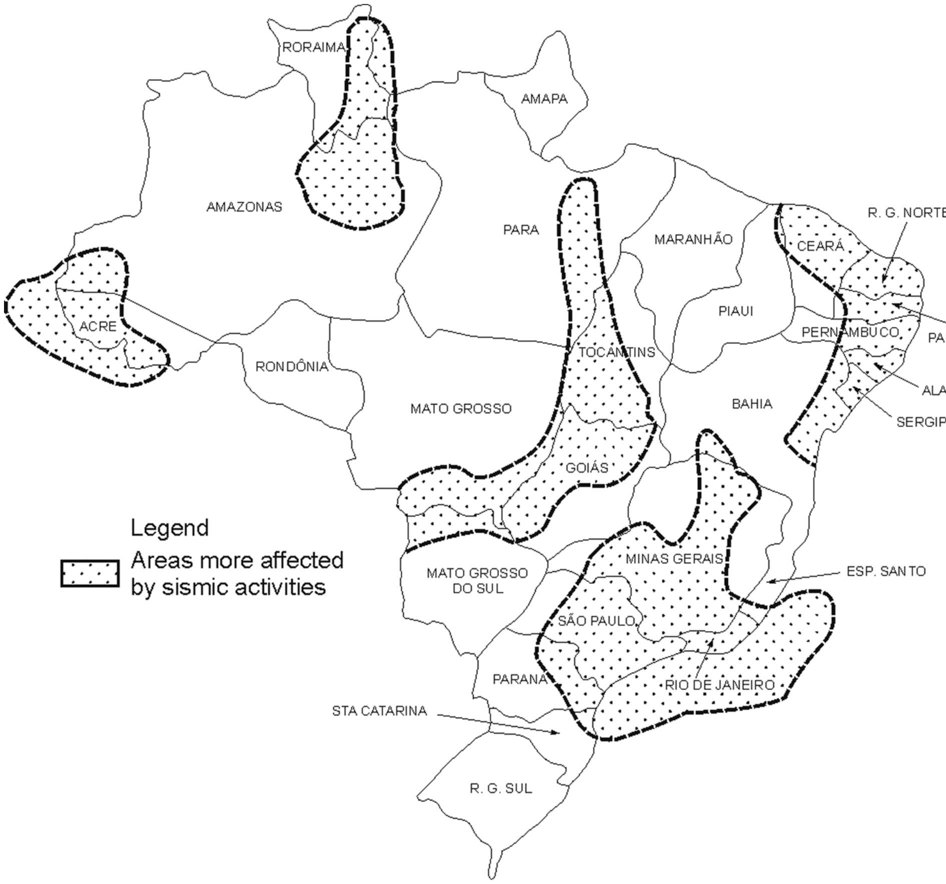

Figure 15 - The regions most affected by earthquakes in Brazil. Modified from (Mioto, 1993), OBSIS (2010) and IAG/USP (2010).

7.7. Zone 7 - Areas composed of carbonate rocks

These regions are composed of calcitic and dolomitic limestones, marbles, and calcareous rocks in different proportions associated with other sedimentary and metamorphic rocks (Fig. 16); carbonate rocks crop out in approximately 10% of Brazil. Depressions, sinkholes and caverns of various sizes occur. In urban areas, this generates problems for construction and the environment. Cities ranging in size from 10 thousand to 2 million inhabitants are affected. Subsidence in rural areas generates problems, such as water accumulation, and prevents the use of heavy machinery in the plantations and even prevents the area from being used as a pasture. There are multiple examples of urban areas (see locations in Fig. 16) affected by subsidence: 1 - The metropolitan region of Curitiba (Paraná State); 2 - Lagoa Santa (Minas Gerais State); 3 - Sete Lagoas (Minas Gerais State), 4 - Laussance (Minas Gerais State); 5 - Vazantes, related to mining (Minas Gerais State); 6 - Cajamar (São Paulo State); 7 - Nobres (Mato Grosso State); 8 - Teresina (Piauí State); 9 - Matozinhos (Minas Gerais State); 10 - Morro do Chapéu (Bahia State); and 11 - Mossoró (Rio Grande do Norte State). In these regions, hundreds of sinkholes have been recorded in the last 20 years, mostly induced by groundwater exploitation. The metropolitan area of Curitiba is the largest of the 11 cited and, consequently, presents the greatest economic losses, mainly in the form of building damage and groundwater exploitation.

7.8. Zone 8 - Areas affected by natural disasters

This zone is the region most affected by natural hazards and disasters, including the 10 largest disasters in Brazil. It includes areas with very steep slopes (greater than 65°) and composed of igneous and metamorphic rocks, mainly granites, migmatites, gneisses, schists, phyllites and limestones (Fig. 17). The altitude is predominantly below 2,000 m, and rainfall can reach 4,500 mm, with daily values of 550 mm. However, the average maximum daily value is approximately 250 mm. These lithologies are associated with weathering profiles with a range of thicknesses and degrees of heterogeneity as well as slopes with different inclinations, from gentle to steep. The variability in the geological materials is very high, which increases the likelihood of diverse natural hazards. In these areas, almost all types of gravitational mass movements and linear erosion occur. These processes are caused by the geological-geotechnical characteristics of the weathering profiles or the unconsolidated materials that are associated with the specific conditions of infiltration, slopes of greater than 65 degrees, discontinuities from different sources parallel to the land surface, artificial embankments with inclinations above the geotechnical limits and earth fills with different degrees of compaction along their slopes. In the last five years, more than 15,000 gravitational mass movements and erosion events have occurred in this area. Among these events, more than 1,000 were classified as hazards, and some became disasters, with a predominance of gravitational mass movements, erosion, sinkholes, peat fires and anthropogenic disasters, such as the leakage of chemicals. Since 1990, large natural hazards have occurred in this

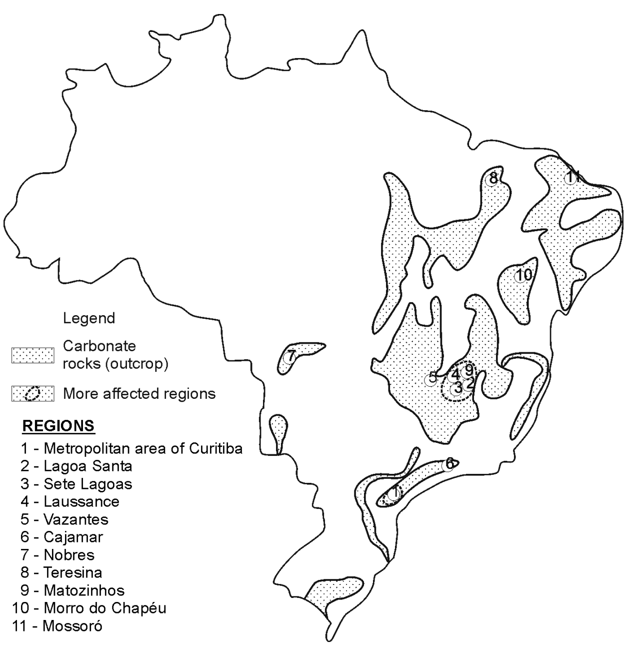

Figure 16 - The distribution of carbonate rocks and the main affected urban areas in Brazil.

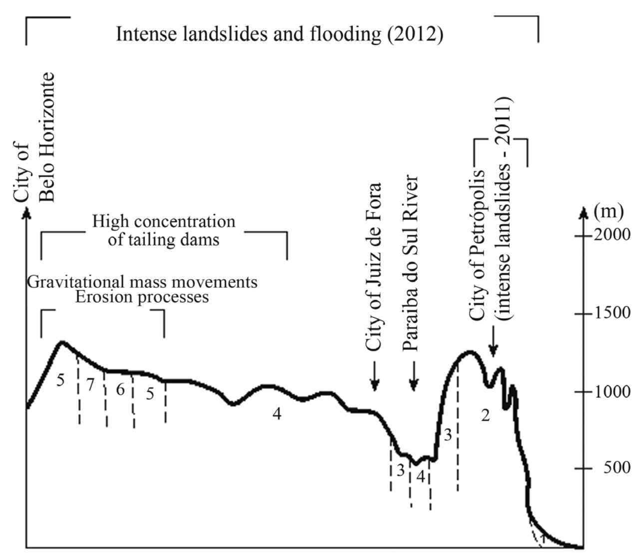

Figure 17 - A schematic vertical geological section of Zone 8 (section F - Fig. 5). Legend: 1 - Alluvial and colluvial sediments (Quaternary, Tertiary); 2 - Granites (late Proterozoic); 3 - Gneisses, migmatites, schists, amphibolites and quartzites (late Proterozoic); 4 - Granulitic gneisses, migmatites, granitoids, gabbros and schists (Archean); 5 - Volcano-sedimentary sequence, quartzites, schists, phyllites and iron formations (Archean); 6 - Quartzites, phyllites, itabirites and schists (early Proterozoic); and 7 - Migmatites, gneisses and granitoids (Archean).

zone, with significant economic losses, and have resulted in the deaths of thousands of people. In December 2010 and January 2011, approximately 400 cities were affected by flooding and landslides of different intensities and magnitudes, including the metropolitan regions of São Paulo, Curitiba and Belo Horizonte. The metropolitan region of São Paulo, the biggest and most economically important urban area in Brazil, is located in this region and is affected annually by intense floods and moderate gravitational mass movements, mostly induced by human interference with the valleys and slopes, which has changed the morphometry and the water dynamics. The annual economic losses can reach 1 billion USD per year, considering that the total extent of the metropolitan region of São Paulo covers 2,500 km^2 and has approximately 20 million inhabitants.

Of the 100 largest disasters in Brazil, many occurred in this zone. Table 3 shows the disasters and the deaths and the economic, social and environmental losses associated with each disaster (the locations are shown in Fig. 5). Table 3 shows that this zone has had, on average, one large disaster every 5 years. The number of hazardous events per year in this zone is very high, but only a small number of these events qualified as disasters, even in urban areas. Landslides normally occur due to changes in the mechanical strength of the geological materials, the inclination of the slope and favourable discontinuities, but landslides normally qualify as disasters if they develop into earth flows due to surface water accumulation and the number of rock blocks transported with the unconsolidated materials. In 2011, there were the same types of rain (intensity and duration) as in 2008 in the state of Santa Catarina; the rain resulted in flooding but not gravitational mass movement. Similar conditions were present in 1967, when major disasters occurred in the Serra das Araras region (city of Piraí) and the city of Caraguatatuba but not at other sites with the same geological characteristics (even though those sites experienced more rain). The fundamental factor for triggering gravitational mass movement in this zone is the rain distribution during the months before the occurrence of the hazardous events rather than high rain intensity over a short du-

Table 3 - The largest disasters occurring in Zone 8.

Year	Site	Type of hazard	Economic, social and environmental losses	Number of casualties
1800 to the present	São Paulo, São Paulo State	Flooding (average frequency less than 5 years)	Disruption of services until high economic losses occurred, with the destruction of buildings, roads and bridges	
1811, 1906, 1924	Rio de Janeiro, Rio de Janeiro State	Flooding	Disruption of services until high economic losses occurred, with the destruction of buildings, roads and bridges	100?
1911	Blumenau, Santa Catarina State	Flooding	People and infrastructure services were severely affected	
1928	Santos, São Paulo State	Landslides	Partial destruction of a hospital	60
1929	São Paulo, São Paulo State	Flooding	People were injured, and services were severely damaged	
1944	Caraguatatuba, São Paulo State	Landslides, flooding		
1948	Rio Paraiba do Sul Valley	Group of landslides	Hundreds of buildings	250
1956	Santos, São Paulo State	Landslides	Destruction of 100 houses	70
1966	Rio de Janeiro, Rio de Janeiro State	Landslides	Destruction of buildings and houses	200
1967	Serra das Araras - city of Piraí (Rio de Janeiro State)	Landslides	Roads, hydroelectric power and dozens of buildings	1,800
1967	Caraguatatuba, São Paulo State	Landslides	Destruction of 500 buildings and roads	150
1972	Campos do Jordão, São Paulo State	Landslides	Destruction of 80 buildings	20
1983	Blumenau, Santa Catarina State	Flooding	200,000 people were affected	50
1986	Lavrinhas, São Paulo state	Landslides	Destruction of houses, roads and bridges	20
1986	Cajamar, São Paulo State	Subsidence (karst)	Destruction of dozens buildings	

Table 3 (cont.)

Year	Site	Type of hazard	Economic, social and environmental losses	Number of casualties
1987	Rio de Janeiro	Flooding	20,000 people affected	300
1988	Cubatão, São Paulo State	Landslides and earth flow	Destruction of dozens of buildings	15
1988	Petrópolis, Rio de Janeiro State	Landslides	1,500 houses were destroyed ,and more than 5000 people were affected	200
1988	Rio de Janeiro	Landslides	Destruction of dozens of buildings	40
1989	São Paulo	Flooding, landslides	Destruction of dozens of buildings	20
1990	Blumenau, Santa Catarina State	Landslides, flooding	Houses, roads and bridges were destructed	20
1992	Belo Horizonte, Minas Gerais State	Landslides, flooding	Houses and roads were destroyed	20
1992	Contagem, Minas Gerais State	Landslides	Hundreds of buildings were destroyed	40
1995	Araranguá, Santa Catarina State	Landslides, flooding	Houses, roads, and plantations were damaged	40
1997	Ouro Preto, Minas Gerais State	Landslides, flooding	High economic, environmental and artistic losses	15
1999/2000	Campos do Jordão, São Paulo State	Landslides	Houses and roads were damaged	20
2002	Angra dos Reis, Rio de Janeiro State	Landslides, flooding	Railroads, buildings	52
2004	Santa Catarina State	Hurricane (wind speed higher than 155 km/h - category 1 on the Saffir-Simpson scale)	1,500 houses destroyed and 40,000 damaged. Economic losses higher than 500,000 USD	75
2008	Blumenau, Santa Catarina State	Landslides, flooding	More than 2 billion in economic losses. 1.5 million people were affected	300
2010	Angra dos Reis, Rio de Janeiro State	Landslides	300 houses and roads	50
2010	Paraty, Rio de Janeiro State	Landslides, flooding	Roads, houses and others types of buildings were damaged	10
2010	São Luiz da Paraitinga, São Paulo State	Flooding, landslides	Hundreds of buildings were destroyed	50
2010	Niterói, Rio de Janeiro State	Landslides	Destruction of hundreds of houses	180
2010	Rio de Janeiro	Flooding, landslides	Destruction of hundreds of houses	300
2011	Mountain region, Rio de Janeiro State	Landslides, flooding	10 billion USD in damages	1000
2012	Mountain region, Rio de Janeiro State	Landslides	2 billion USD in damage and damage to hundreds of buildings	50
2012	Minas Gerais State (110 cities were affected)	Landslides, flooding	More than 3 million people affected and economical losses higher than 3 billion	30
2012	Rio Grande do Sul State (50 municipalities affected)	Drought	3 billion USD	10
2012	Santa Catarina State	Landslides, flooding	500,000 USD	
2013	Mountain region, Rio de Janeiro State	Landslides, flooding	100 houses destroyed and hundreds damaged. Economic losses higher than 3000,000 USD	20

ration. Hundreds of datasets describing the relationships between rain and gravitational mass movements have been collected by CNR/IRPI (2010), and the results indicate that each region is characterised by specific interactions between geological materials and rain. In Brazil alone, there are dozens of examples of this type of relationship for regions separated by only short distances (Guidicini & Iwasa, 1976; Tatizana, 1987; Elbachá *et al.*, 1992; D'Orsi *et al.*, 1997). These complex relationships reflect the fact that gravitational mass movements depend on the combination of several factors, mainly geological, geotechnical and hydrogeological. Some of the disasters presented in Table 3 were chosen as examples, and a small group of characteristics is presented below to show the general intensities and magnitudes of losses. During the period from January to March of 1967, Serra do Mar Mountain, mainly in the states of São Paulo and Rio de Janeiro, suffered daily from intense rainfall of as much as 450 mm per day, with values reaching 300 mm in 3 hours at some sites. In January, a large group of landslides and earth flows reached the Serra das Araras region (near the city of Piraí, Rio de Janeiro state) over an area of approximately 3,000 km^2 (this is well described by Jones, 1973), and another group of landslides and earth flows occurred in the city of Caraguatatuba (São Paulo State). Both disasters killed more than 2,000 people, destroyed hundreds of buildings, cars, roads, and plantations and seriously affected public health and social public services (Fig. 18). Intense gravitational mass movements occurred in 1995 in the Araranguá region (Santa Catarina State - Fig. 5) at altitudes between 600 and 1,100 m, affecting 11 municipalities. This event was associated with a rain event with an intensity of 550 mm/day and with a duration of 4.5 hours, and more than 40 people were killed and 20,000 people affected. These shallow landslides and earth flows began mostly at the crests of very steep slopes (scarps), and the earth masses displaced flows down to the feet of the scarps and continued in drainage channels, reaching high velocities and covering great distances. Fig. 19 shows examples of disasters that occurred in the Itajaí River Basin (SC) in December 2008, with losses greater than 2 billion USD. The landslides and earth flows of various intensities (dimensions and volumes) reached infrastructure works, including roads, bridges, buildings and plantations, causing major economic and environmental losses. Landslides began in different positions on the slopes. Part of the materials transformed into earth flows,

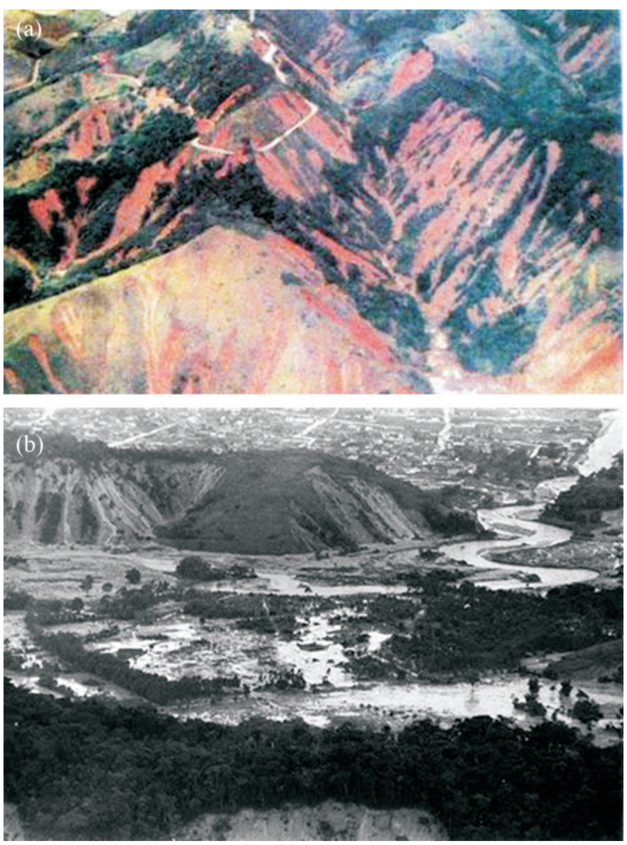

Figure 18 - Landslides in (a) Serra das Araras, Rio de Janeiro State (Site 36 - Fig. 5), and (b) the city of Caraguatatuba, São Paulo State (Site 10 - Fig. 5), in 1967. From Arquivo Base DER.

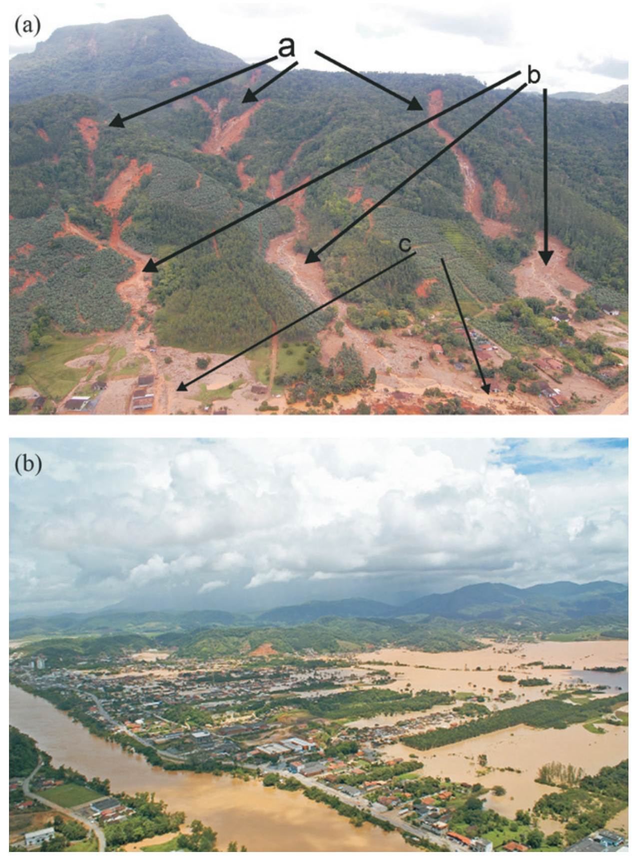

Figure 19 - Examples of natural disasters in the Blumenau region (Itajai Valley, Santa Catarina State; Site 5 - Fig. 5). (a) Gravitational mass movements (a - translational slide, b - earth flow covering buildings, c - valley with geological material transported by several earth flows) and (b) - Intense flooding.

reaching the valleys with accumulated sediments up to 10 m thick. The water level, as a result of flooding, reached 12 m above the normal level of the Itajaí River (although this limit is less than the maximum registered of 17 m) and killed more than 300 people. Flooding presented differently based on the type of valley; narrow valleys frequently suffer more losses than wide valleys. There were also gravitational mass movements in the Angra dos Reis region (Rio de Janeiro State) during the months of March and April 2010. During these events, dozens of people died, and the direct and indirect economic damages surpassed $500 million USD. During April 2010, the cities of Niteroi and Rio de Janeiro were strongly affected by landslides and earth flows that killed more than 400 people and resulted in more than 3 billion USD in damages. During January 2011, January 2012 and March 2013 the mountain region (Rio de Janeiro State) was strongly affected by rainfall on some days, triggering many large gravitational mass movements (*e.g.*, landslides, earth flows, rock falls) and flooding in the municipalities of Teresópolis, Nova Friburgo, Petrópolis, Areal, Sumidouro, São José do Vale do Rio Preto and Itaipava, affecting more than 100,000 people and killing more than 1,000. The intensities and sizes of the landslides varied significantly depending on the spatial arrangement of geological material layers, slope shape, slope profile and inclination. The economic losses exceeded 5 billion USD. The environmental and social losses are impossible to estimate because the cities, people, plantations and environment were strongly modified by the geological material displacement within the valleys and flood plains. In the first days of March of 2011, the region of Antonina and Morretes, in Paraná State, (Site 40 - Fig. 5) was heavily affected by more than 3,000 gravitational mass movements during the second week of March 2011. The volume of the displaced geological material varied from 10 to 200,000 m^3 (Fig. 20). Geologically, the region is composed of amphibolites and gneisses covered by weathered rock, saprolite and unconsolidated material layers, and talus and colluviums occur on some parts of the slopes. The slope inclinations vary from 10 to 70°. Approximately 20% of the gravitational mass movements occurred at locations with morphometric changes due to human interference, and the rest occurred in natural terrain with dense vegetation. These events injured more 10,000 people (approximately 20% of the total population), resulted in deaths, and generated high economic and social losses as well as significant environmental losses due to very large sediment load transported by earth flow to the ocean with its chemical products, including liquid and solid urban wastes and other types of dangerous chemical products (Fig. 20). From December 2011 to January 2012, the southern and southeastern regions of Brazil were affected by natural disasters, causing the destruction of roads, buildings, bridges and other facilities and killing hundreds people.

Figure 20 - Gravitational mass movements in the Antonina and Morretes region, Paraná State (site 40 - Fig. 5). a) General view, b) Sediment load generated by gravitational mass movements with chemical and organic compounds in the water of Antonina Bay (shown by the different colours of water).

8. Analysis

In Brazil, the perception of the problem varies; a natural or anthropogenic event can be classified as a disaster only if it leads to a casualty, irrespective of the magnitude or intensity. Therefore, even if a major disaster causes large economic losses, such as by damaging large plantations, it might not be classified as such. This perception complicates the study of hazards and disasters. Dozens of major hazardous events (*e.g.*, landslides and flooding) have occurred in areas with small populations and thus did not result in fatalities or large economic or social losses. However, in the last 30 years, hazardous events have occurred in urban areas, causing disasters with billions of dollars of losses and thousands of deaths. Considering both the distribution of the hazard types and the disasters in each state and their characteristics, an assessment was made to classify each hazard/disaster type per state into one of the 6 levels, as described in item 8 in the methods section. The results are presented in Table 4.

Considering the data from Table 4, the states most affected by hazards and disasters are Santa Catarina, São Paulo, Rio de Janeiro, Paraná and Minas Gerais; the most affected cities are the metropolitan regions of São Paulo, Rio de Janeiro, Belo Horizonte, Curitiba, Florianopolis,

Table 4 - Gradation of the levels of hazards and disasters for the states.

States/hazard/disaster sources	AP	RR	PA	AM	MA	PI	CE	RN	PB	PE	AL	SE	BA	MG	ES	RJ	SP	PR	SC	RS	MS	MT	RO	AC	GO	TO
1-Seismic activities			2	2		1	2	3	3	3			2	2		3	3				1	1		3	2	2
2-Wind						2	3	3									1									
3-High tides	1		1		1	1	2	2	1	1	1	1	1		1	1	1	2	2	2						
4-Drought				1	2	4	4	3	3	2	1	1	2	2						3	1					
5-Air pollution														1	3	3	5									
6-Saline soils/Salinization						1	2	2	2	1	1	1	1	1	1	1	1	1	1	2	1	1	1			
7-Flood (natural and induced)	1	1	2	4	2	1	2	1	1	2	2	1	2	2	1	5	6	3	4	3	1	2	1	1	1	1
8- Continental and coastal Erosion	2	2	2	1	2	2	3	2		2	1		1	3	1	4	5	4	4	4	4	4	2	1	3	2
9-River, lake and reservoir sedimentation.		2	2	2	1	2	2	1	1	1		1	1	2	1	2	3	2	2	2	3	3	1	1	3	2
10-Subsidences (Karst and underground excavation)				1									1	4		1	2	4	1	1	1	2			1	1
11- Gravitational mass movements				1	1		2	1		2	1		2	4	2	5	6	4	4	3		1				
12-Expansive soils and rocks							2	1		1			1	2		1	2	3	1	1		1		1		
13-Groundwater pollution							2	1		2			2	3		4	5	2	2	2		1	1			
14-Settlement and collapsible soils	1		2	2						2			1	2		2	3	3		2	2	1		1	1	1
15- Pipeline and power and tailing dam ruptures														4	1	2	3	2	1			1	1		1	1
16-Spontaneous fire in peat														1		1	2	1	1	1		1				
17-Desertification		2	1		2	3	2	2	1					1			1			2	1	2			1	1
18-Surface water pollution			2	2	1	1	2	1					1	2	1	3	4	2		2		1	1			
19-Soil pollution		1	2	2						1			2	3		2	3	2		2		2	1			
20-Dangerous components in soil and water																1	2	1		1						
21-Hoarfrost condition																		1	1	1						
22-Soil liquefaction																1	1									
23-Dune movements					2		3	4		1																

Table 4 (cont.)

States/hazard/disaster sources	AP	RR	PA	AM	MA	PI	CE	RN	PB	PE	AL	SE	BA	MG	ES	RJ	SP	PR	SC	RS	MS	MT	RO	AC	GO	TO
24-Radioactivity spill														1		2	2									
25-Natural radioactivity													1	1			1									
26-Uncontrolled earthfill and waste disposal on slopes			1		1		2			1			1	3		3	4	2	2	2	1	1			1	1
27-Concentrated surface water flow																	2	1		1		1			1	
28-Pollutant sources							1			1			1	3	1	3	3	2	1	2	2	2				

Legend: AP – Amapá, RR – Roraima, PA – Pará, AM - Amazônia, MA – Maranhão, PI – Piauí, CE – Ceará, RN – Rio Grande do Norte, PB – Paraíba, PE – Pernambuco, AL – Alagoas, SE – Sergipe, BA - Bahia, MG - Minas Gerais, ES - Espírito Santo, RJ - Rio de Janeiro, SP - São Paulo, PR – Paraná, SC - Santa Catarina, RS – Rio Grande do Sul, MS - Mato Grosso do Sul, MT - Mato Grosso, RO – Rondônia, AC – Acre, GO - Goiás, TO – Tocantins.

Salvador and Recife. Half of the Brazilian population lives in these states (Fig. 3).

Zones 3 and 5 are most affected by agriculture; in Zone 5, due to deforestation and changes in the surface layers of the soils, whereas Zone 3 presents problems related to relief and runoff changes, decreases in the water infiltration and other problems. Zone 2 is the one most affected by urbanization because it contains the majority of the large cities. The relief and runoff changes in this zone have been significant, which have resulted in very dangerous flooding.

In Zone 8, man-made hazards are commonly related to several sources, but tailing dams and sanitary landfills are responsible for significant economic and environmental losses. Tailing-dam ruptures have destroyed buildings, bridges and plantations in large areas, contaminated river waters and occasionally even reached the ocean. The sanitary landfills and others types of waste deposits generate environmental problems related to groundwater contamination and sometimes result in economic and environmental losses due to the rupture of waste masses. In this zone, thousands of land areas are degraded around hundreds of sanitary landfills (controlled and uncontrolled).

Continental erosion, silting, salinization, pollutant sources, desertification and water pollution have generated very high environmental losses, mainly in Zone 1, followed in decreasing order of severity by Zones 2, 5 and 3. However, floods and gravitational mass movements are responsible for more than 80% of the fatalities. For example, erosion has deeply affected the facilities in urbanized areas, even in small cities, mainly damaging streets, water pipes, pluvial drainage systems and sanitation systems; in rural areas, floods have affected unpaved roads, man-made slopes, and the ability to use heavy machines on plantations and pastures.

Zones 2 and 8 experienced the greatest economic, social and environmental losses and disasters that killed hundreds of people. Based on the population distribution (Fig. 3), both zones occupy 80% of the areas with more than 50 inhabitants per km^2. These zones are associated with the climatic conditions (Fig. 2) in which rainfall reaches values as much as 4,500 mm/year and can occur throughout the year. Eighteen of the large cities cited in Table 3 and more than a dozen of the cities considered in Table 3 are located in these zones, including the metropolitan regions of São Paulo, Rio de Janeiro, Belo Horizonte, Curitiba and Porto Alegre. In these zones, disasters appear to have been primarily caused by natural and man-made hazards over the past 25 years.

Considering the distribution of the hazards and the frequency of the disasters found in the eight zones and combined with the population distribution (Fig. 3), we assessed the preliminary direct vulnerability of selected environmental factors (Table 5). The vulnerability assessment was developed considering two characteristic scenarios: (i)

Table 5 - The vulnerability for each hazard and disaster zone considering the environmental elements, population, infrastructure and construction.

Zone	Hazard and degraded land sources	Vulnerability								
		Environmental aspects			Population			Facilities and constructions		
	Vulnerability degree based on hazard types, frequency and intensity	High	Moderate	Low	High	Moderate	Low	High	Moderate	Low
1	Silting	Lakes and Rivers				1*		Water reservoirs		
	Erosion	Landscapes	Rivers			1		Roads		
	Contamination	Surface water	Sediments			1		Water reservoirs		
	Flooding	Lakes and Rivers			3			Build-ings, roads, bridge, dams		
2	Coastal erosion	Beach			2			Buildings, ports	Roads	Pipelines
	Flooding	Rivers, flooding plain			3			Buildings, roads, bridge, dams		
	Gravitational mass move-ments	Relief	Rivers		2			Building, roads	Pipelines	Power lines
3	Erosion	Landscapes	Rivers		1			Roads	Building	
	Silting	Rivers, lakes				1		Water reservoirs		
	Contamination	Groundwater	Soil		1				Industries	
4	Contamination	Groundwater	Superficial water		2			Industries		
	Desertification	Landscapes	Rivers, lakes		1			Agriculture		
	Erosion	Landscapes, rivers				1		Pastures	Cultivations	
	Groundwater lowering	Groundwater, springs			2			Industries		
5	Erosion	Landscape, rivers	Lakes			1			Roads, buildings	
	Desertification	Rivers, landscape			1			Agriculture		
	Streambank erosion	Rivers	Lakes ,reservoirs			1		Fluvial transporta-tion, bridges, ports	Buildings, pipe-lines, roads	
	Flooding	Floodplains			3			Buildings, ports	Roads	
6	Earthquakes						1			Buildings, roads, dams
7	Desertification	Superficial and groundwater, soil fertility			2			Cultivations	Buildings	Roads
8	Sinkholes	Groundwater				2		Buildings, roads	Pipelines	
	Depressions (uvalas and others)	Groundwater and surface water				1		Buildings, roads		

Table 5 (cont.)

Zone	Hazard and degraded land sources	Vulnerability								
		Environmental aspects			Population			Facilities and constructions		
	Vulnerability degree based on hazard types, frequency and intensity	High	Moderate	Low	High	Moderate	Low	High	Moderate	Low
9	Caverns	Groundwater				1		Buildings, roads		
	Contamination	Groundwater			2			Industries		
	Gravitational mass movement	Relief, rivers			3			Building, roads	Pipelines, power lines	
	Erosion	Rivers				1		Roads	Pipelines	Power lines
	Flooding	Rivers, flooding plain			3			Building, roads	Pipelines	Power lines
	Tailing dam ruptures	Rivers				1		Bridges, cultivations		
	Uncontrolled sanitary landfills	Groundwater	Surface water, soil			1			Water reservoirs	

Legend: 1* - magnitude of the vulnerable people.

based on the distribution of the hazards in the 8 zones and considering the possibilities of the most important natural components, construction and infrastructure factors, which resulted in a classification involving high, moderate and low vulnerability levels; and (ii) based only on the population to determine the specific vulnerability of the people related to specific hazard types based on the population and density distribution. The latter analysis was used to evaluate the magnitude of vulnerable people in each zone. Three levels were used, from 1 (low magnitude) to 3 (high magnitude), according to item 10 of the materials and methods section.

9. Conclusions

Brazil urgently needs governmental legislation for the creation of an organization responsible for territorial planning, including geological and geotechnical studies on hazard forecasting, with the objective of avoiding disasters and decreasing the associated economic, social, human and environmental losses.

Between 2008 and 2012, at least 400 disasters occurred in Brazil, generating high economic and social losses, affecting more than 10 million people and killing more than 3,000 people. However, only a few events were recorded, either in the EM-DAT database or in the Brazilian databases.

The inventory of this study allowed us to collect a large amount of data on the occurrence of hazards and disasters in Brazil. The eight most affected zones make up more than 40% of the territory of Brazil and consist of more than 70% of the Brazilian population.

Results from this study provide evidence that there is a need for a countrywide policy to forecast these hazards. All Brazilian states experience hazards and disasters, and these hazards are irregularly distributed. Unfortunately, there is a lack of basic knowledge about the environmental factors responsible for such hazards (*e.g.*, rock, unconsolidated materials, geotechnical characterization, climatic behaviors and land uses) in Brazil that is required for a technical understanding of the natural processes that are instrumental in bringing about these dangerous events and disasters.

The hazards and disasters, in terms of their distribution, magnitude and intensity, can be divided into four groups: 1 - hazards of great magnitude and intensity that are responsible for major disasters and economic losses, such as flooding, gravitational mass movements, continental and coastal erosion, subsidence, silting, desertification, tailing dam ruptures, dune movements and drought; 2 - spatially widespread hazards of moderate magnitude and intensity but high economic and social costs (*e.g.*, surface water pollution, saline soils/salinization, groundwater pollution, uncontrolled earth fills, collapsible soils and waste disposal on slopes); 3 - problems registered over smaller areas, such as soil pollution, natural radioactivity, soil liquefaction and expansive geological materials; 4 - occasional problems associated with low economic losses, such as spontaneous fires in peat, dangerous components released in the soil and water, high tides, seismic activities and radioactive spills.

The coastal zone (Zone 2) and mountain zone (Zone 8) are the most affected by disasters originating from gravitational mass movements, flooding, subsidence, tailing dams, sanitary landfills and erosional processes. The states most affected by such hazards, disasters and land degradation are Santa Catarina, São Paulo, Rio de Janeiro, Paraná, Pernambuco and Minas Gerais. The disasters have occurred in these zones at a frequency of once every 5 years and are associated with significant economic (500,000 USD) and social losses (damage to houses and infrastructure). Some urban areas in these zones experience disasters on an annual basis, whereas disasters due to gravitational mass movements occur once every 5 years in these areas.

Erosion, collapsible soils and silting are the common problems encountered in the regions classified as zones 1 and 3. There are rare fatalities associated with these events, but the economic and environmental costs can be significant and pertain largely to restoration and mitigation efforts. The rivers, lakes and reservoirs are very vulnerable, and people suffer from the indirect effects associated with human, industrial and livestock water requirements.

Zone 4 comprises the recharge areas of the main aquifer in Brazil. This zone is affected by contamination, and the groundwater level has lowered over time. In the long term, the problems inherent to this zone will limit groundwater exploitation, and hundreds of urban areas will suffer greatly as a result. In addition, there are changes in the nature of water infiltration from the ground surface because of agriculture and urbanization.

Zone 5 is intensely affected in terms of the associated environmental losses because of overcultivation and overgrazing, resulting in major changes to the natural condition of the geological materials, water dynamics and relief.

Annually, Brazil loses more than 1,000 people and 2 billion USD due to disasters originating from natural hazards, and Brazil has spent less than 10% of this amount on the forecasting of hazards and in adopting measures to minimize deaths and economic, social and environmental losses.

The spatio-temporal distribution of the triggering events does not follow a defined pattern in terms of trends or regional behavior, although the events are strongly related to geological and geotechnical aspects. Although hazards are distributed throughout the country, those involving gravitational mass movements, flooding and erosional processes deserve special attention because they are responsible for a significant portion of the economic and social losses. Gravitational mass movements occur mainly in areas with unconsolidated residual or transported materials overlying igneous and metamorphic terrane. Although laminar erosion has stabilized in the country since the adoption of improved agricultural management practices, the number of rills and gullies has increased significantly due to the redirection of superficial water flow. Studies of hazard forecasting that includes the mapping of hazard areas should be developed to make more informed disaster management plans.

The results of the inventory and analyses verify that there is an urgent need to develop systematic programs for specific geological and geotechnical research. These programs can develop engineering geological maps to support the elaboration of hazard maps and thus prepare adequate risk charts. These maps will provide fundamental information about the geological and geotechnical background of a region and the distribution of the hazard types and disasters in Brazil so that governmental institutions can adopt measures to control and avoid disasters caused by hazards.

Acknowledgments

We would like to thank the CNPQ (Conselho Nacional de Pesquisa), FAPESP (Fundação de Amparo a Pesquisa do Estado de São Paulo), CAPES (Coordenação de Apoio a Pesquisa e Educação Superior), MINEROPAR (Minerais do Paraná) and CENACID (Centro de Apoio Cientifico em Desastres) for their support of this study.

References

ABGE (2007) Banco de dados sobre a cartografia geotécnica e geoambiental do Brasil. http://itarget.com.br/newclients/abge.com.br/carto/, São Paulo, Brasil. Acesso em: 15/12/ 2006, 15/12/ 2007, 15/12/ 2008, 15/12/ 2009, 15/12/ 2010.

Ab'Saber, A.N. (1964) O Relevo Brasileiro e seus Problemas. Azevedo, A. (ed.). O Brasil, a Terra e o Homem. São Paulo, Ed. Nacional, p. 135-217.

Ab'Saber, A.N. (1988) O Pantanal Mato-Grossense e a Teoria dos Refúgios. Revista Brasileira de Geografia: Reflexões sobre Geografia, Rio de Janeiro, v. 50, n. especial.

Ahrendt, A. & Zuquette, L.V. (2003) Triggering factors of landslides in Campos do Jordão city, Brazil. Bull Eng Geol Env, v. 62:3, p. 231-244.

Alcántara-Ayala, I. (2002) Geomorphology, natural hazards, vulnerability and prevention of natural disasters in developing countries. Geomorphology, v. 47:2, p. 107-124.

Alcántara-Ayala, I. (2004.) Hazard assessment of rainfall-induced landsliding in Mexico. Geomorphology, v. 61:1/2, p. 19-40.

Alexander, D.C. (1993a) Natural Disasters. Academic Publishers, Kluwer, 630 pp.

Alexander, D.C. (1993b) Confronting catastrophe: New Perspectives on Natural Disasters. Terra Publishing, Harpenden, p. 340.

Alheiros, M.M. (1998) Riscos de Escorregamentos na Região Metropolitana do Recife. Tese de Doutorado em Geologia Ambiental, UFBA, 135 pp.

Amaral, C.P. (1996) Escorregamentos no Rio de Janeiro: Inventário, Condicionantes e Redução do Risco. Tese de Doutorado em Eng. Civil, PUC, Rio de Janeiro, 350 pp.

Amaral, C. & Palmeiro, F. (1997) Local landslide inventory of Rio de Janeiro: state of the art and access. ABMS, ABGE & ISSMGE (ed) Proc. 2nd Pan-American Symposium on landslides, II PSL/ 2a COBRAE, Rio de Janeiro, pp. 195-200.

Amaral Júnior, A.F. (2007) Mapeamento Geotécnico com Ênfase na Análise de Atributos Geológico-Geotécnicos Predisponentes aos Processos de Movimento de Massa Gravitacional: Costa Verde-RJ. Dissertação de Mestrado em Geotecnia, Escola de Engenharia de São Carlos, São Carlos, 150 pp.

Augusto Filho, O. (1994) Cartas de Risco a Escorregamentos: Uma Proposta Metodológica e sua Aplicação no Município de Ilha Bela, São Paulo. Dissertação Mestrado em Engenharia, Escola Politécnica, São Paulo, 150 pp.

Augusto Filho, O. (2004). Mass movements identification, modeling, analysis and mapping: some experiences in the southern of Brazil, São Paulo state. Lacerda, W.A.; Elrlich, M.; Fontoura, S.A.B. & Sayão, A.S.F. (eds) Landslides - Evaluation and Stabilization. Balkema - Rotterdam, Rio de Janeiro, v. 1, pp. 57-68.

Bacellar, L.A.P.; Lacerda, W.A. & Coelho Neto, A.L. (2004) Amphiteatre-like headwaters: areas of mudflow hazard in southeastern Brazil. Lacerda, W.A.; Elrlich, M.; Fontoura, S.A.B. & Sayão, A.S.F. (eds) Landslides - Evaluation and Stabilization. Balkema - Rotterdam, Rio de Janeiro, v. 1, pp. 565-570.

Balteanu, D.; Chendes, V.; Sima, M. & Enciu, P. (2010) A country-wide spatial assessment of landslide susceptibility in Romania. Geomorphology, v. 124:3/4, p. 102-112.

Barata, F.E. (1969) Landslides in the tropical region of Rio de Janeiro. Anais do Internacional Conference on Soil Mechanics and Foundation Engineering, 7, México, México: Sociedad Mexicana de Suelos, v. 2, pp. 41-68.

Bolt, B.A.; Horn, W.L.; Macdonald, G.A. & Scott, R.F. (1975) Geological Hazards. Springer-Verlag, New York, 328 pp.

Bonachea, J.; Bruschi, V.M.; Hurtado, M.A.; Forte, L.M.; Silva, M.; Etcheverry, R.; Cavallotto, J.L.; Dantas-Ferreira, M.; Pejon, O.J.; Zuquette, L.V.; Bezerra, M.A.O.; Remondo, J.; Rivas, V.; Gómez-Arozamena, J.; Fernández, G. & Cendrero, A. (2010) Natural and human forcing in recent geomorphic change; case studies in the Rio de la Plata basin. Science of the Total Environment, v. 408:13, p. 2674-2695.

Bonuccelli, T.J. (1999) Movimentos Gravitacionais de Massa e Processos Erosivos com Aplicação na Área Urbana de Ouro Preto, MG - Escala 1:10.000. Tese de Doutorado, Escola de Engenharia de São Carlos, São Carlos, 191 pp.

Brasil, Ministério da Integração Nacional (2010) Centro Nacional de Gerenciamento de Riscos e Desastres. http://www.defesacivil.gov.br/cenad/index.asp, Brasília, Brasil. Acesso em 15/12/ 2006, 15/12/ 2007, 15/12/ 2008, 15/12/ 2009, 15/12/ 2010.

Brasil, Ministério das Ciências e Tecnologia e Inovação. (2012) CEMADEN - Centro Nacional de Monitoramento e Alertas de Desastres Naturais. http://www.cemaden.gov.br/, Brasília, Brasil. Acesso em Março, Maio e Agosto de 2012.

Brasil, Ministério da Integração Nacional (2011) Atlas Brasileiro de Desastres Naturais. http://www.integracao.gov.br/atlas-brasileiro-de-desastres-naturais. Acessado em diferentes períodos.

Carvalho, C.S. (1996) Gerenciamento de Riscos Geotécnicos em Encostas Urbanas: Uma Proposta Baseada na Análise de Decisão. Tese de Doutorado em Engenharia de Solos, Escola Politécnica, São Paulo, 192 pp.

Carvalho, C.S. & Galvão, T. (2006) Ação de apoio a prevenção e erradicação de riscos em assentamentos precários. Carvalho, C.S & Galvão, T (Eds) Prevenção de Riscos de deslizamentos em Encostas: Guia para Elaboração de Políticas Municipais. Ministerio das Cidades, Brasília, pp. 10-17.

CENACID, Centro de Apoio Cientifico em Desastres. (2010) Mapa de Desastres no Brasil. http://www.cenacid.ufpr.br. Acessed em: 15/12/ 2006, 15/12/ 2007, 15/12/ 2008, 15/12/ 2009, 15/12/ 2010.

Cerri, L.E.S. (1993) Riscos Geológicos Associados a Escorregamentos: Uma Proposta para a Prevenção de Acidentes. Tese de Doutorado, Instituto de Geociências e Ciências Exatas, Rio Claro, 197pp.

Claessens, L.; Knapen, A.; Kitutu, M.G.; Poesen, J. & Deckers, J.A. (2007) Modelling landslide hazard, soil redistribution and sediment yield of landslides on the Ugandan footslopes of Mount Elgon. Geomorphology, v. 90:1/2, p. 23-35.

CNR/IRPI (2010) Rainfall thresholds for the initiation of landslides. http://rainfallthresholds.irpi.cnr.it. Visited in May of 2010.

CPRM (1983) Mapa Hidrogeológico do Brasil - Escala 1:5.000.000. Ministério das Minas e Energia, Brasil.

CPRM (2006) Projeto Rio de Janeiro - Inventário de Escorregamentos.

http://www.cprm.gov.br/publique/cgi/cgilua.exe/sys/start.htm?infoid=615&sid=26, Rio de Janeiro, Brazil. Acesso em: 15/12/ 2006, 15/12/ 2007, 15/12/ 2008, 15/12/ 2009, 15/12/ 2010.

CPRM (2007) Programa geologia do Brasil. http://www.cprm.gov.br/publique/cgi/cgilua.exe/sys/start.htm?infoid=79&sid=26, Rio de Janeiro, Brazil.

CPRM (2010) Geobank. http://geobank.sa.cprm.gov.br/, Rio de Janeiro, Brazil. Accessed in 12/12/2011.

Crozier, M. & Glade, T. (2004) Landslide hazard and risk: issues, concepts and approach. Landslide hazard and risk. Thomas Glade, M. Anderson & M. Crozier (eds). J. Willey & Sons, Ltd, West Sussex, p. 1-40.

Cruz, O. (1974) A Serra do Mar e o Litoral na Área de Caraguatatuba-SP: Contribuição á Geomorfologia Litorânea Tropical. Inst. de Geografia, Universidade de São Paulo, São Paulo-SP, Serie Teses e Monografias, 11, 181 pp.

DAEE/UNESP (1984) Mapas Geológicos do Estado de São Paulo - Escala 1:250.000. www.sigrh.sp.gov.br/sigrh/ARQS/RELATORIO/, São Paulo, Brazil. Accessed in 12/12/2011.

Dantas-Ferreira, M. (2008) Proposta de Índice para Processos Erosivos Acelerados a Partir de Levantamento e Diagnóstico Geológico-Geotécnico de Áreas Degradadas. Tese de Doutorado, Escola de Engenharia de São Carlos, São Carlos, 191 p.

Déstro, G.F.G.; Inojosa, F.C.P.; Dias, J. & Bottura, G. (2009) Áreas de risco ambiental por barragens no Estado de Minas Gerais. Anais XIV Simpósio Brasileiro de Sensoriamento Remoto, Natal, Brasil, pp. 5193-5200.

Dias, E. & Zuquette, L.V. (2004) Methodology adopted for probabilistic assessment of landslides in Ouro Preto, Brazil. In: Lacerda, W.A.; Elrlich, M.; Fontoura, S.A.B. & Sayão, A.S.F. Landslides - Evaluation and Stabilization. Balkema- Rotterdam, Rio de Janeiro, v. 1, pp. 287-292.

Dilley, M.; Chen, R.S.; Deichmann, U.; Lerner-Lam, A.L.; Arnold, M.; Agwe, J.; Buys, P.; Kjekstad, O.; Lyon, B. & Yetman, G. (2005) Natural Disaster Hotspots: A Global Risk Analysis (Synthesis Report). International Bank for Reconstruction and Development/The World Bank and Columbia University, p.210.

DNPM, Departamento Nacional de Produção Mineral (1984) Mapa Geológico do Brasil. Escala 1:2,500,000. Ministério das Minas e Energia, Brasil.

D'orsi, R.N.; Feijó, R.L. & Paes, N.M. (2004) 2,500 operational days of Alerta Rio System: history and technical improvements of Rio de Janeiro Warning System for severe weather. Lacerda, W.A.; Elrlich, M.; Fontoura, S.A.B. & Sayão, A.S.F. Landslides - Evaluation and Stabilization. Balkema- Rotterdam, Rio de Janeiro, v. 1, pp. 831-836.

D'Orsi, R.N.; D'Ávila, C.; Ortigão, J.A.R.; Dias, A.; Moraes, L. & Santos, M.D. (1997) Rio-Watch: The Rio de Janeiro landslide watch system. Proc Pan Am Symp on Landslides, 2, COBRAE, Rep 1, pp. 21-30.

DRM-RJ (2011) Megadesastre da Serra em Janeiro de 2011. www.drm.rj.gov.br/index.php?option=com_phocadownload&view=category&id=13:regio-serrana&Itemid=188. Rio de Janeiro, Brazil. Visited in July, 2011.

Elbachá, T.A. (1992) Estudo da Estabilidade de Encostas em Áreas pauperizadas de Salvador. UFBA, Salvador, 184 pp.

Elbachá, A. T.; Campos, L. E. P. & Bahia, R.F.C. (1992) Tentativa de correlação entre precipitação e deslizamentos na cidade de Salvador. Anais da Conferência Brasileira Sobre Estabilidade de Encostas - COBRAE, 1, 1992, Rio de Janeiro. v. II, pp. 647-656.

EM-DAT, Emergency Events Database (2010) The OFDA/CRED International Disaster Database. http://www.em-dat.net, UCL - Brussels, Belgium.

Fell, R.; Corominas, J.; Bonnard, C.; Cascini, L.; Leroi, E. & Savage, W.Z. (2008) Guidelines for landslide susceptibility, hazard and risk zoning for land use planning. Engineering Geology, v. 102:1/2, p. 85-98.

FIBGE, Fundação Instituto Brasileiro de Geografia e Estatística (1990) Mapa de Unidades de Relevo. Escala 1:5.000.000. Rio de Janeiro, Brasil.

GEORIO, Fundação Instituto de Geotécnica do Município do Rio de Janeiro. (2011) Alerta Rio. http://www2.rio.rj.gov.br/georio/site/principal.htm, Rio de Janeiro, Brazil.

Glade, T. & Crozier, M.J. (2005) A review of scale dependency in landslide hazard and risk analysis. Glade, T.; Anderson, M.G. & Crozier, M.J. (eds) Landslide Hazard and Risk. John Wiley, New York, pp. 75-138.

Gramani, M.F. (2001) Caracterização Geológica-Geotécnica das Corridas de Detritos ("Debris Flows") no Brasil e Comparação com Alguns Casos Internacionais. Dissertação de Mestrado em Engenharia de Solos, Escola Politécnica, São Paulo, 372 pp.

Guidicini, G. & Iwasa, O.Y. (1976) Ensaio de Correlação Entre Pluviosidade e Escorregamento em Meio Tropical. Publ 1080. IPT, São Paulo, 48 pp.

Guimarães, R.F.; Fernandes, N.F.; Gomes, R.A.T.; Greenberg, H.M.; Montgomery, D.R. & Carvalho Jr, O.A. (2003) Parameterization of soil parameters for a model of the topographic controls on shallow landsliding. Engineering Geology, v. 69:1/2, p. 99-108.

Guzzetti, F.; Cardinali, M. & Reichenbach, P. (1994) The AVI Project: A bibliographical and archive inventory of landslides and floods in Italy. Environmental Management, v. 18:4, p. 623-633.

Guzzetti, F.; Salvati, P. & Stark, C.P. (2005) Evaluation of risk to the population posed by natural hazards in Italy. Hungr, O., Fell, R.; Couture, R. & Eberhardt, E. (eds) Landslide Risk Management. Taylor & Francis Group, London, pp. 381-389.

Guzzetti, F.; Stark, C.P. & Salvati, P. (2005) Evaluation of flood and landslide risk to the population of Italy. Environmental Management, v. 36:1, p. 15-36.

Hach Hach, A. (1998) Inventário dos Movimentos de Massa Gravitacionais na Região Leste da Grande Curitiba-Paraná - Escala 1:20. 000. Dissertação de Mestrado em Geotecnia, Escola de Engenharia de São Carlos, São Carlos, 201 pp.

Herrmann, M.L.P. (2001) Levantamento dos Desastres Naturais Causados pelas Adversidades Climáticas no Estado de Santa Catarina Período de 1980 a 2000. Ed. Imprensa Oficial, Florianópolis, 97 pp.

Herrmann, M.L.P.; Pellerin, J.R.G.M. & Saito, S.M. (2004) Análise das ocorrências de escorregamentos no Estado de Santa Catarina com base nos formulários de avaliação de danos da Defesa Civil - 1980 a 2003. In: Anais Simpósio Brasileiro De Desastres Naturais, 1, Florianópolis. GEDN/UFSC, Florianópolis, pp 159-173 (CD-ROM).

IAG/USP (2010) Boletim Sísmico Brasileiro. http://moho.iag.usp.br/sismologia/boletim.php. São Paulo, Brasil.

IBGE (2007) Geociências - mapas. ftp://geoftp.ibge.gov.br/mapas/, Brasilia, Brazil.

IBGE (2010) Censos Demográficos: Resultados Preliminares do Censo Demográfico 2010. http://www.ibge.gov.br/estadosat/. Visited in March of 2011.

ISSMGE (2004) TC32 - Technical Committee on Risk Assessment and Management Glossary of Risk Assessment Terms - Version 1. http://jyching.twbbs.org/issmge/tc304.htm.

INPE/CPTEC (2007) Banco de dados. http://bancodedados.cptec.inpe.br/, São José dos Campos, Brazil. Visited in December, 2011.

IPT, Instituto de Pesquisas Tecnológicas (1995) Mapa de Erosão do Estado de São Paulo. Escala 1:1.000.000. 1ª edição. Convenio IPT - DAEE. São Paulo.

Jones, F. (1973) Landslides of Rio de Janeiro and the Serra das Araras Escarpment, Brazil. Geological Survey Professional Paper 697, 42 pp.

Kirschbaum, D.B.; Adler, R.; Hong, Y. & Lerner-Lam, A. (2010) A global landslide catalog for hazard applications: Method, results, and limitations. Natural Hazards, v. 52:3, p. 561-575.

Korup, O. (2005) Geomorphic hazard assessment of landslide dams in South Westland, New Zealand: Fundamental problems and approaches. Geomorphology, v. 66:2, p. 167-188.

Lacerda, W.A. (1997) Stability of natural slopes along the tropical coast of Brazil. Almeida, M. (ed), Proceeding of the International Symposium on Recent Developments in Soil and Pavement Mechanics. A.A. Balkema, Rotterdam, pp. 17-39.

Lollo, J.A. (2008) Solos Colapsíveis: Identificação, Comportamento, Impactos, Riscos e Soluções Tecnológicas. Edunesp, Ilha Solteira, 280 pp.

Macedo, E.S.; Costa, M. & Salles, A.E.R. (1999) Informatização do cadastramento de acidentes de escorregamentos com vítimas fatais ocorridos no Brasil no período de 1988 a 1999. Proc. 9º Congresso Brasileiro de Geologia de Engenharia, São Pedro, pp. 1-10 (CD-ROM).

MINEROPAR, Minerais do Paraná (2005.) Geologia e gestão territorial. http://www.mineropar.pr.gov.br/, Curitiba, Brazil. Visited in December, 2011.

Mioto, J.A. (1993) Sismicidade e Zonas Sismogênicas do Brasil. Tese de Doutorado, Instituto de Geociências e Ciências Exatas, Rio Claro, 2 v., 500 pp.

Miranda, E.E. de & Coutinho, A.C. (2004) Brasil Visto do Espaço. Campinas: Embrapa Monitoramento por Satélite. Disponível em: http://www.cdbrasil.cnpm.embrapa.br. Acessed in: 22 mar. 2007.

Nimer, E. (1989) Climatologia do Brasil. Secretaria de Planejamento e Coordenacao da Presidencia da República e IBGE, Rio de Janeiro, 421 pp.

Novelo-Casanova, A. & Suárez, G. (2012) Natural and man-made hazards in the Cayman Islands. Natural Hazard, v. 61:3, p. 1277-1292.

Nunes Bandeira, A.P. & Coutinho, R.Q. (2008) Landslide risk management: Experiences in the metropolitan area of Recife - Pernambuco, Brazil. Chen, Z.; Zhang, J.; Li, Z.; Wu F. & Ho K. (eds) Proceeding of the tenth International Symposium on Landslides and Engineered Slopes, Xí An, v. 2, pp. 1887-1892.

OAS, Department of Regional Development and Environment (1990) Primer on natural hazard management in integrated regional development planning. Washington, D.C; OAS, p.413 ilus, mapas, tab.

OBSIS (2010) Sismicidade no Brasil. http://www.obsis.unb.br. Brasília. Brasil. Visited in November, 2011.

Pichler, E. (1957) Aspectos geológicos dos escorregamentos de Santos. Boletim da Sociedade Brasileira de Geologia, v. 6:2, p. 69-77.

Ploey, J. de & Cruz, O. (1979) Landslides in the Serra do Mar, Brazil. Catena, Giessen, Germany, v. 6:2, p. 111-122.

Remondo, J.; Soto, J.; González-DIéz, A.; DIáz de Terán, J.R. & Cendrero, A. (2005) Human impact on geomorphic processes and hazards in mountain areas in northern Spain. Geomorphology, v. 66:1, p. 69-84.

Silva, A.F. & Zuquette, L.V. (2010) Landslide hazard assessment from the 3D safety factor: Campos do Jordão, SP, Brazil. Proceeding of the 11th International Congress of the International Association of Engineering Geology and Environment, Auckland, New Zealand, pp. 1435-1441 (CD-ROM).

Tatizana C.; Ogura A.T.; Cerri L.E.S. & da Rocha M.C.M. (1987) Análise de correlação entre chuvas e escorregamentos-Serra do Mar, município de Cubatão. Proc Anais do Congresso Brasileiro de Geologia de Engenharia, v. 5:1, p. 225-236.

UNB, Instituto de Geociências (2008) Esboços e mapas geológicos de algumas pesquisas e teses. http://vsites.unb.br/ig/mapgeo.htm, Brasília, Brasil. Visited in July, 2011.

UNDRO (1984) "UNDRO preparedness aspects", Disaster Prevention and Mitigation, A Compendium of Current Knowledge. United Nations, New York, 221 pp.

UNDRO (1991) United Nations Disaster Relief Office. UNDRO'S Approach to Disaster Mitigation. UNDRO News, jan-febr. Office of the United Nations Disaster Relief Coordinator, Geneva, 20 pp.

UN/ISDR (2010) Disaster Statistic. http://www.unisdr.org/disaster-statistics/introduction.htm (Verified in May of 2010).

Van Den Eeckhaut, M. & Hervás, J. (2012) State of the art of national landslide databases in Europe and their potential for assessing landslide susceptibility, hazard and risk. Geomorphology, v. 139-140:1, p. 545-558.

Varnes, D.J. & the International Association of Engineering Geology Commission on Landslides and Other Mass Movements (1984) Landslide Hazard Zonation: A Review of Principles and Practice. Natural Hazards. UNESCO, Paris, v. 3, p. 63.

White, G.F. & Haas, J.E. (1975) Assessment of Research on Natural Hazards. The Massachusetts Institute of Technology Press, Cambridge, 487 pp.

Wolle, C.M. (1988) Análise dos Escorregamentos Translacionais Numa Região da Serra do Mar no Contexto de uma Classificação de Mecanismos de Instabilização de Encostas. Tese de Doutorado em Geociências, Escola Politécnica, São Paulo, 320 pp.

Wolle, C.M. & Carvalho, C.S. (1989) Deslizamentos em encostas na Serra do Mar-Brasil. Solos e Rochas, v. 12:1, p. 27-36.

Yang, X.; Zhang, K.; Jia, B. & Ci, L. (2005) Desertification assessment in China: an overview. Journal of Arid Environments, v. 63:2, p. 517-531.

Zaruba, Q. & Mencl, V. (1969) Landslides and Their Control. Elsevier, New York, p.205.

Zhou, H.; Wang, J.; Wan, J. & Jia, H. (2010) Resilience to natural hazards: A geographic perspective. Natural Hazards, v. 53:1, p. 21-41.

Zuquette, L.V.; Pejon, O.J.; Sinelli, O. & Gandolfi, N. (1991) Carta de risco da região de Ribeirão Preto (SP). Proc. Simpósio de Geologia do Sudeste. SBG, São Paulo, v. 2, pp. 360-265.

Zuquette, L.V.; Pejon, O.J.; Sinelli, O. & Gandolfi, N. (1992) Preliminary zoning of risk and geotechnical conditions of Northeast Region of São Paulo State. Proc. II Simpósio Latino Americano de Riesgos Geológicos. Colombia, v. 1, pp. 495-501.

Zuquette, L.V. (1993) Importância do Mapeamento Geotécnico no Uso e Ocupação do Meio Físico: Fundamentos e Guia para Elaboração. Tese de Livre Docência, Escola de Engenharia de São Carlos, São Carlos, 2 v., 330 pp.

Zuquette, L.V.; Pejon, O.J. & Sinelli, O. (1994a) Engineering geological zoning mapping of the Ribeirão Preto city-Brazil. Geoscience in urban planning. AGID-IAEG-INQUA, Beijing, pp. 407-417.

Zuquette, L.V.; Pejon, O.J.; Sinelli, O.; Gandolfi, N.; Paraguassu, A.B.; Rodrigues, J.E & Vilar, O.M. (1994b) Engineering geological zoning of São Paulo State-Scale 1:500,000. Seventh International IAEG Congress, Lisbon, v. 2, pp. 1187-1195.

Zuquette, L.V.; Pejon, O.J.; Sinelli, O. & Gandolfi, N. (1994c) Carta de Riscos Potenciais de Erosão da Cidade de Franca (SP) - Escala 1:25.000. AGID Geosciences Series, Cochabamba, n. 21, p. 25-38.

Zuquette, L.V.; Pejon, O.J. & Collares, J. (2004) Land degradation assessment based on environmental geoindicators in the Fortaleza metropolitan region, state of Ceará, Brazil. Environmental Geology, v. 45:3, p. 408-425.

Application of Risk Analysis Methods on Tailings Dams

T. Espósito, L.R. Palmier

Abstract. One of the procedures adopted in a Safety Management System is the use of Risk Analysis for which analytical, iterative, descriptive and qualitative methods, such as the FMEA "Failure Modes and Effects Analysis", have been applied in order to identify and analyse potential failures from a given failure mode, its causes and consequences, as well as the means of detection and prevention of failure modes and mitigation of their effects. In Brazil the FMEA method has been used to evaluate the safe conditions of tailings dams. On the other hand a specific tool for the Risk Analysis of dams, the LCI "Analysis by Diagrams Location, Cause and Failure Indicators" semi-quantitative method, has been developed and in the United Kingdom under the name of "Risk Management for UK Reservoirs" and applied in Europe but not for tailings dams. Recently the LCI MOD-REJ version – an adaptation of the LCI method – has been proposed and applied to one Brazilian tailings dam to explicit deal with the Risk Analysis of this type of structure. Considering the promising results of the former application, the aim of this paper is to evaluate the LCI MOD-REJ version applicability and efficiency by comparing the results of its and the FMEA method applications to two Brazilian tailings dams.

Keywords: tailings dams, risk analysis, LCI, LCI MOD-REJ, FMEA, safety management.

1. Introduction

Tailings are the inevitable consequences of the ore treatment processes, being generated in parallel to the product of interest. Nowadays, these tailings are produced in large amounts, affecting qualitatively and quantitatively the environment. The large production of tailings has generated a growing concern in companies that seek to minimize environmental impacts and costs associated with the processes of containment and disposal of this material. Thus, the tailings have been the subject of great interest of mining companies, which have been looking for inexpensive and safe alternative disposal of these materials. Among the various methods, the deposition of tailings surface using containment of tailings dams has been a preference of Brazilian mining companies. Such dams may be constructed in stages, with successive and raisings over time and in many cases the tailings may constitute the building material (Esposito, 2000). Nonetheless, tailings dams failures continue to occur despite the modern technology available for their design, construction and operation. The consequences of these failures have been economic losses and environmental degradation, and, in many cases, loss of human life. The main causes of the failures include, in some cases, complex geotechnical characteristics that require special care to overcome the adverse conditions.

However, the causes are also possible situations to be solved with the use of already available technologies. This demonstrates the necessity of a more systematic application of the current specialized knowledge. In this sense, "Tailings Dams Engineering" must act in the design, construction, operation, monitoring and maintenance, as well as in emergency situations, and deactivation and decommissioning of tailings dams. The dam security can be achieved in the light of an effective Safety Management. In this context it is worth the use of the Risk Analysis procedure on the Safety Management System of Tailings Dams, which aims to estimate the probabilities of failure events of the components or system and the magnitude of the consequences. However, that application in Geotechnics is not common, although users of this tool in conventional dams (except tailings dams) perceive an increase in the practice of these structures safety, as well as a better understanding of their behaviour. It is concluded that the Risk Analysis in Geotechnics, although not yet a routine application, can be extremely useful in works whose potential risks are high and associated with important consequences such as in tailings dam, as it allows to manage the risks efficiently.

In light of these considerations the aim of this paper is to discuss the application of two Risk Analysis methods, the FMEA and an adapted version of the LCI method (LCI MOD-REJ), to two Brazilian tailings dams.

2. Principles and Procedures of the LCI Method "Analysis by Diagrams Location, Cause and Failure Indicators"

In the past, risk assessment methodologies, as developed for use in other industries, have not been applied to dams and reservoirs on a regular basis. According to Hughes *et al.* (2000), this fact can be explained by the following reasons: the data inadequacy, the uniqueness nature of each dam, the complex interactions involved in the dam behaviour, the wrong perception of negligible risk of dam failure, the concern about the cost of risk assessment, the scepticism, the difficulties of understanding or applying the

Terezinha Espósito, DSc, Associate Professor, Universidade Federal de Minas Gerais, Belo Horizonte, MG, Brazil. e-mail: esposito@etg.ufmg.br.
Luiz Rafael Palmier, Associate Professor, Universidade Federal de Minas Gerais, Belo Horizonte, MG, Brazil. e-mail: palmier@ehr.ufmg.br.
Submitted on May 29, 2012; Final Acceptance on March 27, 2013; Discussion open until August 30, 2013.

output resulting from any form of risk assessment, and, finally, the lack of knowledge of risk assessment techniques by the dam community. According to Hughes *et al.* (2000), the application of risk assessment should help to improve existent dam and reservoir safety, would be useful in identifying the potential consequence of failure and would allow risk classification of reservoirs and prioritization of the future interventions. It is essential that the dam risk assessment should include the primary mechanisms associated with dam incidents and failures, such as seepage/internal erosion, overtopping, instability/overstress, and settlement/deformation. In this context, taking into account the failure mechanisms and the actual maintenance of the embankment dams with different ages, the LCI method was developed for scoring the individual hazard, vulnerability and acquired knowledge of those structures, constituting one phase of a risk portfolio assessment.

The Location, Cause and Indicator (LCI) diagrams have been used for the risk assessment of reservoirs in the United Kingdom, specifically for risk analysis of dams with storage volumes greater than or equal to 25,000 m^3. These three diagrams include the location of the dam component under study, the cause of failure of that component and signs or evidences (indicators) of failure effects in terms of the response of the system, and exclude the consequences evaluation. As an example, Pimenta *et al.* (2005) and Pimenta (2009) discussed the application of this method in Portugal, but without considering tailings dams, which is one of the aims of the current paper.

2.1. Principles and procedures of the LCI Method

Hughes *et al.* (2000) produced a series of Location, Cause, Indicator (LCI) Diagrams, based on known failure modes of different types of dams and on historical data and engineering judgment of existing dams in order to assist the FMECA (Failures Mode, Effects and Criticality Analysis) process in the risk assessment. Each LCI diagram analysis is performed on the basis of the dam characteristics, such as: type (concrete or embankment), height (less than 15 m, 15-30 m, greater than 30 m) and age (pre 1840, between 1840 and 1960, post 1960).

It should be noted that the FMECA complements the FMEA (Failure Modes and Effects Analysis) and is a systematic approach to analyse how a system can fail (failure mode), to determine the effects associated to each failure mode and to assess the likelihood of its occurrence and the severity of its effects to the system operation, through a criticality index, in other words, how critical that type of failure will be to the operation of the system.

Hughes *et al.* (2000) related that to characterize the causes and the indicators three score categories were used (scores from 1 to 5):

i Effects or consequences in the system (Cons.) to reflect the way as the failure of the element is directly related to complete (or partial) failure of the dam;

ii Likelihood (Like.) corresponding to the likelihood of the failure of the element;

iii Confidence degree (Conf.) of the analyst in its consequences and likelihood estimatives, to take into account the uncertainty in knowledge of the dam or of its components; this factor allows the consideration of an uncertainty measure.

During the process, the consequences in the downstream valley are evaluated through a Global Impact Index (GII) and the product of the score of each category (Cons., Like. and Conf.) gives a Criticality index for each set of causes or indicators of problems related to dam elements. The product of those indexes (Criticality index and Global Impact Index) gives the risk score.

Outputs include Location, Cause, Indicator (LCI) Diagram, indicating problematic areas and a list of criticality and risk scores associated with specific problem causes and indicators, allowing prioritisation of resources for single or multiple sites. The stages of this method are:

Stage 1: Impacts evaluation, that includes: information gathering, site visit, prediction of discharge and potential floodwater levels caused by dam failure, assessment and scoring of specific impacts from flooding and combination of scores.

Stage 2: Calculation of the Global Impact Index by the reduction of the different impact scores to a single value impact.

Stage 3: Development and application of LCI diagrams by considering the components of a dam and its contribution to its possible failure. Dam failure with different causes and with different indicators is considered. A criticality score is calculated for each cause/indicator element thus accreting for the overall dam safety.

In the first stage, information is collected along a stretch of 30 km in the downstream valley, including the main characteristics of land occupation, structures and infrastructure, and environmental resources. It is recommended to perform an inspection visit to the near valley along the first 5 km from the dam.

The identification of consequences involves the estimative of the discharge at the dam section, the rupture time and the levels reached by the flood wave in the valley sections previously defined. In order to achieve this, numerical models of dam-break type or simplified techniques are used for calculations of the hydrographs along the valley, as described by Hughes *et al.* (2000). Once the occupation of the valley and the downstream water levels, as affected by the flood wave, are estimated, stage 2 is initiated with the evaluation of the Global Impact Index (GII) by a weighted combination of the potential loss of human life (PLL) and economic losses (EL), along the near valley (first 5 km) and the remaining valley (until 30 km).

To calculate the PLL, the number of people at risk (PAR) is calculated taking into account the types of land occupations, *i.e.*, residential properties, non-residential properties, transportation infrastructure and recreational sites potentially affected by the flood, and considering the estimates presented in Table 1. In formal terms, the PLL is calculated by the following equations:

$$PLL = 0.5\ PAR\ (\text{near valley}) \quad (1)$$

$$PLL = PAR^{0.6}\ (\text{far valley}) \quad (2)$$

The figure for the EL is obtained from the weighted sum of the scores associated with losses in the near and in the far away valleys. In this context, the following weights are used: 0.15 for residential properties; 0.15 for non-residential properties; 0.10 for transportation infrastructure; 0.05 for recreational sites; 0.25 for industrial sites; 0.25 for utilities; and 0.05 for agriculture areas and natural habitats.

The GII is then determined by this equation:

$$GII = 100\ EL_{<5\,km} + PLL_{<5\,km} + 30\ EL_{5\text{-}30\,km} + PLL_{5\text{-}30\,km} \quad (3)$$

After calculating the GII, the next step (stage 3) is to classify the causes and subsequent effects through the application of the LCI diagrams, in order to estimate and classify the Ordination, Confidence, Criticality and Risk indexes.

The causes and the failure indicators are classified within a scale ranging from 1 to 5 by using the previously described three attributes: i) Consequences on the dam (Cons. 1 low, 5 high); ii) Likelihood (Like. 1 low, 5 high); and iii) degree of Confidence (Conf.) (5 low, 1 high).

According to Hughes *et al.* (2000), Caldeira (2005), Pimenta *et al.* (2005) and Pimenta (2009) after the classification of the attributes it is possible to calculate four indexes for each set Location/Cause/Indicator:

- Ordinance Index (Ind_{Ord}), as determined by the product of attributed ratings to the Consequence and Likelihood.
- Confidence Index (Ind_{Conf}), taken equal to the Confidence score.
- Criticality Index (Ind_{Crit}), defined by the product of the ratings assigned to the Consequence, Likelihood and Confidence.
- Risk Index (Ind_{Risk}), as determined by the product of Criticality Index and the Global Impact Index.

2.2. Proposal of a version of the LCI method for tailings dams (LCI MOD-REJ)

An adapted version of the LCI method – the LCI MOD-REJ version – has been proposed in order to adjust a former structure developed specifically for dams to an even more explicit one to focus on the risk assessment of tailings dams by including a "Tailings impoundment" item in the general analysis. The main aim of this adapted version is to identify the structural elements that most contribute for the total collapse of tailing dams. So far the LCI MOD-REJ version was applied to just one Brazilian tailings dam with promising results – Esposito *et al.* (2011a) and Esposito (2011b). It is important to emphasize that the LCI MOD-REJ version does not constitute a new system as specific and common adaptations were considered over the LCI method.

Pimenta *et al.* (2005) emphasize that when GII is below 175 (from the original LCI method) it is not recommended to apply the second step of the original method and therefore there is no need to estimate the Ordinance Index (Ind_{Ord}), the Criticality Index (Ind_{Crit}), the Confidence Index (Ind_{Conf}) and the Risk Index (Ind_{Risk}). In the LCI MOD-REJ version, based on a more conservative approach, the failure modes and the rates of risk must always be estimated. Tailings dams do not always have effective construction control, which also occurs in stages, following the generation and disposal of tailings. These tailings, in turn, have characteristics that change over time, making the quality control of the construction even more necessary. As in practice, since there is not yet a systematic control for these structures, especially in small and medium-sized mining companies, the suggestion is to always apply the proposed LCI MOD-REJ version following the three mentioned stages.

Another aspect is that LCI MOD-REJ diagrams considered the item "Location" with its subdivisions "Dam body, foundations and abutments" and "Spillway and its components", like the original LCI method, adding, as mentioned before, the "Tailings impoundment" subdivision.

3. Principles and Basic Procedures of the "Failure Modes And Effects Analysis" (FMEA) Method

In order to evaluate the LCI MOD-REJ version applicability and efficiency it is proposed a comparison of the results from its application with those from the use of the FMEA method, a much diffused one, to two Brazilian tailings dams. In this item only the basic procedures of the latter method will be shown as it is very well known and has been normally applied by Brazilian mines companies in the evaluation of the risk assessment on tailings dams. The FMEA method is a technique suited to define, identify and analyze potential failures from a given failure mode, its causes and consequences of effects, as well as the means of detection and prevention failure modes and mitigate their effects. To apply the FMEA method it is important to constitute a group of people to identify the product/process in question, in order words, to identify the system with its elements considering theirs functions, the types of failures that can occur, the effects and possible causes of this failure in each element (Hartford & Baecher, 2004).

The FMEA method can be conducted primarily in six steps (Caldeira, 2005 and Santos, 2006): (i) Structuring the system; (ii) Definition of features/requirements of each system component; (iii) Identification of potential failure modes associated with each function of each component; (iv) Identification of potential causes; (v) Description of the direct effects, and other components in the system; and (vi)

Table 1 - Economic losses (PE) and people at risk estimated PAR (Hughes *et al.*, 2000).

Impact 1 – Residential properties			
Properties flooded	Number of properties flooded	Score	PAR
None	0	0	0
Minor	1 to 15	1	30
Appreciable	16 to 50	2	100
Significant	51 to 250	3	500
Major	> 250	4	2 x estimate
Impact 2 – Non-residential properties			
Disruption	Number of people affected	Score	PAR
None	0	0	0
Minor	1 to 150	1	150
Appreciable	151 to 500	2	500
Significant	501 to 1000	3	1000
Major	> 1000	4	Estimate
Impact 3 – Transportation infrastructure			
Disruption	Infrastructures affected	Score	PAR
None	None	0	0
Minor	Minor roads only	1	25
Appreciable	Major regional	2	50
Significant	Major national	3	100
Major	Major international	4	Estimate
Impact 4 – Recreational sites			
Disruption	Number of people affected	Score	PAR
None	0	0	0
Minor	1 to 10	1	10
Appreciable	11 to 50	2	50
Significant	51 to 100	3	100
Major	> 100	4	Estimate
Impact 5 – Industrial sites			
Disruption	Type of industrial site	Score	
None	None	0	
Minor	Light industrial	1	
Appreciable	Public health industries	2	
Significant	Heavy industry	3	
Major	Nuclear petrochemical	4	
Impact 6 – Utilities			
Disruption	Impact on utilities	Score	
None	None	0	
Minor	Local loss of distribution	1	
Appreciable	Local loss of distribution/supply	2	
Significant	Regional loss of distribution/supply	3	
Major	Significant impact on national services	4	
Impact 7 – Agriculture/habitats			
Disruption	Type of site	Score	
None	Uncultivated/grassland	0	
Minor	Pasture	1	
Appreciable	Widespread farming	2	
Significant	Intensive farming/vulnerable natural habitats/monuments	3	
Major	Loss of internationally recognise habitats/monuments	4	

Identification of measures available to detect the causes or failure modes and to control or mitigate their effects. It is common to present the FMEA results by calculating the RPNi (Risk Priority Number) and elaborating the Risk Matrix.

4. Main Characteristics of the Tailings Dams A and B

The data used in the applications of the LCI (the LCI MOD-REJ version) and FMEA methods were based on actual information obtained from Tailings Dams A and B. Technical visits for visual inspection have been done and full dam-break studies were used to assess the floodplain in the downstream valley. The characteristics of both tailings dams are shown in Table 2. It should be noted that Tailings Dam A is currently receiving iron ore tailings differently from Tailings Dam B that is not receiving tailings and its reservoir is full of bauxite tailings.

5. Results and Discussions

5.1. Application of the LCI MOD-REJ diagrams

The purpose of applying the Location, Causes and Indicators of Failure diagrams is to identify and assess the failure modes in terms of likelihood and effects in the global system, based on exterior signs or deficiencies in the dam performance. This section illustrates the application of the LCI-MOD REJ diagrams to two tailings dam, named, in this paper, as Tailings Dam A and Tailings Dam B. Previously to the application of the LCI MOD-REJ diagrams, the GII was calculated. In the sequence, the causes and indicators of failures modes were classified according to the consequences (Cons.), likelihood (Like.) and confidence (Conf.) attributes (Figs. 1 and 2). Then, the following four indices were calculated: I_{Ord}, I_{Crit}, I_{Conf} and I_{Risk}.

The GII (Global Impact Index) was calculated considering the potential loss of lives (PLL) and the economic losses (EL), as estimated for the near downstream (< 5 km) and the far away valleys (5 to 30 km), as shown in Tables 3 and 4. The GII values are showed in Table 5.

The causes and indicators were classified according to three attributes (Figs. 1 and 2): Consequence (Cons.); Likehood (Like.); Confidence (Conf.).

The Tables 6 and 7 present the justification of the values of attributes. In addition, the four indices, Ordinance Index (Ind_{Ord}), Criticality Index (Ind_{Crit}), Confidence Index (Ind_{Conf}), and Risk Index (Ind_{Risk}), were calculated as shown in Table 8.

5.2. Tailings dams A and B: The LCI MOD-REJ diagrams results

The Tailings Dam A and B Safety Reports were consulted and both dams were visited in order to elaborate their LCI MOD-REJ Diagrams. In the Tailings Dam A the Safety Reports was consistently emphasized great concerns about the freeboard, which explains the highest value of the Risk Index (Ind_{Risk}) for overtopping presented in Table 8 for

Table 2 - Characteristics of Tailings Dams A and B.

Characteristics/Dam	Tailings Dam A	Tailings Dam B
Section	Homogeneous	Homogeneous
Function storage reservoir	Iron ore tailings	Bauxite tailings
Classification of tailings stored (according FEAM – State Foundation of Environment)	III	III
Downstream human occupancy	Medium	Medium
Downstream environmental interest	High	High
Concentration of facilities in the downstream area	High	Medium
Analysis	Stability flow	Stability flow
Final dam height (m)	53	64
Crest	Width: 7.50 m Length: 267.97 m	Width: 5.00 m Length: 145.0 m
Upstream slope	1V:2H	1V:2H
Downstream slope	1V:2H	1V:2H
Surface drainage system	Concrete channels on the verges	Concrete channel on the verges and cut-water on the abutments
Internal drainage system	Vertical sand filter type chimney connected to a horizontal drainage and a foot drain	Vertical sand filter connected to a horizontal drainage. It has drains at the bottom of the valley and on the abutments
Spillway system	Channel side	Stop logs
Final volume of the reservoir (m^3)	6.72×10^6	3.87×10^6

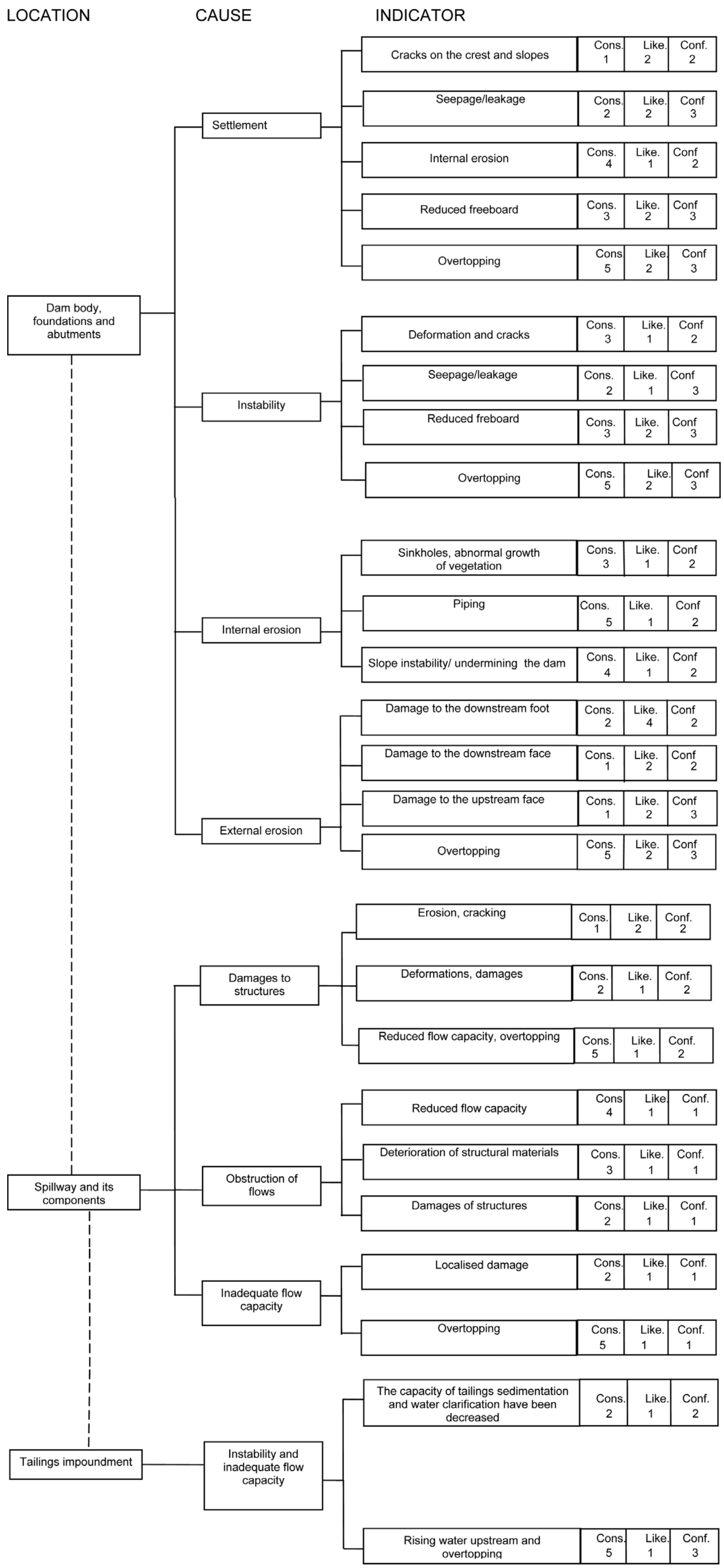

Figure 1 - Diagram LCI MOD-REJ Tailings Dam A - Attributes Consequence (Cons.), Likelihood (Like.) and Confidence (Conf.).

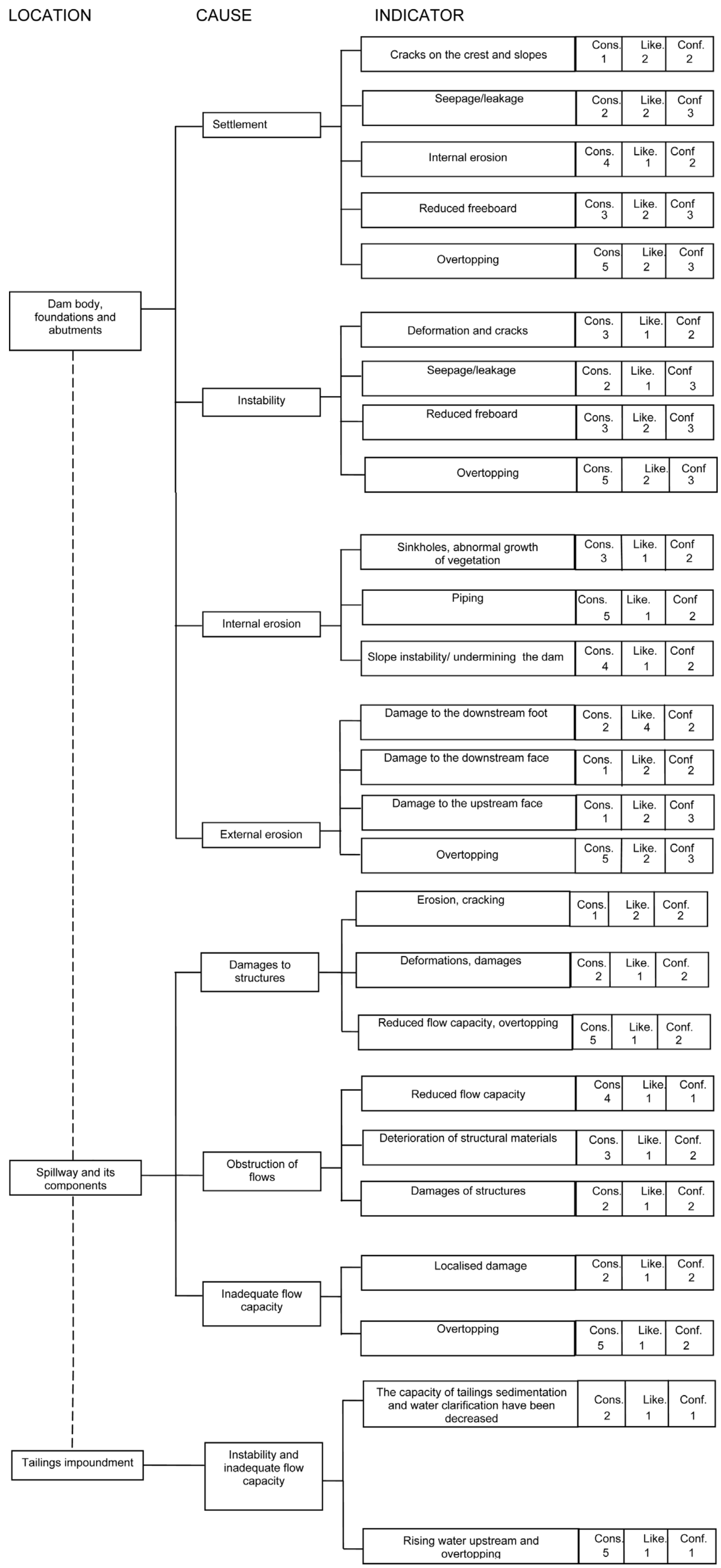

Figure 2 - Diagram LCI MOD-REJ Tailings Dam B - Attributes Consequence (Cons.), Likelihood (Like.) and Confidence (Conf.).

Table 3 - Near valley (< 5 km) – Tailings Dams A and B.

Impact	Dam A Impact score	Dam B Impact score	Value	Dam A Final score	Dam B Final score	Dam A *PAR*	Dam B *PAR*	Dam A *PLL*	Dam B *PLL*
1	4	4	0.15	0.60	0.60	600	800	300	400
2	2	3	0.15	0.30	0.45	500	1000	250	500
3	3	4	0.10	0.30	0.40	100	200	50	100
4	4	4	0.05	0.20	0.20	200	450	100	225
5	1	4	0.25	0.25	1.00	-	-		
6	2	2	0.25	0.50	0.50	-	-		
7	4	4	0.05	0.20	0.20	-	-		
Total				2.65	3.35			700	1225

Table 4 - Far valley (5 to 30 km) – Tailings Dams A and B.

Impact	Dam A Impact score	Dam B Impact score	Value	Dam A Final score	Dam B Final score	Dam A *PAR*	Dam B *PAR*	Dam A *PLL*	Dam B *PLL*
1	2	4	0.15	0.30	0.60	100	150000	16	1275
2	0	4	0.15	0	0.60	0	60000	0	736
3	4	4	0.10	0.40	0.40	10000	200	251	24
4	4	4	0.05	0.20	0.20	500	50000	42	658
5	4	4	0.25	1.00	1.00	-	-		
6	2	2	0.25	0.50	0.50	-	-		
7	4	4	0.05	0.20	0.20	-	-		
Total				2.60	3.50			511	2693

Table 5 - Global Impact Index – Tailings Dams A and B.

Tailings Dam A	GII = 1002.65 + 700 + 302.60 + 511 GII = 1554
Tailings Dam B	GII = 1003.35 + 1225 + 303.50 + 2693 GII = 4358

Dam A, although the probability of its occurrence is low. On the other hand the biggest concern for Tailings Dam B is due to internal erosion because it could generate a significant effect on this dam.

As no evidence of this phenomenon was detected, the probability of occurrence appears to be very small, especially considering the dam long operation time and the good practice used during its construction. However, as there are no monitoring devices, it has been assigned in this paper (Table 8) a high level for the Risk Index (Ind_{Risk}) for this indicator.

Another indicator associated with a high level for the Risk Index (Ind_{Risk}) for the Tailings Dam B was the overtopping. But it should be remembered that its probability of occurrence is low. It is interesting to note that the GII value is almost three times greater for Tailings Dam B than the same for Tailings Dam A even though the former is no longer in operation. This reflects the importance given by the method to the overall consequences on the downstream valley.

The determination of a threshold value for the Risk Index (Ind_{Risk}) may allow an overall picture over a state of alert. Considering the results for Dams A and B, just as an example, the Location/Cause/Indicator for Ind_{Risk} values greater than 40,000 are presented in Table 9. This could be considered a preliminary estimate and it is recommended the application of the method to a great number of tailings dams to make it possible to establish a more reliable reference number for this index.

5.3. Application of the FMEA method

This section illustrates the application of the FMEA method to two tailings dams, named, in this paper, as Tail-

Table 6 - LCI MOD-REJ Tailings Dam A - Justification of the values of Cons., Like. and Conf.

Location	Cause	Indicator	Justification
Dam body, foundations and abutments	Settlement	Cracks on the crest and slopes	No cracking observed.
		Seepage/leakage	No resurgences or wetlands observed, however the inspection was carried out in a dry season.
		Internal erosion	No internal erosion detected. There are no monitoring devices.
		Reduced freeboard	There is no evidence.
		Overtopping	There is no evidence; however there are no monitoring devices.
		Deformations and cracks	There is no evidence; however there are no monitoring devices.
	Instability	Seepage/leakage	There is evidence of vegetation, but no resurgences or wetlands. However, the inspection was carried out in a dry season.
		Reduced freeboard	There is no evidence of reduction of freeboard. The probability is small, but it is an important concern of the design related in the reports.
		Overtopping	There is no evidence; however there are no monitoring devices.
	Internal erosion	Sinkholes, abnormal growth of vegetation	There is evidence of vegetation, but no resurgences or wetlands. However, the inspection was carried out in a dry season.
		Piping	Considering that the dam was built following all the technical requirements and piezometers were installed, the piping probability is very small.
		Slope instability/undermining the dam	The instability of slopes could create the dam global destabilization, so the effect would be significant. The probability is very small, since the dam was built following all the technical requirements. However, there are no monitoring devices.
	External erosion	Damage to the downstream foot	The deterioration of the downstream foot caused by erosion external could generate instability in the dam.
		Damage to the downstream face	The deterioration of the downstream face would not cause significant effects on the dam. The probability of occurrence is very small.
		Damage to the upstream face	The deterioration of the downstream face would not cause significant effects on the dam. The probability of occurrence is very small.
		Overtopping	There is no evidence; however there are no monitoring devices.
Spillway and its components	Damages to structures	Erosion cracking	There is no evidence.
		Deformations damages	There is no evidence.
		Reduced flow capacity overtopping	There is no evidence.
	Obstruction of flows	Reduced flow capacity	There is no evidence.
		Deformations of structural materials	There is no evidence.
		Damages of structures	There is no evidence.
	Inadequate flow capacity	Localised damage	There is no evidence.
		Overtopping	There is no evidence.

Table 7 - LCI MOD-REJ Tailings Dam B - Justification of the values of Cons., Like. and Conf.

Location	Cause	Indicator	Justification
Dam body, foundations and abutments	Settlement	Cracks on the crest and slopes	No cracking observed
		Seepage/leakage	No resurgences or wetlands observed, however the inspection was carried out in a dry season.
		Internal erosion	No internal erosion detected. There are no monitoring devices.
		Reduced freeboard	There is no evidence.
		Overtopping	There is no evidence.
	Instability	Deformations and cracks	There is no evidence; however there are no monitoring devices.
		Seepage/leakage	There is evidence of vegetation, but no resurgences or wetlands. However the inspection was carried out in a dry season.
		Reduced freeboard	There is no evidence of reduction of freeboard.
		Overtopping	There is no evidence; however there are no monitoring devices.
	Internal erosion	Sinkholes, abnormal growth of vegetation	There is evidence of vegetation, but no resurgences or wetlands. However the inspection was carried out in a dry season.
		Piping	Considering that the dam was built following all the technical requirements and piezometers were installed, the piping probability is very small.
		Slope instability/undermining the dam	The instability of slopes could create the dam global destabilization, so the effect would be significant. The probability is very small, since the dam was built following all the technical requirements. However, there are no monitoring devices.
	External erosion	Damage to the downstream foot	There is no evidence.
		Damage to the downstream face	There is no evidence.
		Damage to the upstream face	The deterioration of the downstream face would not cause significant effects on the dam. The probability of occurrence is very small.
		Overtopping	There is no evidence; however there are no monitoring devices.
Spillway and its components	Damages to structures	Erosion, cracking	There is no evidence.
		Deformations, damages	There is no evidence.
		Reduced flow capacity, overtopping	There is no evidence.
	Obstruction of flows	Reduced flow capacity	There is no evidence.
		Deformations of structural materials	There is no evidence.
		Damages of structures	There is no evidence.
	Inadequate flow capacity	Localised damage	There is no evidence.
		Overtopping	There is no evidence.
Tailings impoundment	Instability and inadequate flow capacity	The capacity of tailings sedimentation and water clarification have been decreased	The effects caused by the non-sedimentation of the tailings and the non-clarification of the water are small. This dam is not in operation.
		Rising water upstream and overtopping	There is no evidence; however there are no monitoring devices. This dam is not in operation.

Table 8 - LCI MOD-REJ Tailings Dams A and B - Ordinance Index (Ind_{Ord}), Criticality Index (Ind_{Crit}), Confidence Index (Ind_{Conf}), and Risk Index (Ind_{Risk}).

Location	Cause	Indicator	Dam A Ind_{Ord}	Dam B Ind_{Ord}	Dam A Ind_{Crit}	Dam B Ind_{Crit}	Dam A Ind_{Conf}	Dam B Ind_{Conf}	Dam A Ind_{Risk}	Dam B Ind_{Risk}
Dam body foundations and abutments	Settlement	Cracks on the crest and slopes	2	1	4	2	2	2	6216	8716
		Seepage/leakage	4	2	12	4	3	2	18648	17432
		Internal erosion	4	4	8	8	2	2	12432	34864
		Reduced freeboard	6	3	18	6	3	2	27972	26148
		Overtopping	10	5	30	10	3	2	**46620**	**43580**
	Instability	Deformations and cracks	3	3	6	9	2	3	9324	39222
		Seepage/leakage	2	2	6	4	3	2	9324	17432
		Reduced freeboard	6	3	18	6	3	2	27972	26148
		Overtopping	10	5	30	10	3	2	**46620**	**43580**
	Internal erosion	Sinkholes abnormal growth of vegetation	3	3	6	6	2	2	9324	26148
		Piping	5	5	10	10	2	2	15540	**43580**
		Slope instability/undermining the dam	4	4	8	8	2	2	12432	34864
	External erosion	Damage to the downstream foot	8	2	16	2	2	1	24864	8716
		Damage to the downstream face	2	1	4	2	2	2	6216	8716
		Damage to the upstream face	2	3	6	9	3	3	9324	39222
		Overtopping	10	5	30	5	3	1	**46620**	21790
Spillway and its components	Damages to structures	Erosion, cracking	2	2	4	4	2	2	6216	17432
		Deformation, damages	2	2	4	4	2	2	6216	17432
		Reduced flow capacity, overtopping	5	5	10	10	2	2	15540	**43580**
	Obstruction of flows	Reduced flow capacity	4	4	4	4	1	1	6216	17432
		Deformations of structural materials	3	3	3	6	1	2	4662	26148
		Damages of structures	2	2	2	4	1	2	3108	17432
	Inadequate flow capacity	Localised damage	2	2	2	4	1	2	3108	17432
		Overtopping	5	5	5	10	1	2	7770	**43580**
Tailings impoundment	Instability and inadequate flow capacity	The capacity of tailings sedimentation and water clarification have been decreased	2	2	4	2	2	1	6216	8716
		Rising water upstream and overtopping	5	5	15	5	3	1	23310	21790

ings Dam A and Tailings Dam B. Firstly the Systems of the Tailings Dam A and B (Table 10) were defined. The dams are very similar, so the same system was used for both dams and only the item "1.1.6.4 Drain on the abutments" was incorporated in Tailings Dam B. For each element of the system the FMEA method incorporates its Function, Failure, Final Effect, Severity Index (Si), Cause, Occurrence Index (Oi), Control, Control Type, Detection Index (Di) and

Table 9 - Location/Cause/Indicator with associated Risk Index (Ind_{Risk}) higher than 40,000.

Location	Cause	Indicator
Dam body foundations and abutments	Settlement	Overtopping (Tailing Dam A and B)
	Instability	Overtopping (Tailing Dam A and B)
	Internal erosion	Piping (Tailing Dam B)
	External erosion	Overtopping (Tailing Dam A)

Table 10 - System of the Tailings Dams A and B

System of the Tailings Dams A and B	
1.1	Dam body
1.1.1	Crest
1.1.2	Core
1.1.3	Upstream slope
1.1.3.1	Free board
1.1.4	Downstream slope
1.1.5	Surface drainage system
1.1.5.1	Concrete channels
1.16	Internal drainage system
1.1.6.1	Bottom drain
1.1.6.2	Vertical filter
1.1.6.3	Foot drain
1.1.6.4	Drain on the abutments (only in Tailings Dam B)
1.2	Spillway system
1.3	Abutments
1.3.1	Abutment right
1.3.2	Abutment left
1.4	Foundation
1.5	Tailings impoundment

RPNi (Risk Priority Number). It is emphasized that the Severity Index (Si) shows how severe are the consequences (effects) of each failure mode, the Occurrence Index (Oi) shows how often occurs the cause of failure and the Detection Index (Di) shows what is the chance to be detected the cause of failure (Table 11). RPNi is equal to the product of Si, Oi and Di for each failure mode. The results are presented in Tables 12 and 13.

5.4. Tailings Dams A and B: the FMEA method results

The variation range for the RPNi numbers was from 4 to 225. The following criterion is proposed based on the RPNi values: 1 < RPNi < 50 Acceptable Risk; 50 < RPNi < 120 Tolerable Risk; and RPNi > 120 Intolerable Risk. The Table 14 shows the locations where the values of RPNi were greater than 120 (Intolerable Risk), to both dams.

Moreover the Risk Matrix may be plotted considering the Severity Index (Si) and the Occurrence Index (Oi). For the current cases both indexes would appear on the far left and higher positions, which can be interpreted as an alert situation. The critical items were "1.1.3.1 Free board" (Tailing Dam A) and "1.1.6.3 Foot drain" (Tailing Dam B).

Table 11 - Severity Index (Si), Occurrence Index (Oi) and Detection Index (Di).

Severity index (Si)		Occurrence index (Oi)		Detection index (Di)	
Si	Effect	Oi	Probability	Di	Probability
1	Very low	1	Improbable (0.1%)	1	Almost right
2 3	Low	2 3	Remote (0.1 to 1%)	2	Very high
4 5	Medium	4 5 6	Occasional (1 to 10%)	3	High
6 7 8	Severe	7 8 9	Probable (10 to 20%)	4	Moderately high
9	Very severe	10	Frequent (> 20%)	5	Moderate
10	Catastrophic			6	Low
				7	Very low
				8	Remote
				9	Very remote
				10	Almost impossible

Table 12 - FMEA Results: System of the Tailings Dam A.

Function	Failure	Final effect	Si	Cause	Oi	Control	Control type	Di	RPNi
1.1 Dam body									
Containment of tailings	Insufficient capacity to contain tailings	Global instability of the dam	10	Inadequacy of the project and/or construction	2	Adjustment of the project	Prevention	3	60
						Visual Inspection and Instrumentation	Detection		
1.1.1 Crest									
Allow access to dam	Not allow access to dam	Inability to carry out inspections	4	Inadequacy of the project and/or construction	2	Adjustment of the project	Prevention	1	8
						Visual Inspection	Detection		
1.1.2 Core									
Reduce the hydraulic conductivity	Excessive seepage	Piping	9	Alterability of the materials	2	Recompaction	Prevention	6	108
						Visual Inspection	Detection		
				Dissolution of the materials	4	Recompaction	Prevention	6	216
						Visual Inspection and Instrumentation	Detection		
				High hydraulic load increase the saturation line	4	Recompaction	Prevention	2	72
						Visual Inspection and Instrumentation	Detection		
				Hydraulic fracturing	2	Recompaction	Prevention	4	72
						Visual Inspection and Instrumentation	Detection		
1.1.3 Upstream slope									
Confer mechanical stability	Instability associated with movements of the soil mass	Global instability of the dam	10	Deficient compaction of the embankment	4	Adequacy of the geometry	Prevention	2	80
						Recompaction	Prevention		
						Instrumentation	Detection		
				Alterability of the materials	2	Adequacy of the geometry	Prevention	6	120
						Recompaction	Prevention		
						Visual Inspection	Detection		
	Excessive deformation	Overtopping	9	Alterability of the materials	2	Recompaction	Prevention	6	108
						Visual Inspection	Detection		
				Collapse	2	Recompaction	Prevention	3	54
						Visual Inspection and Instrumentation	Detection		
				Deficient compaction of the embankment	4	Recompaction	Prevention	2	72
						Visual Inspection and Instrumentation	Detection		
1.1.3.1 Free board									
Not allow over-topping of the dam	Allow overtopping of the dam	Overtopping	9	Inadequacy of the project and/or construction	7	Adequacy of the geometry	Prevention	1	63
						Adjustment of the project	Prevention		
						Visual Inspection and Instrumentation	Detection		
1.1.4 Downstream slope									
Confer mechanical stability	Instability associated with movements of the soil mass	Global instability of the dam	10	Deficient compaction of the embankment	4	Adequacy of the geometry	Prevention	2	80
						Recompaction	Prevention		
						Instrumentation	Detection		
				Alterability of the materials	2	Adequacy of the geometry	Prevention	6	120
						Recompaction	Prevention		
						Visual Inspection	Detection		
	External erosion	Local instability of the dam	5	Deficient compaction of the embankment	4	Recompaction	Prevention	2	40
						Visual Inspection and Instrumentation	Detection		
	Excessive deformation	Overtopping	9	Alterability of the materials	2	Recompaction	Prevention	6	108
						Visual Inspection	Detection		
				Deficient compaction of the embankment	4	Recompaction	Prevention	2	72
						Visual Inspection and Instrumentation	Detection		

Table 12 (cont.)

Function	Failure	Final effect	Si	Cause	Oi	Control	Control type	Di	RPNi
1.1.5 Surface drainage system									
Collect surface water that flow through the embankment	Insufficient capacity to collect surface water that flow through the embankment	Local instability of the dam	5	Inadequacy section	1	Structural maintenance of channels	Prevention	4	20
						Visual Inspection	Detection		
				Obstruction of channels	2	Unblocking of channels	Prevention	2	20
						Visual Inspection	Detection		
Collect surface water outside the dam	Insufficient capacity to collect surface water outside the dam	Local instability of the dam	5	Inadequacy section	1	Unblocking of channels	Prevention	4	20
							Detection		
				Obstruction of channels	2	Visual Inspection	Prevention	2	20
							Detection		
1.1.5.1 Concrete channels									
Collect the surface water that flow through the embankment	Insufficient capacity to collect surface water that flow through the embankment	Local instability of the dam	4	Inadequacy section	1	Structural maintenance of channels	Prevention	4	16
						Visual Inspection	Detection		
				Obstruction of channels	2	Unblocking of channels	Prevention	2	16
						Visual Inspection	Detection		
Collect the surface water outside the dam	Insufficient capacity to collect surface water outside the dam	Local instability of the dam	4	Inadequacy section	1	Unblocking of channels	Prevention	4	16
							Detection		
				Obstruction of channels	2	Visual Inspection	Prevention	2	16
1.1.6 Internal drainage system									
Collect the seepage	Inadequate functioning of the internal drainage	Piping	9	Inadequacy of the project and/or construction	2	Adequacy of particle size	Prevention	6	108
						Visual Inspection and Instrumentation	Detection		
1.1.6.1 Bottom drain									
Collect the seepage from dam	Insufficient drainage capacity	Piping	9	Inadequate particle size	2	Adequacy of particle size	Prevention	5	90
						Visual Inspection and Instrumentation	Detection		
				Insufficient thickness	2	Adequacy of particle size	Prevention	5	90
						Visual Inspection and Instrumentation	Detection		
				Alterability of the materials	2	Adequacy of particle size	Prevention	6	108
						Visual Inspection	Detection		
Collect the seepage from nature mass	Insufficient drainage capacity	Piping	9	Inadequate particle size	2	Adequacy of particle size	Prevention	5	90
						Visual Inspection and Instrumentation	Detection		
				Insufficient thickness	2	Adequacy of particle size	Prevention	5	90
						Visual Inspection and Instrumentation	Detection		
				Alterability of the materials	2	Visual Inspection	Prevention	6	108
							Detection		
Collect the seepage from foundation	Insufficient drainage capacity	Piping	9	Inadequate particle size	2	Adequacy of particle size	Prevention	5	90
						Visual Inspection and Instrumentation	Detection		
				Insufficient thickness	2	Adequacy of particle size	Prevention	5	90
						Visual Inspection and Instrumentation	Detection		
				Alterability of the materials	2	Visual Inspection	Prevention	6	108

Table 12 (cont.)

Function	Failure	Final effect	Si	Cause	Oi	Control	Control type	Di	RPNi
1.1.6.2 Vertical filter									
Collect the seep-age from dam	Insufficient drainage capacity	Piping	9	Inadequate of particle size	2	Adequacy of particle size	Prevention	5	90
						Visual Inspection and Instrumentation	Detection		
				Insufficient thickness	2	Adequacy of particle size	Prevention	5	90
						Visual Inspection and Instrumentation	Detection		
				Alterability of the materials	2	Adequacy of particle size	Prevention	6	108
						Visual Inspection	Detection		
Collect the seep-age from nature mass	Insufficient drainage capacity	Piping	9	Inadequate of particle size	2	Adequacy of particle size	Prevention	5	90
						Visual Inspection and Instrumentation	Detection		
				Insufficient thickness	2	Adequacy of particle size	Prevention	5	90
						Visual Inspection and Instrumentation	Detection		
				Alterability of the materials	2	Adequacy of particle size	Prevention	6	108
						Visual Inspection	Detection		
1.1.6.3 Foot drain									
Collect the seep-age from dam	Insufficient drainage capacity	Piping	9	Inadequate of particle size	2	Adequacy of particle size	Prevention	5	90
						Visual Inspection and Instrumentation	Detection		
				Insufficient thickness	2	Adequacy of particle size	Prevention	5	90
						Visual Inspection and Instrumentation	Detection		
				Alterability of the materials	2	Adequacy of particle size	Prevention	6	108
						Visual Inspection	Detection		
Collect the seep-age from nature mass	Insufficient drainage capacity	Piping	9	Inadequate of particle size	2	Adequacy of particle size	Prevention	5	90
						Visual Inspection and Instrumentation	Detection		
				Insufficient thickness	2	Adequacy of particle size	Prevention	5	90
						Visual Inspection and Instrumentation	Detection		
				Alterability of the materials	2	Adequacy of particle size	Prevention	6	108
						Visual Inspection	Detection		
1.2 Spillway system									
Conduct water	Insufficient drainage capacity	Overtopping	9	Inadequate dimensioning of the spillway	3	Correct dimensioning of the spillway	Prevention	2	54
						Visual Inspection and Instrumentation	Detection		
Not allow over-topping of the dam	Allow overtopping of the dam	Overtopping	9	Inadequate dimensioning of the spillway	3	Correct dimensioning of the spillway	Prevention	2	54
						Visual Inspection and Instrumentation	Detection		
1.3 Abutments									
Confer stability of embankment	Instability associated with movements of the soil mass	Local instability of the dam	4	Reduction of strength	3	Sealing of cracks	Prevention	3	36
						Adequacy of the geometry	Prevention		
						Visual Inspection and Instrumentation	Detection		
1.3.1 Abutment right									
Confer stability of embankment	Instability associated with movements of the soil mass	Local instability of the dam	4	Reduction of strength	3	Sealing of cracks	Prevention	3	36
						Adequacy of the geometry	Prevention		
						Visual Inspection and Instrumentation	Detection		

Table 12 (cont.)

Function	Failure	Final effect	Si	Cause	Oi	Control	Control type	Di	RPNi
1.3.2 Abutment left									
Confer stability of embankment	Instability associated with movements of the soil mass	Local instability of the dam	4	Reduction of strength	3	Sealing of cracks	Prevention	3	36
						Adequacy of the geometry	Prevention		
						Visual Inspection and Instrumentation	Detection		
1.4 Foundation									
Provide support for dam	Instability associated with movements of the soil mass	Global instability of the dam	10	Foundation treatment insufficient	2	Reinforcement in the foundation treatment	Prevention	4	80
						Visual Inspection and Instrumentation	Detection		
Confer global stability of embankment	Excessive seepage	Piping	9	Foundation treatment insufficient	2	Reinforcement in the foundation treatment	Prevention	5	90
						Visual Inspection and Instrumentation	Detection		
1.5 Tailings impoundment									
Store water	Insufficient capacity for store water	Overtopping	9	Inadequacy of the project and/or construction	4	Visual Inspection and Instrumentation	Prevention	2	72
Retain sediments	Insufficient capacity for retain sediments	Reduction temporary of the storage capacity	5	Inadequacy of the project and/or construction	4	Visual Inspection and Instrumentation	Prevention	2	40
Water clarification	Insufficient capacity to clarify the water	Reduction temporary of the storage capacity	4	Inadequacy of the project and/or construction	3	Visual Inspection and Instrumentation	Prevention	2	20

Table 13 - FMEA Results: System of the Tailings Dam B.

Function	Failure	Final effect	Si	Cause	Oi	Control	Control type	Di	RPNi
1.1 Dam body									
Containment of tailings	Insufficient capacity to contain tailings	Global instability of the dam	10	Inadequacy of the project and/or construction	2	Adjustment of the project	Prevention	3	60
						Visual Inspection and Instrumentation	Detection		
1.1.1 Crest									
Allow access to dam	Not allow access to dam	Inability to carry out inspections	4	Inadequacy of the project and/or construction	2	Adjustment of the project	Prevention	1	8
						Visual Inspection	Detection		
1.1.2 Core									
Reduce the hydraulic conductivity	Excessive seepage	Piping	9	Alterability of the materials	2	Recompaction	Prevention	6	108
						Visual Inspection	Detection		
				Dissolution of the materials	4	Recompaction	Prevention	6	216
						Visual Inspection and Instrumentation	Detection		
				High hydraulic load increase the saturation line	4	Recompaction	Prevention	2	72
						Visual Inspection and Instrumentation	Detection		
				Hydraulic fracturing	2	Recompaction	Prevention	4	72
						Visual Inspection and Instrumentation	Detection		

Table 13 (cont.)

Function	Failure	Final effect	Si	Cause	Oi	Control	Control type	Di	RPNi
1.1.3 Upstream slope									
Confer mechanical stability	Instability associated with movements of the soil mass	Global instability of the dam	10	Deficient compaction of the embankment	4	Adequacy of the geometry	Prevention	2	80
						Recompaction	Prevention		
						Instrumentation	Detection	6	120
				Alterability of the materials	2	Adequacy of the geometry	Prevention		
						Recompaction	Prevention		
						Visual Inspection	Detection		
	Excessive deformation	Overtopping	9	Alterability of the materials	2	Recompaction	Prevention	6	108
						Visual Inspection	Detection		
				Collapse	2	Recompaction	Prevention	3	54
						Visual Inspection and Instrumentation	Detection		
				Deficient compaction of the embankment	4	Recompaction	Prevention	2	72
						Visual Inspection and Instrumentation	Detection		
1.1.3.1 Free board									
Not allow overtopping of the dam	Allow overtopping of the dam	Overtopping	9	Inadequacy of the project and/or construction	4	Adequacy of the geometry	Prevention	1	36
						Adjustment of the project	Prevention		
						Visual Inspection and Instrumentation	Detection		
1.1.4 Downstream slope									
Confer mechanical stability	Instability associated with movements of the soil mass	Global instability of the dam	10	Deficient compaction of the embankment	4	Adequacy of the geometry	Prevention	2	80
						Recompaction	Prevention		
						Instrumentation	Detection	6	120
				Alterability of the materials	2	Adequacy of the geometry	Prevention		
						Recompaction	Prevention		
						Visual Inspection	Detection		
	External erosion	Local instability of the dam	5	Deficient compaction of the embankment	4	Recompaction	Prevention	2	80
						Visual Inspection and Instrumentation	Detection		
	Excessive deformation	Overtopping	9	Alterability of the materials	2	Recompaction	Prevention	6	108
						Instrumentation	Detection		
				Deficient compaction of the embankment	4	Recompaction	Prevention	2	72
						Visual Inspection and Instrumentation	Detection		
1.1.5 Surface drainage system									
Collect surface water that flow through the embankment	Insufficient capacity to collect surface water	Local instability of the dam	5	Inadequacy section	1	Structural maintenance of channels	Prevention	4	20
						Visual Inspection	Detection		
				Obstruction of channels	2	Unblocking of channels	Prevention	2	20
						Visual Inspection	Detection		
Collect surface water outside the dam	Insufficient capacity to collect surface water	Local instability of the dam	5	Inadequacy section	1	Unblocking of channels	Prevention	4	20
							Detection		
				Obstruction of channels	2	Visual Inspection	Prevention	2	20
							Detection		
1.1.5.1 Concrete channels									
Collect the surface water that flow through the embankment	Insufficient capacity to collect surface water	Local instability of the dam	4	Inadequacy section	1	Structural maintenance of channels	Prevention	4	16
						Visual Inspection	Detection		
				Obstruction of channels	2	Unblocking of channels	Prevention	2	16
						Visual Inspection	Detection		

Table 13 (cont.)

Function	Failure	Final effect	Si	Cause	Oi	Control	Control type	Di	RPNi
Collect the surface water outside the dam	Insufficient capacity to collect surface water	Local instability of the dam	4	Inadequacy section	1	Unblocking of channels	Prevention Detection	4	16
				Obstruction of channels	2	Visual Inspection	Prevention	2	16
1.1.6 Internal drainage system									
Collect the seepage	Inadequate functioning of the internal drainage	Piping	9	Inadequacy of the project and/or construction	3	Adequacy of particle size Visual Inspection and Instrumentation	Prevention Detection	6	162
1.1.6.1 Bottom drain									
Collect the seepage from dam	Insufficient drainage capacity	Piping	9	Inadequate particle size	2	Adequacy of particle size Visual Inspection and Instrumentation	Prevention Detection	5	90
				Insufficient thickness	2	Adequacy of particle size Visual Inspection and Instrumentation	Prevention Detection	5	90
				Alterability of the materials	2	Adequacy of particle size Visual Inspection	Prevention Detection	6	108
Collect the seepage from nature mass	Insufficient drainage capacity	Piping	9	Inadequate particle size	2	Adequacy of particle size Visual Inspection and Instrumentation	Prevention Detection	5	90
				Insufficient thickness	2	Adequacy of particle size Visual Inspection and Instrumentation	Prevention Detection	5	90
				Alterability of the materials	2	Visual Inspection	Prevention Detection	6	108
Collect the seepage from foundation	Insufficient drainage capacity	Piping	9	Inadequate particle size	2	Adequacy of particle size Visual Inspection and Instrumentation	Prevention Detection	5	90
				Insufficient thickness	2	Adequacy of particle size Visual Inspection and Instrumentation	Prevention Detection	5	90
				Alterability of the materials	2	Visual Inspection	Prevention	6	108
1.1.6.2 Vertical filter									
Collect the seepage from dam	Insufficient drainage capacity	Piping	9	Inadequate of particle size	2	Adequacy of particle size Visual Inspection and Instrumentation	Prevention Detection	5	90
				Insufficient thickness	2	Adequacy of particle size Visual Inspection and Instrumentation	Prevention Detection	5	90
				Alterability of the materials	2	Adequacy of particle size Visual Inspection	Prevention Detection	6	108
Collect the seepage from nature mass	Insufficient drainage capacity	Piping	9	Inadequate of particle size	2	Adequacy of particle size Visual Inspection and Instrumentation	Prevention Detection	5	90
				Insufficient thickness	2	Adequacy of particle size Visual Inspection and Instrumentation	Prevention Detection	5	90
				Alterability of the materials	2	Adequacy of particle size Visual Inspection	Prevention Detection	6	108

Table 13 (cont.)

Function	Failure	Final effect	Si	Cause	Oi	Control	Control type	Di	RPNi
1.1.6.3 Foot drain									
Collect the seepage from dam	Insufficient drainage capacity	Piping	9	Inadequate of particle size	5	Adequacy of particle size	Prevention	5	225
						Visual Inspection and Instrumentation	Detection		
				Insufficient thickness	5	Adequacy of particle size	Prevention	5	225
						Visual Inspection and Instrumentation	Detection		
				Alterability of the materials	2	Adequacy of particle size	Prevention	6	108
						Visual Inspection	Detection		
Collect the seepage from nature mass	Insufficient drainage capacity	Piping	9	Inadequate of particle size	5	Adequacy of particle size	Prevention	5	225
						Visual Inspection and Instrumentation	Detection		
				Insufficient thickness	5	Adequacy of particle size	Prevention	5	225
						Visual Inspection and Instrumentation	Detection		
				Alterability of the materials	2	Adequacy of particle size	Prevention	6	108
						Visual Inspection	Detection		
1.1.6.4 Drain on the abutments									
Collect the seepage from dam	Insufficient drainage capacity	Piping	9	Inadequate of particle size	3	Adequacy of particle size	Prevention	4	108
						Visual Inspection and Instrumentation	Detection		
				Insufficient thickness	3	Adequacy of particle size	Prevention	4	108
						Visual Inspection and Instrumentation	Detection		
				Alterability of the materials	2	Adequacy of particle size	Prevention	6	108
						Visual Inspection	Detection		
Collect the seepage from nature mass	Insufficient drainage capacity	Piping	9	Inadequate of particle size	3	Adequacy of particle size	Prevention	4	108
						Visual Inspection and Instrumentation	Detection		
				Insufficient thickness	3	Adequacy of particle size	Prevention	4	108
						Visual Inspection and Instrumentation	Detection		
				Alterability of the materials	2	Adequacy of particle size	Prevention	6	108
						Visual Inspection	Detection		
1.2 Spillway system									
Conduct water	Insufficient drainage capacity	Overtopping	9	Inadequate dimensioning of the spillway	1	Correct dimensioning of the spillway	Prevention	3	27
						Visual Inspection and Instrumentation	Detection		
Not allow overtopping of the dam	Allow overtopping of the dam	Overtopping	9	Inadequate dimensioning of the spillway	1	Correct dimensioning of the spillway	Prevention	3	27
						Visual Inspection and Instrumentation	Detection		
1.3 Abutments									
Confer stability of embankment	Instability associated with movements of the soil mass	Local instability of the dam	4	Reduction of strength	2	Sealing of cracks	Prevention	2	16
						Adequacy of the geometry	Prevention		
						Visual Inspection and Instrumentation	Detection		
1.3.1 Abutment right									
Confer stability of embankment	Instability associated with movements of the soil mass	Local instability of the dam	4	Reduction of strength	2	Sealing of cracks	Prevention	2	16
						Adequacy of the geometry	Prevention		
						Visual Inspection and Instrumentation	Detection		

Table 13 (cont.)

Function	Failure	Final effect	Si	Cause	Oi	Control	Control type	Di	RPNi
1.3.2 Abutment left									
Confer stability of embankment	Instability associated with movements of the soil mass	Local instability of the dam	4	Reduction of strength	2	Sealing of cracks Adequacy of the geometry Visual Inspection and Instrumentation	Prevention Prevention Detection	2	16
1.4 Foundation									
Provide support for dam	Instability associated with movements of the soil mass	Global instability of the dam	10	Foundation treatment insufficient	2	Reinforcement in the foundation treatment Visual Inspection and Instrumentation	Prevention Detection	4	80
Confer global stability of embankment	Excessive seepage	Piping	9	Foundation treatment insufficient	2	Reinforcement in the foundation treatment Visual Inspection and Instrumentation	Prevention Detection	5	90
1.5 Tailings impoundment									
Store water	Insufficient capacity for store water	Overtopping	9	Inadequacy of the project and/or construction	1	Visual Inspection and Instrumentation	Prevention	1	9
Retain sediments	Insufficient capacity for retain sediments	Reduction temporary of the storage capacity	5	Inadequacy of the project and/or construction	1	Visual Inspection and Instrumentation	Prevention	1	5
Water clarification	Insufficient capacity to clarify the water	Reduction temporary of the storage capacity	4	Inadequacy of the project and/or construction	1	Visual Inspection and Instrumentation	Prevention	1	4

Table 14 - Intolerable Risk - RPNi > 120.

Location	Function	Failure	Final effect	Cause	Tailing Dam
1.1.2 Core	Reduce the hydraulic conductivity	Excessive seepage	Piping	Dissolution of the materials	A and B
1.1.6 Internal drainage system	Collect the seepage	Inadequate functioning of the internal drainage	Piping	Inadequacy of the project and/or construction	B
1.1.6.3 Foot drain	Collect the seepage from dam	Insufficient drainage capacity	Piping	- Inadequate of particle size - Insufficient thickness	B
	Collect the seepage from nature mass	Insufficient drainage capacity	Piping	- Inadequate of particle size - Insufficient thickness	B

6. Conclusions

Risk analysis methods have been recently applied to dams, also including tailings dams however there is still a lack of confident threshold risk values to subsidize general analysis of risk situations. A preliminary attempt was carried out in this paper for the LCI (LCI MOD-REJ version) and the FMEA methods (Ind_{Risk} greater than 40,000 and RPNi were greater than 120, respectively).

It can be concluded that those two methods allowed a better understanding of the behaviour of the analyzed dams proving that the use of risk analysis methods is a tool for the decision on making process of the risk management.

In a general view the results of both methods are similar in terms of risk situations though there are specific differences on the determination of failure modes for the two dams considered in this study case. The emphasis for the LCI MOD-REJ version was the indications of failures caused by overtopping while for the FMEA method only problems with piping were detected. It should be reinforced that by no means there is an immediate evidence of failures as both methods only specify to which aspects one must concentrate efforts in order to diminish the risk associated to potential failures of the structures.

These differences in the results are probably related to the way the methods were proposed and have been applied on risk analysis. The LCI one, the basis for the LCI MOD-REJ version, is more general and the calculation of the risk is carried out after an evaluation of the impacts on the downstream valley. On the other hand the evaluation process of the FMEA method is more detailed as the risk for each element of the system is considered in the analysis.

Based on the current results a preliminary recommendation is to apply, whenever possible, these two risk analysis methods to a single or a portfolio of tailings dams. In the first case the idea is to allow the elaboration of an ordination hierarchy and a list of procedures for security. In the latter case the combined application may define the dams that should be prioritized to an immediate maintenance and repairs.

It is important to emphasize the importance to extend the applications of these methods to several tailings dams for a real evaluation of their suitability and effectiveness. For the case of the LCI MOD-REJ version, this extension would be essential to its calibration and verification.

Acknowledgments

The authors thank FAPEMIG (Foundation of Support of Research of Minas Gerais) for financial support for this research and FEAM (State Foundation of Environmental) for logistic support.

References

Caldeira, L. (2005) Análise de Risco em Geotecnia. Aplicação a Barragens de Aterro. Programa de Investigação para Otenção de Habilitação para Funções de Coordenação Científica (*in Portuguese*). LNEC, Lisbon, 238 pp.

Espósito, T.J. (2000) Metodologia Probabilística e Observacional Aplicada a Barragens de Rejeito Construídas por Aterro Hidráulico. Tese de Doutorado, Publicação G.TD-004A/00, Departamento de Engenharia Civil e Ambiental, Universidade de Brasília, Brasília, 359 pp.

Espósito, T.; Caldeira, L. & Naghettini, M. (2011a) Application of Location, Cause and Failure Indicators diagrams (LCI) to Tailings Dams. Proc. 6th International Conference on Dam Engineering. Lisbon, Portugal.

Espósito, T.; Caldeira, L. & Naghettini, M. (2011b) Aplicação da metodologia análise por diagramas de localização, causa e indicadores de falhas (LCI) em barragens de contenção de rejeitos. Proc. VII Congresso Brasileiro de Geotecnia Ambiental, REGEO' 2011, e VI Simpósio Brasileiro de Geossintéticos, Geossintéticos' 2011. Belo Horizonte, Brazil.

Hartford, D.N.D. & Baecher, G.B. (2004) Risk and Uncertainly in Dam Safety. Thomas Telford Limited Ed., London, 391 pp.

Hughes, A.; Hewlett, H.; Samuels, P.; Morris, M.; Sayers, P.; Moffat, I.; Harding, A. & Tedd, P. (2000) Risk Management for UK Reservoirs, Construction Industry Research and Information Association (CIRIA) C542, London, 213 pp.

Pimenta, L. (2009) Abordagens de Riscos em Barragens de Aterro. Tese de Doutorado, Universidade Técnica de Lisboa, Lisbon, 534 pp.

Pimenta, L.; Caldeira, L. & Silva Gomes, A. (2005) Análise de riscos da ensecadeira de Odelouca. Aplicação de uma metodologia simplificada com base em diagramas LCI. Seminário de Barragens Tecnologia, Segurança e Interação com a Sociedade, LNEC, Lisbon, Vol. T4.C7, pp. 609-627.

Santos, R. (2006) Enquadramento das Análises de Riscos em Geotecnia. Dissertação de Mestrado em Geotecnia para Engenharia Civil, Faculdade de Ciências e Tecnologia, Universidade Nova de Lisboa, Lisbon, 257 pp.

Performance of In-Line Sediment Control Devices Under Field Conditions

C.P. Cavalhieri, S.J.A.M. Campos, A.L.C.F. Gallardo, O.Y. Bitar

Abstract. A wide variety of structural best management practices (BMPs) has been developed in the last few decades to control erosion-related problems at construction sites. Even though many BMPs exist to control erosion and sediment accumulation, there is very little research on their performance and this is even more pronounced when considering the performance of these devices working together and under field conditions. In an effort to address this issue, this study analyzes the performance of in-line devices installed at six drainage exits of a new highway under construction, all of them located upstream and 1.0 km to 2.5 km far from a surface intake in a public water supply reservoir. Altogether, three categories of devices were studied: gabions, silt fences and turbidity curtains. The performance of each device was assessed based on inspections at the construction site after heavy rains, by visually checking changes in the apparent color of the water and accumulation of sediments. Complementary, water quality monitoring data collected at the water intake were analyzed by comparing two different periods: before (from 2002 to 2007) and during (from 2008 to 2010) the construction of the highway. Results indicated that the six drainage exits with BMPs installed in-line did not affect the quality of the water at the surface intake. In addition to that, although each of these devices could not function properly due to unsatisfactory maintenance and sometimes by their own low filtration rates, all of them contributed to retain sediment and keep it close to the limits of the construction site.
Keywords: sediment accumulation control, in-line best management practices, highway construction.

1. Introduction

Construction activities usually disturb many elements of the natural environment. These land-disturbing activities include vegetation removal, earthworks and civil works, which concentrate stormwater runoff and, according to Barret *et al.* (1995), increase soil loss and pollutant discharges.

Among all the pollutants that can be carried away in a stormwater runoff, sediment is the most commonly documented and it is a significant component of nonpoint source pollution (USEPA, 2008). When runoff transports eroded soil to water bodies, many resulting adverse environmental impacts may affect aquatic ecosystems (Hedrick *et al.*, 2010), vegetation (Benjankar & Yager, 2012) and use of water resources. In doing so, it is imperative that construction activities incorporate all kinds of mitigation measures in order to reduce discharges of sediments and other pollutants in water bodies (Zech *et al.*, 2008).

In order to minimize negative impacts, especially those related to the intensification of erosion and its effects on water bodies (Forsyth *et al.*, 2006), a wide variety of structural best management practices (BMPs) is usually installed at construction sites (Theisen, 1992). These BMPs are engineered systems designed to treat runoff inside the boundaries of the construction site itself and, therefore, preventing unwanted material to be discharged into either the storm sewer system or surface water bodies (USEPA, 2004).

Even though many BMPs exist to prevent erosion-related problems from happening (Raskin *et al.*, 2005), there is very little research related to their performance, as emphasized by Faucette *et al.* (2009), and this situation is even more pronounced when considering the performance of these devices under field conditions and, therefore, outside the laboratory controlled conditions. Therefore, in an effort to address this issue, the goal of this study was to analyze the performance of in-line devices installed during the construction of a new highway. These devices were designed to work together in the prevention of erosion-related problems.

Caio Pompeu Cavalhieri, Engineer, Instituto de Pesquisas Tecnológicas do Estado de São Paulo, Av. Prof. Almeida Prado 532, Cidade Universitária, 05508-901 São Paulo, SP, Brazil. e-mail: caiopc@ipt.br.
Sofia Julia Alves Macedo Campos, MSc, Instituto de Pesquisas Tecnológicas do Estado de São Paulo, Av. Prof. Almeida Prado 532, Cidade Universitária, 05508-901 São Paulo, SP, Brazil. e-mail: scampos@ipt.br.
Amarilis Lucia Casteli Figueiredo Gallardo, PhD, Instituto de Pesquisas Tecnológicas do Estado de São Paulo, Av. Prof. Almeida Prado 532, Cidade Universitária, 05508-901 São Paulo, SP, Brazil. e-mail: amacafi@ipt.br.
Omar Yazbek Bitar, PhD, Instituto de Pesquisas Tecnológicas do Estado de São Paulo, Av. Prof. Almeida Prado 532, Cidade Universitária, 05508-901 São Paulo, SP, Brazil. e-mail: omar@ipt.br.
Submitted on July 2, 2012; Final Acceptance on December 11, 2012; Discussion open until August 30, 2013.

2. Methods

This study analyzes the performance of in-line structural BMPs installed during the construction of a new highway close to a public water supply reservoir in the state of São Paulo (Brazil) and on an area predominantly formed by sandy clay and sandy loam soils.

All drainage exits of the construction site located upstream and up to 2.5 km far from a surface water intake were monitored. These drainage exits totaled six monitoring areas and the closest one to the water intake was approximately 1.0 km far from it (Fig. 1).

All six areas had a point of discharge from the construction site to the existing reservoir and in-line devices were installed to control sediment accumulation. At least two of the following devices were installed at each drainage exit: gabions, silt fences and turbidity curtains. The quantity of these structural BMPs, the distance from their respective drainage exits and their position in relation to each other are presented in Table 1, where "1st" refers to the device that was first reached by the runoff, "2nd" refers to the following device in the path of runoff, and so on (Fig. 2). In addition to that, all monitored areas were covered with grass, although slopes had not been necessarily covered right after their construction.

Besides having in common the purpose of preventing sediment from leaving the construction site and entering the existing reservoir, the three types of devices had the same nonwoven geotextile as one of their components. The main characteristics of this type of fabric are listed in Table 2.

The performance of each device was assessed by inspecting the construction site after heavy rains and considering two aspects: visible changes in the apparent color of the water and the accumulation of sediments. Particularly in relation to sediment accumulation, those caused by the presence of a silt fence were identified essentially by means of visual inspections at the construction site. Accumulations related to the existence of turbidity curtains were recognized by means of sediment samples collected by the end of the construction activities from the bottom of the reservoirs, upstream and downstream of this type of barrier (Fig. 3).

Table 1 - Quantity, position and distance from each drainage exit of BMPs.

Drainage exit	In-line structural BMPs								
	Gabion			Silt fence			Turbidity curtain		
	Quantity	Position	Distance (m)	Quantity	Position	Distance (m)	Quantity	Position	Distance (m)
# 1	1	1st	60	2	2nd and 3rd	80 and 120	1	4th	165
# 2	-	-	-	2	1st and 2nd	40 and 50	2	3rd and 4th	60 and 70
# 3	2	1st and 2nd	60 and 120	1	3rd	260	1	4th	295
# 4	1	1st	55	-	-	-	2	2nd and 3rd	85 and 105
# 5	1	1st	45	1	2nd	55	1	3rd	95
# 6	1	1st	90	1	2nd	160	1	3rd	185

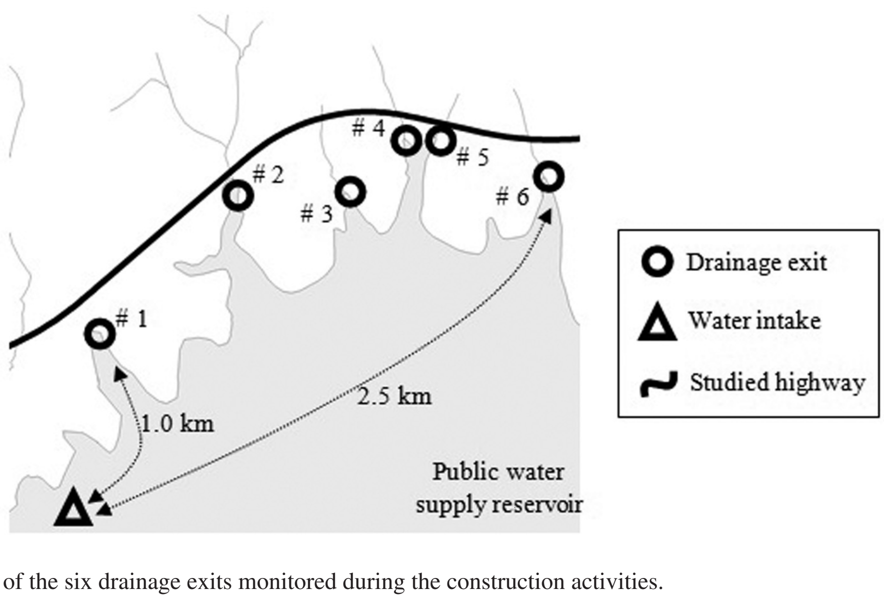

Figure 1 - Location of the six drainage exits monitored during the construction activities.

In addition to that, the water quality monitoring data collected at the surface water intake were analyzed. Two parameters were considered, both affected by the presence of suspended sediment in the water body: turbidity and conductivity. The monitoring data were analyzed by comparing two different periods: before (from 2002 to 2007) and during (from 2008 to 2010) the construction of the new highway. It is important to highlight that, although samples were collected only once every two months and without any reference to the weather conditions during sampling, these monitoring data were relevant to identify any significant changes in the reservoir.

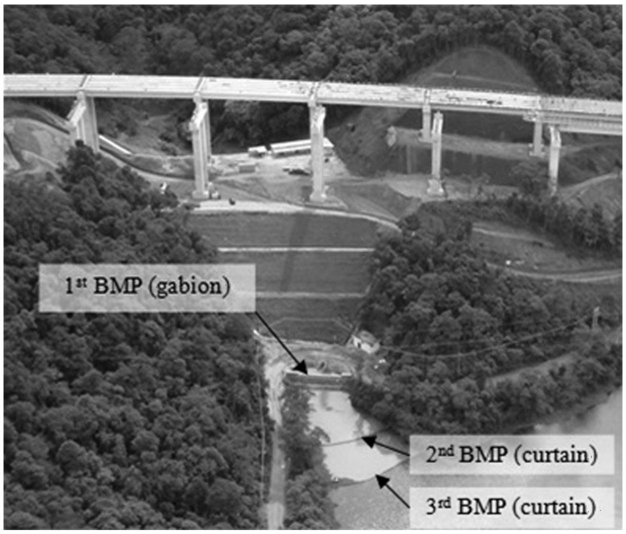

Figure 2 - Drainage exit # 4 and its three structural BMPs installed to control sediment accumulation.

3. Results

The results were grouped into the three categories as follows.

3.1. Visual changes in the apparent color

Based on visual inspections, silt fences and turbidity curtains were effective in reducing the apparent color of the runoff from the construction site.

In the case of silt fences, it was evidenced by the color of the water that passed through the pervious fabric, once it clearer than the runoff ponded behind the fences. However, the fabric clogged relatively fast and, in order to keep the water flowing through the fences, the geotextile had to be either cleaned or replaced very frequently (Fig. 4). In rela-

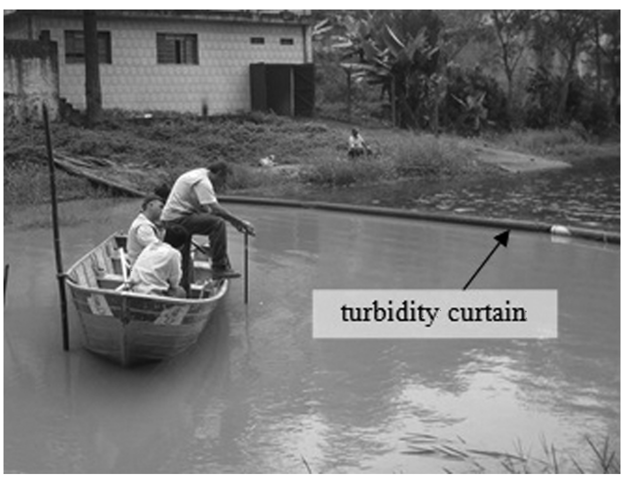

Figure 3 - Sediment sample being collected upstream of a turbidity curtain (3rd BMP at drainage exit # 6) during the monitoring activities.

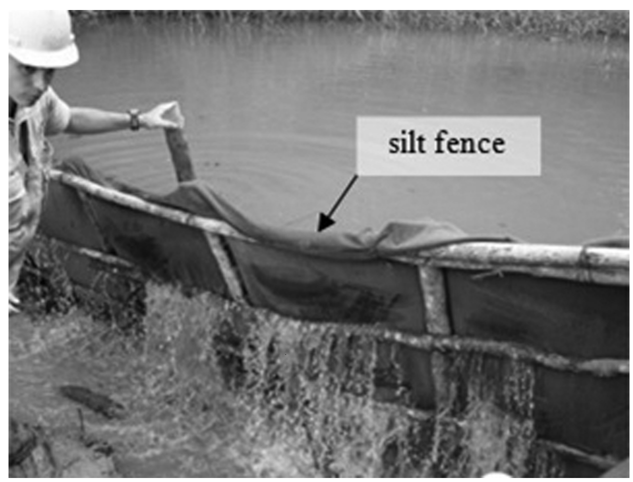

Figure 4 - Runoff passing through the pervious fabric of a silt fence (3rd BMP at drainage exit # 3) right after being partially cleaned.

Table 2 - Properties of the nonwoven geotextile used as a component of the devices.

Mechanical properties	Test method	Geotextile
Wide width tensile strength	NBR 12824	≥ 12 kN/m
Elongation	NBR 12824	≤ 75%
Grab tensile strength	ASTM D 4632	≥ 800 N
CBR Puncture strength	NBR 13359	≥ 2.5 kN
Permeability	ASTM D 4491	≥ 0.35 cm/s
Apparent opening size (AOS)	ASTM 4751	0.11 mm to 0.21 mm

tion to the turbidity curtains, the water retained behind them had too much apparent color, whereas the color of the water right after the curtains was not significantly different from that of the rest of the reservoir (Fig. 5).

Gabions also helped to reduce the apparent color of the runoff. However, based on visual data, reduction of the apparent color performed by this device was not significant when compared to silt fences and turbidity curtains.

3.2. Sediment accumulation

Sediment accumulated behind (upstream) and in front of (downstream) gabions, silt fences and turbidity curtains. In general, material accumulated behind gabions had a larger equivalent diameter in comparison to those found near silt fences and turbidity curtains. In addition, gabions and silt fences that were not properly kept in good conditions were damaged by material overtopping them (Figs. 6 and 7).

Sediment samples were collected downstream up to 12 m far from turbidity curtains. The results indicate that material from the construction site was not completely retained by the floating barriers, which may also be a consequence of unsatisfactory maintenance. The levels of sediments accumulated right before and right after the curtains are listed in Table 3.

Figure 6 - Material accumulated behind the gabion (1st BMP) at drainage exit # 4, almost overtopping it.

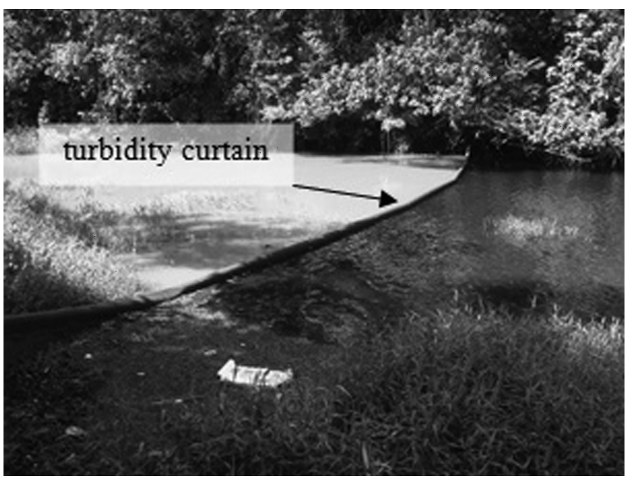

Figure 5 - Apparent color of the water behind (darker) and in front of (lighter) a turbidity curtain (4th BMP at drainage exit # 3).

Figure 7 - Silt fence damaged due to the excess of sediment and the unsatisfactory maintenance (2nd BMP at drainage exit # 5).

Table 3 - Levels of sediments accumulated before and after the turbidity curtains.

Drainage exit*	Level of sediments at different distances from the curtain					
	Upstream (before) the curtain		Downstream (after) the curtain			
	Distance (m)	Level (m)	Distance (m)	High (m)	Distance (m)	High (m)
# 3	2.0	0.36	1.0	0.72	12.6	0.50
# 4**	2.3	1.05	3.7	0.16	-	-
# 5	4.8	0.53	4.0	0.40	16.5	0.31
# 6	2.0	0.75	3.0	0.40	10.1	0.22

(*) Sediment was collected at drainage exits # 1 and # 2 but was not quantified.
(**) Curtain at this drainage refers to the 3rd structural BMP presented in Table 1.

3.3. Comparison of water quality monitoring data

Results of the water quality monitoring for turbidity and conductivity are illustrated in Figs. 8 and 9. In addition to that, the federal turbidity limit of 40 NTU for superficial raw water intended for human consumption is plotted in Fig. 8.

Mean values and standard deviations for turbidity and conductivity are respectively listed in Figs. 10 and 11. These values were calculated based on two different periods: before (2002-2007) and during (2008-2011) the construction.

4. Discussion

The limitations of the methods used in this study are: (a) sampling at the water intake only once every two months without any reference to the weather conditions, (b) positive effects that diffusion naturally exerts on water quality with distance indirectly incorporated into the monitoring data at the water intake, and (c) lack of quantification of sediment collected at two drainage exits. Nevertheless, the results of this study were sufficiently consistent to indicate that the construction of the highway did not cause significant changes in the water reservoir and that the structural BMPs had an important role in that.

According to the water quality monitoring data at the surface intake, turbidity and conductivity were not statically different before and during the construction of the highway (Fig. 10). Therefore, discharges from disturbed areas did not affect the quality of the water in the catchment region and, as a result, had no influence on water treatment activities, such as coagulant dosing and sludge generation and disposal, as it might have happened (Emelko *et al.*, 2011).

In-line devices installed during the highway construction worked as a system that provided slow filtration, as described by Paterniani *et al.* (2011). Either in-line BMPs or slow filtration systems require very low filtration rates to remove suspended particles, which may be accelerated by using either polyacrylamide (Hayes *et al.*, 2005) or an active component from *Moringa oleifera* seeds (Sánchez-Martín *et al.*, 2010). Additionally, both of them must be pre-treated when turbidity levels are high, to prevent them from clogging quickly. Considering in-line BMPs in the context of slow filtration processes, gabions worked as a pre-treatment unit during the construction activities because the relatively large spaces between the blocks tended to retain larger materials, whereas silt fences and turbidity curtains retained smaller particles.

Finally, although gabions, silt fences and turbidity curtains could not function properly due to unsatisfactory maintenance and could not completely retain sediments from the construction site, these three devices contributed

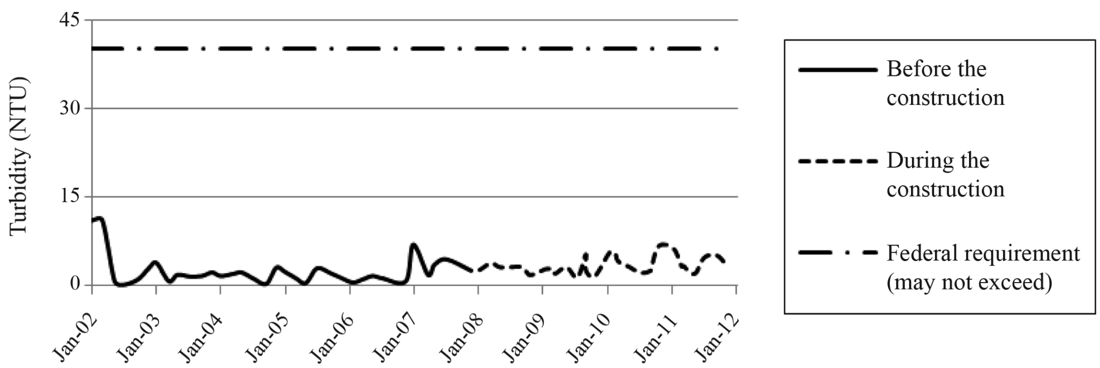

Figure 8 - Turbidity at the superficial water intake before and during the construction. Source: adapted from Cetesb (2003, 2004, 2005, 2006, 2007, 2008, 2009, 2010, 2011 and 2012) and Sabesp (2009, 2010 and 2011).

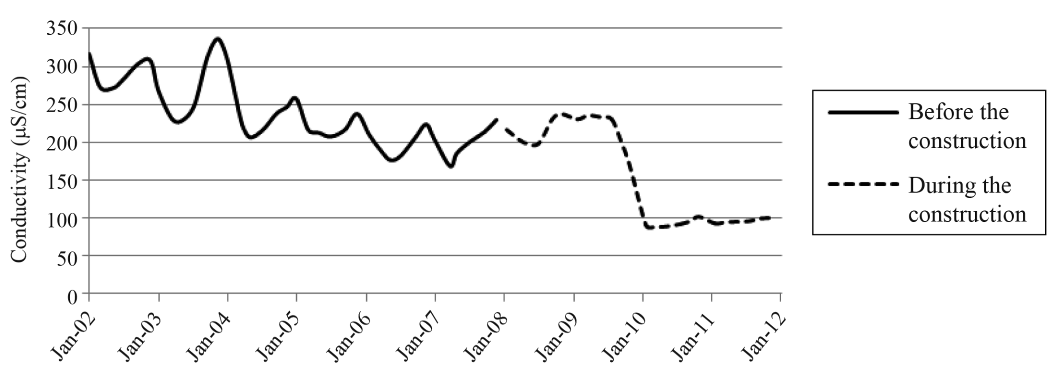

Figure 9 - Conductivity at the superficial water intake before and during the construction. Source: adapted from Cetesb (2003, 2004, 2005, 2006, 2007, 2008, 2009, 2010, 2011 and 2012) and Sabesp (2009, 2010 and 2011).

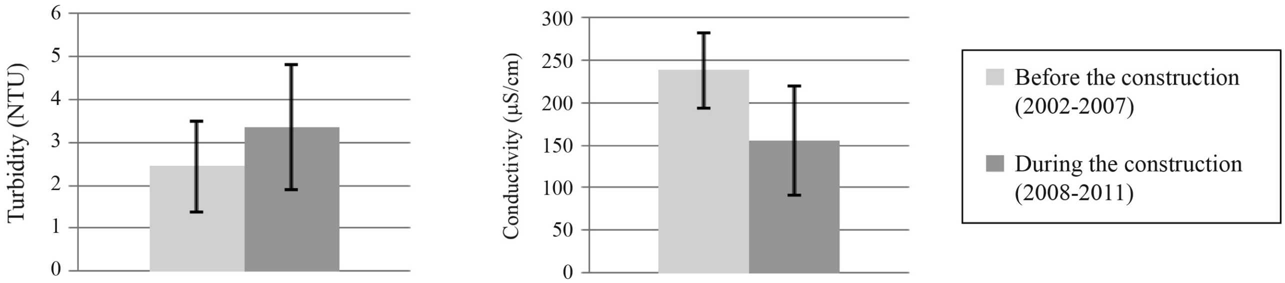

Figure 10 - Turbidity and conductivity mean values and standard deviations at the superficial water intake before and during the construction. Source: adapted from Cetesb (2003, 2004, 2005, 2006, 2007, 2008, 2009, 2010, 2011 and 2012) and Sabesp (2009, 2010 and 2011).

significantly to improve the control on sediment accumulation. It was evidenced, for example, by the sediment spread over a relatively small area, which BMP had positive effects on environmental recovery activities, such as reduction and facilitation of dredging to remove sediment accumulations, as pointed out by Fulazzaky & Abdul Gany (2009).

5. Conclusions

Results observed during the construction of the new highway indicate that structural BMPs, such as those analyzed in this study, have an important role in retaining soil, clarifying water and, therefore, controlling erosion-related problems. In addition to that, the integrated use of these devices results in important gains, such as improvement in controlling sediment accumulation, maintenance of water quality beyond the construction site, and even positive effects on environmental recovery activities.

However, it is important to highlight that gabions, silt fences and turbidity curtains do need maintenance in order to work properly. Continued maintenance is as important as the devices themselves to achieve and maintain the expected performance.

In the same way, in-line structures can be damaged by severe storms, once such configuration requires very low filtration rates to remove the suspended particles from the runoff. That is one of the reasons why advances in technologies that have the potential to accelerate deposition and filtration processes are really relevant in this field of science.

Finally, although gabions, silt fences and turbidity curtains were unable to completely retain sediments from the construction site, our results indicated that in-line structures are able to bring considerable benefits in large infrastructure projects, such as the construction of highways. Therefore, BMPs may be successfully applied to similar contexts as long as continued maintenance, proper installation and design criteria are duly considered.

References

ABNT (1993) Geotêxteis - Determinação da resistência à tração não-confinada - Ensaio de tração de faixa larga - NBR 12824. Associação Brasileira de Normas Técnicas, Rio de Janeiro, Rio de Janeiro, Brazil, 5 p.

ABNT (1995) Geotêxteis - Determinação da resistência ao puncionamento estático - Ensaio com pistão tipo CBR - NBR 13359. Associação Brasileira de Normas Técnicas, Rio de Janeiro, Rio de Janeiro, Brazil, 4 p.

ASTM (2009) Standard Test Method for determining filtering efficiency and flow rate of a geotextile for silt fence application using site-specific soil - D 4491. ASTM International. West Conshohocken, Pennsylvania, USA, 6 p.

ASTM (2008) Standard Test Method for Grab Breaking Load and Elongation of Geotextiles – D 4632. ASTM International. West Conshohocken, Pennsylvania, USA, 4 p.

ASTM (2012) Standard Test Method for Determining Apparent Opening Size of a Geotextile – D 4751. ASTM International. West Conshohocken, Pennsylvania, USA, 7 p.

Barret, M.E.; Kearney, J.E.; McCoy, T.G. & Malina, J.F. (1995) An evaluation of the use and effectiveness of temporary sediment controls. (CRWR Online Report 95-6) Austin: Center for Research in Water Resources, 148 pp.

Benjankar, R. & Yager, E.M. (2012) The impact of different sediment concentrations and sediment transport formulas on the simulated floodplain processes. Journal of Hydrology, v. 450-451:11, p. 230-243.

Cetesb – Companhia de Tecnologia de Saneamento Ambiental (2003) Relatório de qualidade das águas interiores do estado de São Paulo 2002 - 0103-4103. Diretoria de engenharia, tecnologia e qualidade ambiental, São Paulo, São Paulo, Brasil, 279 p.

Cetesb – Companhia de Tecnologia de Saneamento Ambiental (2004) Relatório de qualidade das águas interiores do estado de São Paulo 2003 - 0103-4103. Diretoria de engenharia, tecnologia e qualidade ambiental, São Paulo, São Paulo, Brasil, 273 p.

Cetesb – Companhia de Tecnologia de Saneamento Ambiental (2005) Relatório de qualidade das águas interiores do estado de São Paulo 2004 - 0103-4103. Diretoria de engenharia, tecnologia e qualidade ambiental, São Paulo, São Paulo, Brasil, 307 p.

Cetesb – Companhia de Tecnologia de Saneamento Ambiental (2006) Relatório de qualidade das águas interiores do estado de São Paulo 2005 - 0103-4103. Diretoria de engenharia, tecnologia e qualidade ambiental, São Paulo, São Paulo, Brasil, 488 p.

Cetesb – Companhia de Tecnologia de Saneamento Ambiental (2007) Relatório de qualidade das águas interiores do estado de São Paulo 2006 - 0103-4103. Diretoria de engenharia, tecnologia e qualidade ambiental, São Paulo, São Paulo, Brasil, 327 p.

Cetesb – Companhia de Tecnologia de Saneamento Ambiental (2008) Relatório de qualidade das águas interiores do estado de São Paulo 2007 - 0103-4103. Diretoria de engenharia, tecnologia e qualidade ambiental, São Paulo, São Paulo, Brasil, 537 p.

Cetesb – Companhia de Tecnologia de Saneamento Ambiental (2009) Relatório de qualidade das águas interiores do estado de São Paulo 2008 - 0103-4103. Diretoria de engenharia, tecnologia e qualidade ambiental, São Paulo, São Paulo, Brasil, 528 p.

Cetesb – Companhia Ambiental do Estado de São Paulo (2010) Relatório de qualidade das águas interiores no estado de São Paulo 2009 - 0103-4103. Diretoria de tecnologia, qualidade e avaliação ambiental, São Paulo, São Paulo, Brasil, 310 p.

Cetesb – Companhia Ambiental do Estado de São Paulo (2011) Qualidade das águas superficiais no estado de São Paulo 2010 - 0103-4103. Diretoria de engenharia e qualidade ambiental, São Paulo, São Paulo, Brasil, 298 p.

Cetesb – Companhia Ambiental do Estado de São Paulo (2012) Qualidade das Águas Superficiais no Estado de São Paulo 2011 - 0103-4103. Diretoria de Engenharia e Qualidade Ambiental, São Paulo, 356 pp.

Emelko, M.B.; Silins, U. & Bladon, K.D. (2011) Implications of land disturbance on drinking water treatability in a changing climate: demonstrating the need for “source water supply and protection” strategies. Water Research, v. 45:2, p. 461-472.

Faucette, L.B.; Governo, J.; Tyler, R.; Gigley, G.; Jordan, C.F. & Lockaby, B.G. (2009) Performance of compost filter socks and conventional sediment control barriers used for perimeter control on construction sites. Journal of Soil and Water Conservation, v. 64:1, p. 81-88.

Forsyth, A.R.; Bubb, K.A. & Cox, M.E. (2006) Runoff, sediment loss and water quality from forest roads in a southeast Queensland coastal plain Pinus plantation. Forest Ecology and Management, v. 221:1, p. 194-206.

Fulazzaky, M.A. & Abdul Gany, A.H. (2009) Challenges of soil erosion and sludge management for sustainable development in Indonesia. Journal of Environmental Management, v. 90:8, p. 2387-2392.

Hayes, S.A.; McLaughlin, R.A. & Osmond, D.L. (2005) Polyacrylamide use for erosion and turbidity control on construction sites. Journal of Soil and Water Conservation, v. 60:4, p. 193-199.

Hedrick, L.B.; Welsh, S.A.; Anderson, J.T.; Lin, L.S.; Chen; Y.S. & Wei, X.C. (2010) Response of benthonic macroinvertebrate communities to highway construction in an Appalachian watershed. Hydrobiologia, v. 641:1, p. 115-131.

Fulazzaky, M.A. & Abdul Gany, A.H. (2009) Challenges of soil erosion and sludge management for sustainable development in Indonesia. Journal of Environmental Management, v. 90:8, p. 2387-2392.

Paterniani, J.E.S.; Silva, M.J.M.; Ribeiro, T.A.P. & Barbosa, M. (2011) Pre-filtration in boulder and slow sand filtration with non-woven synthetic layers and granulated vegetal coal to improve quality in wastewater treated by constructed wetlands. Eng. Agríc., v. 31:4, p. 803-812.

Raskin, L.; DePaoli, A. & Singer, M.J. (2005) Erosion control materials used on construction sites in California. Journal of Soil and Water Conservation, v. 60:4, p. 187-192.

Sabesp - Companhia de Saneamento Básico do Estado de São Paulo (2009) available at http://site.sabesp.com.br/uploads/file/monitoramento/conama_357_2009_inorganico.pdf and downloaded on December 10th 2012.

Sabesp - Companhia de Saneamento Básico do Estado de São Paulo (2010) available at http://site.sabesp.com.br/uploads/file/monitoramento/conama_357_2010_inorganico.pdf and downloaded on December 10th 2012.

Sabesp - Companhia de Saneamento Básico do Estado de São Paulo (2011) available at http://site.sabesp.com.br/uploads/file/monitoramento/conama_357_2011_inorganico.pdf and downloaded on December 10th 2012.

Sánchez-Martín, J.; Ghebremichael, K. & Beltrán-Heredia, J. (2010) Comparison of singles-step and two-step purified coagulants from Moringa oleifera seed for turbidity and DOC removal. Bioresource Technology, v. 101:15, p. 6259-6261.

Theisen, M.S. (1992) The role of geosynthetics in erosion and sediment control: an overview. Geotextiles and Geomembranes, v. 11:4, p. 535-550.

USEPA - United States Environmental Protection Agency (2004) The use of best management practices (BMPs) in urban watersheds - EPA/600/R-04/184. Office of research and development, Cincinnati, Ohio, USA, 271 p. Available at: http://nepis.epa.gov/Adobe/PDF/2000D1LM.pdf.

USEPA - United States Environmental Protection Agency (2008) Environmental impact and benefits assessment for proposed effluent guidelines and standards for the construction and development category - EPA-821-R-08-009. Office of water, Washington, District of Columbia, USA, 253 p. Available at: http://water.epa.gov/scitech/wastetech/guide/construction/upload/2008_11_25_guide_construction_proposed_proposed-env-20081120.pdf.

Zech, W.C.; Halverson, J.L. & Clement, T.P. (2008) Intermediate-scale experiments to evaluate silt fence designs to control sediment discharge from highway construction sites. Journal of hydrologic engineering, v. 13:6, p. 497-504.

Technical Note

Explicit Numerial Iterative Methods Applied to the Three-Parameter Infiltration Equation

A.L.B. Cavalcante, L.C.S.M. Ozelim, P.K. Swamee, P.N. Rathie

Abstract. Finding explicit solutions to the partial differential equations governing the infiltration phenomenon tend to be a challenging issue. On account of such complexity, researchers have proposed algebraic equations to model this phenomenon. This paper deals with the solution of the general three-parameter infiltration equation, which is an implicit equation corresponding to the interpolation between the Green-Ampt and Talsma-Parlange infiltration models. By means of the Householders method, the cumulative infiltration is obtained by a rapidly converging iterative procedure. The results are further manipulated in order to obtain the infiltration rate explicitly. The effect of variables involved on the solution is also discussed. A case study is included to demonstrate the use of the proposed algorithm. The formulas proposed provide easy-to-use equations which enable calculations on the fly while considering practical applications.

Keywords: three-parameter infiltration formula, Green-Ampt, Householder's Methods, Talsma-Parlange.

1. Introduction

Originally proposed by Parlange *et al.* (1982), the three parameter infiltration model unifies two other well-known models, introduced by Green-Ampt (1911) and Talsma & Parlange (1972). Green-Ampt's proposition (Green & Ampt, 1911) figures as one of the most explored infiltration models. Green-Ampt's model is based on Darcy's equation and a few other assumptions, namely: the existence of a constant hydraulic pressure head at soil's surface; the hydraulic conductivity in such zone K_t is equivalent to the saturated one K_s; and the formation of a precisely defined wetting front leading to the so-called piston movement (Zonta *et al.* 2010).

The integrated form of Green-Ampt infiltration rate equation is given by Mein & Farrel (1974):

$$t_* = I_* - \ln(1 + I_*) \tag{1}$$

where t_* = nondimensional time; and I_* = nondimensional cumulative infiltration, given by (Mein & Farrel, 1974):

$$t_* = \frac{K_s(t - t_p + t_s)}{(\psi_w - p_s)(\theta_s - \theta_o)} \tag{2}$$

$$I_* = \frac{I}{(\psi_w - p_s)(\theta_s - \theta_o)} \tag{3}$$

wherein I is the cumulative infiltration; t_p = ponding time; t_s = theoretical time necessary to infiltrate the same volume infiltrated until the ponding time, under saturation of the superficial layer of the soil; ψ_w = average wetting front matric potential; p_s = average surface pressure head and θ_s = saturated water content; θ_o = initial water content.

On the other hand Talsma & Parlange (1972) equation for the nondimensional cumulative infiltration and nondimensional time is:

$$(I_* - t_* - 1)\exp(I_* - t_* - 1) + \exp(-t_* - 1) = 0 \tag{4}$$

Equations 1 and 4 were unified by Parlange *et al.* (1982) as

$$t_* = I_* + (1-\alpha)^{-1}\ \ln\left[\frac{\alpha}{1-(1-\alpha)\exp(-\alpha I_*)}\right] \tag{5}$$

where α = a transition parameter lying in the range $0 \le \alpha \le 1$. When $\alpha = 0$, the Green-Ampt equation is recovered from Eq. 5. On the other hand, when $\alpha = 1$, Talsma-Parlange's model follows from Eq. 5.

It has been shown by Parlange *et al.* (2002) that both the Green-Ampt and Talsma-Parlange equations can be explicitly solved in terms of Lambert W-function. On the other hand, Rathie *et al.* (2012) proposed the explicit solution of Eq. 5 in terms of the H-function. When implementations of such special functions are not available, standard trial and error procedures are used to solve Eq. 5.

Practical situations require neither complex nor precisely defined exact solutions. They do demand accurate solutions. This paper presents approximate solutions to the tree-parameter infiltration equation, by means of an iterative algorithm solution whose single iteration order of convergence can be chosen as high as necessary.

André L. Brasil Cavalcante, PhD, Associate Professor, Departamento de Engenharia Civil e Ambiental, Universidade de Brasília, 70910-900 Brasília, DF, Brazil. e-mail: abrasil@unb.br.
Luan Carlos de S.M. Ozelim, PhD Student, Departamento de Engenharia Civil e Ambiental, Universidade de Brasília, 70910-900 Brasília, DF, Brazil. e-mail: luanoz@gmail.com.
Prabhata K. Swamee, PhD, Full Professor, Department of Civil Engineering, National Institute of Technology, 144 011 Jalandhar, India. e-mail: swameefce@yahoo.com.
Pushpa N. Rathie, PhD, Senior Researcher, Departamento de Estatística, Universidade de Brasília, 70910-900 Brasília, DF, Brazil. e-mail: pushpanrathie@yahoo.com.
Submitted on August 12, 2011; Final Acceptance on April 19, 2013; Discussion open until August 30, 2013.

2. Solution of the Three-Parameter Infiltration Equation Using Householder's Method

Consider a function $f(x)$ whose root r needs to be determined. By choosing an initial point, x_0, Householder (1970) proposed the general iteration root-finding recurrence formula:

$$x_{n+1} = x_n + (a+1)\frac{[1/f(x_n)]^{(a)}}{[1/f(x_n)]^{(a+1)}} \tag{6}$$

in which a is a real number which governs the rate at which the iterative scheme tends to the root of the nonlinear equation $f(x) = 0$ and $(1/f)^{(a)}$ represents the a-th derivative of $1/f(x)$.

In fact, it can be shown that $|x_{n+1} - r| \le |K\, x_n - r|^{a+2}$ for some positive real number K, thus if x_0 is sufficiently close to r, the iteration scheme converges to the value of r with rate $a + 2$. Note that this method is a generalization of the Newton-Raphson method, which can be easily obtained by taking $a = 0$ in Eq. 6.

Consider that Eq. 3 can be rewritten as:

$$f(I_*) = t_* - I_* + (1-\alpha)^{-1}\ln\left[\frac{1-(1-\alpha)\exp(-\alpha I_*)}{\alpha}\right] \tag{7}$$

The first and second derivatives of $f(I_*)$ with respect to I_* are:

$$\frac{\partial}{\partial I_*} f(I_*) = -1 + \left[\frac{\alpha}{\exp(\alpha I_*) - (1-\alpha)}\right] \tag{8}$$

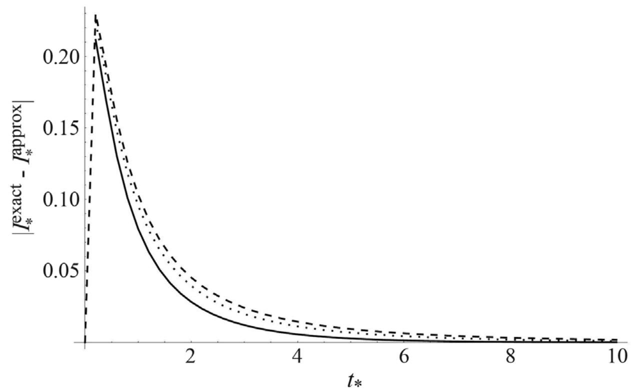

Figure 1 - Absolute Departure of Eq. 11 from exact solution of Eq. 5.

$$\frac{\partial^2}{\partial I_*^2} f(I_*) = \frac{-\alpha^2 \exp(\alpha I_*)}{[\exp(\alpha I_*) - (1-\alpha)]^2} \tag{9}$$

In order to use Houlseholder's iteration formula, let one establish as first guess for I_* the value of t_*. This comes from the fact that as I_* grows, Eq. 7 tends to $f(I_*) \approx t_* - I_*$. Using Eq. 6, I_* is found to be:

(a) For quadratic convergence of the first iteration ($a = 0$)

$$I_* = t_* - \frac{[\exp(\alpha t_*) - (1-\alpha)]\ln\left[\frac{1-(1-\alpha)\exp(-\alpha t_*)}{\alpha}\right]}{(1-\alpha)[1-\exp(\alpha t_*)]} \tag{10}$$

(b) For cubic convergence of the first iteration ($a = 1$)

$$I_* = t_* - \frac{2[1-\exp(\alpha t_*)][\exp(\alpha t_*) - (1-\alpha)]}{\alpha^2 \exp(\alpha t_*) + 2[1-\exp(\alpha t_*)]^2\left\{(1-\alpha)^{-1}\ln\left[\frac{1-(1-\alpha)\exp(-\alpha t_*)}{\alpha}\right]\right\}} \tag{11}$$

It can be noticed that the solution is an iterative algorithm.

In order to compare Eq. 11 to the exact solution of Eq. 5, consider the absolute difference between both solutions. Such departure is shown in Fig. 1. The exact solution has been obtained by trial and error procedures.

Figure 1 reveals that Eq. 11 behaves similarly for different values of the interpolation value α. The latter figure also shows that the maximum departure happens at low values of the nondimensional time, which is fully justified by the "long term" initial guess for nondimensional cumulative infiltration.

It is worth noticing that one may find an optimal initial guess in order to diminish the absolute departure over the whole domain. Also, the results in Fig. 1 correspond to a single iteration of the algorithm. Thus, if more iterations where taken into account, the error would be mitigated. The methodology is, this way, verified to produce good estimations of the solutions.

3. Determination of Some of the Equation Parameters

In order to obtain the values of t_p and t_s, one shall consider the following equation, obtained by means of implicit differentiation of Eq. 5 with respect to t_*:

$$I = \frac{(\psi_w - p_s)(\theta_s - \theta_o)}{\alpha}\ln\left(1 + \frac{\alpha K_s}{r - K_s}\right) \tag{12}$$

in which r is the infiltration rate. If one wants to find the total infiltration until ponding time, I_p, one shall make the substitution $r = i_p$ in Eq. 12, thus

$$I_p = \frac{(\psi_w - p_s)(\theta_s - \theta_o)}{\alpha}\ln\left(1 + \frac{\alpha K_s}{i_p - K_s}\right) \tag{13}$$

where i_p is the rainfall intensity. It's simple to get t_p from Eq. 13 since $t_p = I_p/i_p$, which provides:

$$t_p = \frac{(\psi_w - p_s)(\theta_s - \theta_o)}{\alpha i_p} \ln\left(1 + \frac{\alpha K_s}{i_p - K_s}\right) \quad (14)$$

One shall note that when α tends to 0, the same relation obtained by Mein & Farrel (1974) is retrieved for a Green-Ampt case, which is:

$$t_p = \frac{(\psi_w - p_s)(\theta_s - \theta_o) K_s}{i_p (i_p - K_s)} \quad (15)$$

The value of t_s can be obtained as follows:

$$t_s = \frac{I_p}{K_s} + \frac{(1-\alpha)^{-1} (\psi_w - p_s)(\theta_s - \theta_o)}{K_s} \ln\left[\frac{\alpha}{1-(1-\alpha)\exp(\alpha I_p)}\right] \quad (16)$$

On the other hand, in order to obtain ψ_w the following equation suggested in Cecilio *et al.* (2007) shall be used:

$$\psi_w = \frac{\psi_b (2 + 3\lambda)\left[K_r(\theta_t)^{\frac{3\lambda+1}{3\lambda+2}} - K_r(\theta_0)^{\frac{3\lambda+1}{3\lambda+2}}\right]}{[K_r(\theta_t) - K_r(\theta_0)][3\lambda + 1]} \quad (17)$$

where ψ_b is the air-entry value (mm); λ is the pore size distribution index (nondimensional) and K_r is the relative hydraulic conductivity (nondimensional), expressed as $K(\theta)/K_s$. Based on Brooks & Corey (1964) model, the relative hydraulic conductivity is:

$$K_r(\theta_j) = \left(\frac{\theta_j - \theta_r}{\theta_s - \theta_r}\right)^{\frac{2}{\lambda}+3} \quad (18)$$

where, θ_j is the water content whose relative hydraulic conductivity is sought at; θ_r is the residual water content.

Some propositions related to choosing appropriate parameters which better represent the properties of the soil must be taken into account. Transition zone's water content θ_t can be used instead of the saturation water content θ_s, since θ_t is the water content that most of the soil mass reaches while the infiltration process occurs. Also, the experiments available to obtain the value of K_0 often give a considerable dispersion of the results, what can be minimized by choosing the steady infiltration rate, *Tie*, as representative of the hydraulic conductivity of the soil profile (Cecílio *et al.*, 2007).

4. Examples of the Application of the Proposed Method

The experimental data used in this study are given by Cecílio (2005). Three types of soil will be analyzed, namely: Red Clay Soil (PV), Red Laterite Soil (LV) and Red-Yellow Laterite Soil (LVA). The characteristics of these soils and experimental data obtained (Cecílio, 2005) are presented in Tables 1 and 2 and Figs. 2 and 3.

In order to provide a better characterization of the soils studied, each one is graphically analyzed. It can be verified by experimental data (Cecílio, 2005) that the relative hydraulic conductivity can be graphically related to the volumetric water content as seen on Fig. 2.

It's clear from Fig. 2 that LV soil has a different behavior from LVA and PV soils, which is mainly related to their composition (LV has more sand in its composition while both LVA and PV have more clay), as seen on Table 1.

On the other hand, Fig. 3 shows graphically the relation between the relative hydraulic conductivity and the average wetting front matric potential based on Brooks and Corey model.

Figure 3 also shows that each soil has a unique behavior which mainly depends on the pore size distribution index. This dependence is obtained due to the adoption of Brooks and Corey model for the prediction of the wetting front matric potential.

Based on the data presented by Cecílio (2005) and considering Eq. 11 for predicting the temporal evolution of the cumulative infiltration, the results obtained for the modeling of each soil are presented in Fig. 4.

It can be seen that Eq. 11 provides good predictions of the infiltration behavior. For all the soils analyzed, crescent, however discontinuous, functions have been adjusted

Table 1 - Grain-size distribution of the soils considered.

Soil	Coarse sand (%)	Fine sand (%)	Silt (%)	Clay (%)
LVA	13	10	7	70
LV	26	52	2	20
PV	7	9	25	59

Table 2 - Physical attributes of the soils considered.

Soil	θ_o	θ_s	θ_t	θ_r	ρ (10^3 kgm^{-3})	K_0 (10^{-6} m s^{-1})	Tie (10^{-6} m s^{-1})	i_p (10^{-6} m s^{-1})	ψ_b (10^{-6} m s^{-1})	λ
LVA	0.327	0.541	0.521	0.237	1.05	31.14	36.19	486.0	0.087	0.4032
LV	0.113	0.479	0.398	0.085	1.42	28.50	70.31	530.0	0.132	0.7470
PV	0.300	0.543	0.523	0.237	1.19	9.86	21.92	211.0	0.104	0.3572

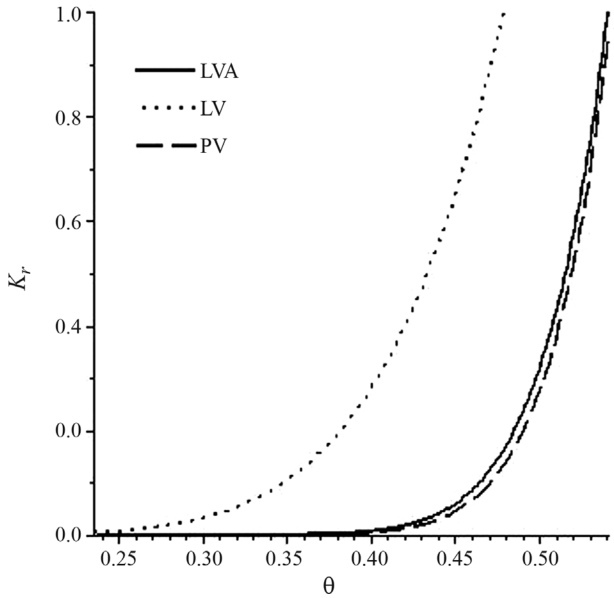

Figure 2 - Relative hydraulic conductivity *vs.* volumetric water content.

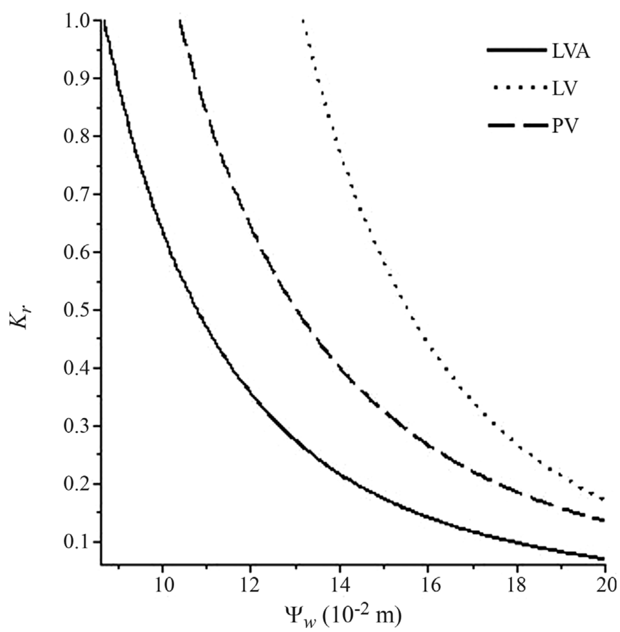

Figure 3 - Relative hydraulic conductivity *vs.* average wetting front matric potential.

for each situation. By choosing α close to 0, the graph tends to overestimate the values of the cumulative infiltration. On the other hand, if such parameter is closer to 1, the values of the cumulative infiltration decrease. It can be seen that the function which predicts the infiltration has a discontinuity when t is equal to t_p. This comes from the assumption that t_p and t_s are obtained by means of the exact three-parameter equation. In order to work out this issue, one shall obtain the explicit equations for each parameter based on the approximated solution proposed. Since such discontinuities do not affect the values of α, this procedure is out of the scope of the present effort. The results are summarized in Table 3.

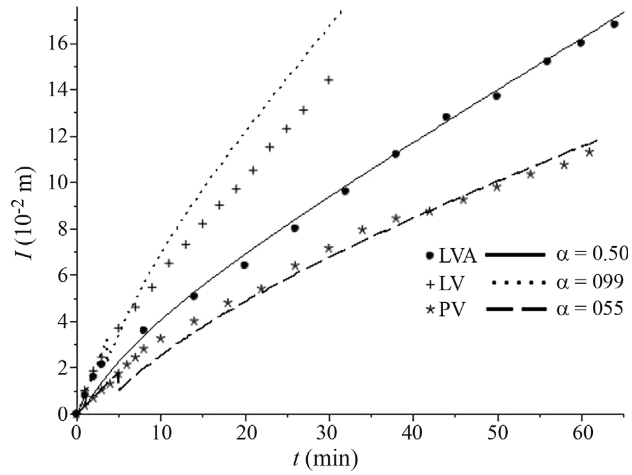

Figure 4 - Cummulative infiltration *vs.* time for the soils analyzed.

Table 3 - Results.

Soil	Classification	$\alpha_{obtained}$
LVA	Red-Yellow Laterite	0.50
LV	Red Laterite	0.99
PV	Red Clay	0.55

5. Conclusions

The three-parameter equation for infiltration prediction has been solved by means of an iterative algorithm whose single-iteration convergence ratio can be chosen as high as desired.

The methodology has been validated by comparing the approximate solutions to the exact ones. The maximum absolute departure of the approximated nondimensional cumulative infiltration is of about 0.23 and happens at low nondimensional times. The results presented considered a single iteration of the algorithm, thus the error could be mitigated by taking more iterations into account.

Based on the three-parameter infiltration equations and the solutions developed, three real cases were studied and the value of the interpolation parameter α has been obtained for each one. For a red clay soil α = 0.55; for a red laterite α = 0.99 and finally, for a red-yellow laterite soil α = 0.50. These values may vary mainly due to the type of soil analyzed.

It’s known that exact solutions are not necessary for practical purposes. The tree-parameter infiltration equation can only be exactly solved in terms of special functions, which ultimately reduces it applicability to practical situations. In the present paper, simple yet powerful approximated solutions with good accuracy are presented. This way, it becomes easier to apply the three-parameter infiltration equation to field studies.

Acknowledgments

The authors acknowledge the support of the following institutions: Brazilian National Research Council (CNPq) and University of Brasilia. The authors would also like to thank two anonymous reviewers for the valuable suggestions on the improvement of the present paper and, finally, Prof. Roberto Cecílio for gently offering the experimental data used in the present effort.

Table of Symbols

a = convergence parameter
I = cumulative infiltration
I_* = nondimensional cumulative infiltration
I_p = cumulative infiltration until ponding time
i_p = rainfall intensity
K_t = hydraulic conductivity in transmission zone
K_r = relative hydraulic conductivity
K_s = saturated hydraulic conductivity
p_s = average surface pressure head
r = infiltration rate
t = time
t_* = nondimensional time
t_p = ponding time
t_s = time necessary to infiltrate the same amount infiltrated until the ponding time, under saturation of the superficial layer of the soil
Tie = steady infiltration rate
α = interpolation parameter;
θ_s = saturated water content
θ_o = initial water content
θ_r = residual water content
λ = pore size distribution index.
ψ_w = average wetting front matric potential
ψ_b = absolute value of the matric potential of air entrance.

References

Brooks, R.H. & Corey, A.T. (1964) Hydraulic properties of porous media. Hydrologic Paper #3, Colorado State University, Fort Collins, 26 p.

Cecilio, R.A. (2005) Modelagem da Infiltração da Água no Solo Fundamentada na Equação de Green-Ampt-Mein-Larson. Tese de Doutorado, Programa de Pós-Graduação em Engenharia Agrícola. Universidade Federal de Viçosa, 164 p (in Portuguese).

Cecilio, R.A.; Martinez, M.A.; Pruski, F.F.; Silva, D.D. & Ataíde, W.F. (2007) Substituição dos parâmetros do modelo de Green-Ampt-Mein-Larson para estimativa da infiltração em alguns solos do Brasil. Rev. Bras. Ciênc. Solo, v. 31:5, p. 1141-1151.

Green, W.H. & Ampt, G.A. (1911) Studies in soil physics. I. The flow of air and water through soils. J Agri. Sci., v. 4:1, p. 1-24.

Householder, A.S. (1970) The Numerical Treatment of a Single Nonlinear Equation. McGraw-Hill, New York, 216 p.

Mein, R.G. & Farrell, D.A. (1974) Determination of wetting front suction in the Green-Ampt equation. Soil Science Society of America Proceedings, v. 38:6, p. 399-417.

Parlange, J.-Y.; Lisle, I.; Braddock, R.D. & Smith, R.E. (1982) The three parameter infiltration equation. Soil Sci, v. 133:6, p. 337-341.

Parlange, J.-Y.; Barry, D.A. & Haverkamp, R. (2002) Explicit infiltration equations and the Lambert W-function. Advances in Water Resources, v. 25:8-12, p. 1119-1124.

Rathie, P.N.; Swamee, P.K.; Cavalcante, A.L.B. & Ozelim, L.C.S.M. (2012) Lagrange's inversion theorem and infiltration. World Academy of Science, Engineering and Technology, v. 67, p. 473-478.

Talsma, T. & Parlange, J.-Y. (1972) One-dimensional vertical infiltration. Australian J. Soil. Res., v. 10:2, p. 143-150.

Zonta, J.H.; Martinez, M.A.; Pruski, F.F.; Silva D.D. & Motebeller, C.A. (2010) Adjustment of Green-Ampt-Mein-Larson model parameters under field conditions. Rev. Bras. Eng. Agric. Ambient., v. 14:10, p. 1021-1029.

SOILS and ROCKS
An International Journal of Geotechnical and Geoenvironmental Engineering

Publication of
ABMS - Brazilian Association for Soil Mechanics and Geotechnical Engineering
SPG - Portuguese Geotechnical Society
Volume 36, N. 1, January-April 2013

Author index

Cavalcante, A.L.B. 129
Cunha, R.P. 21
Dantas-Ferreira, M. 67
Espósito, T. 97
Fahel, A. 1
Gomes, R.C. 37
Guimarães, V. 67
Landi, A. 1
Langone, M.J. 55
Lima, R.E. 67
Ortigao, J.A.R. 1
Ozelim, L.C. de S.M. 129
Paiva, P. 1
Palmier, L.R. 97
Pando, M. 21
Pejon, O.J. 67
Pirete, W. 37
Rathie, P.N. 129
Schnaid, F. 55
Souto, R. 1
Swamee, P.K. 129
Zuquette, L.V. 67

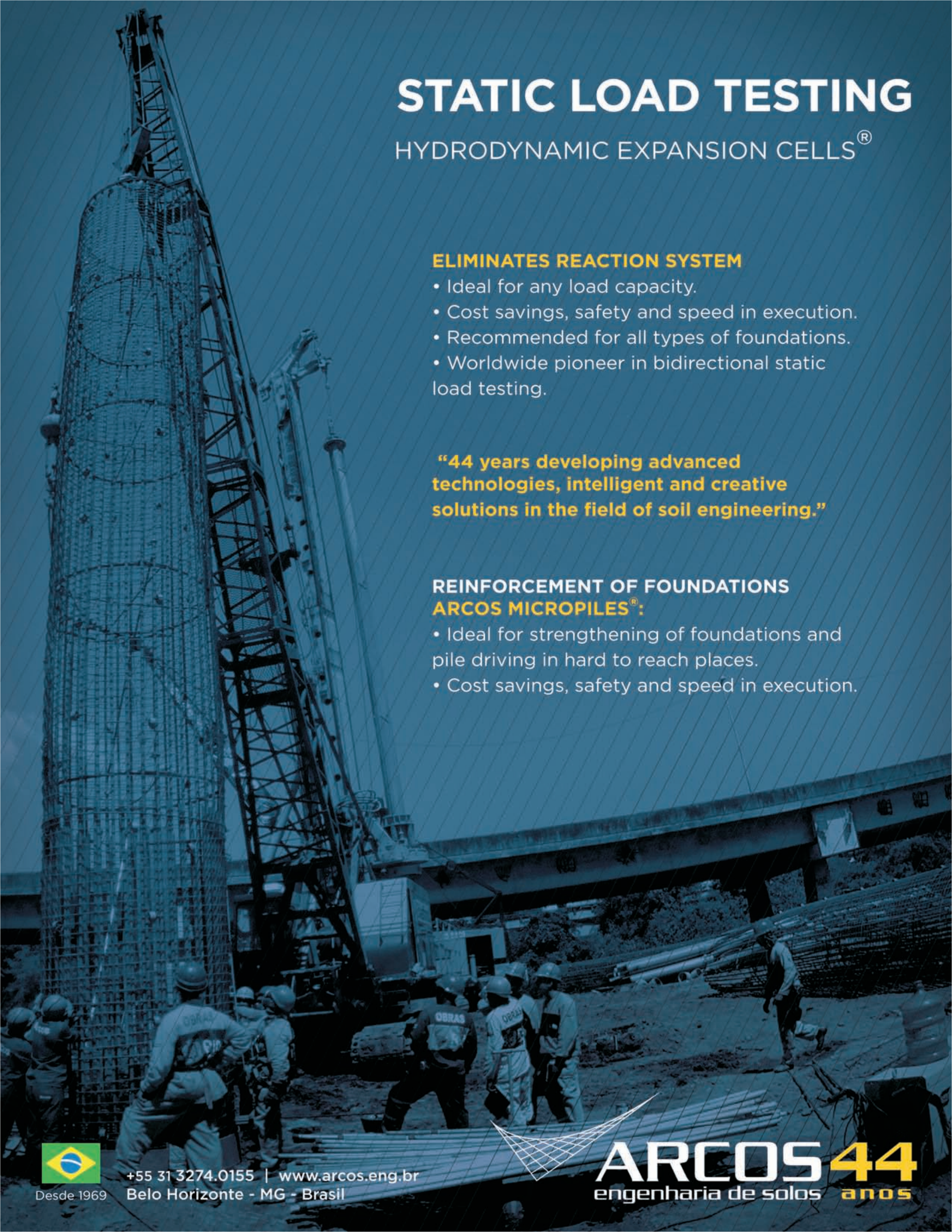
STATIC LOAD TESTING
HYDRODYNAMIC EXPANSION CELLS®
ELIMINATES REACTION SYSTEM
• Ideal for any load capacity.
• Cost savings, safety and speed in execution.
• Recommended for all types of foundations.
• Worldwide pioneer in bidirectional static load testing.
"44 years developing advanced technologies, intelligent and creative solutions in the field of soil engineering."
REINFORCEMENT OF FOUNDATIONS
ARCOS MICROPILES®:
• Ideal for strengthening of foundations and pile driving in hard to reach places.
• Cost savings, safety and speed in execution.
Desde 1969
+55 31 3274.0155 | www.arcos.eng.br
Belo Horizonte - MG - Brasil
ARCOS 44
engenharia de solos anos

1. Mangaratiba RJ

2. Botafogo RJ

3. Copacabana, RJ

1

2

Recorde Mundial: impacto de 20 toneladas métricas à 103km/h contido!

3

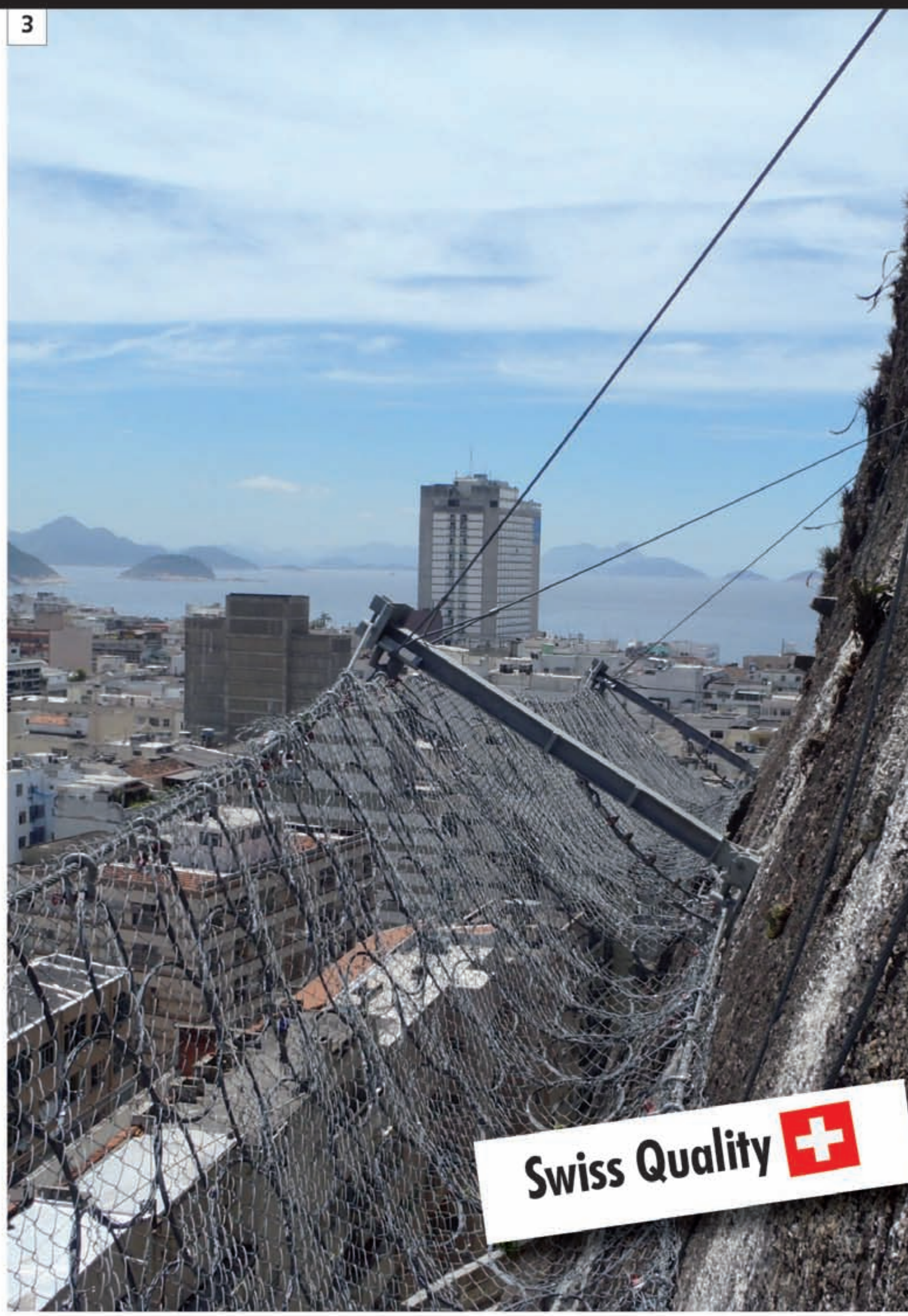

A nova barreira para queda de rochas modelo GBE 8000A estabeleceu novo recorde mundial em teste realizado em Outubro,2011 no campo de testes verticais em Wallenstadt na Suíça. Teste certificado realizado e resultados certificados obtidos de acordo com a norma do ETAG 027 :

- 8,000kj de energia de impacto
- 8.5 metros de deflexão da barreira
- 85% de altura residual da barreira

A barreira modelo GBE-8000A protege contra queda de grandes blocos de rocha que produzem altas cargas de energia cinética, são aplicáveis onde as barragens de retenção não são possíveis e excedem a capacidade de absorção da maioria das galerias de concreto.

Assista ou escaneie o filme do teste em: www.geobrugg.com/GBE-8000A

GEOBRUGG®
BRUGG

Geobrugg AG
Geohazard Solutions
Rua Visconde de Pirajá, 82 sl.606
Ipanema - Rio de Janeiro • 22410-003
Fone: +55 21 3624.1449
Cel: +55 21 9979.1288
info@geobrugg.com • www.geobrugg.com

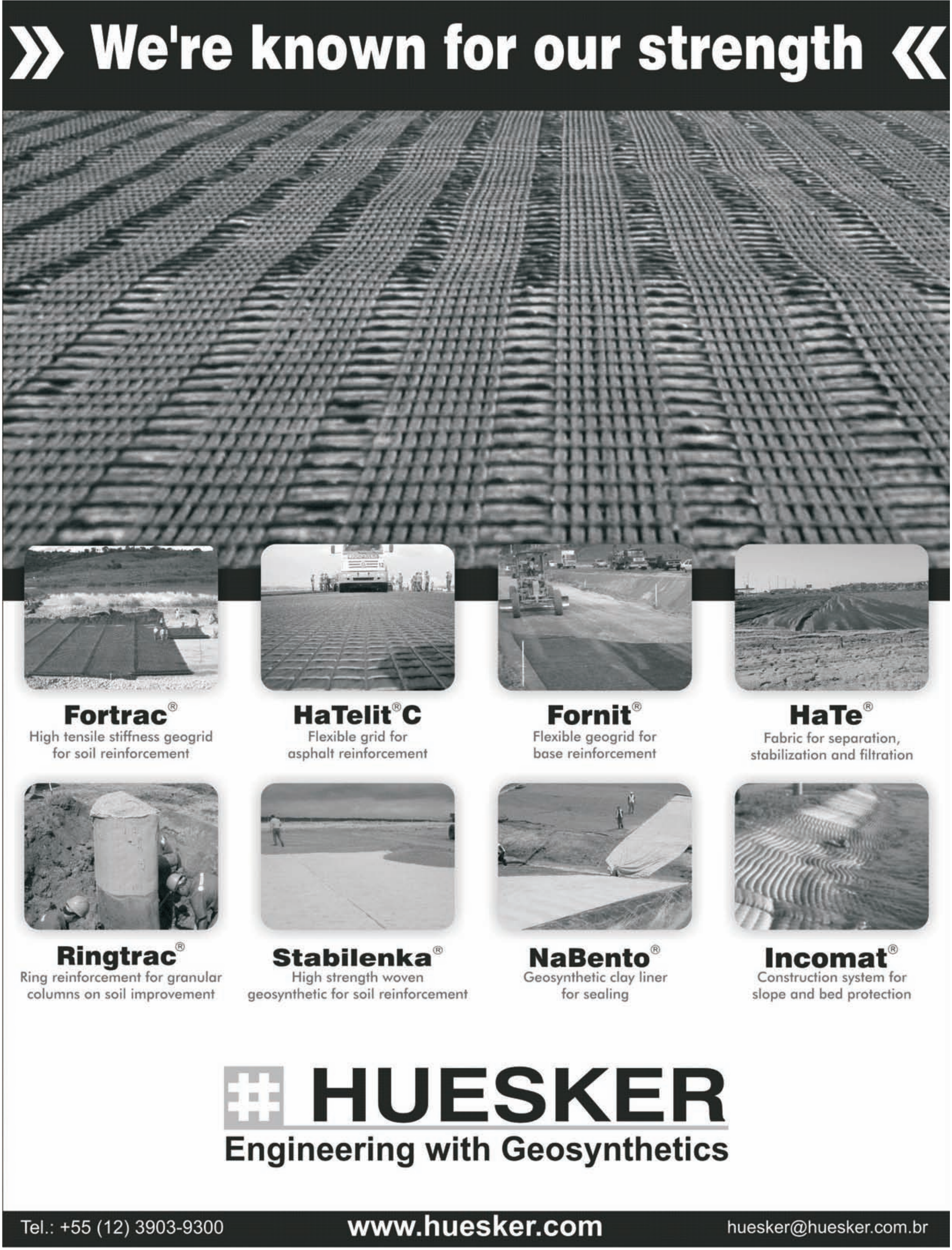
We're known for our strength
Fortrac®
High tensile stiffness geogrid for soil reinforcement
HaTelit®C
Flexible grid for asphalt reinforcement
Fornit®
Flexible geogrid for base reinforcement
HaTe®
Fabric for separation, stabilization and filtration
Ringtrac®
Ring reinforcement for granular columns on soil improvement
Stabilenka®
High strength woven geosynthetic for soil reinforcement
NaBento®
Geosynthetic clay liner for sealing
Incomat®
Construction system for slope and bed protection
HUESKER
Engineering with Geosynthetics
Tel.: +55 (12) 3903-9300
www.huesker.com
huesker@huesker.com.br


SOLOS MOLES?
ENGEGRAUT
www.engegraut.com.br
CPR®
CONSOLIDAÇÃO PROFUNDA RADIAL
O MAIS RÁPIDO E EFETIVO TRATAMENTO PARA SOLOS MOLES
Processo de adensamento de solo mole, eficientemente controlado, monitorando-se o grau de consolidação desejado.
TÉCNICA DE TRATAMENTO DE SOLO MOLE POR CONSOLIDAÇÃO
METODOLOGIA PREMIADA PARA TRATAMENTO DE
SOLO MOLE
Vantagens do CPR
• 100% específico para solos moles;
• Mobilização rápida;
• Ausência de transtornos à obra;
• Ampla gama de aplicações;
• Ausência de aterros, refugos e lama;
• Técnica não destrutiva;
• Alternativa super econômica, além de prazos extremamente curtos em relação à substituição de solos, aterros temporários, colunas granulares e estaqueamentos;
• Alcança profundidades de tratamento onde técnicas clássicas são limitadas;
• Acesso a locais restritos, limitados e difíceis, sem interferência com a rotina do cliente;
• Melhor custo benefício;
• Perfeito para reforço de fundação.
www.engegraut.com.br
Para maiores informações, entre em contato com nosso departamento de geotecnia. A marca CPR® e a tecnologia Consolidação Profunda Radial são patentes da ENGEGRAUT.

GEOLOGY - GEOTECHNICS - SUPERVISION OF GEOTECHNICAL WORKS

EMBANKMENT DAMS - UNDERGROUND WORKS - RETAINING STRUCTURES

SPECIAL FOUNDATIONS - SOIL IMPROVEMENT - GEOMATERIALS

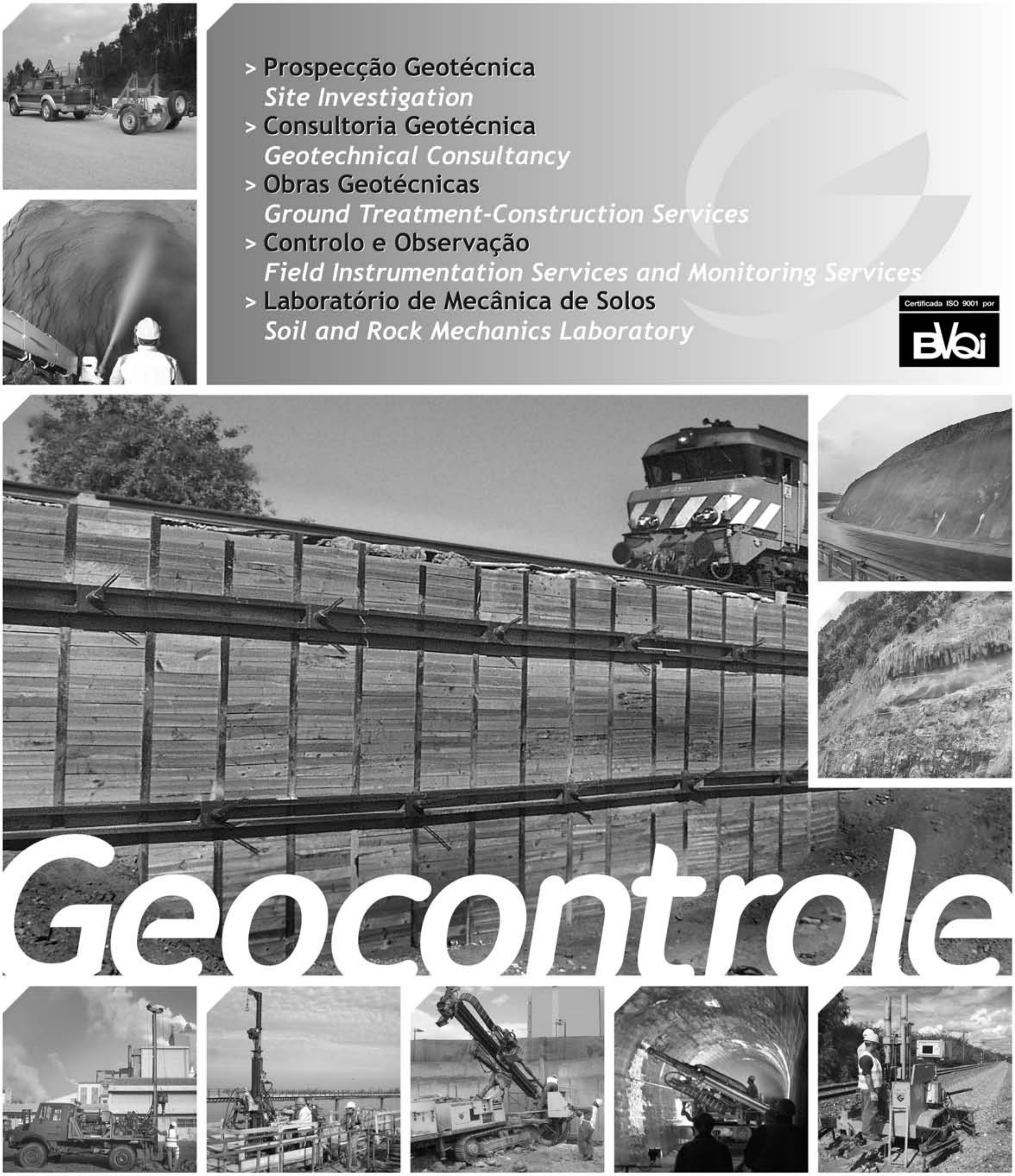
> Prospecção Geotécnica
Site Investigation
> Consultoria Geotécnica
Geotechnical Consultancy
> Obras Geotécnicas
Ground Treatment-Construction Services
> Controlo e Observação
Field Instrumentation Services and Monitoring Services
> Laboratório de Mecânica de Solos
Soil and Rock Mechanics Laboratory
Certificada ISO 9001 por
BVQi
Geocontrole

Instructions to Authors

Category of the Papers

Soils and Rocks is the scientific journal edited by the Brazilian Association for Soil Mechanics and Geotechnical Engineering (ABMS) and the Portuguese Geotechnical Society (SPG). The journal is intended to the divulgation of original research works from all geotechnical branches.

The accepted papers are classified either as an Article paper, a Technical Note, a Case Study, or a Discussion according to its content. An article paper is an extensive and conclusive dissertation about a geotechnical topic. A paper is considered as a technical note if it gives a short description of ongoing studies, comprising partial results and/or particular aspects of the investigation. A case study is a report of unusual problems found during the design, construction or the performance of geotechnical projects. A case study is also considered as the report of an unusual solution given to an ordinary problem. The discussions about published papers, case studies and technical notes are made in the Discussions Section.

When submitting a manuscript for review, the authors should indicate the category of the manuscript, and is also understood that they:

a) assume full responsibility for the contents and accuracy of the information in the paper;

b) assure that the paper has not been previously published, and is not being submitted to any other periodical for publication.

Manuscript Instructions

Manuscripts must be written in English. The text is to be typed in a word processor (MS Word or equivalent), using ISO A4 page size, left, right, top, and bottom margins of 25 mm, Times New Roman 12 font, and line spacing of 1.5. All lines and pages should be numbered. The text should be written in the third person.

The fist page of the manuscript is to include the title of the paper in English, followed by the names of the authors with the abbreviation of the most relevant academic title. The affiliation, address and e-mail is to be indicated below each author's name. An abstract of 200 words is to be written in English after the author's names. A list with up to six keywords at the end of the abstract is required.

Although alteration of the sequence and the title of each section may be required, it is suggested that the text contains the following sections: Introduction, Material and Methods, Results, Discussions, Conclusion, Acknowledgements, References and List of Symbols. A brief description of each section is given next.

Introduction: This section should indicate the state of the art of the problem under evaluation, a description of the problem and the methods undertaken. The objective of the work is to be clearly presented at the end of the section.

Materials and Methods: This section should include all information needed to the reproduction of the presented work by other researchers.

Results: In this section the data of the investigation should be presented in a clear and concise way. Figures and tables should not repeat the same information.

Discussion: The analyses of the results should be described in this section. **Conclusions**: The text of this section should be based on the presented data and in the discussions.

Acknowledgenments: If necessary, concise acknowledgements should be written in this section.

References: References to other published sources are to be made in the text by the last name(s) of the author(s), followed by the year of publication, similarly to one of the two possibilities below:

"*while Silva & Pereira (1987) observed that resistance depended on soil density*" or "*It was observed that resistance depended on soil density (Silva & Pereira, 1987).*"

In the case of three or more authors, the reduced format must be used, *e.g.*: Silva *et al.* (1982) or (Silva *et al.*, 1982). Two or more citations belonging to the same author(s) and published in the same year are to be distinguished with small letters, *e.g.*: (Silva, 1975a, b, c.). Standards must be cited in the text by the initials of the entity and the year of publication, *e.g.*: ABNT (1996), ASTM (2003).

Full references shall be listed alphabetically at the end of the text by the first author's last name. Several references belonging to the same author shall be cited chronologically. Some examples are listed next:

Papers: Bishop, A.W. & Blight, G.E. (1963) Some aspects of effective stress in saturated and unsaturated soils. Géotechnique, v. 13:2, p. 177-197.

Books: Lambe, T.W & Whitman, R.V. (1979) Soil Mechanics, SI Version, 2nd ed. John Wiley & Sons, New York, p. 553.

Book with editors: Sharma, H.D.; Dukes, M.T. & Olsen, D.M. (1990) Field measurements of dynamic moduli and Poisson's ratios of refuse and underlying soils at a landfill site. Landva A. & Knowles, G.D. (eds) Geotechnics of Waste Fills - Theory and Practice, American Society for Testing and Materials - STP 1070, Philadelphia, p. 57-70.

Proceedings (printed matter or CD-ROM): Jamiolkowski, M.; Ladd, C.C.; Germaine, J.T & Lancellotta, R. (1985) New developments in field and laboratory testing of soils. Proc. 11th Int. Conf. on Soil Mech. and Found. Engn., ISSMFE, San Francisco, v. 1, pp. 57-153.(specify if CD – ROM)

Thesis and dissertations: Lee, K.L. (1965) Triaxial Compressive Strength of Saturated Sands Under Seismic Loading Conditions. PhD Dissertation, Department of Civil Engineering, University of California, Berkeley, 521 p.

Standards: ASTM (2003) Standard Test Method for Particle Size Analysis of Soils - D 422-63. ASTM International, West Conshohocken, Pennsylvania, USA, 8 p.

Internet references: Soils and Rocks available at http://www.abms.com.br.

On line first publications must also bring the digital object identifier (DOI) at the end.

Figures shall be either computer generated or drawn with India ink on tracing paper. Computer generated figures must be accompanied by the corresponding digital file (.tif, .jpg, .pcx, etc.). All figures (graphs, line drawings, photographs, etc.) shall be numbered consecutively and have a caption consisting of the figure number and a brief title or description of the figure. This number should be used when referring to the figure in text. Photographs should be black and white, sharp, high contrasted and printed on glossy paper.

Tables shall be numbered consecutively in Arabic and have a caption consisting of the table number and a brief title. This number should be used when referring to the table in text. Units should be indicated in the first line of the table, below the title of each column. Abbreviations should be avoided. Column headings should not be abbreviated. When applicable, the units should come right below the corresponding column heading. Any necessary explanation can be placed as footnotes.

Equations shall appear isolated in a single line of the text. Numbers identifying equations must be flush with the right margin. International System (SI) units are to be used. The symbols used in the equations shall be listed in the List of Symbols. It is recommended that the used symbols be in accordance with Lexicon in 8 Languages, ISSMFE (1981) and the ISRM List of Symbols.

The text of the submitted manuscript (including figures, tables and references) intended to be published as an article paper or a case history should not contain more than 30 pages formatted according to the instructions mentioned above. Technical notes and discussions should have no more than 15 and 8 pages, respectively. Longer manuscripts may be exceptionally accepted if the authors provide proper explanation for the need of the required extra space in the cover letter.

Discussion

Discussions must be written in English. The first page of a discussion paper should contain:

• The title of the paper under discussion in the language chosen for publication;

• Name of the author(s) of the discussion, followed by the position, affiliation, address and e-mail. The discusser(s) should refer himself (herself, themselves) as "the discusser(s)" and to the author(s) of the paper as "the author(s)".

Figures, tables and equations should be numbered following the same sequence of the original paper. All instructions previously mentioned for the preparation of article papers, case studies and technical notes also apply to the preparation of discussions.

Editorial Review

Each paper will be evaluated by reviewers selected by the editors according to the subject of the paper. The authors will be informed about the results of the review process. If the paper is accepted, the authors will be required to submit a version of the revised manuscript with the suggested modifications. If the manuscript is refused for publication, the authors will be informed about the reasons for rejection. In any situation comprising modification of the original text, classification of the manuscript in a category different from that proposed by the authors, or refusal for publication, the authors can reply presenting their reasons for disagreeing with the reviewers' comments

Submission

The author(s) must submit for review:

1. A hard copy of the manuscript to Editors - Soils and Rocks, Av. Prof. Almeida Prado, 532 – IPT, Prédio 54 – DEC/ABMS, 05508-901 - São Paulo, SP, Brazil. The first page of the manuscript should contain the identification of the author(s), or

2. The digital file of the manuscript, omitting the authors' name and any information that eventually could identify them, should be sent to **abms@ipt.br**. The following must be written in the subject of the e-mail message: "*Paper submitted to Soils and Rocks"*. The authors' names, academic degrees and affiliations should be mentioned in the e-mail message. The e-mail address from which the digital file of the paper was sent will be the only one used by the editors for communication with the corresponding author.

Follow Up

Authors of manuscripts can assess the status of the review process at the journal website (www.soilsandrocks.com.br) or by contacting the ABMS secretariat.

Soils and Rocks Volume 36, N. 1 2013

Volume 36, N. 1, January-April 2013

Table of Contents

ARTICLES

Trial Embankment on Gold Mine Tailings
J.A.R. Ortigao, P. Paiva, A. Fahel, A. Landi, R. Souto 1

Influence of Pile-Soil-Raft Parameters on the Behavior of Piled Raft and Conventional Piled Group Foundations
R.P. Cunha, M. Pando 21

Tailings Liquefaction Analysis Using Strength Ratios and SPT/CPT Results
W. Pirete, R.C. Gomes 37

A Method for Predicting Pile Bearing Capacity From Dynamic Penetration Tests
F. Schnaid, M.J. Langone 55

A Preliminary Assessment of the Distribution and Consequences of Natural and Some Anthropogenic Hazards in Brazil
L.V. Zuquette, O.J. Pejon, R.E. Lima, M. Dantas-Ferreira, V. Guimarães 67

Application of Risk Analysis Methods on Tailings Dams
T. Espósito, L.R. Palmier 97

Performance of In-Line Sediment Control Devices Under Field Conditions
C.P. Cavalhieri, S.J.A.M. Campos, A.L.C.F. Gallardo, O.Y. Bitar 119

TECHNICAL NOTE

Explicit Numerial Iterative Methods Applied to the Three-Parameter Infiltration Equation
A.L.B. Cavalcante, L.C.S.M. Ozelim, P.K. Swamee, P.N. Rathie 129